Physik-Department
Technische Universität München
Institut für Theoretische Physik
Lehrstuhl T30e Univ.-Prof. Dr. Manuel Drees

Analysis of constrained CP-phases in the MSSM at future linear colliders

Benedikt Gaißmaier

Vollständiger Abdruck der von der Fakultät für Physik der Technischen Universität München zur Erlangung des akademischen Grades eines

Doktors der Naturwissenschaften (Dr. rer. nat.)

genehmigten Dissertation.

Vorsitzender: Univ.-Prof. Dr. St. Paul

Prüfer der Dissertation:

1. Univ.-Prof. Dr. M. Drees, Universität Bonn
2. Univ.-Prof. Dr. A. J. Buras

Die Dissertation wurde am 13. Juli 2004 bei der Technischen Universität München eingereicht und durch die Fakultät für Physik am 6. August 2004 angenommen.

Contents

Part I

Introduction and Basics

Chapter 1

Introduction

1.1 Introducing the MSSM

1.1.1 Motivation, basic idea and first implications of SUSY

Among all the currently discussed extensions of the Standard Model (SM) Supersymmetry (SUSY) has to be considered as a particular interesting one. SUSY has risen this particular attraction and interest since it offers several virtues [1, 2]. Firstly, weak scale SUSY has a natural answer to the gauge hierarchy problem [3–6] and achieves the gauge unification without the ad hoc introduction of additional particles [7–10]. Moreover, it is able to explain the electroweak symmetry breaking (EWSB) radiatively [11] and offers a compelling candidate for the cold dark matter component of the Universe [12, 13].
Speaking in simplifying terms, the basic idea of SUSY consists in imposing an additional symmetry between fermions and bosons. As a consequence each known particle of the SM obtains a SUSY partner with spin differing by one half. However, since none of these SUSY particles (sparticles) has been found yet, the symmetry—if present at all—has to be broken; in exact SUSY the masses of particles and sparticles are identical. If the virtue of the solved gauge hierarchy problem is supposed to remain for broken SUSY, only a certain class of terms are possible for SUSY breaking. Essentially these terms—so called "soft breaking terms"—are not allowed to generate any quadratic divergencies, which are absent in exact SUSY. Unfortunately, adding all of these phenomenologically required and theoretically allowed soft breaking terms to the exact SUSY generates an "inflation" of parameter space unless additional assumptions on the—a priori completely unknown and undetermined—underlying mechanism of SUSY breaking are made. Here it should be remarked that imposing assumptions on the mechanism of SUSY breaking, i.e. assuming a specific model for SUSY breaking, decorates the used model of SUSY breaking among all possible ones and hence implies a significant loss of generality. However, many of the parameters which are in general introduced to parameterize the possible soft breaking terms arising from an unknown breaking mechanism are complex and hence offer new sources of CP-violation.
Experimentally CP-violation was first observed in the neutral kaon system [14] and has recently been confirmed by measurements in B-meson decays [15,16]. In the SM with massless neutrinos and only one physical neutral Higgs boson the only source of CP-violation is given

by the complex phase[1] of the Cabbibo-Kobayashi-Maskawa-matrix (CKM-matrix) [20]. Moreover, it is known that CP-violating phases are necessary to describe the observed baryon asymmetry of the Universe [21] and that the phase in CKM-matrix is most likely not large enough for this purpose. Therefore the presence of CP-violating phases in soft breaking terms can be interpreted as another virtue of broken SUSY itself. However, even today, with no direct signal of SUSY observed yet, these phases are constrained by the current measurements [18] of the electric dipole moments of the electron (d_e), the muon (d_μ), the neutron (d_n), and the mercury atom (d_{Hg}). Generally speaking the consequences and implications of these measurements for the SUSY parameter space depend strongly on the SUSY model used for interpreting the measurements. Several of these models offer possibilities to obtain sizeable values for some of these phases while still being consistent with the mentioned experimental results—for example by cancellations among various SUSY contributions to the electric dipole moments [22–26] or by making parts of the SUSY spectrum rather heavy [27, 28]. However, regardless in which manner sizeable CP-phases can be made consistent with the constraints from data, the implication that such CP-phases cannot be neglected in the study of (possible) SUSY signals at future colliders should be obvious. To estimate the danger of neglecting CP-phases in collider physics just recall that any observable associated with sparticles at a collider—masses, cross sections, branching ratios—depends not only on the *absolute values* of the involved SUSY parameters, but also on their *phases*, if non-trivial. Hence such CP-phases should be treated unbiased by the constraints mentioned above and be included as free parameters in any analysis of possible SUSY signals at colliders. To be more pathetic, a clear and convincing strategy to establish CP-violation by using SUSY signals at colliders and extracting the new CP-phases, if present, from data is absolutely necessary.
This thesis is devoted to participate in the development of such strategies.

1.1.2 Low-energy Lagrangian of the MSSM

As the technical details of constructing supersymmetric field theories are well known nowadays and are of no further interest for the thesis, this point is not treated here and the motivated reader is referred to textbooks such as [29,30] or review articles such as [31–33]; only a compact summary of the MSSM Lagrangian and its parameters as relevant in this thesis is given. To be more specific than in Sec. 1.1.1 the framework of this thesis is not given by a general supersymmetric extension of the SM but by its minimal one—the Minimal Supersymmetric Standard Model (MSSM). This extension is minimal in a sense that it only duplicates the known particles in the lepton, quark and gauge sector of the SM by introducing their supersymmetric partners. For technical reasons the Higgs sector of the SM—a one Higgs dublett model—has to be extended towards a two Higgs dublett model (2HDM). The interactions and mass spectra are then described by a Lagrangian which is conveniently decomposed into a SUSY exact part, $\mathcal{L}_{\mathrm{exact}}$, and a part containing all possible soft breaking terms, $\mathcal{L}_{\mathrm{soft}}$. In the case that R-parity conservation[2] is imposed on the MSSM

[1] The observation of neutrino flavor oscillations opens the possibility that the neutrino mass matrix contains nontrivial CP-violating phases, but this has not yet been confirmed experimentally. For a recent review see for example [17]. In principle, CP could also be violated in the SM by the QCD θ term, but bounds on the electric dipole moment of the neutron [18] imply [19] $|\theta_{\mathrm{QCD}}| \lesssim 10^{-10}$.

[2] R-parity is an additional transformation acting on superfields; if this parity is violated, i.e. the Lagrangian is not invariant under such a transformation, neither baryon nor lepton number would be

the SUSY exact part contains—beside the differing Higgs sectors—exactly the same number of parameters as the SM does[3], i.e. three gauge couplings and three Yukawa couplings f^n_{ij} in the form of complex 3×3 matrices in generation space. More details on $\mathcal{L}_{\text{exact}}$ are not required at this stage they may either be found in the before mentioned introductory review articles [31–33] or are presented in the later course if relevant.
Contrarily, the soft breaking part attracts more attention here since it generates most of the SUSY parameter space. The most general parametrization of the soft breaking terms is given as

$$\begin{aligned}
\mathcal{L}_{\text{soft}} = &- \left[f^u_{ij} A^u_{ij} h_2 \cdot (\tilde{q}_L)_i \, (\tilde{u}_R)^\star_j + f^d_{ij} A^d_{ij} h_1 \cdot (\tilde{q}_L)_i \left(\tilde{d}_R\right)^\star_j + f^l_{ij} A^l_{ij} h_1 \cdot \left(\tilde{l}_L\right)_i \left(\tilde{l}_R\right)^\star_j + h.c. \right] \\
&- \Big[(\tilde{q}_L)^\dagger_i \left(m^2_{\tilde{q}_L}\right)_{ij} (\tilde{q}_L)_j + (\tilde{u}_R)^\dagger_i \left(m^2_{\tilde{u}_R}\right)_{ij} (\tilde{u}_R)_j + \left(\tilde{d}_R\right)^\dagger_i \left(m^2_{\tilde{d}_R}\right)_{ij} \left(\tilde{d}_R\right)_j \\
&\quad + \left(\tilde{l}_L\right)^\dagger_i \left(m^2_{\tilde{l}_L}\right)_{ij} \left(\tilde{l}_L\right)_j + \left(\tilde{l}_R\right)^\dagger_i \left(m^2_{\tilde{l}_R}\right)_{ij} \left(\tilde{l}_R\right)_j \Big] \\
&- \frac{1}{2} \left[M_1 \bar{\lambda}_1 \lambda_1 + M_2 \bar{\lambda}_2 \lambda_2 + M_3 \bar{\lambda}_3 \lambda_3 + h.c. \right] \\
&- m^2_1 |h_1|^2 - m^2_2 |h_2|^2 - \left[m^2_{12} h_1 \cdot h_2 + h.c \right],
\end{aligned} \tag{1.1}$$

where the m^2_n are hermitian, 3×3 matrices in generation space and give explicit masses to the SUSY partners of left- and right-handed SM fermions. Additional mass terms for these sparticles arise from the quantities A^n, being complex 3×3 matrices in generation space; note that these—so called Yukawa like soft breaking—terms not only imply flavor transitions but also generate left-right mixing after EWSB. The real parameters m^2_1 and m^2_2 as well as the complex parameter m^2_{12} contribute to the masses of the physical, scalar Higgs fields, whereas the three complex parameters M_1, M_2, and M_3 generate explicit mass terms for the fermionic components of the gauge fields. More details on $\mathcal{L}_{\text{soft}}$ and the standard notations for fields in the MSSM may again be found in [31–33].
Counting parameters at this stage of the discussion reveals that the model, including an additional complex parameter—the μ parameter—from the SUSY exact Higgs sector, contains the enormous overall number of 94 real parameters and 74 phases. Fortunately not all of these 168 parameters are physical as some of them can be removed by using additional symmetries of the Lagrangian [34–36]. After using these symmetries "only" 79 real parameters and 44 phases remain as physical parameters of the model. Including Θ_{QCD} as free parameter this model is normally referred to as "MSSM-124". Since most of these parameters are associated with soft breaking terms it is indeed correct to claim that these terms cause an inflation of parameter space.
Following [36] it is rather clear that the MSSM-124 possesses at least two dangerous properties; these are potentially large flavor changing neutral currents (FCNC) and the violation of the lepton family numbers L_e, L_μ, and L_τ. In a general MSSM-124 these features may serve as severe constraints on parameter space, e.g. from the very tight experimental bounds [18] on the branching ratios of lepton flavor violating decays like $\mu \to e\gamma$, $\mu \to 3e$ it could be concluded that lepton flavor violating parameters are absent in the soft breaking

conserved and hence problems with the stability of the proton would arise, for example see [32]. The conservation of R-parity is assumed throughout the complete thesis.

[3] Before the standard reduction of parameter space towards physical parameters.

terms, or at least very small. Motivated by such observations it is convenient to impose one of the following ad hoc assumptions on the soft breaking parameters m_n^2 and A^n:

i.) horizontal universality [34, 35]:
matrices m_n^2 and A^n are generation-independent

$$\left(m_n^2\right)_{ij} \propto m_{n,i}^2 \delta_{ij}, \tag{1.2a}$$

$$\left(A^n\right)_{ij} \propto A_i^n \delta_{ij}, \tag{1.2b}$$

ii.) universality [34, 35]:
matrices m_n^2 and A^n are generation-independent *and* universal

$$\left(m_n^2\right)_{ij} \propto m^2 \delta_{ij}, \tag{1.3a}$$

$$\left(A^n\right)_{ij} \propto A \delta_{ij}, \tag{1.3b}$$

iii.) flavor alignment [37]:
matrices m_n^2 and A^n are diagonal in a basis which diagonalizes quark and lepton mass matrices.

All three assumptions share in common that a separate conservation of L_e, L_μ, and L_τ is achieved [36] and that FCNC are absent at tree level. Certainly, all these assumptions are equivalent to a significant restriction of the parameter space of MSSM-124, but are phenomenological well motivated; at least for first studies of SUSY signals and first data analyses these assumptions should be sufficient for first attempts to construct the low-energy Lagrangian of the MSSM.
An alternative way to reduce the immense parameter space of the MSSM-124 consists in assuming a specific model for SUSY breaking; such a model could be given by mSugra (e.g. [1]) or GMSB [38, 39]. In such an approach a rather small set of parameters is defined at some GUT scale and the low-energy parameters of the MSSM are replaced a set of renormalization group equations, describing the evolution of the parameters from the GUT scale to the weak scale. Note that for such an approach a gain of predictive power due to a small set of input parameters at the GUT scale is accompanied by a loss of generality.
As a conclusion of this section it should be summarized that the MSSM possesses, when compared to the SM, a significantly enlarged parameter space with many physical phases and that several possibilities to reduce this parameter space are available, being either theoretically or phenomenologically well motivated.

1.2 Future collider experiments

The next collider project in the close future is the Large Hadron Collider (LHC) [40], currently being built at CERN and hopefully commencing operation 2007. Using proton proton collisions it is expected to reach a center of mass (CMS) energy of about 10TeV and to offer an integrated luminosity of around 100fb^{-1} per (collider) year to the experiments. The physical goal of this machine is for sure to establish "new physics", or in the worst case at least to find the extensively hunted SM Higgs boson. In the case "new physics"

is indeed found in the form of SUSY, the experiments at LHC are expected to measure parts of its mass spectrum and to determine some of its parameters or at least to constrain its parameter space further. For more details on SUSY searches at the LHC, see [41] and references within.
However, nowadays a certain consensus has been reached that a linear collider using electron positron collisions is significantly better suited for a precise determination of SUSY parameters than LHC. This expectation is essentially associated with the elementary nature of electrons and positrons compared to the constituent structure of the proton. As a consequence of these differing structures the CMS energy and polarizations of the "actually" colliding particles can be controlled much better at a linear collider than at LHC.
Inspired by this expectation worldwide effort is being spent both on the technical details of building and operating such a "Future Linear Collider" (FLC) and on the physics program that could be completed with it. Among all the various FLC projects (for example, GLC [42] in Japan, NLC [43] in the US or Tesla [44] at DESY) the Tesla project has made most progress in the last years. At the current stage a complete technical design report [45] has been released, containing a broad and detailed physics program [46], which in turn includes detailed studies on SUSY signals at Tesla. Moreover, most of the technical solutions suggested for this machine have been tested successfully. Due to this rather highlighted position of the Tesla project among others my thesis uses its expectations for the central machine parameters (CMS energy $\sqrt{s}$, integrated luminosity $\mathcal{L}$ per year, polarization rates of electron (P_{e^-}) and positron beams (P_{e^+})) as reference numbers for an FLC. These reference numbers are summarized in Tab. 1.1 for the 500GeV option of Tesla; note that Tesla and most other projects foresee an upgrade to $\sqrt{s} = 800\text{GeV}$ at least. Unfortunately it has to be admitted that the realization of such a presumably powerful tool as an FLC is to some extent indeed rather far away; even in the most optimistic estimates Tesla is expected to start data taking in 2015.
Nevertheless, it should be remarked that—assuming SUSY is realized by nature—one of the core missions of an FLC is the precise determination of fundamental SUSY parameters, as this is the first step to reveal the mechanism of SUSY breaking and opens a window to the Planck scale [47, 48].
Finally, note that also the e^-e^- option for an FLC is intensively discussed; here a much cleaner experimental environment could be achieved at the price of a reduction of the luminosity.

$\sqrt{s}$	$\mathcal{L}$	P_{e^-}	P_{e^+}
500GeV	300fb^{-1} per year	80%	60%

Table 1.1: Tesla parameters used as reference parameters for an FLC.

1.3 Motivation, goals and course of the thesis

The elementary idea and motivation for this thesis is best understood by taking the following observations carefully into account:
Firstly, the unconstrained MSSM offers a rather big number of phases as a priori free parameters. The current experimental measurements of various electric dipole moments do not necessarily force these phases to be negligibly small.

Secondly, it can be assumed that an FLC with a CMS energy $\sqrt{s}$ sizeable for "New Physics" and a sufficiently large enough integrated luminosity $\mathcal{L}$ will commence operation within the next three decades. As a matter of fact several detailed analyses [46, 49–53] investigating SUSY signals at an FLC have been presented. These analyses show that sparticles with a mass of up to $\sqrt{s}/2$ can be discovered at an FLC and that their properties such as masses, spins and couplings can determined precisely from data. However, when studying these works it can also be observed that some of them [49, 50] show the dangerous tendency to neglect phases completely. This neglect of phases, which are not necessarily small and correctly should be treated as free parameters of the model, has to be considered as a highly problematic simplification since both kinematical masses and couplings depend on them. In turn these phases have a direct impact on observables like cross sections and branching ratios. Hence neglecting possibly non-vanishing phases during the determination of real parameters from experimental data could result in wrong inputs for the reconstruction of the underlying theory at the unification scale.
Thirdly, the construction of sizeable and experimentally accessible CP-asymmetries is rather difficult for most production channels at an FLC. These difficulties arise as at least one secondary decay has to be included. Moreover, at tree-level asymmetries are only available if the decaying particle has non-zero spin. For the measurement of such an asymmetry the spin of the decaying particle then has to be partly reconstructed by using its decay products. Due to experimental issues such as background processes and event identification the profit of a given decay chain in establishing the CP-violating MSSM strongly depends on the chosen parameters points, i.e. the chosen parameter point can not necessarily be considered as representative for larger regions of parameter space.
Making all the observations summarized above led to the following, elementary questions which are broadly discussed in Part II of this thesis:

- How strong are the constraints from leptonic dipole moments?
- How does the "cancellation mechanism" work in detail?
- Which cross sections show a strong dependence on phases, which a weak dependence?
- What are the reasons for such differing behaviors, if present?
- Can a reasonable measure for the impact of CP-odd phases on CP-even cross sections be introduced?
- Do cross sections accumulate enough sensitivity to phases to establish CP-violation within the MSSM?
- Are phase-sensitivities of cross sections correlated among each other, are they correlated with leptonic dipole moments?

The basic idea of the "combined analysis" presented in Part II is to take today's low-energy data (mass bounds and leptonic dipole moments) as a set of constraints for a scan of parameter space and then to use the resulting low-energy compatible parameter points to check whether high-energy experiments at an FLC can provide additional information on phases.
My elementary assumption on the parameter space given by the MSSM is horizontal universality within the soft breaking parameters associated sfermions and strict universality

of these parameters for first and second generation sfermions. Since no specific model on SUSY breaking is used here all parameters are directly specified at the typical energy scale of an FLC. Furthermore the restrictive set of unpolarized, total cross sections for the following production channels[4] at an FLC is used here

$$e^+e^- \to \tilde{\chi}_i^0 \tilde{\chi}_j^0 \qquad i,j = 1,\ldots,4; \tag{1.4a}$$

$$e^+e^- \to \tilde{\chi}_i^+ \tilde{\chi}_j^- \qquad i,j = 1,2; \tag{1.4b}$$

$$e^+e^- \to \tilde{e}_i^+ \tilde{e}_j^- \qquad i,j = 1,2; \tag{1.4c}$$

$$e^-e^- \to \tilde{e}_i^- \tilde{e}_j^- \qquad i,j = 1,2; \tag{1.4d}$$

whereas the leptonic dipole moments used as constraints are restricted to the electric dipole moment of the electron d_e and the anomalous magnetic moment of the muon a_μ. Note that this selection of low- and high–energy observables yields a complementarity: several diagrams involving neutralinos as well as charginos contribute coherently to the low-energy observables, hence these observables can only give bounds on *combinations* of phases. Contrariwise, as different vertices whose combinations contributed to the leptonic dipole moments now appear *separated* from each other in different amplitudes, high-energy observables can be used to investigate *separate* sectors of the theory.
Since the major aim within Part II is to study the impact of CP-odd phases on CP-even cross sections, a significance $\mathcal{S}(f_1 f_2)$ is assigned to each of the final states given by the reactions in Eqs. 1.4. This significance is defined as the difference in counting rates between a CP-conserving point[5] (CPC point) and a CP-violating point[6] (CPV point) normalized to the statistical error of the cross section in the CPC point. In order to distinguish between phase-dependences from a variation of the couplings with phases and phase-dependences from a variation of kinematical masses with phases a second significance $\bar{\mathcal{S}}(f_1 f_2)$ is introduced. For the calculation of this significance the CPV point is chosen such that parts of the mass spectrum are kept fixed by absorbing the variation of (some) kinematical masses into a variation of the absolute values of (some) SUSY parameters.
A detailed numerical analysis using several points in SUSY parameter space shows that some of the reactions (mainly some among those given by Eqs. 1.4a and 1.4d) yield very large sensitivities to phases, whereas others (all chargino production modes in Eq. 1.4b) are almost insensitive to phases once the low-energy bounds are taken into account. Moreover, the numerical analysis also reveals that both significances do not correlate with d_e. Contrariwise, the significances of two different production modes are in most cases strongly correlated among each other. Slightly weaker correlations are observed between significances and a_μ.
On the way to these results remarkable insight into the cancellation mechanism concerning leptonic dipole moments and into the phase-dependences of cross sections is achieved by a semi-analytical treatment of these observables using perturbative treatments of sparticle mixing. These semi-analytical treatments constitute a major difference or improvement

[4] In the MSSM fermionic partners of gauge bosons and of scalar Higgses mix if they have same quantum numbers. The corresponding mass eigenstates are referred to as neutralinos and charginos, denoted by $\tilde{\chi}_i^0$ and $\tilde{\chi}_i^\pm$. Similarly, $\tilde{e}_i^\pm$ denotes selectrons, which are the mass eigenstates obtained from the mixing of the scalar partners of left- and right-handed electrons.

[5] A CP-conserving point is defined by a set of real parameters and all phases being either 0 or π.

[6] A CP-violating point is given by the same set of real parameters together with non-trivial, but low-energy compatible choices for at least one phase.

compared to related work concerning both low [22–26, 54, 55] and high-energy observables [56, 57].
However, despite all gains in understanding and quantifying the impact of CP-odd phases on CP-even cross sections, it is rather clear that no cross section, regardless of its sensitivity to phases, is sufficient to establish CP-violation in the MSSM. Note that the significances introduced above only quantify the deviation from the CP-conserving MSSM, but do not contain any information on the source of such a deviation. This implies that production modes with high significances can be used to determine CP-odd phases only once CP-violation has been established by measuring some CP-odd observables. To obtain a first estimate of how large such CP-odd observables in the investigated production modes can be the CP-odd components of the polarization vector of the produced charginos and neutralinos are included to the combined analysis of Part II. Numerically it is observed that these CP-odd polarization vector components are sizeable in most neutralino production modes, but rather small in chargino production modes with the exception of a few privileged points in parameter space.
Motivated by the obviously unavoidable necessity to measure CP-odd observables to establish CP-violation at an FLC and by the promising size of the CP-odd polarization vector component in neutralino production as well as by several works devoted to similar attempts [58–60], a specific decay chain following $\tilde{\chi}_1^0\tilde{\chi}_2^0$ production is studied in Part III. As general framework the MSSM is still used, but differing assumptions are applied. Here an inverted hierarchy for sfermions is assumed, i.e. sfermions of the first and second generation are assumed to be significantly heavier than third generation sfermions. Note that such assumptions are motivated by some GUT models for SUSY breaking [61–63] and that such an assumption naturally cures the problems associated with electric dipole moments allowing phases to be of $\mathcal{O}(1)$.
Using these assumptions the focus of Part III is on the production $e^+e^- \to \tilde{\chi}_1^0\tilde{\chi}_2^0$ followed by the two step decay $\tilde{\chi}_2^0 \to \tilde{\tau}_1^\pm\tau^\mp \to \tilde{\chi}_1^0\tau^\mp\tau^\pm$ as signal process and the production of a stau pair $e^+e^- \to \tilde{\tau}_i^\pm\tilde{\tau}_j^\mp$ succeeded by two stau decays $\tilde{\tau}_1^\pm \to \tilde{\chi}_1^0\tau^\pm$ as background process. Concerning the goal of sizeable and experimentally accessible CP-odd observables separate discussions of signal and background production cross sections and of both decays are required to obtain first estimates of the size and accessibility of possible asymmetries. Several experimental issues such as the distinction between signal and background events, the assignment of τ leptons in the final state to primary and secondary vertices and the measurement of the τ lepton polarization vector through its decay products are discussed and used to derive criteria for "optimized" parameter sets. Finally the complete decay chain has to be modeled and experimentally measurable CP-asymmetries have to be defined in terms of quantities measurable in the laboratory frame. As a final result of a case study using two optimized parameter sets and Monte Carlo techniques for the modeling of the complete decay chains (signal and background process) it is found numerically that some of these CP-asymmetries defined in the laboratory frame can reach an excess of up to 30% confirming the highlighted position of $\tilde{\chi}_1^0\tilde{\chi}_2^0$ production that was already observed in Part II. Note also that all the difficulties concerning the construction and measurement of CP-asymmetries at an FLC which motivated the work in Part II are nicely illustrated by the contents and efforts of Part III.

1.4 Organization and structure of the work

Despite the logical structure of the thesis is already laid out in Sec. 1.3 the organization of the thesis in the remainder is summarized now. Chapter 2 starts with recalling and briefly discussing the assumptions on the MSSM used in Parts II and III, the issue of rephasing invariance is covered here. In Sec. 2.2 the relevant mixing patterns are investigated both analytically and perturbatively. Afterwards the relevant parameters are summarized in Sec. 2.3 and the interaction Lagrangian as relevant through this thesis is presented in Sec. 2.4. Note that the results of Secs. 2.2, 2.3, and 2.5 are valid for Parts II and III.
Chapter 3, being the first step of the combined analysis of low- and high-energy observables presented in Part II, treats leptonic dipole moments, in particular d_e and a_μ, in great detail. Beginning with a short introduction to leptonic dipole moments and their current experimental status in Sec. 3.1, the restriction to d_e and a_μ as the only leptonic dipole moments relevant for the combined analysis is justified here. Afterwards analytical and semi-analytical results for the neutralino and chargino contributions to d_e and a_μ are presented in Sec. 3.2. These results are in turn used in Sec. 3.3 for a detailed discussion of numerical results concerning low-energy observables and their impact on parameter space.
Chapter 4 is devoted to the investigation of the relevant production cross sections. After defining the kinematical situation in Sec. 4.2 the elementary steps in the calculation of these cross sections are presented. Using the perturbative treatments of sparticle mixing the results for production cross sections from Sec. 4.3 are treated semi-analytically with the goal to work out the dominant sources of phase-dependences for each production cross section in Sec. 4.4. At the end of this chapter it will be obvious which cross sections develop strong dependences on phases and for what reasons. Chapter 5 introduces and discusses polarization vectors for produced fermions. Before a few generalities and definitions for the calculation of polarization vector components are introduced in Sec. 5.3, the problems associated with the construction of CP-asymmetries without including secondary decays to the investigated production channels are reviewed in Secs. 5.1 and 5.2. The results for polarization vector components in the presence and in the absence of initial state polarization are presented in Secs. 5.3.2 and 5.3.3. The most interesting ones of these components (in the absence of initial state polarization) are finally discussed semi-analytically in Secs. 5.4 and 5.5. Chapter 6 introduces the significances $\mathcal{S}(f_1 f_2)$ and $\bar{\mathcal{S}}(f_1 f_2)$, describes their numerical calculation and overviews the information contained in them critically. The elementary properties of both significances and of their correlations are investigated in Sec. 6.2 for the general case and illustrated using simplified toy-models for phase-dependent cross sections. Finally Part II is completed by the presentation of numerical results for high-energy observables in Chapter 7; these results and various sets of correlations of high-energy observables among each other and with low-energy observables are broadly discussed with respect to the findings of Chapters 3, 4 and 5.
The analysis of a decay chain presented in Part III starts with a short introduction to models with inverted hierarchy and their phenomenological implications in Chapter 8. Approaches to construct CP-asymmetries from SUSY decay chains and first experimental consequences of these are summarized in Sec. 8.2. This section also applies known results to obtain for restrictions on parameter space from the experimental accessibility of CP-asymmetries and from theoretical predictions on their size. In Chapter 9 the relevant production cross sections and sparticle decays are briefly addressed and investigated numerically for a parameter set optimized by the findings of Chapter 8, this numerical

investigation serves as "pre-study" for possible asymmetries. Afterwards several experimental issues are discussed in Sec. 9.3, these issues finally complete the criteria for the "optimized" parameters sets, which are in turn used as inputs for the case studies in the same section. Within these case studies the previously introduced CP-asymmetries in terms of laboratory frame observables are investigated numerically using Monte Carlo techniques for the phase space integration. The discussion of the results of these case studies is also contained in Sec. 9.3.
The results of Parts II and III are summarized in Chapter 10. First the results of Parts II and III are summarized separately in Secs. 10.1 and 10.2, respectively; first conclusions are also drawn in these sections. Consequently, Sec. 10.3 is a kind of synthesis of the findings of Parts II and III, more common conclusions are given here. Finally the thesis closes with a short outlook on the issue of CP-violation in the MSSM. Note that various details of technical nature appearing through the course of the thesis are given in the appendices.

Chapter 2

Masses and interactions

After collecting the basic assumptions on SUSY parameters and investigating the physical phases as relevant for the thesis, the appearing mixing patterns between current eigenstates are briefly discussed using analytical and perturbative results. The relevant parameters are summarized briefly. The chapter closes with a collection of the relevant parts of the interaction Lagrangian.

2.1 Assumptions on SUSY-parameters

As laid out in Sec. 1.1.2 experimental data strongly indicates that flavor mixing in the slepton sector is negligible. This observation is most easily accommodated by assuming the soft breaking parameters for sleptons—A^l_{ij}, $(m^2_{\tilde{l}_L})_{ij}$, and $(m^2_{\tilde{l}_R})_{ij}$,—to be diagonal in generation space. Such an assumption is made in Part II and III, with the extension that the soft breaking parameters for first and second generation sleptons are even identical. Note that under this assumption of diagonality in generation space the only mixing in the slepton sector occurs between $SU(2)$ dublett and singlet sleptons, $\tilde{l}_L$ and $\tilde{l}_R$, respectively. Neglecting the "colored sector" (quarks, squarks, gluons and gluinos) from the further discussion[1] the physical phases of this simplified model are now (re)addressed. In the limiting case of universal A terms for all slepton generations and working in a basis for (lepton) superfields where the Yukawa coupling f^l_{ij} is diagonalized with real and positive eigenvalues, the remaining complex parameters are μ, m^2_{12}, A, M_1, and M_2. According to [36] the supersymmetric Lagrangian possesses two global $U(1)$ symmetries,[2] of which one is broken[3] by μ and m^2_{12} and the second by by μ, A, M_1, and M_2. Therefore these symmetries can be used to eliminate two phases of these five complex parameters by suitable redefinitions of the fields. The remaining three phases, being combinations of the initial five phases, are the so called "physical phases" or "rephasing invariant combinations of phases". In the case of the discussed, simplified model these physical phases are given as

$$\Phi_A = \mathrm{Arg}\left[M_1 M_2^\star\right], \tag{2.1a}$$

$$\Phi_B = \mathrm{Arg}\left[\mu M_2 m_{12}^{2\star}\right], \tag{2.1b}$$

[1] This is a suitable simplification since only purely leptonic observables are involved in this thesis.

[2] These two symmetries were already included during the counting of physical phases of the general MSSM in Sec. 1.1.2.

[3] This is to say, terms linear in these parameters are not invariant under the two $U(1)$ symmetries.

$$\Phi_C = \mathrm{Arg}\,[A M_2^\star]\,. \tag{2.1c}$$

Since physical observables are invariant under such redefinitions of the fields, their phase-dependence can only arise from the physical phases in Eqs. 2.1 and from combinations of these phases. For example, in a convention where m_{12}^2 is real, the combination $\phi_\mu + \phi_1$ is expressed in terms of rephasing invariant quantities as

$$\phi_\mu + \phi_1 = \Phi_A + \Phi_B. \tag{2.2}$$

The consideration of physical phases (rephasing invariant quantities) is rather helpful since the requirement that physical observables only depend on them offers a stringent check for the consistency of calculations performed with unfixed conventions for the complex parameters. This is the elementary reason for treating M_2 as complex in Chapter 2 and Sec. 3.2.2. The convention $\phi_2 = 0$ is applied from Sec. 3.2.3 onwards if not noted otherwise. Note that the convention $\mathrm{Arg}[m_{12}^2] = 0$ is invoked throughout the thesis, this convention removes CP-violation from the tree-level Higgs potential [2]. For more details on rephasing invariance see [54] or, more elementary, [64].

2.2 Mixing of superparticles - analytical results

All mixing patterns between the current eigenstates relevant within the framework of this thesis can be calculated analytically. The results for the mixing of sleptons, charginos and neutralinos are briefly summarized in the next three subsections. All our results have been obtained by calculations independent from the ones published so far by other groups. The results within this thesis are found to be consistent with these.

2.2.1 Sfermions

Using the above assumptions the generic slepton mass term is given by [2]

$$\mathcal{L}_M^{\tilde{l}_\alpha \tilde{l}_\beta} = -(\tilde{l}_L, \tilde{l}_R)^\star \begin{pmatrix} X_{\tilde{l}} & Z_{\tilde{l}}^\star \\ Z_{\tilde{l}} & Y_{\tilde{l}} \end{pmatrix} \begin{pmatrix} \tilde{l}_L \\ \tilde{l}_R \end{pmatrix} = -\tilde{l}_\alpha^\star (M_{\tilde{l}}^2)_{\alpha\beta} \tilde{l}_\beta, \tag{2.3}$$

where the entries of the mass matrix $M_{\tilde{l}}^2$ are defined as

$$X_{\tilde{l}} = m_l^2 + m_{\tilde{l}_L}^2 + \frac{\cos 2\beta}{2}(M_Z^2 - 2M_W^2), \tag{2.4a}$$

$$Y_{\tilde{l}} = m_l^2 + m_{\tilde{l}_R}^2 + \cos 2\beta (M_Z^2 - M_W^2), \tag{2.4b}$$

$$Z_{\tilde{l}} = m_l \left| A_l^\star + \mu \tan\beta \right| e^{i\phi_{\tilde{l}}}, \tag{2.4c}$$

where m_l is the mass of the charged lepton l, $m_{\tilde{l}_{L,R}}^2$ and A_l are soft SUSY breaking parameters, μ is the Higgsino mass parameter, and $\tan\beta$ is the ratio of the vacuum expectation values of the two neutral Higgs fields. In general, $\mu \equiv |\mu| e^{i\phi_\mu}$ and $A_l \equiv |A_l| e^{i\phi_A}$ can be complex, while all other parameters appearing in Eqs. 2.4 are real. Here, $\phi_{\tilde{l}}$ is the argument of the off-diagonal entry, which is given by

$$\phi_{\tilde{l}} = \arg(-A_l - \mu^\star \tan\beta) \tag{2.5a}$$

$$= \phi_{A_l} - \arctan\left(\frac{|\mu|\sin(\phi_{A_l}+\phi_\mu)}{\cot\beta|A_l| + |\mu|\cos(\phi_{A_l}+\phi_\mu)}\right). \tag{2.5b}$$

The hermitian mass matrix $M^2_{\tilde{l}}$ is diagonalized by a unitary transformation $U_{\tilde{l}}$

$$U^\dagger_{\tilde{l}} M^2_{\tilde{l}} U_{\tilde{l}} = \mathrm{diag}(m^2_{\tilde{l}_1}, m^2_{\tilde{l}_2}), \tag{2.6}$$

which may be parametrized as [65]

$$U_{\tilde{l}} = \begin{pmatrix} \cos\theta_{\tilde{l}} & -\sin\theta_{\tilde{l}} e^{-i\phi_{\tilde{l}}} \\ \sin\theta_{\tilde{l}} e^{i\phi_{\tilde{l}}} & \cos\theta_{\tilde{l}} \end{pmatrix} = \begin{pmatrix} U_{\tilde{l}L} \\ U_{\tilde{l}R} \end{pmatrix}, \tag{2.7}$$

where $-\pi/2 \leq \theta_{\tilde{l}} \leq \pi/2$ and $0 \leq \phi_{\tilde{l}} \leq 2\pi$ and the eigenvalues are sorted in an increasing order. After introducing the quantities

$$\overline{M}^2_{\tilde{l}} = \frac{m^2_{\tilde{l}_2} + m^2_{\tilde{l}_1}}{2} = \frac{X_{\tilde{l}} + Y_{\tilde{l}}}{2}, \tag{2.8a}$$

$$\Delta_{\tilde{l}} = m^2_{\tilde{l}_2} - m^2_{\tilde{l}_1} = \sqrt{(X_{\tilde{l}} - Y_{\tilde{l}})^2 + 4\,|Z_{\tilde{l}}|^2}, \tag{2.8b}$$

one obtains for the mass eigenvalues and mixing angle

$$m^2_{\tilde{l}_1,\tilde{l}_2} = \overline{M}^2_{\tilde{l}} \mp \frac{\Delta_{\tilde{l}}}{2}, \tag{2.9a}$$

$$\sin 2\theta_{\tilde{l}} = -2\frac{|Z_{\tilde{l}}|}{\Delta_{\tilde{l}}}, \qquad \cos 2\theta_{\tilde{l}} = \frac{X_{\tilde{l}} - Y_{\tilde{l}}}{\Delta_{\tilde{l}}}. \tag{2.9b}$$

Some simple observations on slepton mixing should be mentioned after all these formulae were given: first of all, I denoted the first and second line of $U_{\tilde{l}}$ in Eq. 2.7 by $U_{\tilde{l}L}$ and $U_{\tilde{l}R}$ in order indicate to which entry of $U_{\tilde{l}}$ results in a $SU(2)$-doublet (singlet) component of the i.th mass eigenstate:

$$\tilde{l}_i = (U_{\tilde{l}})_{Li}\,\tilde{l}_L + (U_{\tilde{l}})_{Ri}\,\tilde{l}_R.$$

This notation will allow an easy back-tracing of contributions in observables to interactions with $SU(2)$ or $U(1)$ gauge bosons. Second, Eqs. 2.4 and 2.9 show that the amount of left-right mixing in the slepton sector is controlled by the absolute value of the off-diagonal entry in the mass matrix. In the case of the absolute value of this entry being negligible compared to the diagonal entries, left-right mixing is absent and only the two choices $\theta_{\tilde{l}} = 0$ or $\theta_{\tilde{l}} = \pi/2$ corresponding to $m_{\tilde{l}_L} \leq m_{\tilde{l}_R}$ and $m_{\tilde{l}_R} \leq m_{\tilde{l}_L}$ for $\theta_{\tilde{l}}$ are possible. Therefore, in the case of collider physics concerning processes which involve first and/or second generation sleptons, slepton mixing can safely be neglected, since $m_{\mathrm{e},\mu} \ll m_{\tilde{l}_{L,R}}$. This is no longer correct, either if leptonic dipole moments are considered since then the corresponding operators involve at least one power of the lepton mass, or if high energy signals with third generation sleptons are studied. Furthermore, Eqs. 2.4 and 2.9 also indicate that increasing values for $|\mu|$ and/or $\tan\beta$ enhance left-right mixing. Finally, Eq. 2.5b clearly illustrates that ϕ_l *itself* is no rephasing-invariant quantity and therefore cannot solely enter a physical quantity.

As sneutrinos are only present as components of left-handed superfields in the MSSM, there is no partner to mix with and their mass simply reads

$$m_{\tilde{\nu}} = m^2_{\tilde{l}_L} + \frac{1}{2}\cos 2\beta M^2_Z. \tag{2.10}$$

2.2.2 Charginos

The Dirac mass matrix for charginos mixes the $SU(2)$ gaugino $\tilde{W}^{\pm}$ and the charged Higgsino $\tilde{H}^{\pm}$. The corresponding mass term reads as [2]

$$\mathcal{L}_M^{\bar{\tilde{\chi}}_\alpha^- \tilde{\chi}_\beta^+} = -\left(\bar{\Psi}_R M_C \Psi_L + \text{h.c}\right). \tag{2.11}$$

Using the basis $\left(\tilde{W}^-, \tilde{H}^-\right)$ the Dirac mass matrix M_C is found to be

$$M_C = \begin{pmatrix} M_2 & \sqrt{2} M_W \cos\beta \\ \sqrt{2} M_W \sin\beta & \mu \end{pmatrix}, \tag{2.12}$$

where the soft breaking mass parameter $M_2 \equiv |M_2| e^{i\phi_2}$ for $SU(2)$ gauginos is taken to be complex here for the reasons given in Sec. 2.1. In general it can be made real without loss of generality by appropriate field redefinitions. This mass matrix is asymmetric and hence has to be diagonalized by bi-unitary transformations U_R and U_L,

$$U_R M_C U_L^\dagger = \text{diag}(m_{\tilde{\chi}_1^-}, m_{\tilde{\chi}_2^-}). \tag{2.13}$$

It follows that the increasingly ordered mass eigenstates $(\tilde{\chi}_i^-)_\alpha$ are given as

$$\begin{pmatrix} \tilde{\chi}_1^- \\ \tilde{\chi}_2^- \end{pmatrix}_{L,R} = U_{L,R} \begin{pmatrix} \tilde{W}^- \\ \tilde{H}^- \end{pmatrix}. \tag{2.14}$$

For the mixing matrices U_L and U_R the following structure can be assumed [66]

$$U_L = \begin{pmatrix} \cos\phi_L & \sin\phi_L e^{-i\beta_L} \\ -\sin\phi_L e^{i\beta_L} & \cos\phi_L \end{pmatrix}, \tag{2.15a}$$

$$U_R = \begin{pmatrix} e^{i\gamma_1} & 0 \\ 0 & e^{i\gamma_2} \end{pmatrix} \begin{pmatrix} \cos\phi_R & \sin\phi_R e^{-i\beta_R} \\ -\sin\phi_R e^{i\beta_R} & \cos\phi_R \end{pmatrix}. \tag{2.15b}$$

with $-\pi/2 \leq \phi_{L,R} \leq \pi/2$ and $0 \leq \gamma_{1,2}, \beta_{L,R} \leq 2\pi$. Here γ_1 and γ_2 denote two possible Dirac phases which have to be introduced to ensure that the eigenvalues of M_C are real and positive. The parameters of U_L and U_R can be determined from $M_C^\dagger M_C$ and $M_C M_C^\dagger$, respectively. Introducing the quantity

$$\begin{aligned} \Delta_C = &\Big\{ \left(|M_2|^2 - |\mu|^2\right)^2 + 4M_W^4 \cos^2(2\beta) + 4M_W^2 \left(|M_2|^2 + |\mu|^2\right) \\ &+ 8M_W^2 |\mu||M_2| \sin 2\beta \cos(\phi_\mu + \phi_2) \Big\}^{\frac{1}{2}} \\ = &\, m^2_{\tilde{\chi}_2^\pm} - m^2_{\tilde{\chi}_1^\pm}, \end{aligned} \tag{2.16}$$

we obtain for the mass eigenvalues

$$m^2_{\tilde{\chi}^\pm_{1,2}} = \frac{1}{2}\left(|M_2|^2 + |\mu|^2 + 2M_W^2 \mp \Delta_C\right). \tag{2.17}$$

The mixing angles can be computed from

$$\cos 2\phi_L = \frac{-|M_2|^2 + |\mu|^2 + 2M_W^2 \cos 2\beta}{\Delta_C}, \tag{2.18a}$$

$$\sin 2\phi_L = \frac{-4M_W}{\sqrt{2}\Delta_C}\left(|M_2|^2\cos^2\beta + |\mu|^2\sin^2\beta + |M_2||\mu|\cos(\phi_\mu+\phi_2)\sin 2\beta\right)^{\frac{1}{2}}, \quad (2.18b)$$

$$\cos 2\phi_R = \frac{-|M_2|^2 + |\mu|^2 - 2M_W^2\cos 2\beta}{\Delta_C}, \quad (2.18c)$$

$$\sin 2\phi_R = \frac{-4M_W}{\sqrt{2}\Delta_C}\left(|M_2|^2\sin^2\beta + |\mu|^2\cos^2\beta + |M_2||\mu|\cos(\phi_\mu+\phi_2)\sin 2\beta\right)^{\frac{1}{2}}, \quad (2.18d)$$

and the phases read

$$\tan\beta_L = -\frac{|\mu|\sin\phi_\mu - \cot\beta|M_2|\sin\phi_2}{|\mu|\cos\phi_\mu + \cot\beta|M_2|\cos\phi_2}, \quad (2.19a)$$

$$\tan\beta_R = \frac{|\mu|\sin\phi_\mu - \tan\beta|M_2|\sin\phi_2}{|\mu|\cos\phi_\mu + \tan\beta|M_2|\cos\phi_2}, \quad (2.19b)$$

$$\cot\gamma_1 = \frac{M_W^2|\mu|\sin 2\beta\cos\phi_\mu + M_2(m^2_{\tilde{\chi}_1^\pm} - |\mu|^2)\cos\phi_2}{M_W^2|\mu|\sin 2\beta\sin\phi_\mu - M_2(m^2_{\tilde{\chi}_1^\pm} - |\mu|^2)\sin\phi_2}, \quad (2.19c)$$

$$\cot\gamma_2 = -\frac{|\mu|(m^2_{\tilde{\chi}_2^\pm} - M_2^2)\cos\phi_\mu + M_W^2 M_2\sin 2\beta\cos\phi_2}{|\mu|(m^2_{\tilde{\chi}_2^\pm} - M_2^2)\sin\phi_\mu - M_W^2 M_2\sin 2\beta\sin\phi_2}. \quad (2.19d)$$

Eqs. 2.18 and 2.19 show that the mixing angles which contain only rephasing invariant combinations of ϕ_μ and ϕ_2 can be physical quantities while no phase, all of them containing ϕ_μ and ϕ_2 separately, can enter an observable solely.

2.2.3 Neutralinos

The most dedicated mixing pattern occurs in the neutralino mass matrix as it mixes the neutral components of both Higgsinos $\tilde{H}^0_{1,2}$ with hypercharge $\pm 1/2$, the $U(1)_Y$ gaugino $\tilde{B}^0$ and the $SU(2)$ gaugino $\tilde{W}_3$. Using the basis $\xi^0 = \left(\tilde{B}^0, \tilde{W}_3, \tilde{H}^0_1, \tilde{H}^0_2\right)^T$, the mass term reads [2]

$$\mathcal{L}^{\tilde{\chi}^0}_M = -\frac{1}{2}\left(\xi^0\right)^T M_{\tilde{\chi}^0}\xi^0 + \text{h.c.}, \quad (2.20)$$

with the mass matrix $M_{\tilde{\chi}^0}$

$$M_{\tilde{\chi}^0} = \begin{pmatrix} M_1 & 0 & -M_Z\cos\beta\sin\theta_W & M_Z\sin\beta\sin\theta_W \\ 0 & M_2 & -M_Z\cos\beta\cos\theta_W & M_Z\sin\beta\cos\theta_W \\ -M_Z\cos\beta\sin\theta_W & -M_Z\cos\beta\cos\theta_W & 0 & -\mu \\ M_Z\sin\beta\sin\theta_W & M_Z\sin\beta\cos\theta_W & -\mu & 0 \end{pmatrix}. \quad (2.21)$$

The $U(1)_Y$ gaugino mass parameter $M_1 \equiv |M_1|e^{i\phi_1}$ generally is complex. This mass matrix is symmetric and hence has to be diagonalized by a unitary transformation N as follows

$$N^T M_{\tilde{\chi}^0} N = \text{diag}(m_{\tilde{\chi}^0_1}, m_{\tilde{\chi}^0_2}, m_{\tilde{\chi}^0_3}, m_{\tilde{\chi}^0_4}), \quad (2.22)$$

where once more an increasing order of the mass eigenvalues is assumed. Therefore the n-th mass eigenstate is given by the complex conjugate of the n-th column of N

$$\left(\tilde{\chi}^0_i\right)_j = N^\star_{ji}, \quad (2.23)$$

and satisfies

$$M_{\tilde{\chi}^0}\left(\tilde{\chi}_n^0\right)^\dagger = m_{\tilde{\chi}_n^0}\left(\tilde{\chi}_n^0\right)^T, \tag{2.24}$$

when written in the given basis, and is not an eigenvector of M_N in the usual sense.

The mass eigenvalues and the mixing matrix elements can even be calculated analytically for arbitrary CP-phases ϕ_μ, ϕ_1, and ϕ_2 [67,68], but the general expressions are too lengthy and allow little insight in the involved physics, so they are not presented here. Contrarily, a better physical understanding of neutralino mixing is achieved by performing a perturbative diagonalization of the mass matrix as presented in the next section. Of course, a numerical calculation of N is straightforward.

2.3 Mixing of superparticles - perturbative results

As already stated above, the analytical results allow only limited insight into the dynamics of particle mixing. A much deeper insight into the parameter dependence of mixing parameters is obtained if the mass matrices can be diagonalized by using a perturbative approach. In the case of all three mixing patterns which have already been treated analytically a suitable expansion parameter can be found. Hence such an approach is possible. The most important results of the perturbative treatment of particle mixing will be illustrated in this section.

2.3.1 Sfermions

In the case of slepton mixing the necessary conditions for a perturbative treatment are given by

$$m_l \ll |m_{\tilde{l}_L} - m_{\tilde{l}_R}|, \tag{2.25a}$$

$$M_Z^2 - M_W^2 \ll m_{\tilde{l}_L}^2 - m_{\tilde{l}_R}^2, \tag{2.25b}$$

$$|A_l^\star + \tan\beta\mu| \approx m_{\tilde{l}_L} + m_{\tilde{l}_R}. \tag{2.25c}$$

If these conditions are fulfilled (the trigonometric functions of) the mixing angles are given as

$$\cos 2\theta_{\tilde{l}} \simeq \frac{m_{\tilde{l}_L}^2 - m_{\tilde{l}_R}^2}{m_{\tilde{l}_1}^2 - m_{\tilde{l}_2}^2} = \begin{cases} 1 & \text{if} \quad m_{\tilde{l}_L} < m_{\tilde{l}_R}, \\ -1 & \text{if} \quad m_{\tilde{l}_L} > m_{\tilde{l}_R}, \end{cases} \tag{2.26a}$$

$$\sin 2\theta_{\tilde{l}} \simeq \frac{m_l|A_l^\star + \mu\tan\beta|}{2(m_{\tilde{l}_1}^2 - m_{\tilde{l}_2}^2)} = \begin{cases} \frac{1}{2}\frac{m_l|A_l^\star+\mu\tan\beta|}{m_{\tilde{l}_L}^2 - m_{\tilde{l}_R}^2} & \text{if} \quad m_{\tilde{l}_L} < m_{\tilde{l}_R}, \\ -\frac{1}{2}\frac{m_l|A_l^\star+\mu\tan\beta|}{m_{\tilde{l}_L}^2 - m_{\tilde{l}_R}^2} & \text{if} \quad m_{\tilde{l}_L} > m_{\tilde{l}_R}, \end{cases} \tag{2.26b}$$

and the mixing angle reads

$$\theta_{\tilde{l}} \simeq \begin{cases} \left(\frac{1}{4}\right)\frac{m_l|A_l^\star+\mu\tan\beta|}{m_{\tilde{l}_L}^2 - m_{\tilde{l}_R}^2} & \text{if} \quad m_{\tilde{l}_L} < m_{\tilde{l}_R}, \\ \frac{\pi}{2} - \left(\frac{1}{4}\right)\frac{m_l|A_l^\star+\mu\tan\beta|}{m_{\tilde{l}_L}^2 - m_{\tilde{l}_R}^2} & \text{if} \quad m_{\tilde{l}_L} > m_{\tilde{l}_R}. \end{cases} \tag{2.27}$$

In contrast to the mixing angle $\theta_{\tilde{l}}$ the phase $\phi_{\tilde{l}}$ is independent of the lepton mass, Eq. 2.5b yields explicitly

$$\phi_{\tilde{l}} = \phi_{A_{\tilde{l}}} + \pi + \arctan\left[\frac{-|\mu|\sin(\phi_\mu + \phi_A)}{|\mu|\cos(\phi_A + \phi_\mu) + \cot\beta|A|}\right]. \tag{2.28}$$

This expression simplifies only if an assumption on the relative size of the entering SUSY-parameters is made

$$\phi_{\tilde{l}} \simeq \begin{cases} -\phi_\mu + \pi & \text{if} \quad |\mu|\tan\beta \gg |A|, \\ \phi_A + \pi & \text{if} \quad |\mu|\tan\beta \ll |A|. \end{cases} \tag{2.29}$$

Note that the reliability of the perturbative treatment of slepton mixing is not only limited by Eqs. 2.25a and 2.25b, but also by Eq. 2.25c: overlarge values of the off-diagonal entry $|A_{\tilde{l}}^\star + \mu\tan\beta|$ compared with $m_{\tilde{l}_L} + m_{\tilde{l}_R}$ can (over)compensate the negligible ratio $m_l/(m_{\tilde{l}_L} - m_{\tilde{l}_R})$ and may therefore lead to a break-down of the perturbative ansatz. Due to the rather large mass of the τ lepton, perturbative treatment of stau-mixing should only be used with great care.

2.3.2 Charginos

A perturbative treatment of the chargino matrix is possible, if

$$M_W \ll ||\mu| - |M_2|| \tag{2.30}$$

holds. As ansatz the following expansion of the mixing matrices U_L and U_R into powers of M_W is chosen:

$$U_L = \begin{pmatrix} 1+\epsilon_{11} & \epsilon_{12} \\ \epsilon_{21} & 1+\epsilon_{22} \end{pmatrix}, \qquad U_R = PV_R = P\begin{pmatrix} 1+\beta_{11} & \beta_{12} \\ \beta_{21} & 1+\beta_{22} \end{pmatrix}, \tag{2.31}$$

where the matrix $P = \mathrm{diag}\,(e^{i\gamma_1}, e^{i\gamma_2})$ separates the Dirac phases from the mixing matrix U_R. The ϵ_{ij} and β_{ij} denote possible contributions to chargino mixing in $\mathcal{O}(M_W)$. The mass eigenvalues are expanded analogously

$$m^2_{\tilde{\chi}_i^\pm} = m^{2(0)}_{\tilde{\chi}_i^\pm} + \delta m^{2(1)}_{\tilde{\chi}_i^\pm} + \delta m^{2(2)}_{\tilde{\chi}_i^\pm}, \tag{2.32}$$

where $\delta m^{2(n)}_{\tilde{\chi}_i^\pm}$ indicates the n.-th order correction to the squared mass of the i.th chargino and $m^{2(0)}_{\tilde{\chi}_i^\pm}$ is the corresponding, squared mass in 0.th order. Keeping only terms up to $\mathcal{O}(M_W^2)$ one finds for the entries ϵ_{ij} and β_{ij}

$$\epsilon_{11} = \epsilon_{22} = \beta_{11} = \beta_{22} = 0, \tag{2.33a}$$

$$\epsilon_{12} = -\epsilon_{21}^\star = \frac{-M_W\sqrt{2}}{|\mu|^2 - |M_2|^2}\left[M_2\sin\beta + \mu^\star\cos\beta\right], \tag{2.33b}$$

$$\beta_{12} = -\beta_{21}^\star = \frac{-M_W\sqrt{2}}{|\mu|^2 - |M_2|^2}\left[M_2^\star\cos\beta + \mu\sin\beta\right], \tag{2.33c}$$

while the corrections to the squared eigenvalues ($m^{2(0)}_{\tilde{\chi}_i^\pm} = (|M_2|, |\mu|)$) are

$$\delta m^{2(1)}_{\tilde{\chi}_1^\pm} = 0, \quad \delta m^{2(1)}_{\tilde{\chi}_2^\pm} = 0, \tag{2.34a}$$

$$\delta m^{2(2)}_{\tilde{\chi}^\pm_1} = \frac{-2M_W^2|M_2|}{|\mu|^2 - |M_2|^2}\left[|M_2| + |\mu|\sin 2\beta\cos(\phi_\mu + \phi_2)\right], \tag{2.34b}$$

$$\delta m^{2(2)}_{\tilde{\chi}^\pm_2} = \frac{2M_W^2|\mu|}{|\mu|^2 - |M_2|^2}\left[|\mu| + |M_2|\sin 2\beta\cos(\phi_\mu + \phi_2)\right], \tag{2.34c}$$

if the hierarchy $|\mu| > |M_2|$ is assumed. Then the correction to the masses themselves read

$$\delta m^{(2)}_{\tilde{\chi}^\pm_1} = \frac{-M_W^2}{|\mu|^2 - |M_2|^2}\left[|M_2| + |\mu|\sin 2\beta\cos(\phi_\mu + \phi_2)\right], \tag{2.35a}$$

$$\delta m^{(2)}_{\tilde{\chi}^\pm_2} = \frac{M_W^2}{|\mu|^2 - |M_2|^2}\left[|\mu| + |M_2|\sin 2\beta\cos(\phi_\mu + \phi_2)\right]. \tag{2.35b}$$

Finally, the expressions for the Dirac phases γ_1 and γ_2 read

$$\tan\gamma_1 = -\tan\phi_2 - \frac{M_W^2}{|\mu|^2 - |M_2|^2}\frac{|\mu|}{|M_2|}\sin 2\beta\frac{\sin(\phi_2 + \phi_\mu)}{\cos^2\phi_2}, \tag{2.36a}$$

$$\tan\gamma_2 = -\tan\phi_\mu + \frac{M_W^2}{|\mu|^2 - |M_2|^2}\frac{|M_2|}{|\mu|}\sin 2\beta\frac{\sin(\phi_2 + \phi_\mu)}{\cos^2\phi_\mu}. \tag{2.36b}$$

Basically these results can also be derived by a perturbative expansion of the analytical formulae given in Sec. 2.2.2, but the illustrated ansatz is more straightforward and can easily be extended to higher orders in M_W. Furthermore, a violation of the condition in Eq. 2.30 indicates a breakdown of the perturbative diagonalization of the chargino mass matrix. More details on the approach for a perturbative diagonalization of the chargino mass matrix may be found in App. A.1 and App. A.2.

2.3.3 Neutralinos

For a perturbative treatment of neutralino mixing the sufficient conditions are

$$M_Z \ll |\mu|, |M_1|, |M_2|, \tag{2.37a}$$

$$M_Z \ll ||\mu| - |M_1||, ||\mu| - |M_2||. \tag{2.37b}$$

The basic idea in the perturbative treatment is to expand then eigenvectors and masses into powers of M_Z

$$m_{\tilde{\chi}^0_i} \simeq m^{(0)}_{\tilde{\chi}^0_i} + \delta m^{(1)}_{\tilde{\chi}^0_i} + \delta m^{(2)}_{\tilde{\chi}^0_i}, \tag{2.38a}$$

$$\tilde{\chi}^0_i \simeq \frac{e^{i\phi_i^{(0)}}}{N_i}\left[(\tilde{\chi}^0_i)^{(0)} + \left(\delta^{(1)}_{i1}, \delta^{(1)}_{i2}, \delta^{(1)}_{i3}, \delta^{(1)}_{i4}\right) + \left(\delta^{(2)}_{i1}, \delta^{(2)}_{i2}, \delta^{(2)}_{i3}, \delta^{(2)}_{i4}\right)\right]. \tag{2.38b}$$

where $\phi_i^{(0)}$ denotes the phase associated with the i.th eigenstate in $\mathcal{O}(M_Z^0)$ and N_i is a normalization factor. Explicitly, the 0.th order eigenstates are [69]

$$(\tilde{\chi}^0_1)^{(0)} = \left(e^{i\phi_1/2}, 0, 0, 0\right), \tag{2.39a}$$

$$(\tilde{\chi}^0_2)^{(0)} = \left(0, e^{i\phi_2/2}, 0, 0\right), \tag{2.39b}$$

$$(\tilde{\chi}^0_3)^{(0)} = (0, 0, 1, 1)\frac{e^{i(\phi_\mu+\pi)/2}}{\sqrt{2}}, \tag{2.39c}$$

$$(\tilde{\chi}_4^0)^{(0)} = (0,0,1,-1)\,\frac{e^{i\phi_\mu/2}}{\sqrt{2}}. \tag{2.39d}$$

In contrast to the perturbative treatment of chargino mixing, where a degeneration of the mass eigenstates only occurs for $|M_2| = |\mu|$, the two Higgsino-like eigenstates are always degenerate in the neutralino sector. This point may lead to some problems in the entries containing Higgsino-Higgsino mixing, however it can be shown that these entries are irrelevant for Part II. For more details on the perturbative treatment of neutralino mixing in general and on this problem see App. A.1 and App. A.3. Using the results in App. A.3, the corrections to the masses are given as

$$\delta m^{(1)}_{\tilde{\chi}_i^0} = 0, \tag{2.40a}$$

$$\delta m^{(2)}_{\tilde{\chi}_1^0} \simeq \frac{-M_Z^2 \sin^2\theta_W}{|\mu|^2 - |M_1|^2}\left[|M_1| + |\mu| \sin 2\beta \cos(\phi_\mu + \phi_1)\right], \tag{2.40b}$$

$$\delta m^{(2)}_{\tilde{\chi}_2^0} \simeq \frac{-M_Z^2 \cos^2\theta_W}{|\mu|^2 - |M_2|^2}\left[|M_2| + |\mu| \sin 2\beta \cos(\phi_\mu + \phi_2)\right], \tag{2.40c}$$

$$\begin{aligned}\delta m^{(2)}_{\tilde{\chi}_{3,4}^0} \simeq &\left\{[|\mu| \mp |M_1|\cos(\phi_\mu+\phi_1)] + \cot^2\theta_W \frac{|\mu|^2 - |M_1|^2}{|\mu|^2 - |M_2|^2}\left[|\mu| \mp |M_2|\cos(\phi_\mu+\phi_2)\right]\right\} \\ &\times \frac{M_Z^2 \sin^2\theta_W}{|\mu|^2 - |M_1|^2}\frac{1 \mp \sin 2\beta}{2}.\end{aligned} \tag{2.40d}$$

The first order corrections to the eigenstates relevant for the later calculations are

$$\delta^{(1)}_{13} = \frac{M_Z \sin\theta_W}{|\mu|^2 - |M_1|^2}\left(M_1^\star \cos\beta + \mu \sin\beta\right), \tag{2.41a}$$

$$\delta^{(1)}_{14} = -\frac{M_Z \sin\theta_W}{|\mu|^2 - |M_1|^2}\left(M_1^\star \sin\beta + \mu \cos\beta\right), \tag{2.41b}$$

$$\delta^{(1)}_{23} = -\frac{M_Z \cos\theta_W}{|\mu|^2 - |M_2|^2}\left(M_2^\star \cos\beta + \mu \sin\beta\right), \tag{2.41c}$$

$$\delta^{(1)}_{24} = \frac{M_Z \cos\theta_W}{|\mu|^2 - |M_2|^2}\left(M_2^\star \sin\beta + \mu \cos\beta\right), \tag{2.41d}$$

$$\delta^{(1)}_{31} = -\frac{M_Z \sin\theta_W}{|\mu|^2 - |M_1|^2}\left(\sin\beta - \cos\beta\right)\left(\mu^\star - M_1\right), \tag{2.41e}$$

$$\delta^{(1)}_{32} = \frac{M_Z \cos\theta_W}{|\mu|^2 - |M_2|^2}\left(\sin\beta - \cos\beta\right)\left(\mu^\star - M_2\right), \tag{2.41f}$$

$$\delta^{(1)}_{41} = -\frac{M_Z \sin\theta_W}{|\mu|^2 - |M_1|^2}\left(\sin\beta + \cos\beta\right)\left(\mu^\star + M_1\right), \tag{2.41g}$$

$$\delta^{(1)}_{42} = \frac{M_Z \cos\theta_W}{|\mu|^2 - |M_2|^2}\left(\sin\beta + \cos\beta\right)\left(\mu^\star + M_2\right), \tag{2.41h}$$

while the second order corrections to the relevant off-diagonal entries read

$$\delta^{(2)}_{12} = -\frac{M_Z^2 \sin\theta_W \cos\theta_W \left[|M_1|^2 + M_1^\star M_2 + \sin 2\beta(\mu^\star M_1^\star + \mu M_2)\right]}{(|M_2|^2 - |M_1|^2)(|\mu|^2 - |M_1|^2)}, \tag{2.42a}$$

$$\delta_{21}^{(2)} = \frac{M_Z^2 \sin\theta_W \cos\theta_W \left[|M_2|^2 + M_1 M_2^\star + \sin 2\beta(\mu^\star M_2^\star + \mu M_1)\right]}{(|M_2|^2 - |M_1|^2)(|\mu|^2 - |M_2|^2)}. \tag{2.42b}$$

For the $\mathcal{O}(M_Z^2)$-corrections to the diagonal entries $\delta_{ii}^{(2)}$, no closed formulae can be found; hence their real and imaginary parts have to be calculated separately. The real parts $\mathcal{R}\mathrm{e}\left[\delta_{ii}^{(2)}\right]$ are related by the unitary conditions with $\mathcal{O}(M_Z)$-corrections via

$$\mathcal{R}\mathrm{e}\left[\delta_{ii}^{(2)}\right] = -\frac{1}{2}\sum_{k,\, k\neq i}\left|\delta_{ik}^{(1)}\right|^2, \tag{2.43}$$

whereas the imaginary parts of the relevant diagonal entries read

$$\mathcal{I}\mathrm{m}\left[\delta_{11}^{(2)}\right] = \frac{1}{2}\frac{M_Z^2 \sin^2\theta_W}{|\mu|^2 - |M_1|^2}\frac{|\mu|}{|M_1|}\sin(\phi_\mu + \phi_1)\sin 2\beta, \tag{2.44a}$$

$$\mathcal{I}\mathrm{m}\left[\delta_{22}^{(2)}\right] = \frac{1}{2}\frac{M_Z^2 \cos^2\theta_W}{|\mu|^2 - |M_2|^2}\frac{|\mu|}{|M_2|}\sin(\phi_\mu + \phi_2)\sin 2\beta. \tag{2.44b}$$

Eqs. 2.41 to 2.44 show that the expansion will already break down if the condition in Eq. 2.37b is not fullfilled. In other words this implies that even if all dimensionful parameters in the neutralino mass matrix are $\gg M_Z$ a large mixing between gaugino and Higgsino can be generated. Furthermore it should be mentioned that corrections of $\mathcal{O}(M_Z)$ only affect gaugino-Higgsino mixing, which is absent in order $\mathcal{O}(M_Z^0)$. Contrarily, corrections of $\mathcal{O}(M_Z^2)$ only affect gaugino-gaugino mixing and Higgsino-Higgsino mixing.

2.4 Summary of involved parameters

	$\tan\beta$	$\lvert\mu\rvert$	ϕ_μ	$\lvert M_1\rvert$	ϕ_1	$\lvert M_2\rvert$	ϕ_2	$\lvert A_l\rvert$	ϕ_A	$m_{\tilde{l}_L}$	$m_{\tilde{l}_R}$
slepton sector	×	×	×	—	—	—	—	×	×	×	×
chargino sector	×	×	×	—	—	×	×	—	—	—	—
neutralino sector	×	×	×	×	×	×	×	—	—	—	—

Table 2.1: Summary of relevant SUSY parameters. Here "×" denotes the presence of a parameter in a sector of the model, whereas "—" indicates its absence.

Under the assumptions given in Sec. 2.1 the mixing patterns in the part of the SUSY spectrum relevant for this work depend on 11 SUSY parameters. Some of these parameters ($m_{\tilde{l}_L}$, $m_{\tilde{l}_R}$, $|A_l|$, ϕ_A, $|M_1|$, ϕ_1) only enter into a single sector (sleptons and neutralinos, respectively), while $|M_2|$ and ϕ_2 appear in both the neutralino and chargino mass matrix, and $|\mu|$, ϕ_μ, and $\tan\beta$ affect all three sectors. Therefore the mixing patterns in the separate sectors are partly correlated to each other. In particular, choosing the parameters of the neutralino mass matrix completely determines the chargino mass matrix as well. Moreover, increasing $|\mu|$ suppresses gaugino-Higgsino mixing but enhances left-right mixing in the slepton sector. Finally, taking $\tan\beta \gg 1$ again enhances left-right mixing but reduces the impact of all phases on the physical masses. The relevant SUSY parameters and their impact on the three discussed mixing patterns are summarized in Tab. 2.1. Of course, all observables that will be investigated later on contain dependences on SM parameters like M_Z or $\sin\theta_W$ whose values are already known to a good accuracy.

2.5 Interaction Lagrangian

In order to make this work self-contained as well as to fix the notations the next three subsections present a short collection of the relevant pieces of interaction Lagrangian expressed in terms of mass eigenstates. I start with the interactions involving only SM-particles, continue with interactions between SM-particles and superparticles and close with pure supersymmetric interactions.

2.5.1 SM part

The only part of the SM interaction Lagrangian relevant for this work is the well known coupling between charged leptons and gauge bosons

$$\mathcal{L}_{l\bar{l}\gamma,Z} = e\bar{l}\gamma^{\mu}\left(A_{\mu}Q_{\gamma}^{\alpha,l}P_{\alpha} + Z_{\mu}Q_{Z}^{\alpha,l}P_{\alpha}\right)l, \tag{2.45}$$

where e is the QED coupling constant and P_{α}, $\alpha \in \{+,-\} \equiv \{R,L\}$, are the standard chirality projection operators defined as $P_{\pm} = (1 \pm \gamma_5)/2$. The linear charges in Eq. 2.45 are

$$Q_{\gamma}^{+,l} = 1, \qquad Q_{Z}^{+,l} = -\tan\theta_W, \tag{2.46a}$$

$$Q_{\gamma}^{-,l} = 1, \qquad Q_{Z}^{-,l} = \frac{-1}{\sin\theta_W\cos\theta_W}\left(\sin^2\theta_W - \frac{1}{2}\right). \tag{2.46b}$$

Other parts of the SM interaction Lagrangian are not required here.

2.5.2 Gauge interactions with sparticles

Slepton left-right mixing does not affect the coupling between sleptons and photon, it only enters the coupling between sleptons and Z-boson. Therefore the vertices with two charged sleptons and a gauge boson are defined via the momentum-space Lagrangian

$$\mathcal{L}_{\tilde{l}_i\tilde{l}_j\gamma,Z} = e\left(A_{\mu}Q_{\gamma}^{\tilde{l},ij} + Z_{\mu}Q_{Z}^{\tilde{l},ij}\right)(k_i+k_j)^{\mu}\tilde{l}_i(k_i)\tilde{l}_j(k_j)^{\star}, \tag{2.47}$$

where $i,j \in \{R,L\}$. The corresponding linear charges $Q_{\gamma,Z}^{\tilde{l},ij}$ are

$$Q_{\gamma}^{\tilde{l},ij} = \delta_{ij}, \tag{2.48a}$$

$$Q_{Z}^{\tilde{l},ij} = -\delta_{ij}\left[\tan\theta_W - \frac{1}{2\cos\theta_W\sin\theta_W}\left(U_{\tilde{l}}\right)_{1i}^{\star}\left(U_{\tilde{l}}\right)_{1j}\right]. \tag{2.48b}$$

In the case of high-energy applications with selectrons involved, left-right mixing can safely be neglected within the coupling between sleptons and Z-boson. Hence the coupling reduces to [4]

$$Q_{Z}^{\tilde{l},ij} = -\delta_{ij}\left[\tan\theta_W - \frac{1}{2\cos\theta_W\sin\theta_W}\delta_{iL}\right]. \tag{2.49}$$

[4] As only the d_e and the a_{μ} are considered the coupling to the Z-boson is irrelevant for the low-energy observables and the neglect of selectron (smuon) mixing within this vertex is without consequences.

The couplings between physical Majorana neutralinos and the Z boson are given by

$$\mathcal{L}_{\tilde{\chi}_i^0\tilde{\chi}_j^0 Z} = \frac{e}{2\sin\theta_W\cos\theta_W} Z_\mu \overline{\tilde{\chi}_i^0}\gamma^\mu Q^{\alpha,ij}_{\tilde{\chi}^0} P_\alpha \tilde{\chi}_j^0, \tag{2.50}$$

where the linear charges $Q^{\alpha,ij}_{\tilde{\chi}^0}$ are defined as

$$Q^{+,ij}_{\tilde{\chi}^0} = -\left(Q^{-,ij}_{\tilde{\chi}^0}\right)^\star = \frac{1}{2}\left(N_{3i}N^\star_{3j} - N_{4i}N^\star_{4j}\right) \equiv Z_{ij}. \tag{2.51}$$

The first equality in Eq. 2.51 follows from the Majorana nature of the neutralinos. Of course, there is no neutralino-photon coupling.
Finally, the interactions between neutral gauge bosons and charginos are given by

$$\mathcal{L}_{\tilde{\chi}_i^\pm\tilde{\chi}_j^\pm\gamma,Z} = e\overline{\tilde{\chi}_i^-}\gamma^\mu\left(Q^{\alpha,ij}_{\tilde{\chi}^\pm,\gamma}P_\alpha A_\mu + P_\alpha Z_\mu Q^{\alpha,ij}_{\tilde{\chi}^\pm,Z}\right)\tilde{\chi}_j^-, \tag{2.52}$$

with

$$Q^{+,ij}_{\tilde{\chi}^\pm,\gamma} = Q^{-,ij}_{\tilde{\chi}^\pm,\gamma} = \delta_{ij}, \tag{2.53a}$$

$$Q^{\pm,ij}_{\tilde{\chi}^\pm,Z} = \frac{-1}{\cos\theta_W\sin\theta_W}\left(\sin^2\theta_W\delta_{ij} - (W_\pm)_{ij}\right). \tag{2.53b}$$

The matrices $(W_\pm)_{ij}$ can be obtained from the chargino mixing matrices U_L and U_R via

$$(W_\pm)_{ij} = (U_\pm)_{i1}(U_\pm)^\star_{j1} + \frac{1}{2}(U_\pm)_{i2}(U_\pm)^\star_{j2} \qquad [+,-\equiv R,L], \tag{2.54}$$

and read explicitly in terms of chargino mixing angles and phases as

$$W_- = \begin{pmatrix} \frac{3}{4}+\frac{1}{4}\cos 2\phi_L & -\frac{1}{4}\sin 2\phi_L e^{-i\beta_L} \\ -\frac{1}{4}\sin 2\phi_L e^{i\beta_L} & \frac{3}{4}-\frac{1}{4}\cos 2\phi_L \end{pmatrix}, \tag{2.55a}$$

$$W_+ = \begin{pmatrix} \frac{3}{4}+\frac{1}{4}\cos 2\phi_R & -\frac{1}{4}\sin 2\phi_R e^{i(\gamma_1-\beta_R-\gamma_2)} \\ -\frac{1}{4}\sin 2\phi_R e^{-i(\gamma_1-\beta_R-\gamma_2)} & \frac{3}{4}-\frac{1}{4}\cos 2\phi_R \end{pmatrix}. \tag{2.55b}$$

2.5.3 Pure SUSY interactions

The relevant "pure" SUSY interactions are the ones between sleptons and chargino or neutralino. The neutralino-slepton-lepton vertices receive contributions from both gauge and Yukawa interactions

$$\mathcal{L}_{\tilde{l}l\tilde{\chi}_i^0} = \frac{e}{\sqrt{2}\sin\theta_W}\bar{l}\left(G^\alpha_{ij} + Y^\alpha_{ij}\right)P_\alpha\tilde{\chi}_i^0\tilde{l}_j + h.c., \tag{2.56}$$

with

$$Y^-_{ij} = -\sqrt{2}Y_l N_{3i}(U_{\tilde{l}})_{1j}, \quad G^-_{ij} = -2\tan\theta_W N_{1i}(U_{\tilde{l}})_{2j}, \tag{2.57a}$$

$$Y^+_{ij} = -\sqrt{2}Y_l N^\star_{3i}(U_{\tilde{l}})_{1j}, \quad G^+_{ij} = (\tan\theta_W N^\star_{1i} + N^\star_{2i})(U_{\tilde{l}})_{2j}. \tag{2.57b}$$

Here the dimensionless, rescaled Yukawa coupling Y_l is given by

$$Y_l = \frac{m_l}{\sqrt{2}M_W\cos\beta}. \tag{2.58}$$

Note that terms proportional to Y_l as well as a non-trivial sleptonic mixing matrix $U_{\tilde{l}}$ have to be kept when computing leptonic dipole moments. On the other hand, for high-energy applications Y_e can be set to zero, which implies $Y_{ij}^{\pm} = 0$ in case of selectrons. In the same limit left-right mixing can be neglected, in which case the gauge contributions $G_{ij}^{\pm}$ simplify to

$$G_{ij}^{-} = -2 \tan\theta_W N_{1i} \delta_{Rj}, \tag{2.59a}$$

$$G_{ij}^{+} = \left(\tan\theta_W N_{1i}^{\star} + N_{2i}^{\star}\right) \delta_{Lj}. \tag{2.59b}$$

The coupling between chargino, sneutrino and lepton also receives gauge and Yukawa contributions

$$\mathcal{L}_{\tilde{\nu}_l l \tilde{\chi}_i^{\pm}} = \frac{e}{\sin\theta_W} \overline{\tilde{\chi}_i^{-}} N_{\alpha,i} P^{\alpha} l \tilde{\nu}_l^{\star} + h.c., \tag{2.60}$$

where

$$N_{\alpha,i} = -\delta_{\alpha L} \left(U_R\right)_{i1} + \delta_{\alpha R} \left(U_L\right)_{i2} Y_l. \tag{2.61}$$

As before, the term proportional to Y_e in Eq. 2.61 can be dropped in collider physics applications, but it has to be kept when computing the leptonic dipole moments.

Part II

Combined analysis

Chapter 3

Leptonic dipole moments

This chapter starts with a short summary of the introduction of leptonic dipole moments, the current status of experiments concerning leptonic dipol moments, and a derivation of the bounds on the possible SUSY contributions. Next the analytical results for these contributions as relevant for this work are summarized to some extent and perturbative expressions for these low energy observables are given. The chapter concludes with a presentation of the parameter scenarios which will be explored in the remainder of the thesis and a detailed numerical analysis of the low energy compatible phase ranges within these scenarios.

3.1 Status and relevance of leptonic dipole moments

3.1.1 Introducing leptonic dipole moments

This introduction to dipole form factors closely follows Ref. [54]. First of all, the most general effective Lagrangian describing the interaction of a neutral vector boson V with two fermions can be written as

$$\begin{aligned}\mathcal{L}_{Vff} = V^{\mu}(x)\overline{\Psi}(x)\left[\gamma_{\mu}(g_V - g_A\gamma_5) + i\overset{\leftrightarrow}{\partial}_{\mu}(g_M - ig_E\gamma_5) + i\overset{\leftrightarrow}{\partial^{\nu}}\sigma_{\mu\nu}(g_{TS} - ig_{TP}\gamma_5)\right]\Psi(x) \\ + \left[i\partial^{\mu}V^{\nu}(x)\right]\overline{\Psi}(x)\left[g_{\mu\nu}(ig_S + g_P\gamma_5) + \sigma_{\mu\nu}(ig_{TM} + g_{TE}\gamma_5)\right]\Psi(x) + h.c. \qquad (3.1)\end{aligned}$$

Only operators of dimension four or five are included here. The reason for this restriction will be clarified later. When $\mathcal{L}_{Vff}$ is restricted to dimension four and five operators, the given operators and complex coefficients g_i are independent from each other and describe the Vff interaction completely.
The next step is to classify these operators with respect to their chirality behavior and their transformation properties under $\mathcal{C}$-, $\mathcal{P}$-, and $\mathcal{T}$-transformations. This is done by using

$$\begin{aligned}(1, \gamma_5) &= P_+^2 \pm P_-^2, \\ \overline{\Psi}\,(1, \gamma_\mu, \sigma_{\mu\nu})\,P_\pm &= \left(\overline{\Psi}_\mp, \overline{\Psi}_\pm\gamma_\mu, \overline{\Psi}_\mp\sigma_{\mu\nu}\right),\end{aligned}$$

as well as the properties of V^{μ} and Ψ under these transformations as they can be found in standard text books such as [70, 71]. The results of this classification are summarized in Tab. 3.1. In accordance with Ref. [54] it may be observed that out of the dimension

operator	coefficient	$\mathcal{C}$	$\mathcal{P}$	$\mathcal{T}$	$\mathcal{CP}$	chirality flip
$V^\mu\overline{\Psi}\gamma_\mu\Psi$	g_V	+	+	+	+	NO
$V^\mu\overline{\Psi}\gamma_\mu\gamma_5\Psi$	g_A	−	−	+	+	NO
$V^\mu\overline{\Psi}i\overset{\leftrightarrow}{\partial_\mu}\Psi$	g_M	+	+	+	+	YES
$V^\mu\overline{\Psi}\overset{\leftrightarrow}{\partial_\mu}\gamma_5\Psi$	g_E	+	−	−	−	YES
$V^\mu\overline{\Psi}i\overset{\leftrightarrow}{\partial^\nu}\sigma_{\mu\nu}\Psi$	g_{TS}	−	+	−	−	YES
$V^\mu\overline{\Psi}\overset{\leftrightarrow}{\partial^\nu}\sigma_{\mu\nu}\gamma_5\Psi$	g_{TP}	−	−	+	+	YES
$(\partial\cdot V)\,\overline{\Psi}\Psi$	g_S	−	+	−	−	YES
$(i\partial\cdot V)\,\overline{\Psi}\gamma_5\Psi$	g_P	−	−	+	+	YES
$(\partial^\mu V^\nu)\,\overline{\Psi}\sigma_{\mu\nu}\Psi$	g_{TM}	+	+	+	+	YES
$(i\partial^\mu V^\nu)\,\overline{\Psi}\sigma_{\mu\nu}\gamma_5\Psi$	g_{TE}	+	−	−	−	YES

Table 3.1: Classification of the operators in Eq. 3.1 by their properties under $\mathcal{C}$-, $\mathcal{P}$-, and $\mathcal{T}$-transformations and their helicity flipping behavior. A similar table is given in Ref. [54].

four operators only those two that are proportional to the usual vector and axial couplings g_V and g_A are chirality conserving while all dimension five operators are chirality flipping. Furthermore the operators associated with g_V, g_A, g_M, g_P, g_{TM}, and g_{TP} are even under a CP-transformation, whereas the operators proportional to g_E, g_{TS}, g_S, and g_{TE} are odd under such a transformation. Therefore the presence of non-vanishing g_E, g_{TS}, g_S, and g_{TE} implies a CP-violating theory. As dimension five operators at the tree level would make the theory unrenormalizable, all chirality flipping operators and the associated coefficients can only originate from quantum corrections in renormalizable theory.
The effective Lagrangian in Equation 3.1 is Fourier transformed to obtain the effective Vff vertex in momentum space as [54]

$$\begin{aligned}\Gamma_\mu^{Vff} = i\,[&\gamma_\mu(f_V - f_A\gamma_5) + (q-\bar{q})_\mu(f_M + if_E\gamma_5) + (q+\bar{q})_\mu(if_S + f_P\gamma_5)\\ &+ (q-\bar{q})^\nu\sigma_{\mu\nu}(f_{TS} + if_{TP}\gamma_5) + (q+\bar{q})^\nu\sigma_{\mu\nu}(f_{TM} + if_{TE}\gamma_5)]\,,\end{aligned} \tag{3.2}$$

where q and $\bar{q}$ are the outgoing momenta of the fermions. The complex form factors f_i are functions of the kinematical invariants. Eq. 3.2 gives the most general Lorentz structure of the effective Vff which justifies the restriction to dimension five operators in Eq. 3.1 by the following argument [54]: Adding an additional dimension six operator to the effective Lagrangian $\mathcal{L}_{Vff}$ would indeed lead to a new coefficient g_6 in $\mathcal{L}_{Vff}$, but by the Fourier transformation to obtain the effective vertex Γ_μ^{Vff} this operator can not result in a new Lorentz structure. Hence the contribution of the Fourier transformed dimension six operators can be absorbed into a redefinition of the corresponding form factor f_i obtained by the Fourier transformation of dimension four or five operators.[1] Therefore the form factors f_i can be considered to be more general than the coefficients g_i. The second reason for

[1] As an example consider the dimension six operator $g_6\partial_\nu\partial^\nu V^\mu\overline{\Psi}\gamma_\mu\Psi$ which Fourier transforms into a contribution $\propto g_6(q+\bar{q})^2\gamma_\mu$ and hence can be absorbed into the contributions of the Fourier transformed dimension four operator $V^\mu\overline{\Psi}\gamma_\mu\Psi$.

restricting the operators in Eq. 3.1 to dimension four and five is that additional dimension six operators in the discussed case can arise only from inserting an additional derivative acting either on the bosonic or the fermionic field. Hence we expect an additional, relative suppression of contributions from such operators by the ratio of external momentum to internal mass scale. In the case of SUSY contributions to d_e or a_μ, this ratio is either the vanishing momentum of the photon or the lepton mass divided by the mass scale of the internal SUSY particles, and hence can be safely neglected for lepton dipole moments.
The number of independent form factors f_i can be reduced significantly by imposing on-shell conditions both for the fermions and the gauge bosons. Using Gordon identities as in App.B.3 eliminates[2] f_{TM}, f_{TE}, f_{TS}, and f_{TP}, whereas f_S and f_P are removed from Γ_μ^{Vff} by using the gauge bosons on-shell condition $(q+\bar{q})_\mu \epsilon^\mu = 0$. After these simplifications the effective Vff vertex for two on-shell fermions and one on-shell gauge boson is conventionally represented by [54]

$$\Gamma_\mu^{Vff}(s) = ie\left\{\gamma_\mu\left[V_f^V(s) - A_f^V(s)\gamma_5\right] + \sigma_{\mu\nu}(q+\bar{q})^\nu\left[i\frac{a_f^V(s)}{2m_f} - \frac{d_f^V(s)}{e}\gamma_5\right]\right\}, \tag{3.3}$$

where m_f is the fermion mass and e is the standard QED coupling constant. The form factors $V_f^V(s)$ and $A_f^V(s)$ are connected with chirality conserving, CP-even operators. Contrarily, the form factors $a_f^V(s)$ and $d_f^V(s)$ are associated with chirality flipping, CP-even, respectively CP-odd operators. All of them only depend on the gauge boson's momentum via $s^2 = (q+\bar{q})^2$. In a renormalizable theory the two chirality flipping form factors, known as anomalous magnetic dipole form factor and electric dipole form factor respectively, can only receive contributions from quantum corrections from operators with dimension five (or higher).
The electric dipole moments are obtained by specifying $V \equiv \gamma$ and taking the limit $s \to 0$. Finally, the anomalous magnetic dipole moment of a fermion (AMDM_f) and the electric dipole moment of a fermion (EDM_f) are

$$\mathrm{EDM}_f \equiv d_f^\gamma(0), \tag{3.4a}$$

$$\mathrm{AMDM}_f \equiv a_f^\gamma(0). \tag{3.4b}$$

The most important conclusions from this introduction to dipole form factors are these: Firstly, $a_f^\gamma(0)$ and $d_f^\gamma(0)$ are associated with chirality flipping dimension five operators. This implies that in the explicit calculation of the SUSY contributions to these form factors the Yukawa coupling may not be neglected, even for electrons and muons. Furthermore, as counterterms can only be given for dimension four operators, the SUSY contributions to $a_f^\gamma(s)$ and $d_f^\gamma(s)$ have to be UV-finite, i.e. all ϵ-divergences from dimensional regularization of the various appearing tensor loop integrals have to cancel out in each of these two contributions. Finally, $d_f^\gamma(0)$ is connected to CP-variant operators, hence a non-vanishing SUSY contribution to $d_f^\gamma(0)$ is only possible in the presence of CP-violating phases. Contrarily, $a_f^\gamma(0)$ arises from CP-invariant operators and therefore the SUSY contribution is expected to be non-vanishing even in the absence of CP-violating phases.

[2] More accurate, they allow the absorption of f_{TM}, f_{TE}, f_{TS}, and f_{TP} into f_V, f_A, f_M and f_E when the condition of on-shell gauge bosons is used simultaneously.

3.1.2 Selection of relevant leptonic dipole moments

As already stated in Sec. 1.4, purely leptonic processes are the main subject of this thesis. Therefore the (quite stringent) experimental constraints on the electric dipole moments of the neutron and the mercury atom are ignored, the main reason being that leptonic dipole moments suffer much less from uncertainties due to non-perturbative strong interactions. For example, Ref. [72] finds that different models relating the electric dipole moments of quarks to that of the neutron or Hg typically differ by a factor of two. Since large phases in the hadronic sector can be tolerated if there are cancellations between contributions which have different hadronic matrix elements, a conservative interpretation of the experimental bounds on d_n tends to give significantly weaker constraints on model parameters than does the bound on the electric dipole moment of the electron [22]. This holds even if one assumes some connection between the CP-violating phases in the squark and slepton sectors. The only CP-violating (more exactly, T-violating) low-energy quantity of relevance to this work is therefore the electric dipole moment of the electron d_e. Given our assumption of flavour universality of the soft breaking terms in the slepton sector, at least as far as the first and second generation are concerned, the bound on the electric dipole moment of the muon [18] need not be considered separately: since $(d_l)_{\rm SUSY} \propto m_l$, all combinations of parameters that satisfy the constraint on the SUSY contributions to d_e will be at least five orders of magnitude below the maximally allowed SUSY contribution to d_μ.[3]
On the other hand, our assumption of universal sleptonic soft breaking terms for the first two generations also implies [73] that the measurement [74, 75] of the anomalous magnetic moment of the muon, $a_\mu = (g_\mu - 2)/2$, gives a *tighter* constraint of SUSY parameters than does the anomalous magnetic moment of the electron. The reason for this is that for universal soft breaking masses the SUSY contribution to these leptonic dipole moments is essentially proportional to the squared mass of the lepton, and the experimental errors satisfy [18, 74, 75] $\delta a_\mu/m_\mu^2 \lesssim \delta a_e/m_e^2$. This implies that the size of a possible SUSY contribution to a_l relative to m_l^2 can be extracted more accurately from a_μ than from a_e. Therefore the second leptonic dipole moment relevant for this work is a_μ. Note that the SUSY contributions to d_e and a_μ show very similar dependences on the absolute values of the relevant parameters; however, d_e receives non-vanishing contributions only in the presence of nontrivial phases, i.e. $\phi \neq (0, \pi)$, while the contributions to $|a_\mu|$ become maximal if all phases are zero or π.

3.1.3 Derivation of bounds on SUSY contributions

The derivation of an allowed range for a possible SUSY contribution to d_e is straightforward. This is because the prediction for the SM contribution is smaller by more than 5 orders of magnitude (see e.g. [76]) than the current experimental limit [18]

$$(d_e)_{\rm exp} = (0.069 \pm 0.074) \times 10^{-26} e \cdot \text{cm}. \tag{3.5}$$

Therefore the SM prediction can be neglected and the experimental limit can be directly translated into a 2σ range for the supersymmetric contribution to d_e

$$-0.079 \times 10^{-26} e \cdot \text{cm} \leq (d_e)_{\rm SUSY} \leq 0.217 \times 10^{-26} e \cdot \text{cm}. \tag{3.6}$$

[3] The experimental bounds on d_e and d_μ satisfy $d_e/d_\mu \simeq 10^{-8}$ [18]; this ratio is not compensated by $m_\mu/m_e \simeq 200$.

The interpretation of the most recent measurement [74, 75] of a_μ,

$$(a_\mu)_{\text{exp}} = (11659208 \pm 6) \times 10^{-10}, \tag{3.7}$$

is less clear, since that non-perturbative hadronic terms do contribute to a_μ, at about the 10^{-8} level. In principle this contribution can be calculated from experimental data using dispersions relations [77–79]. Unfortunately, calculations based on different data do not quite agree, although the discrepancy has become smaller following the recent release of corrected data by the CMD-2 collaboration [80]. Using e^+e^- annihilation data as input tends to give a SM prediction which falls a little short of the experimental value in Eq. 3.7. A recent analysis [81] which includes all existing e^+e^- data finds[4]

$$(a_\mu)_{\text{SM}} = (11659180.9 \pm 8.0) \times 10^{-10}. \tag{3.8}$$

Adding all errors in quadrature, this results in a $\sim 2.7\sigma$ discrepancy. On the other hand, using data from τ decays gives [81]

$$(a_\mu)_{\text{SM}} = (11659195.6 \pm 6.8) \times 10^{-10}, \tag{3.9}$$

which is only $\sim 1.4\sigma$ below the measurements. Since even the e^+e^- data lead to a discrepancy of less than 3σ between the prediction for and the measurement of a_μ, evidence for a non-vanishing SUSY contribution is not claimed within this work. In order to be conservative, the upper limit of the "2σ allowed" range for $(a_\mu)_{\text{SUSY}} = (a_\mu)_{\text{exp}} - (a_\mu)_{\text{SM}}$ is constructed by using as estimate of $(a_\mu)_{\text{SUSY}}$ the lower value as given in Eq. 3.9, reduced by two combined standard deviations. Similarly, the lower end of this "2σ allowed" range is obtained when $(a_\mu)_{\text{SUSY}}$ is estimated by adding two standard deviations to the higher value given by Eq. 3.8. This gives

$$-5.7 \times 10^{-10} \leq (a_\mu)_{\text{SUSY}} \leq 47.1 \times 10^{-10}. \tag{3.10}$$

as a conservatively estimated range for the size of a possible SUSY contribution $(a_\mu)_{\text{SUSY}}$ to the anomalous magnetic moment of the muon.

The upper bound in Eq. 3.10 constrains the SUSY parameter space only for large values of $\tan\beta$, but the lower bound is significant also for moderate values of $\tan\beta$.

3.2 Results for leptonic dipol moments

3.2.1 Analytical results

The supersymmetric one-loop contributions to leptonic dipole moments are shown in Fig. 3.1. The left diagram depicts the neutralino contribution, the right one the chargino contribution. Using the interaction Lagrangians given in Sec. 2.5, we find for the chargino contribution to electric dipole moment of the electron

$$(d_e)^{\tilde{\chi}^\pm}_{\text{SUSY}} = \frac{1}{96\pi^2} \sum_{i=1}^{2} \frac{2}{m_{\tilde{\chi}_i^\pm}} f_1(x_i)\, \mathcal{I}\text{m}\left[c_{Li}^\star c_{Ri}\right]. \tag{3.11}$$

[4] Similar analyses, which are also using both data sets as alternative inputs may be found in [82, 83].

Figure 3.1: SUSY contributions to leptonic dipole operators

The chargino loop contribution to the magnetic anomalous magnetic moment of the muon is

$$(a_\mu)^{\tilde{\chi}^\pm}_{\mathrm{SUSY}} = \frac{1}{192\pi^2}\sum_{i=1}^{2}\left\{\frac{8m_\mu}{m_{\tilde{\chi}_i^\pm}} f_1\left(x_i\right)\mathcal{R}\mathrm{e}\left[c_{Li}^\star c_{Ri}\right] + \frac{m_\mu^2}{m^2_{\tilde{\chi}_i^\pm}} f_3\left(x_i\right)\left[|c_{Li}|^2 + |c_{Ri}|^2\right]\right\}. \tag{3.12}$$

The corresponding results for the neutralino contribution read

$$(d_e)^{\tilde{\chi}^0}_{\mathrm{SUSY}} = \frac{-1}{96\pi^2}\sum_{i=1}^{4}\sum_{\alpha=1}^{2}\frac{1}{m_{\tilde{\chi}_i^0}} f_2\left(y_{i\alpha}\right)\mathcal{I}\mathrm{m}\left[n_{Li\alpha}^\star n_{Ri\alpha}\right], \tag{3.13a}$$

$$(a_\mu)^{\tilde{\chi}^0}_{\mathrm{SUSY}} = \frac{-1}{192\pi^2}\sum_{i=1}^{4}\sum_{\alpha=1}^{2}\left\{\frac{4m_\mu}{m_{\tilde{\chi}_i^0}} f_2\left(y_{i\alpha}\right)\mathcal{R}\mathrm{e}\left[n_{Li\alpha}^\star n_{Ri\alpha}\right] + \frac{m_\mu^2}{m^2_{\tilde{e}_\alpha}} f_3\left(y_{i\alpha}\right)\left[|n_{Li\alpha}|^2 + |n_{Ri\alpha}|^2\right]\right\}. \tag{3.13b}$$

The variables x_i and $y_{i\alpha}$ are defined as

$$x_i = \frac{m^2_{\tilde{\chi}_i^\pm}}{m^2_{\tilde{\nu}}}, \quad y_{i\alpha} = \frac{m^2_{\tilde{e}_\alpha}}{m^2_{\tilde{\chi}_i^0}}, \tag{3.14}$$

and the loop functions f_i are

$$f_1(z) = \frac{3z}{2(z-1)^3}(z^2 - 4z + 3 + 2\log z), \tag{3.15a}$$

$$f_2(z) = \frac{3z}{(z-1)^3}(z^2 - 1 + 2z\log z), \tag{3.15b}$$

$$f_3(z) = \frac{2z}{(z-1)^4}(z^3 - 6z^2 + 3z + 2 + 6z\log z). \tag{3.15c}$$

These functions are normalized such that $f_i(1) = 1, \;\; i = 1, 2, 3$. Finally the couplings c_{Ai} and $n_{Ai\alpha}$ may be written as

$$c_{Li} = \frac{-e}{\sin\theta_W}\left(U_R\right)_{i1}, \tag{3.16a}$$

$$c_{Ri} = \frac{e}{\sin\theta_W} Y_l \left(U_L\right)_{i2}, \tag{3.16b}$$

$$n_{Li\alpha} = \frac{e}{\sqrt{2}\sin\theta_W}\left[\left(N_{2i} + \tan\theta_W N_{1i}\right)\left(U_{\tilde{l}}\right)^\star_{L\alpha} - \sqrt{2} Y_l N_{3i}\left(U_{\tilde{l}}\right)^\star_{R\alpha}\right], \tag{3.16c}$$

$$n_{Ri\alpha} = \frac{-e}{\sqrt{2}\sin\theta_W}\left[2\tan\theta_W N^\star_{1i}\left(U_{\tilde{l}}\right)^\star_{R\alpha} + \sqrt{2}Y_l N^\star_{3i}\left(U_{\tilde{l}}\right)^\star_{L\alpha}\right]. \tag{3.16d}$$

These results agree with those of refs. [22, 54, 55], the neutralino contribution in ref. [24] seems to contain some misprints. For more details on the calculation of the leptonic moments the interested reader is referred to App. B.

3.2.2 Perturbative results

The analytic expressions of Sec. 3.2.1 can be used to rewrite both chargino contributions in terms of the loop functions f_i and the basic SUSY parameters

$$(d_e)^{\tilde{\chi}^\pm}_{\text{SUSY}} = -\frac{m_e}{48\pi^2}\frac{e^2}{\sin^2\theta_W}\frac{\tan\beta|\mu||M_2|\sin(\phi_\mu+\phi_2)}{\Delta_C}\sum_{i=1}^{2}(-1)^i\frac{f_1\left(x_i\right)}{m^2_{\tilde{\chi}^\pm_i}}, \tag{3.17a}$$

$$\begin{aligned}(a_\mu)^{\tilde{\chi}^\pm}_{\text{SUSY}} = -\frac{m_\mu^2}{96\pi^2}\frac{e^2}{\sin^2\theta_W}\Bigg\{&2\sum_{i=1}^{2}\frac{f_1\left(x_i\right)}{m^2_{\tilde{\chi}^\pm_i}} - \frac{1+Y_\mu^2}{4}\sum_{i=1}^{2}\frac{f_3\left(x_i\right)}{m^2_{\tilde{\chi}^\pm_i}}\\ &+2\frac{|M_2|^2+|\mu|^2+2\tan\beta|\mu||M_2|\cos(\phi_\mu+\phi_2)+2M_W^2\cos 2\beta}{\Delta_C}\sum_{i=1}^{2}(-1)^i\frac{f_1\left(x_i\right)}{m^2_{\tilde{\chi}^\pm_i}}\\ &-\frac{1}{4}\frac{(|M_2|^2-|\mu|^2)(1-Y_\mu^2)+2M_W^2\cos 2\beta(1+Y_\mu^2)}{\Delta_C}\sum_{i=1}^{2}(-1)^i\frac{f_3\left(x_i\right)}{m^2_{\tilde{\chi}^\pm_i}}\Bigg\},\end{aligned} \tag{3.17b}$$

where Δ_C has been defined in Eq. 2.16. These results are obtained by re-expressing mixing matrix elements in terms of basic SUSY parameters, and therefore hold for the complete SUSY parameter space. Together with Eqs. 3.15 they show explicitly that the chargino contributions to the leptonic dipole moments decouple like $1/m^2_{\tilde{\chi}^\pm}$ for $m^2_{\tilde{\chi}^\pm} \gg m^2_{\tilde{\nu}}$, and like $1/m^2_{\tilde{\nu}}$ in the opposite limit $m^2_{\tilde{\nu}} \gg m^2_{\tilde{\chi}^\pm}$. For completeness terms proportional to Y_μ^2 have been included, even though Eq. 2.58 shows that $Y_\mu^2 \ll 1$; if these terms are neglected, $(a_\mu)^{\tilde{\chi}^\pm}_{\text{SUSY}} \propto m_\mu^2$, as advertised earlier.
Furthermore, providing a perturbative ansatz for chargino mixing as discussed in Sec. 2.3.2 can be applied, these results can be used to derive approximative expressions for the chargino loop contribution to leptonic dipole moments. These read[5]

$$(d_e)^{\tilde{\chi}^\pm}_{\text{SUSY,per.}} \simeq \frac{e^2 m_e}{48\pi^2\sin^2\theta_W}\frac{\tan\beta\sin(\phi_\mu+\phi_2)}{|\mu||M_2|(|\mu|^2-|M_2|^2)}\left[|\mu|^2 f_1\left(x_1\right) - |M_2|^2 f_1\left(x_2\right)\right], \tag{3.18a}$$

$$\begin{aligned}(a_\mu)^{\tilde{\chi}^\pm}_{\text{SUSY,per.}} \simeq\ &-\frac{e^2 m_\mu^2}{24\pi^2\sin^2\theta_W}\Bigg\{\frac{\tan\beta\cos(\phi_\mu+\phi_2)}{|\mu||M_2|(|\mu|^2-|M_2|^2)}\left[|M_2|^2 f_1\left(x_2\right) - |\mu|^2 f_1\left(x_1\right)\right]\\ &+\frac{1}{|\mu|^2-|M_2|^2}\left[f_1\left(x_2\right)-f_1\left(x_1\right)\right] - \frac{f_3\left(x_1\right)}{8|M_2|^2}\Bigg\}.\end{aligned} \tag{3.18b}$$

Analogous statements also hold for the neutralino contributions, but because of the more complicated nature of neutralino mixing it is extremely difficult to find a simple exact analytic expressions for these contributions. However, making use of the results of the

[5] The ordering $|M_2|^2 < |\mu|^2$ is assumed here.

ansatzes for a perturbative diagonalization of the slepton and neutralino mass matrices as presented in Sec. 2.3.1 and Sec. 2.2.3, one can derive approximate expressions for the neutralino contribution to d_e and a_μ

$$
\begin{aligned}
(d_e)^{\tilde{\chi}^0}_{\text{SUSY,per.}} \simeq & - \frac{e^2 m_e}{96\pi^2} \left\{ \frac{|A_e^\star + \mu \tan\beta|}{\cos^2\theta_W |M_1|} \frac{f_2(x_R) - f_2(x_L)}{m^2_{\tilde{e}_L} - m^2_{\tilde{e}_R}} \sin(\phi_1 - \phi_{\tilde{e}}) \right. \\
& + \frac{\tan\beta \sin(\phi_\mu + \phi_1)}{\cos^2\theta_W |\mu||M_1| \left(|\mu|^2 - |M_1|^2\right)} \\
& \times \left[|\mu|^2 \left(f_2(x_R) - \frac{f_2(x_L)}{2} \right) - |M_1|^2 \left(f_2(z_R) - \frac{f_2(z_L)}{2} \right) \right] \\
& \left. + \frac{\tan\beta \sin(\phi_\mu + \phi_2) \left[|\mu|^2 f_2(y_L) - |M_2|^2 f_2(z_L) \right]}{2\sin^2\theta_W |M_2||\mu| \left(|\mu|^2 - |M_2|^2\right)} \right\}, \qquad (3.19a) \\
(a_\mu)^{\tilde{\chi}^0}_{\text{SUSY,per.}} \simeq & - \frac{e^2 m_\mu^2}{48\pi^2} \left\{ \frac{|A_\mu^\star + \mu \tan\beta|}{\cos^2\theta_W |M_1|} \frac{f_2(x_R) - f_2(x_L)}{m^2_{\tilde{\mu}_L} - m^2_{\tilde{\mu}_R}} \cos(\phi_1 - \phi_{\tilde{\mu}}) \right. \\
& + \frac{\tan\beta \cos(\phi_\mu + \phi_1)}{\cos^2\theta_W |\mu||M_1| (|\mu|^2 - |M_1|^2)} \\
& \times \left[|\mu|^2 \left(f_2(x_R) - \frac{f_2(x_L)}{2} \right) - |M_1|^2 \left(f_2(z_R) - \frac{f_2(z_L)}{2} \right) \right] \\
& + \frac{\tan\beta \cos(\phi_\mu + \phi_2)}{2\sin^2\theta_W |\mu||M_2| (|\mu|^2 - |M_2|^2)} \left[|\mu|^2 f_2(y_L) - |M_2|^2 f_2(z_L) \right] \\
& + \frac{1}{\cos^2\theta_W} \frac{1}{|\mu|^2 - |M_1|^2} \left[f_2(x_R) - \frac{f_2(x_L)}{2} - f_2(z_R) + \frac{f_2(z_L)}{2} \right] \\
& + \frac{1}{2\sin^2\theta_W} \frac{1}{|\mu|^2 - |M_2|^2} \left[f_2(y_L) - f_2(z_L) \right] \\
& \left. + \frac{1}{2} \left\{ \frac{1}{\cos^2\theta_W} \left[\frac{f_3(x_R)}{m^2_{\tilde{\mu}_R}} + \frac{f_3(x_L)}{4m^2_{\tilde{\mu}_L}} \right] + \frac{f_3(y_L)}{\sin^2\theta_W m^2_{\tilde{\mu}_R}} \right\} \right\}, \qquad (3.19b)
\end{aligned}
$$

where $x_\alpha = m^2_{\tilde{e}_\alpha(\tilde{\mu}_\alpha)}/|M_1|^2$, $y_\alpha = m^2_{\tilde{e}_\alpha(\tilde{\mu}_\alpha)}/|M_2|^2$, and $z_\alpha = m^2_{\tilde{e}_\alpha(\tilde{\mu}_\alpha)}/|\mu|^2$. As pointed out before, both the electric dipole moment and the anomalous magnetic moment are chirality flipping and hence proportional to powers of the Yukawa coupling. Therefore slepton mixing, being proportional to the Yukawa coupling, cannot be neglected and an approbate, perturbative treatment of slepton mixing has to be used. This results in the first lines of Eq. 3.19a and Eq. 3.19b, both of which contain the relative phase between M_1 and $\phi_{\tilde{l}}$ from slepton mixing. These lengthy expressions for the perturbative results yield some insight into the physics and the parameter dependences of the SUSY contributions from chargino and neutralino loops to a_μ and d_e. As already mentioned the contributions to d_e and a_μ shows—at least for the phase dependent terms—an almost identical dependence on the SUSY parameters, i.e. the chargino(neutralino) contribution to d_e can be obtained from the chargino(neutralino) contribution to a_μ by dropping the phase-independent terms, replacing cosine with sine as well as the lepton index ($\mu \to e$) and dividing by $2m_e$. Furthermore the appearance of phase-independent and cosine-terms for both contributions to a_μ—in contrast to the exclusive presence of sine-terms for the contributions to d_e—emphasize

once more that the CP-odd observable d_e requires non-trivial phases to be nonvanishing whereas the SUSY contributions to a_μ are non-vanishing even for trivial phases. Note also that the phase dependent $SU(2)$ contributions to $(d_e)^{\tilde{\chi}^0}$ (last line of Eq. 3.19a) and to $(a_\mu)^{\tilde{\chi}^0}$ (third line of Eq. 3.19b) are almost identical to the corresponding terms in the chargino contribution, but relatively suppressed by a factor of four. Hence, if only the $SU(2)$ interactions are considered, the chargino contribution dominates the corresponding neutralino contribution.
Finally, the results show that the relative phase between the gaugino masses M_1 and M_2 does not enter the contributions at all, the only relevant phases entering the contributions being the relative phase between the Higgsino mass parameter μ and the gaugino masses and the relative phase between M_1 and the phase $\phi_{\tilde{l}}$. In our general convention the absence of terms proportional to the relative phase $\phi_2 - \phi_{\tilde{l}}$ between the phase from slepton mixing and the phase of M_2 might seem surprising. But this fact can be understood by noticing that effectively the leading order contributions to $(d_e)^{\tilde{\chi}^0}_{\mathrm{SUSY}}$ and $(a_\mu)^{\tilde{\chi}^0}_{\mathrm{SUSY}}$ have been calculated here. These are of order $M_Z^0 \times m_l^1$. Terms of such order in M_Z can arise from either zeroth order neutralino mixing or first order corrections to the Higgsino content of neutralinos multiplied with the rescaled Yukawa coupling Y_l. Multiplying the second class of terms with first order corrections to slepton mixing (in order to obtain a dependence on $\phi_{\tilde{l}}$) would lead to subleading terms of order $M_Z^0 \times m_l^2$. Therefore, the only terms of order $M_Z^0 \times m_l^1$ with dependence on both ϕ_2 and $\phi_{\tilde{l}}$ are terms from zeroth order neutralino mixing and first order slepton mixing; but for zeroth order neutralino mixing the neutralino mixing matrix element N_{12} appearing in $n_{R2\alpha}$ vanishes, and hence we find no dependence on $\phi_2 - \phi_{\tilde{l}}$.

3.2.3 Possibilities for suppressing the SUSY contributions to d_e and a_μ

It is well established [22–25, 27, 28, 84–86] that the experimental bound in Eq. 3.5 on d_e provides stringent bounds on the MSSM parameter space. For example, the chargino contribution can roughly be estimated as [69]

$$(d_e)^{\tilde{\chi}^\pm}_{\mathrm{SUSY}} \sim 3 \times 10^{-24} \tan\beta \sin\phi_\mu \left(\frac{100\mathrm{GeV}}{m_{\mathrm{SUSY}}}\right)^2 e\mathrm{cm}, \tag{3.20}$$

where m_{SUSY} stands for the relevant sparticle (sneutrino or chargino, whichever is heavier) mass. Also, from now the convention $\phi_2 = 0$ is used.[6] A similar, rough estimate for the chargino loop contribution to $(a_\mu)_{\mathrm{SUSY}}$ reads

$$(d_e)^{\tilde{\chi}^\pm}_{\mathrm{SUSY}} \sim 2 \times 10^{-8} \left(\frac{100\mathrm{GeV}}{m_{\mathrm{SUSY}}}\right)^2 \times (1.2 + \tan\beta\cos\phi_\mu) \tag{3.21}$$

In contrast to the estimate for the chargino contribution to d_e, which is almost four orders of magnitude above the experimental limit, the estimate for the contribution to a_μ is just one order above the allowed limit.[7] Hence the problem of suppressing the chargino contribution to a_μ can be understood to be much less severe than suppressing the corresponding

[6] Keep in mind that up to now I used $\phi_2 \neq 0$ in order to keep results symmetric and to illustrate rephasing invariance. In the following numerical analysis the convention $\phi_2 = 0$ will explicitly be invoked.

[7] To be precise the given estimate holds for $|\mu| \gg |M_2| \simeq m_{\tilde{\nu}}$. Other choices for these three mass scales give even smaller numbers.

contributions to d_e. As a matter of fact the remainder of this section will mainly focus on possibilities for fulfilling the bound on $(d_e)_{\rm SUSY}$.[8]
The chargino contribution by itself can therefore only satisfy the experimental constraint by Eq. 3.6 for a very small phase ϕ_μ and/or very large sparticle masses. For sparticle masses not much above 100GeV, one would need phases of order 10^{-3} (10^{-2}) or less in the chargino (neutralino and slepton) mass matrices; for $\tan\beta \gg 1$, this constraint would become even stronger. Such small phases are unlikely to lead to measurable effects in high energy collider experiments [56, 57] and hence are of no interest for the remainder of this work. Alternatively one can postulate that sparticle masses are very large [27, 28]. Since gaugino masses are coupled to parameters in the Higgs sector via one loop renormalization equations, whereas a similar coupling between first generation sfermion masses and the Higgs sector only exists at two loop level [33, 87], naturalness arguments favor models with large slepton masses and relatively modest gaugino masses. The estimate in Eq. 3.20 indicates that for such scenarios first generation sleptons masses well above 1 TeV would be required if the relevant phases are of $\mathcal{O}(1)$. In that case these sleptons would be beyond the reach of the next linear e^+e^- collider, which will have a center of mass energy $\sqrt{s} \leq 1$TeV. Hence such scenarios are not of interest within Part II where the interest is explicitly on the consequences of non-vanishing sizeable CP-phases on selectron pair production. Moreover, since FCNC constraints would then also indicate very large masses for the second generation sleptons (recall that I assume them to be exactly degenerate with the first generation), a possible excess in a_μ could not be accommodated within the MSSM.
Therefore the focus within Part II is on the third possibility for satisfying the constraint from Eq. 3.6, where the different contributions to d_e largely cancel [22, 23]; i.e., the neutralino contribution must cancel the chargino contribution. In the following numerical analyses I study this possibility qualitatively for three scenarios specified in the next section. Later onwards I will analyze high energy observables that are sensitive to phases within the same three scenarios.

3.3 Numerical analysis

The first subsection briefly introduces the three scenarios discussed within Part II and explains the additional bounds used for the numerical analysis. The numerical analysis first investigates the low energy compatible ranges of phases and then studies correlations between the low energy observables and the allowed ranges for the phases.

3.3.1 Choice of parameters

First of all, for the definition of the studied parameter sets and the following numerical analysis the gaugino mass parameter M_2 is assumed to real and positive, i.e. $\phi_2 = 0$. As mentioned before this reduction of the number of phases can be achieved by suitable field redefinitions and leads to some loss of generality within the analytical results. Note that in this convention together with $\mathrm{Arg}\,[m_{12}^2] = 0$ the physical phases are those of μ, A, and M_1 (see. Eq 2.1). In all cases it is then assumed that the ratio of M_2 and $|M_1|$ is similar

[8] This should not be misunderstood to say that a_μ does not restrict parameters at all. There will later discussion of scenarios where a_μ indeed constrains parameter space.

to that in models with gaugino mass unification at the GUT scale, which predicts [33, 87] $|M_1| \simeq 0.5 M_2$ at the weak scale. Similarly, values for the soft breaking masses of $SU(2)$ singlet and doublet sleptons that are consistent with the assumption of universal scalar masses at the GUT scale are used. Recall that degenerate first and second generation soft breaking parameters in the slepton sector are assumed

$$m_{\tilde{e}_L} = m_{\tilde{\mu}_L} \equiv m_{\tilde{l}_L}, \tag{3.22a}$$

$$m_{\tilde{e}_R} = m_{\tilde{\mu}_R} \equiv m_{\tilde{l}_R}, \tag{3.22b}$$

$$A_e = A_\mu \equiv A. \tag{3.22c}$$

The assumption of universal scalar masses at the GUT scale implies [33, 87] that

$$m^2_{\tilde{l}_L} \simeq m^2_{\tilde{l}_R} + 0.46 M_Z^2, \tag{3.23}$$

at the weak scale. Finally, I'm interested in scenarios where at least $\tilde{l}_L$, $\tilde{l}_R$, $\tilde{\chi}^\pm_1$, and $\tilde{\chi}^0_2$, can be pair-produced at a "first stage" linear collider operating at $\sqrt{s} = 500\text{GeV}$.
This leads to consider three different scenarios, which are referred to as B1, B2, and B3. Scenario B1 has $|\mu| = M_2$, i.e. is characterized by strong mixing between $SU(2)$ gauginos and Higgsinos; this will occur in both the neutralino and chargino sector. Contrariwise, B2 has $|\mu| \gg M_2$, i.e. all Higgsino-gaugino mixing is suppressed. In these two cases a relatively large value of $|A|$, which enhances slepton left-right mixing for small $\tan\beta$, is taken; it will be shown that this increases the possibility of a cancellation between the neutralino and chargino contributions to d_e. On the other hand, selectron left-right mixing, while important for the calculation of d_e, remains negligible as far as selectron production at high energies is concerned. Case B3, which is almost[9] identical to the much–studied Snowmass "benchmark point SPS1A" [88], has intermediate Higgsino-gaugino mixing, as well as slightly reduced slepton masses. In all three cases four different values for $\tan\beta$ are used. Moreover, the three relevant phases ϕ_μ ,ϕ_1, and ϕ_A are allowed to flow freely, i.e. random numbers between 0 and 2π for these phases are picked. These three scenarios are summarized in Tab. 3.2. Of course, during the scan of the three phases ϕ_μ, ϕ_1, and

	$\lvert M_1\rvert$	M_2	$m_{\tilde{l}_L}$	$m_{\tilde{l}_R}$	$\lvert A\rvert$	$\lvert\mu\rvert$	$\tan\beta$	ϕ_1, ϕ_μ, ϕ_A
B1	100	200	235	180	500	200	3, 6, 9, 12	$\in [-\pi, \pi]$
B2	100	200	235	180	500	500	3, 6, 9, 12	$\in [-\pi, \pi]$
B3	102.2	191.8	198.7	138.2	255.5	343.2	5, 10, 15, 20	$\in [-\pi, \pi]$

Table 3.2: The three scenarios studied in Part II. All dimensionful parameters are in GeV.

ϕ_A, all relevant limits from direct searches for superparticles at colliders are respected. In particular, for searches at LEP2 [18] these limits read

$$m_{\tilde{e}} > 95\text{GeV}, \tag{3.24a}$$

$$m_{\tilde{\mu}} > 88\text{GeV}, \tag{3.24b}$$

$$m_{\tilde{\nu}} > 40\text{GeV}, \tag{3.24c}$$

[9] The agreement becomes exact for the "benchmark value" $\tan\beta = 10$ and vanishing phases.

$$m_{\tilde{\chi}_1^0} > 37\text{GeV}, \tag{3.24d}$$

$$\sigma_{\tilde{\chi}_1^\pm \tilde{\chi}_1^\mp} < 0.78\text{pb}, \tag{3.24e}$$

where an upper limit on the production cross section of light chargino pairs instead of a lower bound for the mass of the light chargino is used for technical reasons. Since in all three scenarios the real, dimensionful parameters are chosen so as to be large enough, this second set of "low-energy constraints" essentially has no restrictive impact on parameter points if these are compatible with d_e and a_μ. However, while being of no importance for the studied parameters sets, these bounds are implemented as additional cuts in the program itself. Thus the program can easily be applied to more generalized parameter scans or other scenarios.[10]

3.3.2 Correlations between phases

Before discussing the allowed ranges for the phases ϕ_μ, ϕ_1, and ϕ_A, a brief investigation of the "cutting efficiency" of the bound on $(d_e)_{\text{SUSY}}$ (Eq. 3.6), of the bound on $(a_\mu)_{\text{SUSY}}$ (Eq. 3.10), and of both bounds together is prepended. The absolute number of initial randomly generated sets for $(\phi_\mu,\ \phi_1,\ \phi_A)$ as well as the absolute and relative number of sets passing each separate constraint and the combination of both are given in Tab. 3.3.

First of all, it is observed that the constraints are quite stringent, less than 0.5% of the

	$\tan\beta$	points	d_e-survival		a_μ-survival		combined survival	
B1	3	500 000	1268	0.25%	353218	70.1%	528	0.11%
	6	500 000	593	0.12%	294575	58.9%	291	0.06%
	9	500 000	422	0.08%	279039	55.8%	218	0.04%
	12	500 000	286	0.06%	271547	54.3%	151	0.03%
B2	3	750 000	4327	0.58%	710723	94.8%	3892	0.52%
	6	750 000	2096	0.28%	574163	76.6%	1469	0.19%
	9	750 000	1412	0.19%	508093	67.7%	811	0.11%
	12	750 000	1069	0.14%	467759	62.4%	543	0.07%
B3	5	750 000	1495	0.20%	507068	67.6%	746	0.10%
	10	750 000	675	0.09%	434395	57.9%	340	0.05%
	15	750 000	516	0.07%	414060	55.2%	245	0.03%
	20	750 000	354	0.05%	354988	47.3%	111	0.01%

Table 3.3: Absolute number of the points passing the "low-energy constraints" given by d_e (4.th column), by a_μ (6.th column) and by both (8.th column). The survival rate relative to the number of initially scanned points is given in the 5.th, 7.th and 9.th column.

initially generated points survive after cutting on the low energy observables d_e and a_μ. Furthermore, in all cases the bound from d_e is significantly stronger than the bound from a_μ. At least 99.4% of the initial points fail to meet the constraint from d_e. This reinforces the already stated point that the "cancellation problem" given by Eq. 3.6 is much more

[10] For further details of the code refer to App. E.

severe than the one from Eq. 3.10. The cutting efficiency of d_e in good approximation grows linearly with $\tan\beta$. [11] Concerning the stronger rejections from d_e, this behavior will be discussed to some extent shortly. The significant drops of the survival rate from a_μ in scenarios B1 and B3, when increasing $\tan\beta$ from 3 to 6, reflect the appearing disallowance of negative values for a_μ, which is due to the asymmetric range for a_μ in Eq. 3.10. This asymmetry also explains why the overall survival rate from both bounds is smaller than the one from d_e alone: phases which lead to negative but allowed d_e can give a negative a_μ whose absolute value is too large; and hence these phases are forbidden. Of course, the small numbers of overall surviving points are the reason why $\mathcal{O}(10^5)$ points have to be generated initially, otherwise the numerical analysis could not accumulate enough statistics and could not be considered representative.
For simplicity, and because of limited space for representation, in the remainder only the results for the two extreme choices of $\tan\beta = 3$ and 12 in scenarios B1 and B2 are shown. For scenario B3 $\tan\beta = 10$ is chosen, so that the benchmark point SPS1A is indeed studied, and the extreme value $\tan\beta = 20$. Results for the other, omitted cases are qualitatively similar and can be obtained by extrapolation from the extreme cases. Furthermore, note that the results shown below are projections of a three-dimensional parameter space onto two-dimensional planes. Hence it should be kept in mind that each correlation in the $\phi_x - \phi_y$ plane has been obtained by scanning over the entire allowed range for ϕ_z. In the following we will quote upper bounds on $|\phi_\mu|$ that result from the constraint given by Eq. 3.6. A similar band $\phi_\mu = \pi$ exists for small $\tan\beta$ and large $|\mu|$.
First of all, Fig. 3.2 shows the allowed combinations of the phases ϕ_μ and ϕ_1. Very strong constraints on ϕ_μ are observed in scenario B1, which become stronger as $\tan\beta$ increases. Scenario B2 allows much larger values of $|\phi_\mu|$, which moreover do not decrease much with increasing $\tan\beta$, while scenario B3 is intermediate between these two. This behavior can be understood from Eqs. 3.17a, 3.18a, and 3.19a, describing the chargino and neutralino loop contributions to $(d_e)_{\mathrm{SUSY}}$ analytically/perturbatively in terms of basic SUSY input parameters. It was remarked that the contributions involving $SU(2)$ gauge interactions have very similar structures in both cases, but the chargino loop contribution is bigger by a factor of four than the corresponding term in the neutralino loop contribution. The potentially most important cancellation therefore occurs between the chargino contribution [more exactly: the total contribution involving $SU(2)$ interactions, which, however, is always dominated by the chargino contribution] and the neutralino contributions involving $U(1)_Y$ interactions.
Scenario B1 has $|\mu| = M_2$, i.e. very strong mixing between Higgsinos and $SU(2)$ gauginos. It is obvious that Eq. 3.19a no longer gives an accurate estimate of the neutralino contribution within this limit, but one expects it to remain qualitatively correct; note that it gives a finite answer (involving the derivative of the function f_2) in this case. In particular, the contributions involving the $SU(2)$ gauge coupling would be much bigger than those involving the $U(1)_Y$ interactions if the relevant phases had similar magnitude; in other words, a significant cancellation can only occur if $|\phi_\mu|$ is well below $|\phi_1|$. Furthermore, for this choice of parameters a strong internal cancellation occurs between the two contributions from $U(1)_Y$ interactions that grow proportional to $\tan\beta$, i.e. between the first

[11] This indicates that rather severe fine-tuning is required [57] to obtain the necessary cancellations if all phases are indeed independent quantities. To put it differently, one faces the challenge to construct models that "naturally" explain the required cancellations between these phases. This work will not attempt to do so.

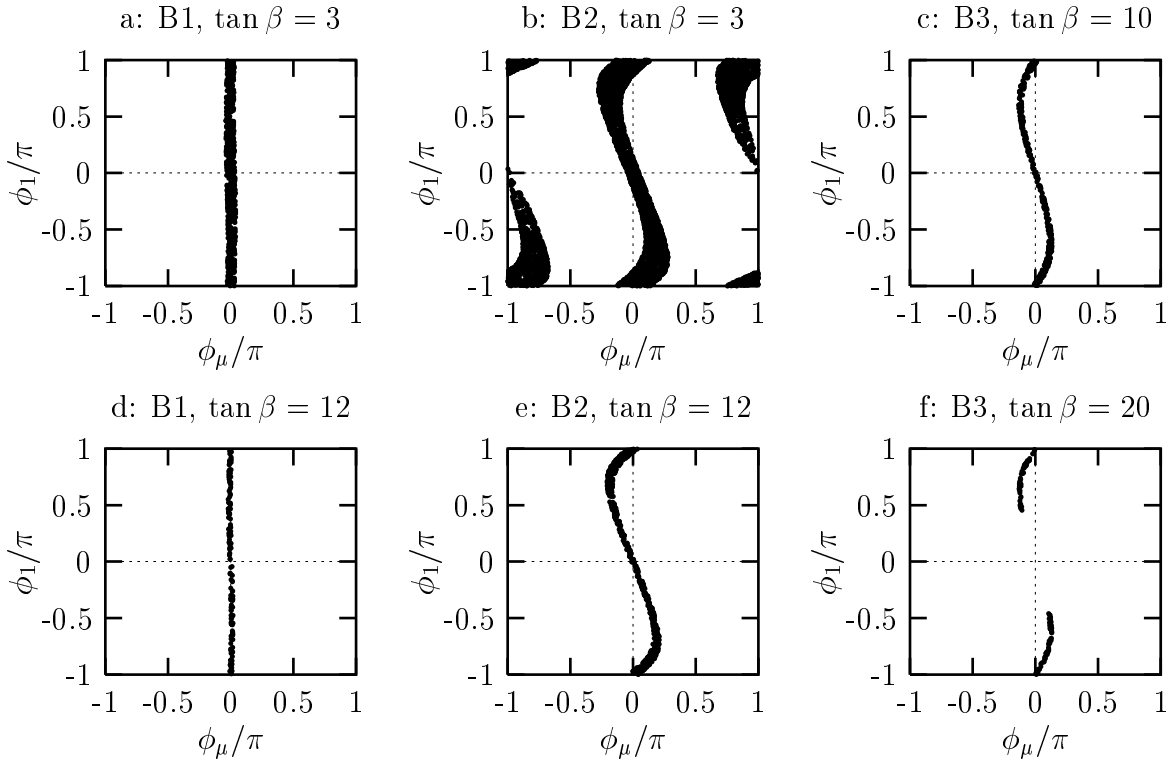

Figure 3.2: Combinations of ϕ_μ and ϕ_1 that are allowed for at least one $\phi_A \in [-\pi, \pi]$.

and the second addend in Eq. 3.19a. As a result we find $|\phi_\mu| \leq \pi/30$ even for $\tan\beta = 3$. Moreover, the dominant contribution from $U(1)_Y$ interactions in this scenario involves A, i.e. is independent of $\tan\beta$, whereas the contribution from $SU(2)$ interactions increases proportional to $\tan\beta$. The upper bound on $|\phi_\mu|$ therefore scales essentially like $\cot\beta$. This scaling basically explains the scaling of the total cutting efficiencies in scenario B1 as well. The importance of ϕ_A in this scenario also explains why there is almost no correlation between the allowed values of ϕ_μ and ϕ_1. Moreover, in this scenario values of ϕ_μ near π are excluded by the lower bound on $(a_\mu)_{\rm SUSY}$ in Eq. 3.10.

Eq. 3.17a shows that increasing $|\mu|$ while keeping all other parameters constant decreases the chargino contribution to d_e. Further, according to Eq. 3.19a it also decreases the neutralino contributions that involve $SU(2)$ interactions, but actually *increases* the neutralino contribution that is sensitive to selectron left-right mixing, i.e., the first line of Eq. 3.19a.[12] Much larger values of $|\phi_\mu|$ therefore become possible for larger $|\mu|$. For the given choice of parameters in scenario B2 the coefficient of the neutralino contribution $\propto \sin(\phi_1 - \phi_{\tilde{e}})$ is still about 5 times smaller than the coefficient of $\sin\phi_\mu$ in the chargino contribution, leading to an upper limit of $\sim \pi/4$ on $|\phi_\mu|$. Since these two coefficients have the same sign, cancellations occur only if $\phi_1 + \phi_\mu$ and ϕ_μ have opposite signs. Note that both of these contributions are (essentially) $\propto \tan\beta$. The upper bound on $|\phi_\mu|$ is therefore almost independent of $\tan\beta$. However, one needs increasingly stronger cancellations as $\tan\beta$ increases; moreover, the relative importance of the phase ϕ_A diminishes with increasing $\tan\beta$,

[12] In principle one could therefore have large cancellations between the chargino and the neutralino contributions even for $M_2 \simeq |\mu|$, if $M_2 \simeq m_{\tilde{\nu}} \gg |M_1|,\ m_{\tilde{e}_R}$. However, if M_2 and $m_{\tilde{\nu}}$ are as in scenario B1, this would require values of $m_{\tilde{e}_R}$ well below the direct search limit ~ 100GeV.

since its contribution to the selectron left-right mixing is not enhanced within this limit. These two considerations explain why the width of the allowed band essentially decreases like $\cot\beta$ for large $\tan\beta$; this behavior directly transfers to the total cutting efficiency in scenario B2.

The increase of $|\mu|$ when going from scenario B1 to B2 also reduces the supersymmetric

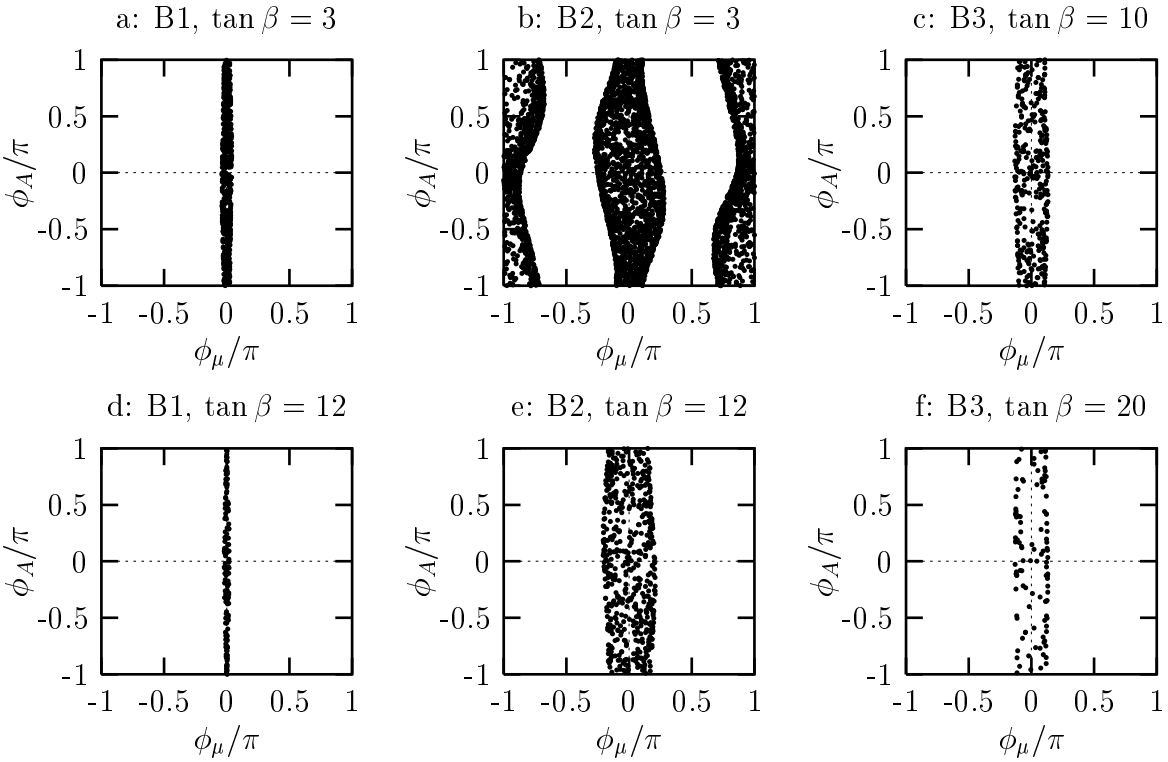

Figure 3.3: Combinations of ϕ_μ and ϕ_A that are allowed for at least one value of $\phi_1 \in [-\pi, \pi]$.

contribution to a_μ. Hence, for $\tan\beta = 3$ an additional allowed band with $\phi_\mu \simeq \pi$ is found; however, this band disappears at $\tan\beta \sim 10$. Note that the phase ϕ_1 enters a_μ mostly in the combination[13] $\cos(\phi_\mu + \phi_1)$. This means that $\phi_1 \simeq 0$ will give positive (negative) contributions to a_μ if $\phi_\mu \simeq 0(\pi)$. In other words, for values of ϕ_1 near zero the $U(1)_Y$ interactions contribute with equal sign to a_μ as the (usually leading) $SU(2)$ interactions do, whereas $\phi_1 \simeq \pi$ leads to a particular cancellation between $U(1)_Y$ and $SU(2)$ contributions. $\phi_\mu \simeq \pi$ therefore remains allowed to slightly higher values of $\tan\beta$ if $\phi_1 \simeq \pi$ as well.
If $|\mu|$ is increased by another factor $\sim\sqrt{5}$, chargino and neutralino loop contributions to d_e can be of the same size, in which case no upper limit can be given either on $|\phi_\mu + \phi_1|$ or $|\phi_\mu|$ separately [22], although a strong (anti-)correlation between these two phases still has to hold. If $|\mu|$ is increased even further, the neutralino contribution becomes dominant. In that case ϕ_μ could take any value (after scanning over the other phases), but significant absolute constraints on the combination $\phi_1 + \phi_\mu$ would emerge that hold even after scanning over all ϕ_A and ϕ_μ. However, most models of supersymmetry breaking prefer [33, 87] values of $|\mu|$ that are not much larger than M_2. Therefore scenarios with $|\mu| \gg M_2$ are not discussed any further.

[13] For $|\mu|\tan\beta \gg |A_l|$, $\cos(\phi_1 - \phi_{\tilde{l}}) \simeq \cos(\phi_\mu + \phi_1)$ as well.

Scenario B3 has a significantly smaller value of $|\mu|$ than scenario B2, although the value

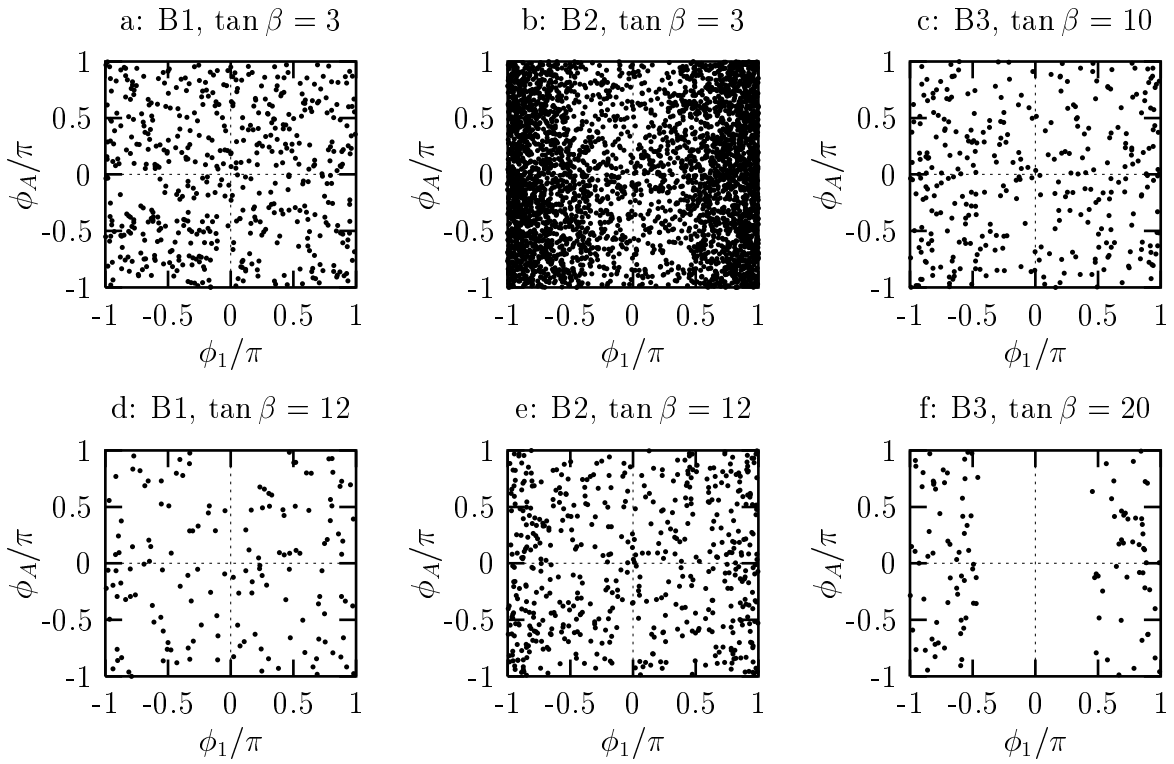

Figure 3.4: Combinations of ϕ_1 and ϕ_A that are allowed for at least one value of $\phi_\mu \in [-\pi, \pi]$.

is larger than in B1. The absolute upper bound on $|\phi_\mu|$ is therefore reduced to $\sim \pi/8$. The allowed bands in Fig. 3.2c,f are narrower than in Fig. 3.2b,e due to the larger values of $\tan\beta$ and the slightly lighter slepton masses; both effects tend to increase the SUSY contributions to d_e, requiring correspondingly more perfect cancellations. Note also that for $\tan\beta = 20$ values of ϕ_1 near zero give a_μ above the range from Eq. 3.10, i.e. in this case the neutralino and chargino contributions to a_μ must not add constructively. Parameter sets with ϕ_μ near π are allowed only for $\tan\beta \lesssim 5$.

The allowed regions in the (ϕ_μ, ϕ_A)-plane are shown in Fig. 3.3. Most of the discussed scenarios have $\tan\beta|\mu|$ significantly above $|A|$, in which case the value of ϕ_A is not very important. Even if ϕ_A is important, as in scenario B1, there is little correlation between ϕ_A and ϕ_μ, since ϕ_A only enters from the combination $\phi_{\tilde{e}} - \phi_1$, and ϕ_1 is scanned in Fig. 3.3. In all cases the bound on $|\phi_\mu|$ is slightly weaker for $\phi_A \simeq 0$ than for $\phi_A \simeq \pi$, since in the former case A and μ add (mostly) constructively to the mixing of selectrons, thereby increasing the first line in Eq. 3.19a.

It was observed from Figs. 3.2 and 3.3 that in all cases the entire range of values for ϕ_1 and ϕ_A is allowed by the d_e constraint for some combinations of the other phases. Fig. 3.4 shows that there is little correlation between the allowed ranges for these two phases. Indeed, the d_e constraint allows all combinations of these two phases, for some value of ϕ_μ. On the other hand, in case B3 with $\tan\beta = 20$ the a_μ constraint form Eq. 3.10 excludes $|\phi_1| \lesssim \pi/2$, see Fig. 3.2.

3.3.3 Correlations between $(a_\mu)_{\rm SUSY}$, $(d_e)_{\rm SUSY}$ and the phases

Sec. 7.3.1 will study correlations between low- and high-energy observables. To that end it is instructive to see how the low-energy observables a_μ and d_e correlate with the SUSY phases in the experimentally allowed region of parameter space. It was observed above that ϕ_μ is tightly constrained, whereas ϕ_A and ϕ_1 are not. Since ϕ_A does not affect high energy observables, the most interesting correlations are those between low-energy observables and ϕ_1, after scanning over ϕ_A and ϕ_μ.

One finds that there is no correlation between d_e and ϕ_1 as shown in Fig. 3.5, whereas in

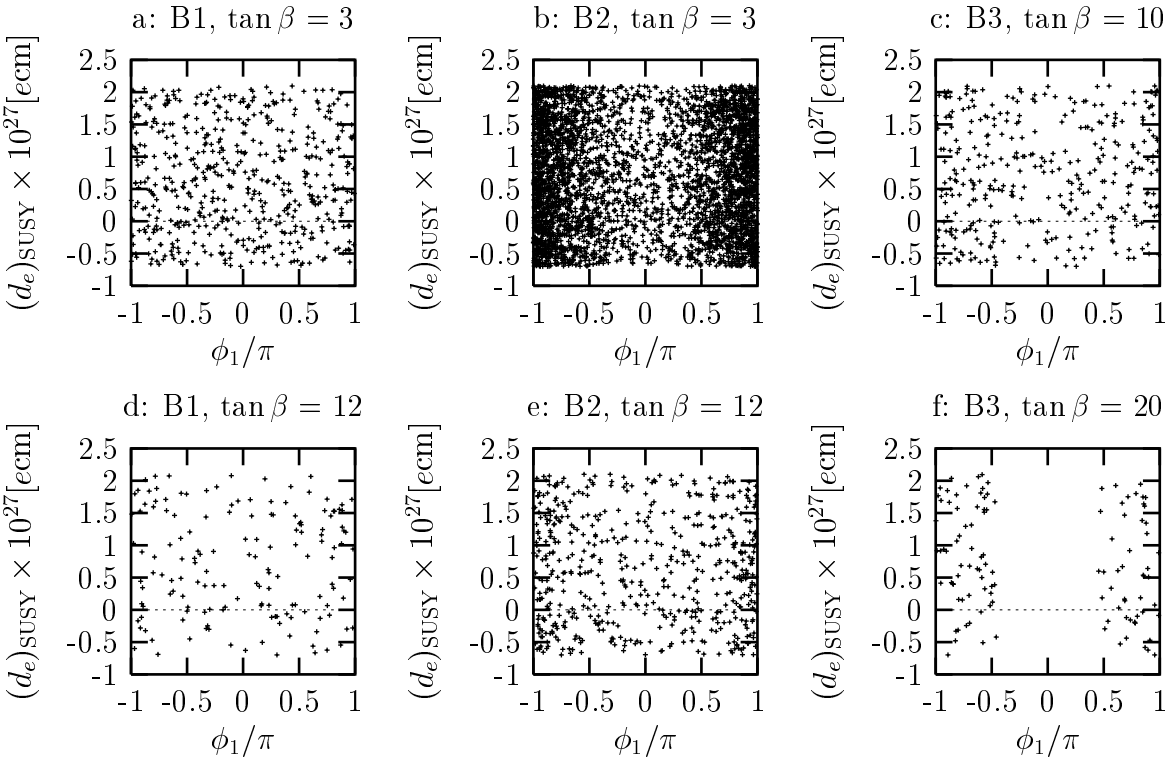

Figure 3.5: $(d_e)_{\rm SUSY}$ vs. ϕ_1 after scanning over ϕ_μ and ϕ_A.

scenarios B2 and B3 a_μ shows a behavior $\propto a\cos\phi_1 + b$ with a finite scatter, see Fig. 3.6. This difference originates from the requirement of very strong cancellations in d_e, discussed above. In particular, the phases ϕ_1 and ϕ_μ have to be correlated such that the leading terms $\propto \sin(\phi_\mu + \phi_1)$ and $\sin\phi_\mu$ cancel each other to an accuracy determined by the size of (subleading) terms $\propto \sin\phi_A$ as well as by the experimental bound on d_e. This completely removes the correlation between d_e and $\sin\phi_1$ that one might naively expect from Eq. 3.19a. The phase-dependent neutralino loop contribution to a_μ is given in Eq. 3.19b. Since for the given examples ϕ_μ is constrained to be small (or near to π), $|\cos\phi_\mu| \simeq 1$, and one finds a cosine-like dependence of a_μ on ϕ_1. The crucial observation is that the ϕ_1-dependent and the ϕ_μ-dependent terms do *not* cancel in this case, so the "naive" dependence of a_μ on ϕ_1 survives. In passing it may be noted that $(a_\mu)_{\rm SUSY}$ can usually not be achieved for a given choice of the absolute parameters once large cancellations in $(d_e)_{\rm SUSY}$ have been required, i.e. one cannot choose the phases such that there are large cancellations both in $(d_e)_{\rm SUSY}$ and $(a_\mu)_{\rm SUSY}$. A better measurement of, and more accurate SM prediction for, a_μ therefore has higher potential to further constrain the SUSY phases than improved measurements

of d_e. Of course, experimentally establishing a nonvanishing value d_e (well above the SM prediction) would be of the greatest importance, since it would require physics beyond the SM. However, while it would require some SUSY phases to be non-zero, it would not further reduce the allowed ranges of any one of these phases after scanning over the two phases.

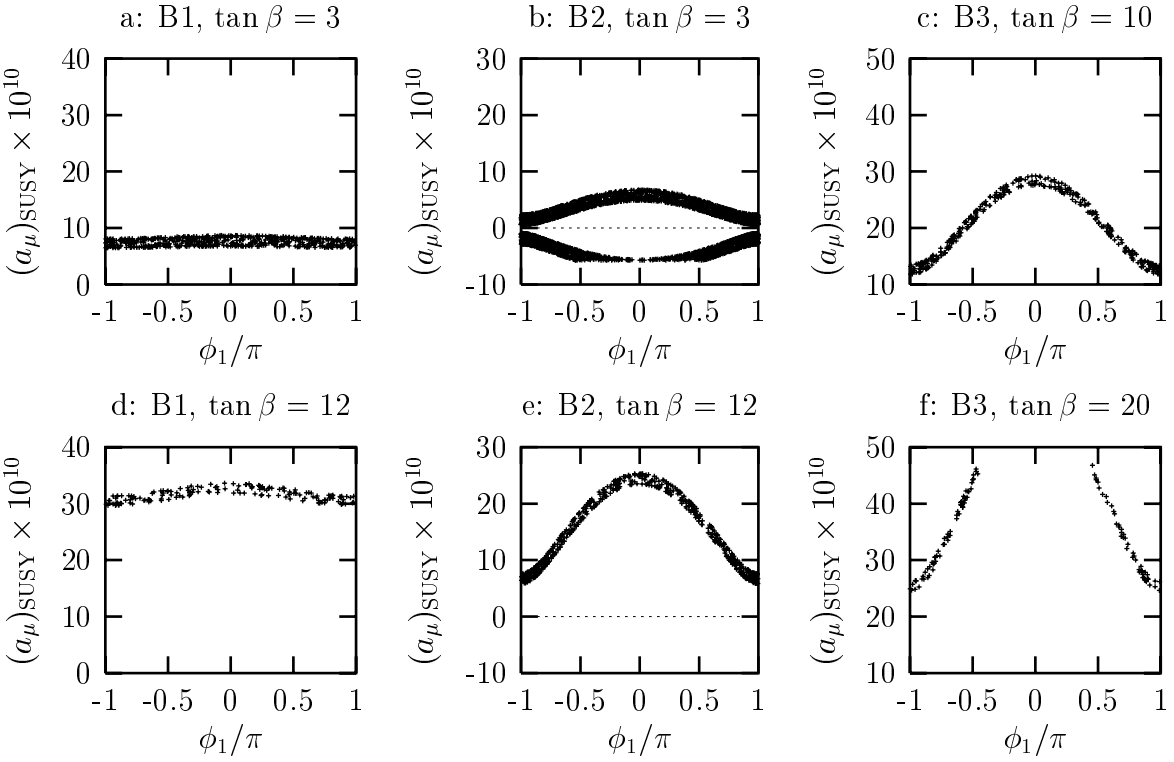

Figure 3.6: $(a_\mu)_{\rm SUSY}$ vs. ϕ_1 after scanning over ϕ_μ and ϕ_A.

Chapter 4

Cross sections

This chapter is devoted to cross sections. It starts with giving a short road map for the calculation of (tree level) cross sections, then gives analytic results for the cross sections of the four processes under discussion. The analytic results are used to derive perturbative expressions for the relevant production processes. Finally the perturbative results are discussed to some extent.

4.1 Road map to the calculation of cross sections

For reasons of completeness I give here the basic steps for calculating tree level cross section in form of a short road map:

1.) Derive Feynman rules

2.) Fix the kinematical situation

3.) Write down all tree level diagrams contributing to the considered process using chirality projection operators

4.) Calculate the helicity amplitudes

5.) Include initial beam polarization by using polarisation density matrices

6.) Include phase space and flux factors to obtain the differential, polarized cross section

7.) Perform the phase space integration to find the total, polarized cross section

8.) Taking the limit of vanishing polarization rates finally delivers the unpolarized differential and total cross section.

Keeping the goal in mind, the first step has already been achieved, the Feynman rules were basically given in Sec. 2.5 and the kinematical situation will be fixed shortly. Details on steps four to six are given in App.C.1, whereas step three has to be taken separately for each cross section.
In general the phase space integration in step 7 could be done numerically using suitable subroutines. However, for the purposes of the numerical analysis, where a great amount of

cross sections has to be evaluated up to 10 times[1] for more than 1000 parameter points, a substantial reduction in computing time can be achieved by finding analytical expressions for the total, unpolarized cross sections. An ansatz to find such results as used for this work is summarized in App. C.3.

4.2 Kinematical situation

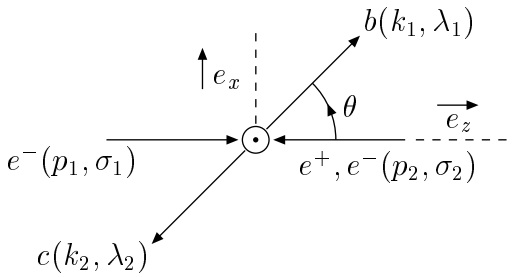

Figure 4.1: Kinematical situation

The kinematic situation is illustrated in Fig. 4.1. The momenta and helicities of the ingoing (first) electron and positron (second electron) are denoted by p_1^μ and σ_1, and p_2^μ and σ_2, respectively. The momenta of the produced superparticles, generally labeled by b and c, are denoted by k_1^μ and k_2^μ. In case of fermions being produced their helicities are denoted by λ_1 and λ_2.
Working in the center of mass (CMS) frame, the z-axis of the coordinate system is defined such that $\vec{p}_1$ points in $+z$ direction. The event plane is then completed by the momentum $\vec{k}_1$ of particle b, this plane defines the (x, z)-plane of the coordinate system. The scattering angle θ is defined as angle between $\vec{p}_1$ and $\vec{k}_1$. The nominal range range for θ which is used when going from the differential to the total cross section extends from 0 to π. However, if the final state consists of two identical particles physically θ has to be $\leq \pi/2$; therefore the cross section for the production of identical particles has to be multiplied with a factor of 1/2. Notice that this convention implies a vanishing azimuthal angle ϕ. This definition of the (x, z) plane is convenient since Part II is only interested in total cross sections for unpolarized $e^\pm$ beams.[2] Of course, the phase space integration, which should be performed in a lab-fixed coordinate system, still gives a factor of 2π from the integration over the azimuthal angle. Explicit expressions for the momenta p_i^μ and k_i^μ may be found in App. C.1.1.

[1] This factor of 10 for each cross section is due to the evaluation of significances; for further details see Chapter 6. Depending $\sqrt{s}$ up to 25 cross sections have to investigated.

[2] A nontrivial dependence on the azimuthal angle would arise only if transversely polarized $e^\pm$ beams were considered, and/or if in the kinematical distribution of the decay products of the produced superparticles b and c were investigated.

4.3 Analytical results for total cross sections

Here I briefly present the calculation of the corresponding unpolarized total cross sections. All these processes have already been discussed in literature: results for $\tilde{e}_i^- \tilde{e}_j^+$ and $\tilde{e}_i^- \tilde{e}_j^-$ production can be found in [89–96] and [97], whereas results for $\tilde{\chi}_i^- \tilde{\chi}_j^+$ and $\tilde{\chi}_i^0 \tilde{\chi}_j^0$ production are given in [66,92,93,98–103] and [67]. Nevertheless I list my own results here in order to provide a self-contained presentation and to illustrate consistency with previous works.

4.3.1 $e^+e^- \to \tilde{e}_i^+ \tilde{e}_j^-$

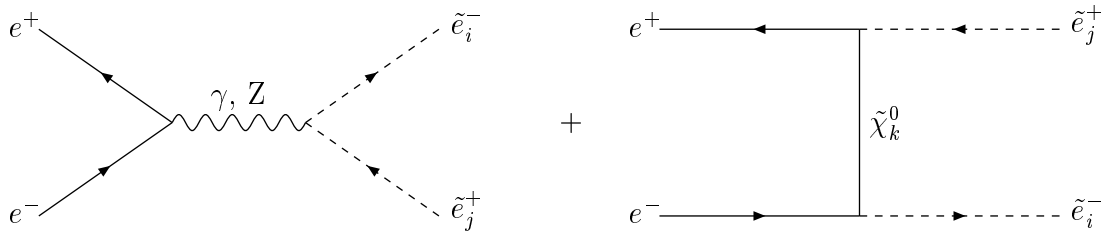

Figure 4.2: Diagrams for $e^+e^- \to \tilde{e}_i^- \tilde{e}_j^+$

Fig. 4.2 shows the s- and t-channel diagram contributing to selectron pair production. By introducing a dimensionless Z propagator

$$D_Z = \frac{s}{s - M_Z^2 + i\Gamma_Z M_Z}, \tag{4.1}$$

and bilinear charges $Z_{ij}^{\pm}$

$$Z_{LL}^- = 1 + \frac{\left(\sin^2\theta_W - \frac{1}{2}\right)^2}{\sin^2\theta_W \cos^2\theta_W} D_Z, \quad Z_{RR}^- = 1 + \frac{\sin^2\theta_W - \frac{1}{2}}{\cos^2\theta_W} D_Z, \tag{4.2a}$$

$$Z_{LL}^+ = 1 + \frac{\sin^2\theta_W - \frac{1}{2}}{\cos^2\theta_W} D_Z, \qquad Z_{RR}^+ = 1 + \frac{\sin^2\theta_W}{\cos^2\theta_W} D_Z, \tag{4.2b}$$

$$Z_{LR}^{\pm} = Z_{RL}^{\pm} = 0, \tag{4.2c}$$

the gauge contribution can be written as

$$\mathcal{M}_{ij}^{\sigma_1\sigma_2,G} = \frac{e^2}{s} \overline{v}\left(p_2, \sigma_2\right) Z_{ij}^{\alpha} P_{\alpha} u\left(p_1, \sigma_1\right) \left(k_i - k_j\right)^{\mu}. \tag{4.3}$$

The neutralino contribution is

$$\mathcal{M}_{ij}^{\sigma_1\sigma_2,\tilde{\chi}_k^0} = -\overline{v}\left(p_2, \sigma_2\right) \left(K_{-\alpha k}^j\right)^{\star} P^{\alpha} (\not{p}_1 - \not{k}_1 + m_{\tilde{\chi}_k^0}) D_t^k K_{\beta k}^i P^{\beta} u\left(p_1, \sigma_1\right). \tag{4.4}$$

The coefficients $K_{\alpha k}^i$ are given by

$$K_{Lk}^L = \frac{e}{\sqrt{2}\sin\theta_W \cos\theta_W} \left(\cos\theta_W N_{2k} + \sin\theta_W N_{1k}\right), \tag{4.5a}$$

$$K_{Rk}^R = \frac{-2e}{\sqrt{2}\cos\theta_W} N_{1k}^{\star}, \tag{4.5b}$$

$$K^R_{Lk} = K^L_{Rk} = 0, \tag{4.5c}$$

and the neutralino propagators are

$$D^k_{t,u} = \frac{1}{(t,u) - m^2_{\tilde{\chi}^0_k}}, \tag{4.6}$$

where $t = (p_1 - k_1)^2$ and $u = (p_1 - k_2)^2$. By introducing a shorthanded notation for the helicity amplitudes

$$\langle \sigma_1 \sigma_2 \rangle_{ij} = \mathcal{M}^{\sigma_1\sigma_2,G}_{ij} + \mathcal{M}^{\sigma_1\sigma_2,\tilde{\chi}^0_k}_{ij}, \tag{4.7}$$

and using the explicit expressions for helicity amplitudes given in App. C.1.3 and the definition of the neutralino functions as in App. C.2 one finds six non-vanishing helicity amplitudes

$$\langle ++ \rangle_{RL} = -2e^2 M_{LR}(s,t), \tag{4.8a}$$

$$\langle -- \rangle_{LR} = 2e^2 M^\star_{LR}(s,t), \tag{4.8b}$$

$$\langle +- \rangle_{RR} = -e^2 \lambda^{\frac{1}{2}}_{RR} \sin\theta \left(N_{RR}(s,t) + Z^+_{RR} \right), \tag{4.8c}$$

$$\langle +- \rangle_{LL} = -e^2 \lambda^{\frac{1}{2}}_{LL} \sin\theta Z^+_{LL}, \tag{4.8d}$$

$$\langle -+ \rangle_{RR} = -e^2 \lambda^{\frac{1}{2}}_{RR} \sin\theta Z^-_{RR}, \tag{4.8e}$$

$$\langle -+ \rangle_{LL} = -e^2 \lambda^{\frac{1}{2}}_{LL} \sin\theta \left(N_{LL}(s,t) + Z^-_{LL} \right). \tag{4.8f}$$

Here, the kinematical factors $\lambda^{\frac{1}{2}}_{ij} \equiv \lambda^{\frac{1}{2}}_{\tilde{e}_i \tilde{e}_j}$ are as in Eq. C.3 and, as defined in Sec. 4.2, θ is the angle between the incident e^- and the produced $\tilde{e}^-$. As usual, the unpolarized cross sections can be obtained by averaging over initial helicities. Alternatively, one can calculate polarized cross sections using polarisation density matrices for the incident beams (as described in App. C.1.4) and taking the limit over vanishing longitudinal and transversal polarizations for both beams. After integrating over the azimuthal angle, in both cases one obtains

$$\frac{d\sigma_{LL}}{d\cos\theta} = \frac{\lambda^{\frac{1}{2}}_{LL}}{128\pi s} \left(|\langle +- \rangle_{LL}|^2 + |\langle -+ \rangle_{LL}|^2 \right), \tag{4.9a}$$

$$\frac{d\sigma_{RR}}{d\cos\theta} = \frac{\lambda^{\frac{1}{2}}_{RR}}{128\pi s} \left(|\langle +- \rangle_{RR}|^2 + |\langle -+ \rangle_{RR}|^2 \right), \tag{4.9b}$$

$$\frac{d\sigma_{LR}}{d\cos\theta} = \frac{\lambda^{\frac{1}{2}}_{LR}}{128\pi s} |\langle -- \rangle_{LR}|^2, \tag{4.9c}$$

$$\frac{d\sigma_{RL}}{d\cos\theta} = \frac{\lambda^{\frac{1}{2}}_{RL}}{128\pi s} |\langle ++ \rangle_{RL}|^2. \tag{4.9d}$$

Finally, for these and following reactions the total, unpolarized cross sections may be obtained by performing the remaining integration over the scattering angle

$$\sigma_{ij} = \int_{-1}^{1} d\cos\theta \left(\frac{d\sigma_{ij}}{d\cos\theta} \right). \tag{4.10}$$

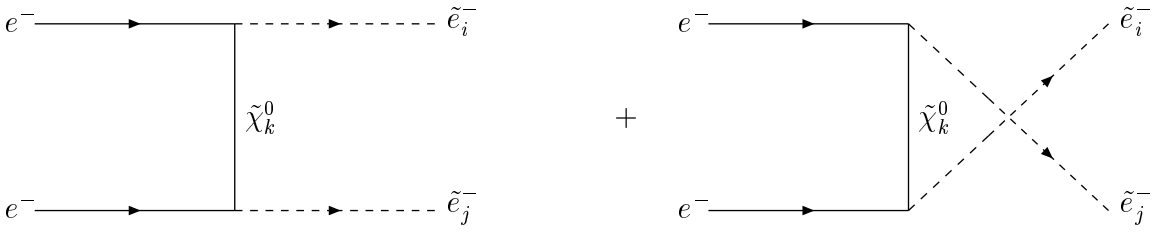

Figure 4.3: Diagrams for $e^-e^- \to \tilde{e}_i^-\tilde{e}_j^-$

4.3.2 $e^-e^- \to \tilde{e}_i^-\tilde{e}_j^-$

The t- and u-channel diagram contributing to $\tilde{e}_i^-\tilde{e}_j^-$ production are shown in Fig. 4.3, the corresponding invariant amplitude can be written as

$$\mathcal{M}_{ij}^{\sigma_1\sigma_2,\tilde{\chi}_k^0} = -K_{\alpha k}^j K_{\beta k}^i \overline{v}\,(p_2,\sigma_2) \times \left\{ \delta_{\beta,-\alpha} \left[\frac{\not{p}_1 - \not{k}_1}{t - m^2_{\tilde{\chi}_k^0}} + \frac{\not{p}_1 - \not{k}_2}{u - m^2_{\tilde{\chi}_k^0}} \right] + \delta_{\beta,\alpha} \left[\frac{m_{\tilde{\chi}_k^0}}{t - m^2_{\tilde{\chi}_k^0}} + \frac{m_{\tilde{\chi}_k^0}}{u - m^2_{\tilde{\chi}_k^0}} \right] \right\} P^\alpha u\,(p_1,\sigma_1)\,. \tag{4.11}$$

Using the results of App. C.1.3 the helicity amplitudes may be evaluated and one finds

$$\begin{aligned} \mathcal{M}_{ij}^{\sigma_1\sigma_2,\tilde{\chi}_k^0} = \langle\sigma_1\sigma_2\rangle_{ij} = &-\frac{s}{2}\sin\theta\lambda_{ij}^{\frac{1}{2}}\delta_{\sigma_2,-\sigma_1}\left(K_{\sigma_1 k}^i K_{-\sigma_1 k}^j D_t^k - K_{-\sigma_1 k}^i K_{\sigma_1 k}^j D_u^k\right) \\ &+ m_{\tilde{\chi}_k^0}\sqrt{s} K_{\sigma_1 k}^i K_{\sigma_1 k}^j \sigma_1 \delta_{\sigma_1,\sigma_2}\left(D_t^k + D_u^k\right). \end{aligned} \tag{4.12}$$

Rewriting these results in terms of neutralino functions as given in App. C.2, one finds four non-vanishing helicity amplitudes. Here θ is the angle between the momenta of an incident e^- and a produced $\tilde{e}^-$. It does not matter which initial and final state particles are chosen, since the cross section is invariant under $\theta \to \pi - \theta$.

$$\langle{+}{+}\rangle_{RR} = 2e^2\left[M_{RR}(s,t) + M_{RR}(s,u)\right]^\star, \tag{4.13a}$$

$$\langle{-}{-}\rangle_{LL} = -2e^2\left[M_{LL}(s,t) + M_{LL}(s,u)\right], \tag{4.13b}$$

$$\langle{-}{+}\rangle_{LR} = e^2\lambda_{LR}^{\frac{1}{2}}\sin\theta N_{LR}(s,t), \tag{4.13c}$$

$$\langle{+}{-}\rangle_{RL} = -e^2\lambda_{LR}^{\frac{1}{2}}\sin\theta N_{LR}(s,u). \tag{4.13d}$$

After calculating the polarization averaged squared matrix elements and including the phase space factor, differential cross sections are

$$\frac{d\sigma_{LL}}{d\cos\theta} = \frac{\lambda_{LL}^{\frac{1}{2}}}{256\pi s}|\langle{-}{-}\rangle_{LL}|^2, \tag{4.14a}$$

$$\frac{d\sigma_{RR}}{d\cos\theta} = \frac{\lambda_{RR}^{\frac{1}{2}}}{256\pi s}|\langle{+}{+}\rangle_{RR}|^2, \tag{4.14b}$$

$$\frac{d\sigma_{LR}}{d\cos\theta} = \frac{\lambda_{LR}^{\frac{1}{2}}}{128\pi s}\left(|\langle{-}{+}\rangle_{LR}|^2 + |\langle{+}{-}\rangle_{RL}|^2\right). \tag{4.14c}$$

Note that σ_{LR} and σ_{RL} are not physically distinguishable in this case, unlike for e^+e^- annihilation.

4.3.3 $e^+e^- \to \tilde{\chi}_i^+\tilde{\chi}_j^-$

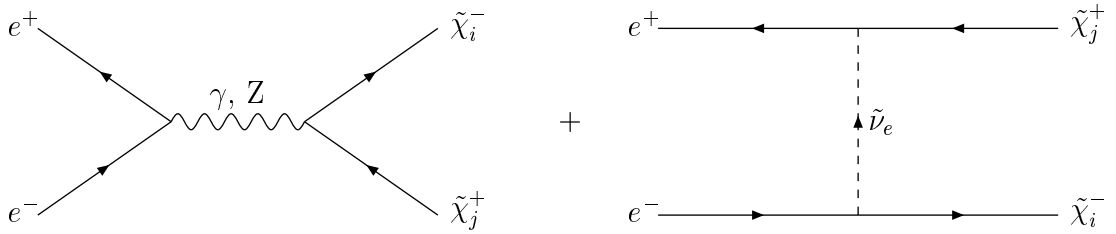

Figure 4.4: Diagrams for $e^-e^+ \to \tilde{\chi}_i^-\tilde{\chi}_j^+$

Fig. 4.4 shows the s- and t-channel contributions to $\tilde{\chi}_i^-\tilde{\chi}_j^+$ production. After a suitable Fierz-rearrangement of the $\tilde{\nu}$ contribution, as described in App. C.1.5, the invariant amplitude can be written as

$$\mathcal{M}_{ij}^{\sigma_1\sigma_2,\lambda_1\lambda_2} = \frac{-e^2}{s}\overline{v}\left(p_2,\sigma_2\right)\gamma_\mu P^\alpha u\left(p_1,\sigma_1\right) Q_{\alpha\beta}^{ij}\overline{u}_i\left(k_1,\lambda_1\right)\gamma^\mu P^\beta v_j\left(k_2,\lambda_2\right), \tag{4.15}$$

where bilinear charges $Q_{\alpha\beta}^{ij}$ have been introduced as (with $x = \sin^2\theta_W$)

$$Q_{LL}^{11} = 1 + \frac{D_Z(2x-1)}{2x(1-x)}\left(x - \frac{3}{4} - \frac{1}{4}\cos 2\phi_L\right), \tag{4.16a}$$

$$Q_{RR}^{11} = 1 + \frac{D_Z}{1-x}\left(x - \frac{3}{4} - \frac{1}{4}\cos 2\phi_R\right), \tag{4.16b}$$

$$Q_{LR}^{11} = 1 + \frac{D_Z(2x-1)}{2x(1-x)}\left(x - \frac{3}{4} - \frac{1}{4}\cos 2\phi_R\right) + \frac{sD_t^{\tilde{\nu}}}{4x}(1+\cos 2\phi_R), \tag{4.16c}$$

$$Q_{RL}^{11} = 1 + \frac{D_Z}{1-x}\left(x - \frac{3}{4} - \frac{1}{4}\cos 2\phi_L\right); \tag{4.16d}$$

$$Q_{LL}^{22} = 1 + \frac{D_Z(2x-1)}{2x(1-x)}\left(x - \frac{3}{4} + \frac{1}{4}\cos 2\phi_L\right), \tag{4.17a}$$

$$Q_{RR}^{22} = 1 + \frac{D_Z}{1-x}\left(x - \frac{3}{4} + \frac{1}{4}\cos 2\phi_R\right), \tag{4.17b}$$

$$Q_{LR}^{22} = 1 + \frac{D_Z(2x-1)}{2x(1-x)}\left(x - \frac{3}{4} + \frac{1}{4}\cos 2\phi_R\right) + \frac{sD_t^{\tilde{\nu}}}{4x}(1-\cos 2\phi_R), \tag{4.17c}$$

$$Q_{RL}^{22} = 1 + \frac{D_Z}{1-x}\left(x - \frac{3}{4} + \frac{1}{4}\cos 2\phi_L\right); \tag{4.17d}$$

$$Q_{LL}^{12} = \left(Q_{LL}^{21}\right)^\star = \frac{D_Z(2x-1)}{8x(1-x)}\sin 2\phi_L e^{-i\beta_L}, \tag{4.18a}$$

$$Q_{RR}^{12} = \left(Q_{RR}^{21}\right)^\star = \frac{D_Z}{4(1-x)}\sin 2\phi_R e^{i(\gamma_1-\beta_R-\gamma_2)}, \tag{4.18b}$$

$$Q_{LR}^{12} = \left(Q_{LR}^{21}\right)^\star = \left(\frac{D_Z(2x-1)}{8x(1-x)} - \frac{sD_t^{\tilde\nu}}{4x}\right)\sin 2\phi_R e^{i(\gamma_1-\beta_R-\gamma_2)}, \tag{4.18c}$$

$$Q_{RL}^{12} = \left(Q_{RL}^{21}\right)^\star = \frac{D_Z}{4x(1-x)}\sin 2\phi_L e^{-i\beta_L}. \tag{4.18d}$$

Here the sneutrino propagator $D_t^{\tilde\nu}$ is defined analogously to the neutralino propagators in Eq. 4.6. Using the results of App. C.1.3, one finds for the generic helicity amplitude (θ is the angle between the momenta of the incident e^- and the produced $\tilde\chi^-$)

$$\mathcal{M}_{ij}^{\sigma_1,-\sigma_1;\lambda_1\lambda_2} = \langle\sigma_1,-\sigma_1;\lambda_1\lambda_2\rangle ij = \frac{-e^2}{2}\sum_\beta \Big\{\lambda_1\delta_{\lambda_1,\lambda_2}\sqrt{1-\eta_{\beta\lambda_1}^2}\sin\theta + \delta_{\lambda_1,-\lambda_2}\sqrt{(1+\beta\lambda_1\eta_{\beta\lambda_1})(1+\beta\lambda_1\eta_{-\beta\lambda_1})}(1+\lambda_1)\Big\}, \tag{4.19}$$

where the kinematical functions $\eta_{\beta\lambda_1}$ are defined in Eq. C.1.3. The unpolarized cross sections can be computed from Eq. 4.19 by averaging over initial helicities and summing over the final ones. Including the phase space factor one finds

$$\frac{d\sigma_{ij}}{d\cos\theta} = \frac{\pi\alpha^2}{8s}\lambda_{ij}^{\frac{1}{2}}\left\{\left[(1-\Delta_{ij}^2)+\lambda_{ij}\cos^2\theta\right]Q_1^{ij} + 8\mu_i\mu_j Q_2^{ij} + 2\lambda_{ij}^{\frac{1}{2}}\cos\theta Q_3^{ij}\right\}, \tag{4.20}$$

where $4\pi\alpha = e^2$, $\mu_i = m_{\tilde\chi_i^\pm}/\sqrt{s}$ and $\Delta_{ij} = \mu_i^2 - \mu_j^2$. The new quartic charges are given by

$$Q_1^{ij} = \left|Q_{++}^{ij}\right|^2 + \left|Q_{+-}^{ij}\right|^2 + \left|Q_{-+}^{ij}\right|^2 + \left|Q_{--}^{ij}\right|^2, \tag{4.21a}$$

$$Q_2^{ij} = \mathcal{R}\mathrm{e}\left[Q_{++}^{ij}Q_{+-}^{ij\star} + Q_{--}^{ij}Q_{-+}^{ij\star}\right], \tag{4.21b}$$

$$Q_3^{ij} = \left|Q_{++}^{ij}\right|^2 - \left|Q_{+-}^{ij}\right|^2 - \left|Q_{-+}^{ij}\right|^2 + \left|Q_{--}^{ij}\right|^2. \tag{4.21c}$$

4.3.4 $e^+e^- \to \tilde\chi_i^0\tilde\chi_j^0$

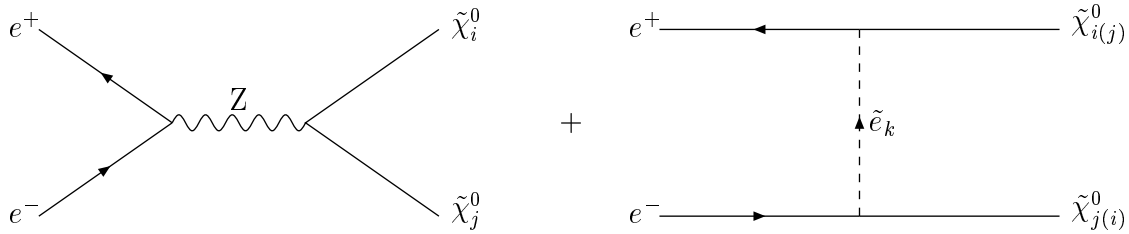

Figure 4.5: Diagrams for $e^-e^+ \to \tilde\chi_i^0\tilde\chi_j^0$

In Fig. 4.5 the s- and t-channel contributions to $\tilde\chi_i^0\tilde\chi_j^0$ production are shown, the additional, destructively interfering u-channel diagram is indicated by the indices in parentheses. Applying a Fierz rearrangement on both the t- and u-channel diagram and re-ordering the u-channel amplitude, the invariant amplitude reads

$$\mathcal{M}_{ij}^{\sigma_1\sigma_2,\lambda_1\lambda_2} = \frac{e^2}{s}\overline{v}(p_2,\sigma_2)\gamma_\mu P^\alpha u(p_1,\sigma_1)\,Q_{\alpha\beta}^{ij}\overline{u}_i(k_1,\lambda_1)\gamma^\mu P^\beta v_j(k_2,\lambda_2). \tag{4.22}$$

Here, the bilinear charges $Q^{ij}_{\alpha\beta}$ are given ($x = \sin^2\theta_W$) as

$$Q^{ij}_{LL} = \frac{D_Z}{2x(1-x)}(2x-1)Z^\star_{ij} - sD^L_u g_{Lij}, \tag{4.23a}$$

$$Q^{ij}_{RR} = -\frac{D_Z}{1-x}Z_{ij} - sD^R_u g^\star_{Lij}, \tag{4.23b}$$

$$Q^{ij}_{LR} = -\frac{D_Z}{2x(1-x)}(2x-1)Z_{ij} + sD^L_t g^\star_{Lij}, \tag{4.23c}$$

$$Q^{ij}_{RL} = \frac{D_Z}{1-x}Z^\star_{ij} + sD^R_t g_{Rij}; \tag{4.23d}$$

with

$$g_{Lij} = \frac{1}{4x}\left(N_{2i} + \tan\theta_W N_{1i}\right)^\star \left(N_{2j} + \tan\theta_W N_{1j}\right), \tag{4.24a}$$

$$g_{Rij} = \frac{1}{1-x}N^\star_{1i}N_{1j}. \tag{4.24b}$$

The selectron propagators are defined as

$$D^{L,R}_{t,u} = \frac{1}{(t,u) - m^2_{\tilde{e}_{L,R}}}. \tag{4.25}$$

Since this amplitude has the same structure as the amplitude for $\tilde{\chi}^-_i\tilde{\chi}^+_j$ production, see Eq. 4.15, the result in Eq. 4.19 from this calculation can be transfered directly; only the bilinear charges have to replaced. Also the result for the unpolarized, total cross section as in Eq. 4.20 can be transfered , but a statistical factor has to be included, so that

$$\frac{d\sigma_{ij}}{d\cos\theta} = 2^{-\delta_{ij}}\frac{\pi\alpha^2}{8s}\lambda^{\frac{1}{2}}_{ij}\left\{\left[(1-\Delta^2_{ij}) + \lambda_{ij}\cos^2\theta\right]Q^{ij}_1 + 8\mu_i\mu_j Q^{ij}_2 + 2\lambda^{\frac{1}{2}}_{ij}\cos\theta Q^{ij}_3\right\}. \tag{4.26}$$

Of course, now the bilinear charges of Eqs. 4.23 have to be used when evaluating the quartic charges defined in Eqs. 4.21.

4.4 Perturbative results for total cross sections

The results presented in the previous subsections allow the exact (tree-level) calculation of the phase-dependences of the selectron, neutralino, and chargino production cross sections. Similar to the results for the chargino and neutralino loop contributions to a_μ and d_e, the results offer little insight into the explicit dependences of the cross sections on SUSY input parameters, i.e. they neither indicate in *which* production mode a strong dependence on the phases is to be expected, nor *where* such a strong dependence may originate from. To obtain such predictions on phase-dependences, the next sections are devoted to a perturbative analysis of the cross sections calculated above. Within this analysis the approximative diagonalization of the neutralino and chargino mass matrices as presented in Sec. 2.3.2 and 2.3.3 is used. Furthermore all kinematical and "SM" factors are dropped wherever doing so is convenient for a more compact presentation. More details on the general perturbative treatment of cross sections may be found in App. C.4.

4.4.1 $e^{\pm}e^{-} \to \tilde{e}_i^{-}\tilde{e}_j^{\pm}$

Since the cross sections for $\tilde{e}_i^{-}\tilde{e}_j^{+}$ and $\tilde{e}_i^{-}\tilde{e}_j^{-}$ production are of very similar structure, see Eqs. 4.8 and 4.13, I will treat both sets of cross sections together. First of all, due to $U_Y(1)$ interactions all six modes receive $\mathcal{O}(M_Z^0)$ contributions from the exchange of the bino-like neutralino. Contrarily, only the $\tilde{e}_L$ pair production modes contain $SU(2)$ interactions also and hence the exchange of a wino-like neutralino also contributes at order M_Z^0. However, all these contributions by themselves do not lead to a phase-dependence of the cross sections at order M_Z^0. The only phase-dependence that can contribute to cross sections at $\mathcal{O}(M_Z^0)$ occurs when $U_Y(1)$ and $SU(2)$ contributions can interfere; this is only possible for the $\tilde{e}_L^{-}\tilde{e}_L^{-}$ mode.[3] For this exquisite mode the cross section is sensitive to the relative phase between M_1 and M_2 independently from $\tan\beta$.
All other cross sections show sensitivity to phases only at $\mathcal{O}(M_Z^2)$. These phase-dependences basically arise from three sources: first from the exchange of heavier, Higgsino-like neutralinos which develop gaugino components at $\mathcal{O}(M_Z)$, secondly from the $\mathcal{O}(M_Z^2)$ corrections to the gaugino components of the gaugino-like neutralinos. Finally, the $\mathcal{O}(M_Z^2)$ shifts $\delta m^{(2)}_{\tilde{\chi}_i^0}$ of the neutralino masses may also contribute to the phase-dependence of the cross sections. The presence of the second source explains why the second order corrections in Eq. 2.42 and 2.43 have been included to the perturbative treatment of Neutralino mixing in Sec. 2.3.3. The effects from the shifts $\delta m^{(2)}_{\tilde{\chi}_i^0}$ are either direct (if the physical masses are allowed to vary with phases[4]) or indirect (if physical masses are kept fixed, in which case the absolute values of the input parameters have to be varied along with the phases). In the second case the variation of the SUSY input parameters $|M_1|$, M_2, and $|\mu|$ is of order M_Z^2 (see App. A.4) and hence the changes of the eigenstates $\tilde{\chi}_i^0$ due to these variations are at least $\mathcal{O}(M_Z^3)$. For all modes this change generates additional phase-dependences which are suppressed by two additional powers of M_Z relative to the leading phase-dependence, hence such indirect effects can safely be ignored in the following.
Since $\tilde{e}_R^{-}$ does not have $SU(2)$ interactions, $\sigma\left(\tilde{e}_R^{-}\tilde{e}_R^{\pm}\right)$ are at $\mathcal{O}(M_Z^2)$ only sensitive to the phase combination $\phi_\mu + \phi_1$, whereas the other modes are also sensitive to ϕ_1 and ϕ_μ.[5] Furthermore it should be remembered that the matrix elements for both diagonal $\tilde{e}^{-}\tilde{e}^{+}$ production modes receive large, phase-independent contributions from γ and Z exchange in the s-channel. In fact, the phase-dependence of these two modes arising from interference terms between s- and t-channel is diluted by the gauge-contributions.
The phase-dependence of the selectron production cross sections for fixed physical neutralino masses[6] is summarized in Tab. 4.1. Here the coefficients of the various phase-dependent terms that can appear relative to the leading (phase-independent) contribution to the cross section are shown. Furthermore I have assumed $|\mu| \gg |M_1|,\ |M_2|$ and omitted both kinematical and numerical factors, as well as factors involving the weak mixing angle. Nevertheless this overview can be used to draw some conclusions on the phase-dependences

[3] For the $\tilde{e}_L^{-}\tilde{e}_L^{+}$ mode the relevant neutralino function perturbatively reads $N_{LL}(s,t/u) \propto D^1_{t(u)} + D^2_{t(u)}$, whereas $M_{LL}(s,t/u) \propto M_1 D^1_{t(u)} + M_2 D^2_{t(u)}$ is involved in $\tilde{e}_L^{-}\tilde{e}_L^{-}$ production. That explains why the $U_Y(1)$-$SU(2)$ interference, although present, does not lead to a phase-dependence at $\mathcal{O}(M_Z^0)$ in $\tilde{e}_L^{-}\tilde{e}_L^{+}$ production.

[4] The phase-dependence then enters via $D^i_{t(u)} \propto D^i_{t(u)} - 2m_{\tilde{\chi}_i^0}\delta m^{(2)}_{\tilde{\chi}_i^0}\left[D^i_{t(u)}\right]^2$, where the propagators on the right hand side are to be evaluated for $m_{\tilde{\chi}_i^0} \equiv m^{(0)}_{\tilde{\chi}_i^0}$.

[5] Again the convention $\phi_2 \equiv 0$ is invoked.

[6] Only phase-dependences that arise from coupling factors are tabulated here.

	$\cos(\phi_\mu+\phi_1)$	$\cos\phi_\mu$	$\cos\phi_1$
$\tilde{e}_L^-\tilde{e}_L^+$	$\sin 2\beta\frac{M_Z^2\lvert M_1\rvert}{M_2^2\lvert\mu\rvert}$	$\sin 2\beta\frac{M_Z^2}{M_2\lvert\mu\rvert}$	$\frac{M_Z^2\lvert M_1\rvert}{M_2\lvert\mu\rvert^2}$
$\tilde{e}_L^-\tilde{e}_R^+$	$\sin 2\beta\frac{M_Z^2}{\lvert M_1\mu\rvert}$	$\sin 2\beta\frac{M_Z^2}{M_2\lvert\mu\rvert}$	$\frac{M_Z^2 M_2}{\lvert M_1\rvert\lvert\mu\rvert^2}$
$\tilde{e}_R^-\tilde{e}_R^+$	$\sin 2\beta\frac{M_Z^2\lvert M_1\rvert}{\lvert\mu\rvert^3}$	none	none
$\tilde{e}_L^-\tilde{e}_L^-$	$\sin 2\beta\frac{M_Z^2}{M_2\lvert\mu\rvert}$	$\sin 2\beta\frac{M_Z^2}{M_2\lvert\mu\rvert}$	$\frac{\lvert M_1\rvert}{M_2}$
$\tilde{e}_L^-\tilde{e}_R^-$	$\sin 2\beta\frac{M_Z^2\lvert M_1\rvert}{M_2^2\lvert\mu\rvert}$	$\sin 2\beta\frac{M_Z^2}{M_2\lvert\mu\rvert}$	$-\frac{M_Z^2\lvert M_1\rvert}{M_2\lvert\mu\rvert^2}$
$\tilde{e}_R^-\tilde{e}_R^-$	$\sin 2\beta\frac{M_Z^2}{\lvert M_1\mu\rvert}$	none	none

Table 4.1: Phase-dependence of the cross sections for selectron pair production in e^+e^- as well as e^-e^- annihilation for fixed physical neutralino masses. Each entry gives the dependence of the coefficient of the indicated (combination of) phase(s) on the supersymmetric parameters relative to the leading (phase–independent) contribution to this cross section, under the assumption $|M_1| < M_2 \ll |\mu|$. "None" means that the corresponding term does not exist to $\mathcal{O}(M_Z^2)$.

of the cross sections. First, all dependences on the phase ϕ_μ shown in the second and third column of Tab. 4.1 vanish like $1/\tan\beta$ for large values of $\tan\beta$.[7] The reason is that the dependence on this phase in the neutralino mass matrix could be rotated[8] into the off-diagonal gaugino-Higgsino entries $\propto \cos\beta$. However, the dependence of the relative phase between the two soft gaugino masses, ϕ_1 in our convention, does not vary with $\tan\beta$, see the fourth column of Tab. 4.1. The $\tilde{e}_L^-\tilde{e}_L^-$ mode contains additional phase-dependences $\propto \cos(\phi_1-\phi_\mu)$ and $\propto \cos(2\phi_1+\phi_\mu)$.[9] The coefficients of these phase-dependences are $|M_1|M_Z^2\sin 2\beta/|\mu|^3$ and $|M_1|^2M_Z^2\sin 2\beta/(|\mu|^3M_2)$, respectively. Due to the additional suppression $\propto 1/|\mu|^2$ relative to the coefficients of $\cos(\phi_\mu+\phi_1)$ and $\cos\phi_\mu$, these phase-dependences are neglected in the following.
Second, with the exception of $\tilde{e}_L^-\tilde{e}_L^-$ mode, all phase-dependence vanishes as $|\mu|\to\infty$, but the $|\mu|$-dependence varies for different modes. In particular, the phase-dependence of the diagonal mode $\tilde{e}_R^-\tilde{e}_R^-$ vanishes $\propto 1/|\mu|^3$ for large $|\mu|$, whereas all other cross sections receive phase-dependent contributions that merely fall as $1/|\mu|$; however, for $\tan\beta\to\infty$ the $|\mu|$-dependence of the total sensitivity becomes stronger, as can be seen in the last column. In most cases the leading phase-dependence derives from the exchange of the lighter, gaugino-like neutralinos.[10] The exception is the $\tilde{e}_R^-\tilde{e}_R^-$ mode, where the exchange of the heavier, Higgsino-like neutralinos contributes dominantly at the same order as the

[7] $\sin 2\beta = \frac{2}{\tan\beta}\frac{1}{1+1/\tan\beta^2}$.

[8] This rotation does not introduce any phase in those parts of $f\tilde{f}\tilde{\chi}$ vertices that come from gauge interactions, but *does* introduce a phase in the Yukawa contributions to these vertices. Recall that these Yukakwa contributions can be ignored when calculating cross sections, but have to be kept when computing leptonic dipole moments. This explains why the ϕ_μ dependence of $(d_e)_{\rm SUSY}$ and $(a_\mu)_{\rm SUSY}$ is not suppressed at large $\tan\beta$.

[9] In a convention with $\phi_2 \neq 0$, the rephasing invariance of the arguments is restored. They read $(\phi_\mu+\phi_1)-(\phi_2-\phi_1)$ and $(\phi_\mu+\phi_2)-(\phi_1-\phi_2)$.

[10] More precisely, for the modes $\tilde{e}_L^-\tilde{e}_L^+$, $\tilde{e}_L^-\tilde{e}_L^-$, and $\tilde{e}_L^-\tilde{e}_R^-$ the contributions from gaugino exchange is dominant. Within the modes $\tilde{e}_R^-\tilde{e}_R^+$ and $\tilde{e}_L^-\tilde{e}_R^+$ gaugino and Higgsino exchange are of same size.

gaugino exchanges do in the other modes with phase-dependences at $\mathcal{O}(M_Z^2)$.
Clearly, as already observed by [96], the $\tilde{e}_L^-\tilde{e}_L^-$ mode will reveal the strongest phase-dependence of all $\tilde{e}^-\tilde{e}^-$ channels, and indeed of all selectron production channels, since it already occurs at $\mathcal{O}(M_Z^0)$, as noted earlier. The phase-dependent terms in $\tilde{e}_L^-\tilde{e}_L^+$ and $\tilde{e}_L^-\tilde{e}_R^+$ production are of similar size. For our choice of parameters the second mode is preferable, since it is accessible at lower energies, and since the cross section near threshold scales like $\lambda^{\frac{1}{2}}$ rather than $\lambda^{\frac{3}{2}}$. The two remaining modes in $\tilde{e}^-\tilde{e}^-$ pair production are also of similar size. For these two modes the better accessibility of the $\tilde{e}_R^-\tilde{e}_R^-$ mode goes in hand with a $\lambda^{\frac{1}{2}}$-scaling of the cross section near threshold compared to s$\lambda^{\frac{3}{2}}$-scaling of the $\tilde{e}_L^-\tilde{e}_R^-$ mode. The only argument in favor of the second mode is the presence of $\tan\beta$ independent terms which will give a sizeable phase-dependence even for large $\tan\beta$. Obviously, the $\tilde{e}_R^-\tilde{e}_R^+$ mode, at least within the reliability of the perturbative treatment, is the most disfavored mode, as the phase-dependence scales like $1/|\mu|^3$ and decouples for large $\tan\beta$. Finally, the relative importance of phase-sensitive and phase-insensitive terms in most selectron production modes does not strongly depend on the beam energy.[11] Therefore the best statistical accuracy for the determination of the relevant phases can be expected when the beam is chosen such that the cross section being investigated is maximal.
So far I have only studied phase-dependences from coupling effects. This corresponds to keeping the physical neutralino masses fixed and varying the parameters $|M_1|$, $|M_2|$, and $|\mu|$ along with the phases. As shown above, this variation of the three parameters affects the cross sections only at $\mathcal{O}(M_Z^2)$ relative to the leading term. If the input parameters are held fixed instead, the physical neutralino masses will vary at $\mathcal{O}(M_Z^2)$ and hence lead to additional phase-dependences originating from the t-(u-)propagators. Since the exchange of gaugino-like states already gives contributions at $\mathcal{O}(M_Z^0)$ for all modes[12] the masses of the two lighter states are of particular interest. Obviously, the $\tilde{e}_L^-\tilde{e}_L^-$ mode with phase-dependence at $\mathcal{O}(M_Z^0)$ only receives additional phase-dependent contributions at subleading order M_Z^2. The relevant $\mathcal{O}(M_Z^2)$ shifts are given in Eqs. 2.40. The phase-dependences from these two shifts, as relevant for the remaining five modes, vanish also like $\propto 1/\tan\beta$ for large $\tan\beta$, but only drop like $1/|\mu|$ for large $|\mu|$. This directly implies that they dominate the total phase-dependence of the $\tilde{e}_R^-\tilde{e}_R^+$ mode. For the other modes, the dependence on $\cos(\phi_\mu + \phi_1)$ and $\cos\phi_\mu$ deriving from the variation of the physical masses of the gaugino-like neutralinos is qualitatively the same as shown in the second and third columns of Tab. 4.1, if factors $|M_1|/M_2 \approx \mathcal{O}(1)$ are ignored. Therefore a more detailed analysis, including the in-cooperation of previously dropped factors, is required to decide which source —variation of kinematical masses or coupling effects— dominates the phase-dependence. Such an analysis, although it has been performed in course of the work presented here, depends strongly on the chosen input values for the SUSY parameters as well as on $\sqrt{s}$ and hence is of little advantage for a deeper understanding of the balance between kinematical and coupling effects. Hence it is not shown or discussed here.

[11] At least, if terms of same order in M_Z^2 are compared.

[12] The exchange of Higgsino-like neutralinos requires gaugino components of these neutralinos. Such components are first generated in $\mathcal{O}(M_Z^1)$ corrections. Hence the contributions from Higgsino exchange are of order M_Z^2 and the shifts $\delta m_{3/4}^{(2)}$ lead to $\mathcal{O}(M_Z^4)$ effects.

4.4.2 $e^+e^- \to \tilde{\chi}_i^+\tilde{\chi}_j^-$

The next cross sections to be studied are the ones for $\tilde{\chi}_i^-\tilde{\chi}_j^+$ pair production. Using the convention $\phi_2 \equiv 0$, the only phase entering the chargino mass matrix is ϕ_μ and all phase-dependence of the chargino production modes is due only to this phase. As it already was found in Sec. 3.3.2, ϕ_μ is strongly constrained, the phase-dependences in all chargino production modes are expected to be rather small. Nevertheless, for reasons of completeness these production channels are discussed here.
First of all, both diagonal modes $\tilde{\chi}_1^-\tilde{\chi}_1^+$ and $\tilde{\chi}_2^-\tilde{\chi}_2^+$ already receive contributions from s- and t-channel diagrams at order M_W^0; but these contributions are all phase-independent. The off-diagonal mode $\tilde{\chi}_1^-\tilde{\chi}_2^+$ requires non-vanishing gaugino-Higgsino mixing and therefore starts directly at $\mathcal{O}(M_W^2)$. For all three modes, phase-dependences that may arise from an adjustment of the parameters $|\mu|$ and M_2 while keeping the physical masses fixed are of order M_W^2 relative to the leading phase-dependence.[13] Therefore the discussion can be focused on the phase-dependences from couplings, i.e. effects from the quartic charges in appearing in Eqs. 4.20 and 4.21, and kinematical effects, i.e. effects from the variation of the physical chargino masses in the kinematical functions of Eq. 4.20. The phase-dependent

	Q_1, Q_3	Q_2
$\tilde{\chi}_1^-\tilde{\chi}_1^+$	$\sin 2\beta \frac{M_W^2}{\lvert\mu\rvert^2}\frac{M_2}{\lvert\mu\rvert}$	$\sin 2\beta \frac{M_W^2}{\lvert\mu\rvert^2}\frac{M_2}{\lvert\mu\rvert}\frac{M_2^2}{s}$
$\tilde{\chi}_1^-\tilde{\chi}_2^+$	$\sin 2\beta \frac{M_2}{\lvert\mu\rvert}$	$\sin 2\beta \frac{M_2\lvert\mu\rvert}{s}$
$\tilde{\chi}_2^-\tilde{\chi}_2^+$	$\sin 2\beta \frac{M_W^2}{\lvert\mu\rvert^2}\frac{M_2}{\lvert\mu\rvert}$	$\sin 2\beta \frac{M_W^2}{s}\frac{M_2}{\lvert\mu\rvert}$

Table 4.2: Phase-dependences of the cross sections for chargino pair production for fixed physical neutralino masses ("coupling effects"). The second column displays phase-dependences from Q_1 and Q_3, the contributions from Q_2 are already multiplied with $\mu_i\mu_j$. All contributions are proportional to $\cos\phi_\mu$ and have been normalized to the leading phase-independent contribution of the cross section.

terms that are found in the quartic charges of Eq. 4.21 are summarized in Tab. 4.2; all kinematical and numerical factors have been neglected. Nevertheless some conclusions about the sensitivities to ϕ_μ can be drawn. First, all phase-dependences are proportional to $\sin 2\beta$ and hence vanish like $1/\tan\beta$ for large $\tan\beta$. Second, the phase-dependences from Q_1 and Q_3 are at least $\propto 1/|\mu|$, the diagonal modes contain an additional suppression factor $M_W^2/|\mu|^2$, and all sensitivities to ϕ_μ from Q_1 and Q_3 hence vanish in the limit of large[14] $|\mu|$. Concerning the contributions from Q_2 including the reduced masses in the diagonal modes generates additional suppression factors of M_2^2/s and $|\mu|^2/s$, respectively.[15] As both factors are smaller than one in the physical region ($\sqrt{s} > M_2 + |\mu|$) the sensitivity of the diagonal modes is not increased. On the contrary, even after including the factor $M_2|\mu|/s$,

[13] However, note that the adjustment of $|\mu|$ leads to a dependence of the chargino modes on the relative phase between M_1 and μ, see Eqs. A.28. But such an indirect dependence on ϕ_1 is of subleading order.

[14] If $|\mu|$ gets too big, the production modes containing at least one heavy chargino are above threshold and vanish kinematically. Therefore, for this part of the discussion, $\sqrt{s}$ is assumed to be a completely free parameter.

[15] An explicit calculation shows $Q_1^{ii} \propto Q_2^{ii}$.

the quartic charge Q_2 yields a somewhat larger phase-sensitivity for the off-diagonal mode than do the corresponding contributions[16] from Q_1 and Q_3. In particular, if $|\mu|$ is increased while remaining in the physical region this sensitivity even increases linearly with $|\mu|$. Altogether the $\tilde{\chi}_1^- \tilde{\chi}_2^+$ mode displays the strongest sensitivity to ϕ_μ. This sensitivity is only apparently independent from $M_W^2/|\mu|^2$ as the production cross section itself vanishes for $M_W^2/|\mu|^2 \to 0$. It is due to the fact that phase-independent and phase-dependent terms are both of $\mathcal{O}(M_W^2)$. In the case of the diagonal modes, the phase-independent contributions already start at $\mathcal{O}(M_W^0)$. This fact explains the small, relative phase-dependences when the $\mathcal{O}(M_W^2)$ phase-dependent terms are normalized to the former contributions.
As long as only phase-dependences from coupling factors are concerned, the off-diagonal mode appears to be preferable to the diagonal modes. However, the attractivity of the $\tilde{\chi}_1^- \tilde{\chi}_2^+$ mode is decreased by its cross section. First, the presence of a heavy chargino might limit the accessibility of this mode in the first stage of an FLC. Secondly, even if the mode is accessible, the cross section is expected to be rather small[17], and accumulating statistics for an accurate determination might turn out to be difficult.
So far, I have only investigated phase-dependences in $\tilde{\chi}_i^- \tilde{\chi}_j^+$ production that arise from coupling effects, i.e. phase-dependences that are present even when the kinematical masses are fixed and the parameters are varied along with the phases. If the absolute values of the parameters are kept fixed and the kinematical masses are allowed to vary along with the phases, additional phase-dependences arise from the shifts $\delta m^2_{\tilde{\chi}_i^\pm}$ via the kinematical functions in Eq. 4.20. However, these shifts in Eqs. 2.35 are only relevant for the diagonal modes. Concerning the off-diagonal mode these shifts can be neglected as they only lead to relatively suppressed effects of order M_W^4, when inserted into the kinematics of a $\mathcal{O}(M_W^2)$ cross section. The phase-dependent parts of the shifts of the squared masses are identical (in absolute value) and basically read as $M_W^2 M_2 \sin 2\beta \cos\phi_\mu/|\mu|$. This shows that these effects per se vanish like $1/|\mu|$ and $1/\tan\beta$ for large $|\mu|$ and large $\tan\beta$, respectively. However, the shifts directly enter the "diagonal" cross sections through the reduced masses μ_i and in the kinematical functions λ_{ii}, hence the final order of magnitude of effects from these shifts is determined by these functions. The simplest example for a kinematical function is $\lambda_{ii}^{\frac{1}{2}}$, which enters the cross section already as an overall factor, see Eq. 4.20. For this example the "complete" phase-dependence due to mass shifts reads

$$\frac{1}{\sqrt{1-4\mu_i^2}} \frac{M_W^2 M_2}{s|\mu|} \sin 2\beta \cos\phi_\mu. \tag{4.27}$$

This example already illustrates the two important features of the phase-dependent terms from mass shifts in chargino pair production. First, the factor $1/\sqrt{1-4\mu_i^2}$ causes a large enhancement of such contributions near threshold. Secondly, the factor $1/s$ reduces them significantly far above threshold. The specifics of this simple example already indicate that a prediction of whether kinematical or coupling effects dominate again strongly depends on the concrete choices for the SUSY input parameters and $\sqrt{s}$. Hence, such an analysis, although possible, leads only to $\sqrt{s}$-dependent predictions for selected parameter points and is of no general use. Nevertheless, it should be emphasized that both diagonal modes may develop a strong dependence on ϕ_μ close to threshold due to kinematical effects.

[16] Here the explicit calculation reveals that Q_1^{12} and Q_2^{12} are independent from each other.

[17] This mode only contains M_W^2-contributions as discussed above, hence the corresponding cross section is suppressed.

4.4.3 $e^+e^- \to \tilde{\chi}^0_i\tilde{\chi}^0_j$

The discussion of phase-dependences of cross sections in a perturbative regime now concludes with an investigation of the neutralino production modes. It is a straightforward conclusion that out of the 10 distinct cross sections for neutralino pair production in e^+e^- annihilation, $\sigma_{ij} \equiv \sigma\left(\tilde{\chi}^0_i\tilde{\chi}^0_j\right)$, only four receive $\mathcal{O}(M_z^0)$ corrections. The cross sections σ_{11}, σ_{12}, σ_{22} describing the production of two gaugino like neutralinos receive contributions from selectron exchange in the t- and u-channel, while σ_{34} receives contributions from Z exchange in the s-channel. The cross sections σ_{33} and σ_{44} describing the production of two equal Higgsino-like states receive non-vanishing contributions at $\mathcal{O}(M_Z^4)$ only, whereas the cross sections for the production of one Higgsino-like and one gaugino-like neutralino start at $\mathcal{O}(M_Z^2)$. This first classification of the cross sections for neutralino production can most easily be understood in a diagrammatical approach as described in App.C.4.2.
Only σ_{12} has sensitivity to some phase (in this case the relative phase between M_1 and M_2) at order M_Z^0. All other cross sections are only sensitive to phases at order M_Z^2 or even M_Z^4. The strong phase sensitivity of σ_{12} can be traced back to the Q_2^{12}-term in Eq. 4.26. It derives from the fact [84] that the production of two Majorana fermions is P-waved suppressed near threshold if they have the same relative CP-phase, whereas any difference in this phase leads to an S-wave contribution to the cross section. This effect can be probed with optimal statistical significance rather close to the threshold, in this case for $\sqrt{s}$ not too much above $|M_1| + M_2$.
For an observation of phase-dependent terms the production of mixed "gaugino-Higgsino" final states should be most suitable since here phase-dependent and phase-independent contributions to the cross sections σ_{13}, σ_{14}, σ_{23}, and σ_{24} both start at $\mathcal{O}(M_Z^2)$. Also, the cross sections for equal Higgsino-like final states, σ_{33} and σ_{44}, only contain phase-independent and phase-dependent terms of same order M_Z; but these modes are clearly disfavored for an observation of phase-dependent contributions as the cross sections are of $\mathcal{O}(M_Z^4)$ and hence tiny. Accumulating statistics for an accurate determination within these modes appears to be almost impossible. Furthermore, within the parameter choices of scenarios B2 and B3 they lie above the discovery limit of a first stage FLC.[18] The two diagonal, gaugino-like modes also are of less interest for an observation of phase-dependent contributions, as the phase-independent contributions to σ_{11} and σ_{22} already are present in $\mathcal{O}(M_Z^0)$ whereas phase-dependent contributions only start at $\mathcal{O}(M_Z^2)$. Hence observing a "signal" (phase-dependent terms) of $\mathcal{O}(M_Z^2)$ in a "background" (phase-independent terms) of $\mathcal{O}(M_Z^0)$ is a tedious task. The same argument holds for σ_{34}. Furthermore, under the given assumptions, $\tilde{\chi}^0_1$ is the LSP and the production of a $\tilde{\chi}^0_1$-pair cannot be observed at all. Therefore the further discussion of phase-dependences in neutralino pair production is restricted to the mixed "gaugino-Higgsino" final states.
Firstly, it has to be noticed that the two Higgsino-like neutralinos are closely mass degenerated within the reliability of our perturbative treatment. This makes it very difficult to experimentally distinguish between the production of $\tilde{\chi}^0_3$ and $\tilde{\chi}^0_4$. Therefore in the following discussion these two Higgsino-like-states always summed over, i.e. the cross sections discussed are

$$\sigma_{i\tilde{H}} \equiv \sigma_{i3} + \sigma_{i4}, \quad i = 1, 2. \tag{4.28}$$

As all kinematical functions in Eq. 4.26 are identical under the assumption $m_{\tilde{\chi}^0_3} \equiv m_{\tilde{\chi}^0_4}$

[18] Within B2 they are even out of reach for foreseen upgrades of an FLC, which typically assume the achievement of $\sqrt{s} = 800\text{GeV}$ in the second stage of operation.

	$\sigma_{1\tilde{H}}$		$\sigma_{2\tilde{H}}$	
$\cos(\phi_\mu + \phi_1)$	$\frac{\sin 2\beta \lvert M_1\rvert}{\lvert\mu\rvert}$	$\frac{\sin 2\beta \lvert M_1\rvert \lvert\mu\rvert}{s}$	$\frac{\sin 2\beta \lvert M_1\rvert}{\lvert\mu\rvert}$	$\frac{\sin 2\beta \lvert M_1\rvert M_2^2}{\lvert\mu\rvert s}$
$\cos\phi_\mu$	$\frac{\sin 2\beta M_2}{\lvert\mu\rvert}$	$\frac{\sin 2\beta \lvert M_1\rvert^2 M_2}{\lvert\mu\rvert s}$	$\frac{\sin 2\beta M_2}{\lvert\mu\rvert}$	$\frac{\sin 2\beta \lvert\mu\rvert M_2}{s}$
$\cos\phi_1$	$\frac{\lvert M_1\rvert M_2}{\lvert\mu\rvert^2}$	$\frac{\lvert M_1\rvert M_2}{s}$	$\frac{\lvert M_1\rvert M_2}{\lvert\mu\rvert^2}$	$\frac{\lvert M_1\rvert M_2}{s}$
$\cos(\phi_1 - \phi_\mu)$	none	$\frac{\sin 2\beta \lvert M_1\rvert M_2^2}{\lvert\mu\rvert s}$	none	none
$\cos(2\phi_1 + \phi_\mu)$	none	none	none	$\frac{\sin 2\beta \lvert M_1\rvert^2 M_2}{\lvert\mu\rvert s}$

Table 4.3: Phase-dependences of $\sigma_{1\tilde{H}}$ and $\sigma_{2\tilde{H}}$ under the assumption $|\mu| \gg |M_1| > M_2$. Columns two and four show the dominant, phase-dependent terms from Q_1 and Q_3, whereas columns three and five display $\sqrt{s}$- and phase-dependent contributions from Q_2. Numerical and all other kinematical factors have been dropped and all contributions are normalized to the characteristic size $M_Z^2/(|\mu|^2 s)$ of the leading phase-independent contribution. "None" denotes that the corresponding phase-dependence does not exist at $\mathcal{O}(M_Z^2)$.

this summation corresponds to summing the quartic charges in Eq. 4.26. The results of the analysis of phase-dependences from coupling effects are summarized in Tab. 4.3. The cross sections also contain terms $\propto \cos(\phi_1 - \phi_\mu)$ and $\propto \cos(2\phi_1 + \phi_\mu)$ which result from combinations of the rephasing invariant quantities $\phi_{1(2)} + \phi_\mu$ and $\phi_1 - \phi_2$ in the convention $\phi_2 = 0$, as noted earlier in Sec. 4.4.1.

Again all terms involving the phase ϕ_μ come with a common factor $\sin 2\beta$ and are suppressed at large $\tan\beta$. Furthermore both modes contain sensitivity to the relative phase between the gaugino masses M_1 and M_2, ϕ_1 in the convention $\phi_2 = 0$. This sensitivity remains for large values of $\tan\beta$. The s-dependent terms $\propto Q_2$, listed in the third and fifth column if present, reveal a different dependence on $|\mu|$ than the terms that survive for $s \to \infty$ do. Some of them still vanish $\propto 1/|\mu|$ for large $|\mu|$, whereas others seem to grow with $|\mu|/\sqrt{s}$ in this limit. However in the physical region $|\mu|/\sqrt{s} < 1$ holds and hence the accessibility limits the growth of these terms. Finally, the results shown in Tab. 4.3 allow the conclusion that $\sigma_{1\tilde{H}}$ might show a slightly stronger overall dependence on phases in the region of parameter space allowed by low-energy data. The expectation of such a stronger phase-dependence for $\sigma_{1\tilde{H}}$ is based on the fact that all contributions involving the rather unconstrained phase ϕ_1 are either of the size for both modes or prefer $\sigma_{1\tilde{H}}$; whereas terms pure in the strongly constrained phase ϕ_μ prefer $\sigma_{2\tilde{H}}$. This preference of $\sigma_{1\tilde{H}}$ is fortunate, since the $\tilde{\chi}_1^0\tilde{H}$ mode is accessible at lower energies.

So far only phase-dependences that arise from couplings have been discussed. Again, similar to selectron and chargino modes, all phase-dependences that may arise from a variation of a the parameters M_2, $|M_1|$, and $|\mu|$ along with the phases while keeping physical neutralino masses fixed may be neglected. The reason for this is that, as already pointed out in Sec. 4.4.1, such adjustments of parameters affect the perturbative neutralino mixing at $\mathcal{O}(M_Z^3)$ only and hence lead to subleading phase-dependences in all modes. The sources of phase-dependences are completed by the shifts of neutralino masses in Eqs. 2.40. These shifts $\delta m^2_{\tilde{\chi}_i^0}$ are relevant when the absolute values of the parameters are kept fixed and the physical masses vary with the phases. Note that these shifts only need to be dis-

cussed when the leading phase-independent and the leading phase-dependent term are not of same order of M_Z, i.e. for σ_{11}, σ_{22} and σ_{34}. In all other modes the mass shifts lead to phase-dependences of subleading order. Concerning the remaining cross sections σ_{11}, σ_{22} and σ_{34}, which were already marked as less helpful for an observation of phase-dependent terms, it may merely be observed that the phase-dependent parts of the mass shifts show phase-dependences similar to those that might be expected from phase-dependent coupling contributions. Hence only a detailed parameter dependent analysis could show which effect —coupling or kinematical— dominates the phase-dependences of these three cross sections. However, it should be remembered from the discussion of kinematical effects in chargino pair production that kinematical effects can be greatly enhanced close to threshold. This point applies to all neutralino production modes.

Chapter 5

Polarization vectors

The numerical analysis presented in Chapter 7 will show that some of the cross sections calculated and discussed in Chapter 4 depend quite sensitively on the CP-violating phases ϕ_1 and/or ϕ_μ. Nevertheless, if measurements of these cross sections establish a deviation from the CP-conserving MSSM, it will necessary to measure some CP-violating asymmetries in order to reach the conclusion that the observed deviation is indeed due to non-vanishing phases, rather than due to some extension of the MSSM. Consequently, this chapter is devoted to the discussion of CP-asymmetries that can be defined at the level of cross sections, i.e. without including any decay chains in the production of SUSY particles. The discussion starts with investigating the possibility of constructing CP-odd observables from the studied production channels. Afterwards the components of final states polarization vectors in 2-fermion production are calculated. Finally, only the CP-violating components are investigated for a perturbative treatment of chargino and neutralino production.

5.1 Rate asymmetries and polarization vectors in two fermion production

To start with, the production of fermionic (charginos or neutralinos) final states and the CP-conjugated process may be summarized as

$$e^-\,(\vec{p}_1,\vec{s}_1)\,e^+\,(\vec{p}_2,\vec{s}_2) \to \tilde{\chi}_i\vec{k}_1,\vec{\tilde{s}}_1\overline{\tilde{\chi}}_j(\vec{k}_2,\vec{\tilde{s}}_2), \tag{5.1a}$$

$$CP:\quad e^+\,(-\vec{p}_1,\vec{s}_1)\,e^-\,(-\vec{p}_2,\vec{s}_2) \to \overline{\tilde{\chi}}_i-(\vec{k}_1,\vec{\tilde{s}}_1)\tilde{\chi}_j-(\vec{k}_2,\vec{\tilde{s}}_2), \tag{5.1b}$$

where the momenta $\vec{p}_{1,2}$ and $\vec{k}_{1,2}$ have been defined in Fig. 4.1, and $\vec{s}_{1,2}$ and $\vec{\tilde{s}}_{1,2}$ are the spin vectors of the initial and final states, respectively.
In the CMS the following relations between the momenta hold

$$\vec{p}_1=-\vec{p}_2, \qquad \vec{k}_1=-\vec{k}_2. \tag{5.2}$$

Therefore the initial state will self-conjugate if $\vec{s}_1=\vec{s}_2$, in particular for unpolarized beams. Comparing reactions (5.1a) and (5.1b) one can introduce two CP-odd asymmetries even after summing over the spins of the final states. A rate asymmetry can be defined for chargino production, essentially $\sigma\left(\tilde{\chi}_1^-\tilde{\chi}_2^+\right)-\sigma\left(\tilde{\chi}_1^+\tilde{\chi}_2^-\right)$, as well as an angular asymmetry for the production of two different neutralinos, proportional to $d\sigma\left(\tilde{\chi}_i^0\tilde{\chi}_j^0,\theta\right)-d\sigma\left(\tilde{\chi}_i^0\tilde{\chi}_j^0,\pi-\theta\right)$.

However, far from the Z pole, both these asymmetries vanish identically at the tree-level. The reason is that they are both odd under a combined $CP\tilde{T}$-transformation, where the "naive time reversal" $\tilde{T}$ reverses the direction of all 3-vectors, but does *not* exchange initial and final state. Quantities that are odd under $CP\tilde{T}$ can be non-zero only in the presence of absorptive phases [104]. Such phases can only be provided by nearly resonant s-channel propagators or by loop corrections if the kinematics allow the particles in the loop to be on-shell. As we are dealing with tree-level cross sections at CMS energies $\sqrt{s}$ far above the Z pole, no absorptive phases are available. Hence the two introduced CP-odd asymmetries, also being $CP\tilde{T}$ odd, vanish.[1]
In the absence of absorptive phases a CP-odd quantity can therefore only be non-zero if it is also $\tilde{T}$-odd. This is true for triple products of momentum and spin vectors. In general, the spin of the final state fermions in (5.1a) can be decomposed into three components: $P_L^{i,ij}$ is the component of $\vec{\tilde{s}}_i$ in direction of $\vec{k}_i$, averaged over many events (with fixed θ); $P_T^{i,ij}$ is orthogonal to $\vec{k}_i$, but lies *in* the event plane; and $P_N^{i,ij}$ is orthogonal to $\vec{k}_i$ *and* orthogonal to the event plane, i.e.

$$P_L^{i,ij} = \langle \vec{\tilde{s}}_1 \cdot \vec{k}_1 \rangle, \quad P_T^{i,ij} = \langle \vec{\tilde{s}}_1 \cdot (\vec{p}_1 \times \vec{k}_1) \rangle, \quad P_N^{i,ij} = \langle \vec{\tilde{s}}_1 \cdot [\vec{k}_1 \times (\vec{p}_1 \times \vec{k}_1)] \rangle, \tag{5.3}$$

where $\langle \ldots \rangle$ denotes averaging over many events for a fixed scattering angle θ. The components $P_{L,T,N}^{j,ij}$ are obtained from Eqs. 5.3 by the replacement $\vec{k}_1 \to \vec{k}_2$ and $\vec{\tilde{s}}_1 \to \vec{\tilde{s}}_2$. Obviously, $P_L^{i,ij}$ and $P_T^{i,ij}$ are $\tilde{T}$-even quantities, but $P_N^{i,ij}$ is $\tilde{T}$-odd.[2]
From this we can conclude that the production of fermionic final states offers some handle on CP-violating phases via the normal components $P_N^{i(j),ij}$ of final state polarization vectors already at the level of differential cross sections. Analytical results for these components will be shown in Sec. 5.3, a discussion of the normal components within the perturbative regime follows in Secs. 5.4 and 5.5. The measurability of these quantities will be commented on during the presentation of numerical results.

5.2 Absence of CP-violating observables in selectron production

Concerning CP-odd observables in both selectron production modes, $\tilde{e}_i^- \tilde{e}_j^+$ and $\tilde{e}_i^- \tilde{e}_j^-$, the situation is quite discouraging. First of all, for $\tilde{e}_i^- \tilde{e}_j^-$ production the reaction and its CP-conjugated reaction are

$$e^-(\vec{p}_1, \vec{s}_1)\, e^-(\vec{p}_2, \vec{s}_2) \to \tilde{e}_i^-(\vec{k}_1) \tilde{e}_j^-(\vec{k}_2), \tag{5.4a}$$

$$CP: \quad e^+(-\vec{p}_1, \vec{s}_1)\, e^+(-\vec{p}_2, \vec{s}_2) \to \tilde{e}_i^+(-\vec{k}_1) \tilde{e}_j^+(-\vec{k}_2). \tag{5.4b}$$

The processes summarized in (5.4a) and (5.4b) illustrate that the CP-conjugated initial state consists of two *positrons*. Therefore, even if any CP-asymmetry could be constructed

[1] In the absence of absorptive phases, "naive time reversal" $\tilde{T}$ and "normal" time T reversal are essentially the same. Hence $CP\tilde{T}$-violation would indicate CPT-violation.

[2] Strictly speaking, $P_N^{i,ij}$ is CP-odd only for self-conjugate final states (any two neutralinos, or $\tilde{\chi}_i^- \tilde{\chi}_i^+$). However, since T and $\tilde{T}$ are essentially the same in the absence of absorptive phases, a non-vanishing $P_N^{i,12}$ in $\tilde{\chi}_1^- \tilde{\chi}_2^+$ production can also be considered evidence for CP-violation.

from the two reactions above, measuring such an asymmetry requires two rather different experimental setups and environments. Hence, even in the quite unlikely case that both environments were available simultaneously, the accurate extraction of any asymmetry from two well distinguished sets of data is a rather sophisticated challenge within the experiment. Since this thesis primarily attempts to determine the accessibility of CP-phases at an FLC, the "experimental doubts" given above explain why no further effort on determing CP-asymmetries in $\tilde{e}_i^- \tilde{e}_j^-$ is made.
Considering the availability of the CP-conjugated initial state, the reaction for $\tilde{e}_i^- \tilde{e}_j^+$ and its CP-conjugated

$$e^-(\vec{p}_1, \vec{s}_1)\, e^+(\vec{p}_2, \vec{s}_2) \to \tilde{e}_i^-(\vec{k}_1)\tilde{e}_j^+(\vec{k}_2), \tag{5.5a}$$

$$CP: \quad e^+(-\vec{p}_1, \vec{s}_1)\, e^-(-\vec{p}_2, \vec{s}_2) \to \tilde{e}_i^+(-\vec{k}_1)\tilde{e}_j^-(-\vec{k}_2), \tag{5.5b}$$

look more promising. However, for the discussion of possible CP-asymmetries available from the reactions given by (5.5a) and (5.5b), reference [65] can be followed closely. In that work we classified and discussed *all* polarization and rate asymmetries available for $\mu^+\mu^- \to \tilde{\tau}_i^- \tilde{\tau}_j^+$ with scalar, pseudoscalar, axial and vectorial couplings as well as with arbitrary initial state polarization. Transferring the conventions and the results from [65] to the reactions in (5.5a) and (5.5b) it can be observed that most contributions to polarized, differential cross section vanish[3] and that only two CP-odd asymmetries are available a priori. Unfortunately, both asymmetries are also odd under $CP\tilde{T}$. Again this implies that they vanish far from the Z pole.
As a consequence of the discussion in Secs. 5.1 and 5.2 it may be noted that the only CP-odd quantity that can be defined without the inclusion of any secondary decays are the normal components of polarization vectors in the production of fermionic final states as discussed in Sec. 5.1.

5.3 Calculation of polarization vectors in $2f \to 2f$

In this section the framework for the calculation of polarization vector components in the presence of initial state polarization is provided and these components are defined. Afterwards the starting point of the calculation and the results for the polarization vector components are given. Finally, I show the results for $P_N^{i(j),ij}$ in absence of initial state polarization and discuss them briefly.

5.3.1 Generalities and definitions

The calculation of polarization vector components starts by defining a suitable coordinate system for the decomposition of $\vec{\tilde{s}}_{i(j)}$: the outgoing momentum $\vec{k}_{i(j)}$ is chosen as z-axis, the y-axis is then introduced as perpendicular to the event plane and finally the x-axis is given as cross product of these two

$$\vec{e}_z^{\,i(j)} = \frac{\vec{k}_{i(j)}}{|k_{i(j)}|}, \tag{5.6a}$$

[3] This is due to the rather restricting structure of the helicity amplitudes in Eq. 4.8; they are either helicity diagonal and mass off-diagonal or vice versa, whereas in the general case mass indices and helicity labels are not correlated.

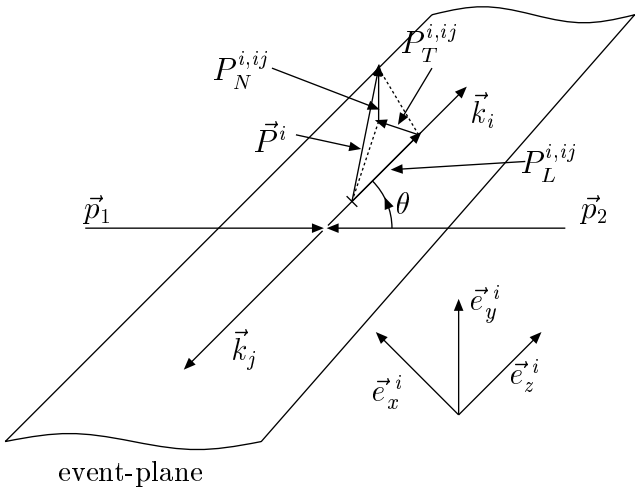

Figure 5.1: Coordinate system for the decomposition of the polarization vector $\vec{\tilde{s}}_i$.

$$\vec{e}_y^{\,i(j)} = \frac{\vec{p}_1 \times \vec{k}_{i(j)}}{|\vec{p}_1 \times \vec{k}_{i(j)}|}, \tag{5.6b}$$

$$\vec{e}_x^{\,i(j)} = \vec{e}_y^{\,i(j)} \times \vec{e}_z^{\,i(j)} = \frac{\vec{k}_{i(j)} \times \left(\vec{p}_1 \times \vec{k}_{i(j)}\right)}{|\vec{k}_{i(j)}||\vec{p}_1 \times \vec{k}_{\,i(j)}|}. \tag{5.6c}$$

Using this right-handed orthonormal system the components of $\vec{\tilde{s}}_{i(j)}$ are projections of $\vec{\tilde{s}}_{i(j)}$ onto the coordinate-axes in the rest frame of $\tilde{\chi}_i$ according to[4]

$$P_L^{i(j),ij} = \vec{\tilde{s}}_{i(j)} \cdot \vec{e}_z^{\,i(j)}, \tag{5.7a}$$

$$P_T^{i(j),ij} = \vec{\tilde{s}}_{i(j)} \cdot \vec{e}_x^{\,i(j)}, \tag{5.7b}$$

$$P_N^{i(j),ij} = \vec{\tilde{s}}_{i(j)} \cdot \vec{e}_y^{\,i(j)}. \tag{5.7c}$$

This description and the resulting decomposition of $\vec{s}_i$ are summarized in Fig. 5.1. Following [66, 105] the initial state polarization averaged, squared matrix element may be expanded into polarization vector components and spin-spin-correlations as

$$\sum_{\sigma_1,\sigma_1',\sigma_2,\sigma_2'} \langle\sigma_1\sigma_2, \lambda\bar{\lambda}\rangle\langle\sigma_1'\sigma_2', \lambda'\bar{\lambda}'\rangle^\star \rho^1_{\sigma_1\sigma_1'}\rho^2_{\sigma_2\sigma_2'} =$$
$$N\left[\delta_{\lambda'\lambda}\delta_{\bar{\lambda}\bar{\lambda}'} + P^i_\alpha(\tau_\alpha)_{\lambda'\lambda}\delta_{\bar{\lambda}\bar{\lambda}'} + P^j_\alpha(\tau_\alpha)_{\bar{\lambda}\bar{\lambda}'}\delta_{\lambda'\lambda} + \mathcal{Q}^{ij}_{\alpha\beta}(\tau_\alpha)_{\lambda'\lambda}(\tau_\beta)_{\bar{\lambda}\bar{\lambda}'}\right], \tag{5.8}$$

where ρ^1 and ρ^2 are the initial state polarization density matrices as defined in Eq. C.20 and Eq. C.21, respectively; N is a general normalization factor. The final state index pair ij has been dropped wherever it can be designated as superfluous. $P_\alpha^{i(j)}$ denote the components[5] of $\vec{\tilde{s}}^{i(j)}$ as defined in Eq. 5.7, and τ_α are the standard Pauli-matrices associated

[4]The average over many events with fixed scattering angle θ, denoted by $\langle\ldots\rangle$ in Eq. 5.3, is neglected here; but still it should be kept in mind since this averaging will determine the measurability.

[5]To clarify the notation: $P_\alpha^{i(j)}$ are the components of polarization vectors in the *presence* of initial state polarization, $P_\alpha^{i(j),ij}$ are the same components in the *absence* of initial state polarization.

with the coordinate system used for the decomposition of $\vec{\tilde{s}}^{i(j)}$, i.e. $P_x^i \tau_x = P_T^i \tau_x$. Finally the spin-spin-correlations are denoted by $\mathcal{Q}_{\alpha\beta}^{ij}$. They are not relevant for the further course of this thesis. For the production processes under consideration the initial helicities are off-diagonal ($\sigma_2 = -\sigma_1$), and Eq .5.8 slightly simplifies to

$$\sum_{\sigma_1,\sigma_1'} \langle \sigma_1 - \sigma_1, \lambda\bar{\lambda}\rangle \langle \sigma_1' - \sigma_1', \lambda'\bar{\lambda}'\rangle^\star \rho^1_{\sigma_1\sigma_1'} \rho^2_{-\sigma_1-\sigma_1'} =$$
$$N \left[\delta_{\lambda'\lambda}\delta_{\bar{\lambda}\bar{\lambda}'} + P_\alpha^i (\tau_\alpha)_{\lambda'\lambda}\delta_{\bar{\lambda}\bar{\lambda}'} + P_\alpha^j (\tau_\alpha)_{\bar{\lambda}\bar{\lambda}'}\delta_{\lambda'\lambda} + \mathcal{Q}_{\alpha\beta}^{ij} (\tau_\alpha)_{\lambda'\lambda}(\tau_\beta)_{\bar{\lambda}\bar{\lambda}'}\right]. \tag{5.9}$$

The normalization N and the polarization vector components $P_\alpha^{i(j)}$ can be extracted from Eq. 5.9 by multiplying with suitable combinations of $\delta_{\lambda'\lambda}$, $\delta_{\bar{\lambda}\bar{\lambda}'}$, $(\tau_\alpha)_{\lambda'\lambda}$, and $(\tau_\alpha)_{\bar{\lambda}\bar{\lambda}'}$ and summing over the final state helicities. An example of this calculation is illustrated in App. C.1. The results obtained by the procedure are summarized in the next two subsections.

5.3.2 Results with initial state polarization

In this subsection the results for polarization vector components with arbitrary initial state polarization are presented. Initial state polarization is described by the longitudinal polarizations $P_L^{1,(2)}$, the transversal polarizations $P_T^{1,(2)}$, and the polarization angles $\alpha_{1(2)}$ for electron and the positron. Focusing on the polarization density matrix elements on the left-hand side of Eq. 5.9, one notices that four "polarization functions" f_i, given as

$$f_1 \equiv f_U = 1 - P_L^1 P_L^2, \tag{5.10a}$$
$$f_2 \equiv f_L = P_L^1 - P_L^2, \tag{5.10b}$$
$$f_3 \equiv f_T = P_T^1 P_T^2 \cos(\alpha_1 + \alpha_2), \tag{5.10c}$$
$$f_4 \equiv f_N = P_T^1 P_T^2 \sin(\alpha_1 + \alpha_2), \tag{5.10d}$$

are sufficient to describe all dependences of the polarization vector components on initial state polarization. Using these four functions, the normalization N and the polarization vector components $P_\alpha^{i(j)}$ may be decomposed as[6]

$$16N = \sum_k N_k f_k, \tag{5.11a}$$
$$P_\alpha^{i(j)} = \frac{\sum_k C_{\alpha,i(j)}^k f_k}{16N}. \tag{5.11b}$$

First the coefficients N_k and $C_{\alpha,i(j)}^k$ are expressed in terms of helicity amplitudes. These intermediate results may be found in App. C.2. When these intermediate results are further reduced to kinematical functions and quartic charges, several new quartic have to be added to Eq. 4.21 and the complete set of quartic charges finally reads

$$Q_1^{ij} = |Q_{++}|^2 + |Q_{+-}|^2 + |Q_{-+}|^2 + |Q_{--}|^2, \tag{5.12a}$$
$$\tilde{Q}_1^{ij} = |Q_{++}|^2 + |Q_{+-}|^2 - |Q_{-+}|^2 - |Q_{--}|^2, \tag{5.12b}$$

[6]The inserted factor 16 serves to cancel common factors both from the normalization of polarization density matrices and from sums over λ, λ', $\bar{\lambda}$, and $\bar{\lambda}'$.

$$Q_2^{ij} = \mathcal{R}\mathrm{e}\left[Q_{++}Q_{+-}^{\star} + Q_{--}Q_{-+}^{\star}\right], \tag{5.12c}$$

$$\tilde{Q}_2^{ij} = \mathcal{R}\mathrm{e}\left[Q_{++}Q_{+-}^{\star} - Q_{--}Q_{-+}^{\star}\right], \tag{5.12d}$$

$$Q_3^{ij} = |Q_{++}|^2 - |Q_{+-}|^2 - |Q_{-+}|^2 + |Q_{--}|^2, \tag{5.12e}$$

$$\tilde{Q}_3^{ij} = |Q_{++}|^2 - |Q_{+-}|^2 + |Q_{-+}|^2 - |Q_{--}|^2, \tag{5.12f}$$

$$Q_4^{ij} = \mathcal{I}\mathrm{m}\left[Q_{++}Q_{+-}^{\star} + Q_{--}Q_{-+}^{\star}\right], \tag{5.12g}$$

$$\tilde{Q}_4^{ij} = \mathcal{I}\mathrm{m}\left[Q_{++}Q_{+-}^{\star} - Q_{--}Q_{-+}^{\star}\right], \tag{5.12h}$$

$$Q_5^{ij} = \mathcal{R}\mathrm{e}\left[Q_{++}Q_{-+}^{\star} + Q_{--}Q_{+-}^{\star}\right], \tag{5.12i}$$

$$\tilde{Q}_5^{ij} = \mathcal{R}\mathrm{e}\left[Q_{++}Q_{-+}^{\star} - Q_{--}Q_{+-}^{\star}\right], \tag{5.12j}$$

$$Q_6^{ij} = \mathcal{I}\mathrm{m}\left[Q_{++}Q_{-+}^{\star} - Q_{--}Q_{+-}^{\star}\right], \tag{5.12k}$$

$$\tilde{Q}_6^{ij} = \mathcal{I}\mathrm{m}\left[Q_{++}Q_{-+}^{\star} + Q_{--}Q_{+-}^{\star}\right], \tag{5.12l}$$

where the bilinear charges $Q_{\alpha\beta}^{ij}$ have been introduced in Eqs. 4.16–4.18 for chargino pair production and in Eq. 4.23 for neutralino pair production. Using the quartic charges above, the components N_k of the normalization are

$$N_1 = 4\left\{\left[\left(1-\Delta^2\right) + \lambda\cos^2\theta\right]Q_1 + 2\lambda^{\frac{1}{2}}\cos\theta Q_3 + 8\mu_i\mu_j Q_2\right\}, \tag{5.13a}$$

$$N_2 = 4\left\{\left[\left(1-\Delta^2\right) + \lambda\cos^2\theta\right]\tilde{Q}_1 + 2\lambda^{\frac{1}{2}}\cos\theta\tilde{Q}_3 + 8\mu_i\mu_j\tilde{Q}_2\right\}, \tag{5.13b}$$

$$N_3 = 8\sin^2\theta\lambda Q_5, \tag{5.13c}$$

$$N_4 = 8\sin^2\theta\lambda Q_6, \tag{5.13d}$$

while the coefficients $C_{L,i(j)}^k$ for the longitudinal components read

$$C_{L,i}^1 = 4\left\{\left[2\left(1-\bar{\Delta}\right)\tilde{Q}_1 + 8\mu_i\mu_j\tilde{Q}_2\right]\cos\theta + \lambda^{\frac{1}{2}}\left[1+\cos^2\theta - \Delta\sin^2\theta\right]\tilde{Q}_3\right\}, \tag{5.14a}$$

$$C_{L,j}^1 = -4\left\{\left[2\left(1-\bar{\Delta}\right)\tilde{Q}_1 + 8\mu_i\mu_j\tilde{Q}_2\right]\cos\theta + \lambda^{\frac{1}{2}}\left[1+\cos^2\theta + \Delta\sin^2\theta\right]\tilde{Q}_3\right\}, \tag{5.14b}$$

$$C_{L,i}^2 = 4\left\{\left[2\left(1-\bar{\Delta}\right)Q_1 + 8\mu_i\mu_j Q_2\right]\cos\theta + \lambda^{\frac{1}{2}}\left[1+\cos^2\theta - \Delta\sin^2\theta\right]Q_3\right\}, \tag{5.14c}$$

$$C_{L,j}^2 = -4\left\{\left[2\left(1-\bar{\Delta}\right)Q_1 + 8\mu_i\mu_j Q_2\right]\cos\theta + \lambda^{\frac{1}{2}}\left[1+\cos^2\theta + \Delta\sin^2\theta\right]Q_3\right\}, \tag{5.14d}$$

$$C_{L,i}^3 = 8\sin^2\theta\lambda^{\frac{1}{2}}\left(1+\Delta\right)\tilde{Q}_5, \tag{5.14e}$$

$$C_{L,j}^3 = -8\sin^2\theta\lambda^{\frac{1}{2}}\left(1-\Delta\right)\tilde{Q}_5, \tag{5.14f}$$

$$C_{L,i}^4 = 8\sin^2\theta\lambda^{\frac{1}{2}}\left(1+\Delta\right)\tilde{Q}_6, \tag{5.14g}$$

$$C_{L,j}^4 = -8\sin^2\theta\lambda^{\frac{1}{2}}\left(1-\Delta\right)\tilde{Q}_6. \tag{5.14h}$$

For the coefficients $C_{T,i(j)}^k$ of the transversal polarization one obtains

$$C_{T,i}^1 = -8\sin\theta\left[\mu_i\left(1-\Delta\right)\tilde{Q}_1 + \mu_i\lambda^{\frac{1}{2}}\cos\theta\tilde{Q}_3 + 2\mu_j\left(1+\Delta\right)\tilde{Q}_2\right], \tag{5.15a}$$

$$C_{T,j}^1 = 8\sin\theta\left[\mu_j\left(1+\Delta\right)\tilde{Q}_1 + \mu_j\lambda^{\frac{1}{2}}\cos\theta\tilde{Q}_3 + 2\mu_i\left(1-\Delta\right)\tilde{Q}_2\right], \tag{5.15b}$$

$$C^2_{T,i} = -8\sin\theta\left[\mu_i\left(1-\Delta\right)Q_1 + \mu_i\lambda^{\frac{1}{2}}\cos\theta Q_3 + 2\mu_j\left(1+\Delta\right)Q_2\right], \tag{5.15c}$$

$$C^2_{T,j} = 8\sin\theta\left[\mu_j\left(1+\Delta\right)Q_1 + \mu_j\lambda^{\frac{1}{2}}\cos\theta Q_3 + 2\mu_i\left(1-\Delta\right)Q_2\right], \tag{5.15d}$$

$$C^3_{T,i} = 16\sin\theta\cos\theta\mu_i\lambda^{\frac{1}{2}}\tilde{Q}_5, \tag{5.15e}$$

$$C^3_{T,j} = -16\sin\theta\cos\theta\mu_j\lambda^{\frac{1}{2}}\tilde{Q}_5, \tag{5.15f}$$

$$C^4_{T,i} = 16\sin\theta\cos\theta\mu_i\lambda^{\frac{1}{2}}\tilde{Q}_6, \tag{5.15g}$$

$$C^4_{T,j} = -16\sin\theta\cos\theta\mu_j\lambda^{\frac{1}{2}}\tilde{Q}_6. \tag{5.15h}$$

Finally the coefficients $C^k_{N,i(j)}$ of the normal polarization are found to be

$$C^1_{N,i} = 16\mu_j\lambda^{\frac{1}{2}}\sin\theta Q_4, \tag{5.16a}$$

$$C^1_{N,j} = -16\mu_i\lambda^{\frac{1}{2}}\sin\theta Q_4, \tag{5.16b}$$

$$C^2_{N,i} = 16\mu_j\lambda^{\frac{1}{2}}\sin\theta\tilde{Q}_4, \tag{5.16c}$$

$$C^2_{N,j} = -16\mu_i\lambda^{\frac{1}{2}}\sin\theta\tilde{Q}_4, \tag{5.16d}$$

$$C^3_{N,i} = -16\mu_i\lambda^{\frac{1}{2}}\sin\theta\tilde{Q}_6, \tag{5.16e}$$

$$C^3_{N,j} = 16\mu_j\lambda^{\frac{1}{2}}\sin\theta\tilde{Q}_6, \tag{5.16f}$$

$$C^4_{N,i} = 16\mu_i\lambda^{\frac{1}{2}}\sin\theta\tilde{Q}_5, \tag{5.16g}$$

$$C^4_{N,j} = -16\mu_j\lambda^{\frac{1}{2}}\sin\theta\tilde{Q}_5. \tag{5.16h}$$

Here λ denotes the kinematical function λ_{ij} as introduced in Eq. C.3; $\Delta \equiv \Delta_{ij}$ is defined in Eq. C.16 and $\bar{\Delta} \equiv \bar{\Delta}_{ij}$ is given by

$$\bar{\Delta}_{ij} = \mu_i^2 + \mu_j^2. \tag{5.17}$$

These are complete results describing the polarization vector of both produced fermions in suitable coordinate systems with arbitrary initial state polarization. Despite being lengthy they are presented here as they will be used again in the later course of this thesis. Another reason for noting these results in full is that apparently have not as yet been published.

5.3.3 Results without initial state polarization

Without initial state polarization the polarization vector components of the produced fermions are generally given by the coefficients $C^1_{\alpha,i(j)}$ and N^1 as

$$P^{i(j),ij}_\alpha \equiv P_{\alpha,i(j)}\big|_{P^i_L=P^i_T=0} = \frac{C^1_{\alpha,i(j)}}{N_1}. \tag{5.18}$$

As only $P^{i(j),ij}_N$ is of further interest within Part II , the results for $P^{i(j),ij}_L$ and $P^{i(j),ij}_T$ are omitted here. The CP-odd normal components are found to be

$$P^{i,ij}_N = \frac{4\mu_j\lambda^{\frac{1}{2}}_{ij}Q^{ij}_4}{\left[\left(1-\Delta^2_{ij}\right)+\lambda_{ij}\cos^2\theta\right]Q^{ij}_1 + 2\lambda^{\frac{1}{2}}_{ij}\cos\theta Q^{ij}_3 + 8\mu_i\mu_j Q^{ij}_2}, \tag{5.19a}$$

$$P_N^{j,ij} = \frac{-4\mu_i \lambda_{ij}^{\frac{1}{2}} Q_4^{ij}}{\left[\left(1-\Delta_{ij}^2\right) + \lambda_{ij}\cos^2\theta\right] Q_1^{ij} + 2\lambda_{ij}^{\frac{1}{2}} \cos\theta Q_3^{ij} + 8\mu_i\mu_j Q_2^{ij}}. \tag{5.19b}$$

These results, as well as the omitted ones, can be compared with [66, 105]. Agreement in all six components without initial state polarization is found.
Firstly, Eqs. 5.19 reveal that the denominator of $P_N^{i(j),ij}$ is essentially given by the corresponding differential cross sections if the phase space factors in Eq. 4.20 are neglected. Thus the results of the discussion of cross sections within the perturbative regime can be transferred directly to these denominators. Secondly, from Eqs. 5.19 one can conclude that $P_N^{i(j),ij}$ vanishes both at the threshold (where $\lambda_{ij} \to 0$) and far above threshold (where $\mu_{j,i} \to 0$). Furthermore, Eqs. 4.16 and 4.17 show that all bilinear charges describing $\tilde{\chi}_i^- \tilde{\chi}_i^+$ production are real. Likewise, Eqs. 4.23 and 4.24 together with Eq. 2.51 illustrate that the couplings appearing in the expressions of Eq. 5.19 of the bilinear charges are real for final states consisting of two identical neutralinos. Thus Q_4^{ij} and hence $P_N^{i(j),ij}$ can only be non-vanishing for off-diagonal chargino or neutralino production modes ($i \neq j$). Moreover, the identity

$$P_N^{j,ij} = -\frac{\mu_i}{\mu_j} P_N^{i,ij}, \tag{5.20}$$

shows that there is only one independent P_N for each distinct $\tilde{\chi}_i\tilde{\chi}_j$ production channel. This amounts to a total of seven independent CP-odd observables.

5.4 $P_N^{1(2),12}$ in perturbative chargino production

The results of the perturbative treatment of chargino mixing are now applied to the normal component $P_N^{1(2),12}$ in $\tilde{\chi}_1^\pm\tilde{\chi}_2^\mp$-production. Remember that these components are the only CP-odd ones available for all chargino production modes. When normalized to the leading phase-independent contributions within the cross section, which are $\propto M_W^2/|\mu|^2$, the quartic charge Q_4^{12} reads[7]

$$Q_4^{12} \propto \sin 2\beta \sin\phi_\mu. \tag{5.21}$$

The quartic charge Q_4^{12} contains pure s-channel contributions as well as contributions from the interference between s- and t-channel. In both cases first order corrections to the Higgsino (gaugino) component of the gaugino-like (Higgsino-like) state are crucial. As $P_N^{1(2),12}$ is given as the $\mathcal{O}(M_W^2)$-quantity Q_4^{12} normalized to an $\mathcal{O}(M_W^2)$ cross section, it is of order $\mathcal{O}(M_W^0)$ itself. Therefore, when the reduced masses $\mu_{1(2)}$ (see Eq. 5.19) are included in Eq. 5.21 in order to obtain the normal polarizations $P_N^{1(2),12}$ are basically given as

$$P_N^{1,12} = \frac{|\mu|}{\sqrt{s}} \sin 2\beta \sin\phi_\mu, \quad P_N^{2,12} = \frac{M_2}{\sqrt{s}} \sin 2\beta \sin\phi_\mu. \tag{5.22}$$

Trivially, but as expected for a CP-odd quantity, here the dependence on ϕ_μ is exclusively through sine functions and vanishes like $1/\tan\beta$ for large $\tan\beta$. The included kinematical terms $\mu_{i(j)}/\sqrt{s}$ yield a suppression of $P_N^{1(2),12}$ in the physical region, where $M_2/\sqrt{s} < |\mu|/\sqrt{s} < 1$. However, this additional suppression "prefers" the normal polarization vector components of the lighter, gaugino-like chargino $\tilde{\chi}_1^\pm$. Additional phase-dependences arising

[7] Again I work with the convention $\phi_2 \equiv 0$ and assume $|\mu| \gg M_2$.

either from the variation of physical masses with the phases or from variations of the absolute values along the phases with fixed kinematical masses need not be included; both lead to contributions of subleading, relative order of M_W^2. Following these arguments $P_N^{1,12}$ could be considered the best CP-odd observable available from chargino pair production, but unfortunately the observed, quite stringent bounds on ϕ_μ (see Sec. 3.3.2) strongly limit its utility. Moreover, the utility of $P_N^{1,12}$ also suffers from being associated with an $\mathcal{O}(M_W^2)$ cross section. This fact narrows down the statistics available for a determination of $P_N^{1,12}$. As a consequence it has to be concluded that normal polarization in chargino production is most probably not sufficient to probe CP-violation directly.

5.5 $P_N^{i(j),ij}$ in perturbative neutralino production

Within the framework of the perturbative treatment of neutralino mixing as given in Sec.2.3.3 it was observed that the two heavier, Higgsino-like neutralino are closely degenerated in mass. Hence only four off-diagonal production channels, i.e $\tilde{\chi}_1\tilde{\chi}_2$, $\tilde{\chi}_1^0\tilde{H}$, $\tilde{\chi}_2^0\tilde{H}$, and $\tilde{H}\tilde{H}$, are available. This reduces the number of independent normal polarizations available in neutralino production from six to four. To start with, P_N for $\tilde{H}\tilde{H}$ $(\tilde{\chi}_3^0\tilde{\chi}_4^0)$ can be neglected in the further course of discussion as Q_4^{34} vanishes to $\mathcal{O}(M_Z^2)$ and therefore P_N itself is an $\mathcal{O}(M_Z^2)$ effect after normalizing Q_4^{34} to the corresponding cross section of $\mathcal{O}(M_Z^0)$. In contrast, one finds that the numerators in Eqs. 5.19 receive $\mathcal{O}(M_Z^0)$ corrections only for the $\tilde{\chi}_1^0\tilde{\chi}_2^0$-mode; in the case of the $\tilde{\chi}_1^0\tilde{H}$ and $\tilde{\chi}_2^0\tilde{H}$ mode the numerator starts at $\mathcal{O}(M_Z^2)$, just like the corresponding total cross sections, and hence the denominators in Eqs. 5.19. In all these cases P_N will be an effect of order M_Z^0. This argument again indicates that additional phase-dependences, which might arise either from the variation of physical masses along with the phases or from the variation of mass parameters, need not be included.
The normal polarization of the heavier, wino-like neutralino in $\tilde{\chi}_1^0\tilde{\chi}_2^0$ is explicitly given as

$$P_N^{2,12} = \frac{-4\lambda_{12}^{\frac{1}{2}}\frac{|M_1|}{\sqrt{s}}\sin\theta\sin\phi_1}{(1-\Delta_{12}^2+\lambda_{12}\cos^2\theta)\frac{\left(D_t^L\right)^2+\left(D_u^L\right)^2}{D_t^L D_u^L} - 8\frac{|M_1|M_2}{s}\cos\phi_1 + 2\lambda_{12}^{\frac{1}{2}}\cos\theta\frac{\left(D_t^L\right)^2-\left(D_u^L\right)^2}{D_t^L D_u^L}}. \quad (5.23)$$

As expected for a CP-odd quantity the dominant dependence on ϕ_1 is through a sine function, while the denominator (basically the differential cross section discussed in Sec. 4.4.3) contains a CP-even dependence on ϕ_1 through a cosine. In general, Eq. 5.20 shows that $\left|P_N^{1,12}\right|$ is larger than $\left|P_N^{2,12}\right|$ by a factor of $M_2/|M_1| \simeq 2$. However, since it has been assumed that $\tilde{\chi}_1^0$ is the LSP and hence stable (if R-parity is conserved), the spin of $\tilde{\chi}_1^0$ cannot be measured.
Due to their mass degeneracy we have to average P_N for the mixed gaugino-higgsino modes over the production of both Higgsino-like neutralinos. Using the event numbers N as weights, we obtain

$$P_N^{i(\tilde{H}),i\tilde{H}} = \frac{N_{i3}P_N^{i(3),i3} + N_{i4}P_N^{i(4),i4}}{N_{i3}+N_{i4}}, \quad i=1,2. \quad (5.24)$$

This amounts to replacing the quartic charges in Eqs. 5.19 with

$$Q_k^{i\tilde{H}} = Q_k^{i3} + Q_k^{i4}. \quad (5.25)$$

With this description the calculation of the relevant quartic charges $Q_4^{i\tilde{H}}$ to $\mathcal{O}(M_Z^2)$ becomes a straightforward, if somewhat tedious procedure. The results of this calculation are summarized in Tab. 5.1, where they have been normalized to the leading phase-independent contribution to the differential cross sections, characterized by $M_Z^2/|\mu|^2$. Due to this normalization the terms in Tab. 5.1 correspond directly to terms in P_N, up to an additional factor of $|M_1|/\sqrt{s}$ ($M_2/\sqrt{s}$ or $|\mu|/\sqrt{s}$) for $P_N^{\tilde{H},1\tilde{H}}$ ($P_N^{\tilde{H},2\tilde{H}}$ or $P_N^{2,2\tilde{H}}$). As expected, the phase-dependence of these terms is through sine functions. All terms that are sensitive to ϕ_μ are suppressed at large $\tan\beta$. A similar behavior has already been observed and discussed in Sec. 4.4.3 for the corresponding contributions to the cross sections. The dominant phase-

	$Q_4^{1\tilde{H}}$	$Q_4^{2\tilde{H}}$
$\sin(\phi_1+\phi_\mu)$	$\sin 2\beta$	$\sin 2\beta \frac{\lvert M_1\rvert M_2}{\lvert\mu\rvert^2}$
$\sin\phi_\mu$	$\sin 2\beta \frac{\lvert M_1\rvert M_2}{\lvert\mu\rvert^2}$	$\sin 2\beta$
$\sin\phi_1$	$\frac{M_2}{\lvert\mu\rvert}$	$\frac{\lvert M_1\rvert}{\lvert\mu\rvert}$
$\sin(\phi_1-\phi_\mu)$	$\sin 2\beta \frac{M_2^2}{\lvert\mu\rvert^2}$	none
$\sin(2\phi_1+\phi_\mu)$	none	$\sin 2\beta \frac{\lvert M_1\rvert^2}{\lvert\mu\rvert^2}$

Table 5.1: Phase-dependences of $Q_4^{1(2)\tilde{H}}$ under the assumption $|\mu| \gg M_2 \gg |M_1|$, normalized to the characteristic size $M_Z^2/|\mu|^2$ of the leading contributions in the denominators of Eqs. 5.19. The terms proportional to $\sin\phi_1$ get additional contributions of the same size, but scaling with $\cos 2\beta$. As these contributions do not affect the following conclusions, they are omitted here.

dependence of $P_N^{\tilde{H},1\tilde{H}}$ is due to $\sin(\phi_1+\phi_\mu)$; this contribution remains finite for $|\mu|\to\infty$, but vanishes $\propto 1/\tan\beta$ for large $\tan\beta$. Taking the additional, kinematical factor $|M_1|/\sqrt{s}$ into account we notice that all contributions to $P_N^{\tilde{H},1\tilde{H}}$ suffer from an additional suppression that increases with increasing $|\mu|$.[8]
On the other hand, in the $\tilde{\chi}_2^0\tilde{H}$-mode the polarization of the lighter, gaugino-like neutralino can be measured, in this case giving rise to an extra factor of $|\mu|/\sqrt{s}$. We thus see that (as long as $\sqrt{s} > |\mu| + M_2$) the contribution to $P_N^{2,2\tilde{H}}$ proportional to $\sin\phi_\mu$ (third entry in the third line of Tab. 5.1) *rises* with increasing $|\mu|$. Unfortunately, for the range of $|\mu|$ of interest to this work, this contribution is suppressed by the stringent upper limit on $|\sin\phi_\mu|$, see Sec. 3.3.2; only in scenario B2 with small $\tan\beta$ magnitude comparable to the contribution proportional to $\sin\phi_1$ (third entry of the fourth line in Tab. 5.1) can be attained. This contribution to $P_N^{2,2\tilde{H}}$ approaches a constant for large $|\mu|$ (when $|\mu|/\sqrt{s}$ is included), *and* remains finite for large $\tan\beta$. Therefore it can be concluded that the production of $\tilde{\chi}_2^0\tilde{H}$ should allow a somewhat more sensitive direct probe of CP-violation than the production of $\tilde{\chi}_1^0\tilde{H}$.

[8] In order to remain within the physical region $\sqrt{s}$ has to be increased with increasing $|\mu|$.

Chapter 6

Significances

In the course of this thesis I have so far explored the possible size of phases as well as developed an expectation about which out of the various production channels considered here might be sensitive to these phases. But a tool to quantify these sensitivities was not yet introduced. This lack is addressed by this chapter. After introducing such a tool, referred to as significance later onwards, a few properties of these significances are studied briefly using simple toy-models of phase-dependent cross sections.

6.1 Introduction of the significances $\mathcal{S}$ and $\bar{\mathcal{S}}$

A major goal of this thesis is to quantify the impact of CP-odd phases on total cross sections, which are CP-even quantities. To this end the difference in counting rates between a CP-conserving point in parameter space (CPC: all phases $\phi_i = 0$ or π) and a CP-violating one (CPV: identical absolute values, but at least one $\phi_i \neq 0$ and low-energy compatible) is compared to the statistical error at the CPC point. This determines the significance $\mathcal{S}$ with which a deviation from the cross section predicted for the CPC point can be measured. It may be written as

$$\mathcal{S} = \frac{\Delta N_{\mathrm{CPC-CPV}}}{\delta N_{\mathrm{CPC}}}. \tag{6.1}$$

Since there are two CP-conserving values (0, π) for each phase, one has to deal with eight CPC points for each set of absolute values, and hence the same number of significances is available for each kinematical accessible cross section. The smallest of these evidently determines the statistical significance with which the presence of CP-violating phases can be inferred from this cross section for given values of the absolute values of all SUSY parameters. Therefore the final measure of the sensitivity of a given cross section to phases the significance is defined as

$$\mathcal{S}\left(f_i f_j\right) = \min_n \left(\frac{\left| \sigma^{\mathrm{CPV}}_{f_i f_j} - \sigma^{\mathrm{CPC}_n}_{f_i f_j} \right|}{\sqrt{\sigma^{\mathrm{CPC}_n}_{f_i f_j}}} \right) \times \sqrt{\mathcal{L}}, \tag{6.2}$$

where $\sigma_{f_i f_j}$ is the total cross section for $e^- e^\pm \to f_i f_j$, and $n = 1, \ldots, 8$; only include CPC points which are low-energy compatible are included.[1] Finally, $\mathcal{L}$ is the integrated

[1] Since $\sigma_{f_i f_j}$ does not depend on ϕ_A, there are only four different values of $\sigma^{\mathrm{CPC_n}}_{f_i f_j}$ for a given CPV point. However, occasionally both $\phi_A = 0$ and $\phi_A = \pi$ have to be checked to find a CPC point that is

luminosity which is expected to be different for the e^-e^+ and e^-e^- options.
In the procedure outlined so far, CPC and CPV points have the same absolute values of M_1, M_2, and μ. This means that these points will in general have *different* physical neutralino and chargino masses [106]. Recall that the phase-dependence of the $\tilde{\chi}$ masses is suppressed by $M^2_{Z(W)}/(|\mu| m_{\tilde{\chi}})$ in the perturbative limit, see Eqs. 2.35 and 2.40. Nevertheless, changes of several percent are possible, in particular in the neutralino sector. This could lead to similar changes[2] in the cross sections through kinematical factors (in $\tilde{\chi}$ production) or through neutralino propagator factors (in $\tilde{e}$ production). Moreover, these masses are often more easily measurable than the cross sections which are the focus of this analysis.
Therefore a second set of significances $\bar{\mathcal{S}}$, where CPC and CPV points have the same physical masses for $\tilde{\chi}^0_1$, $\tilde{\chi}^0_3$ and $\tilde{\chi}^\pm_1$, is introduced. In the limit of large $\tilde{\chi}$ masses and for the choice of $|\mu| \geq M_2 \geq |M_1|$, these three masses essentially fix $|M_1|$, $|\mu|$, and M_2, respectively. Note that only three (dimensionful) absolute values that can be adjusted in the neutralino and chargino mass matrices are available. Therefore it can not be guaranteed that all chargino and neutralino masses are the same in the CPC and CPV points. However, after ensuring that these three $\tilde{\chi}$ masses are the same in both points, the remaining variations of the other three $\tilde{\chi}$ masses between the CPC and CPV points are quite small. For technical reasons $|M_1|$, M_2, and $|\mu|$ are kept fixed (at the values listed in Tab. 3.2) for the CPC points, and are adjusted at the CPV points. Since the eight CPC points have four different $\tilde{\chi}$ mass spectra, a given set of phases now also produces several different CPV points, labeled as $\overline{\text{CPV}}_n$. The new significance can thus be written as

$$\bar{\mathcal{S}}\,(f_i f_j) = \min_n \left(\frac{\left| \sigma^{\overline{\text{CPV}}_n}_{f_i f_j} - \sigma^{\text{CPC}_n}_{f_i f_j} \right|}{\sqrt{\sigma^{\text{CPC}_n}_{f_i f_j}}} \right) \times \sqrt{\mathcal{L}}. \tag{6.3}$$

The algorithm for calculating the significances $\mathcal{S}$ and $\overline{\mathcal{S}}$ can be summarized as follows:

- Select a CPV point: For a set of the absolute values of the relevant SUSY parameters, as listed in Tab. 3.2 for our three scenarios B1, B2, and B3, this amounts to randomly choosing values for the phases ϕ_A, ϕ_μ, and ϕ_1. Repeat this step until a point that is compatible with the low-energy constraints has been found.

- For each process, find the low-energy allowed CPC point that minimizes $\mathcal{S}\,(f_i f_j)$ as defined in Eq. 6.2. Note that there are only eight CPC points for each scenario if $\tan\beta$ is kept fixed, however, this procedure in general selects different CPC points for different processes. This completes the calculation of $\mathcal{S}$.

- Define eight new CPV points $\overline{\text{CPV}}_n$ by adjusting $|M_1|$, M_2, and $|\mu|$ such that $m_{\tilde{\chi}^0_1}$, $m_{\tilde{\chi}^\pm_1}$, and $m_{\tilde{\chi}^0_3}$ are the same in points $\overline{\text{CPV}}_n$ and CPC_n.

- Calculate the significances $\bar{\mathcal{S}}\,(f_i f_j)$ as described in Eq. 6.3.

Note that $\mathcal{S}$ and $\bar{\mathcal{S}}$ only measure *statistical* significances. In addition there will be systematic uncertainties, both from experiment and theory. Little can be said here about

compatible with the bound on a_μ. Trivially, all CPC points satisfy the bound on d_e.

[2] These possible changes have already partially been discussed within Sec. 4.4, under the heading of "kinematical effects".

experimental uncertainties, except to express the hope that they will be small. A theoretical error is introduced since our cross sections can only be predicted with finite precision. At tree-level these cross sections are determined uniquely by the parameters listed in Tab. 3.2, plus a few SM parameters that at this time are already known with high precision. However, explicit calculations for $\tilde{\chi}_1^\pm$ pair production show that quantum corrections can easily amount to $\mathcal{O}(10\%)$ [107,108]. Some of these corrections can be calculated unambiguously once the parameters listed in Tab. 3.2 are specified, but the remaining corrections can still amount to several percent. In particular, the lepton-slepton-gaugino "gauge couplings" depend (logarithmically) on the squark mass scale [109–113]. The production of Higgsino-like charginos [107,108] and, presumably, neutralinos also depends on the parameters appearing in third generation sfermion masses. These corrections will only be calculable once the parameters of the (presumably quite heavy) squark sector have been determined. Until then, out of two processes with roughly equal significances as defined above, the process with the *smaller* cross section should be preferred since here a given significance corresponds to a *larger* relative variation of the cross section with the phases.

6.2 Elementary properties of significances

This section is devoted to a brief analysis of the elementary properties that a significance can reveal if the corresponding cross section is varied along with some phases.[3] I start with giving three statements which allow almost the complete determination of the significance from the corresponding cross section. These statements are briefly motivated and illustrated for three examples. I complete Chapter 6 with deriving an instance of the possible correlation pattern of significances from these examples and studying the case of constrained ranges for the phases.

6.2.1 General case

In order to understand the elementary properties of significances a cross section σ and the associated significance $\mathcal{S}(\sigma)$, where σ is depending on two phases, are studied here.[4] As the general case includes the presence of two phases[5], one has to deal with four CPC points and correspondingly have four CPC cross sections, denoted by σ_i^{CPC}, $i = 1, \ldots, 4$, available as CPC reference points in the definition of $\mathcal{S}(\sigma)$ by Eq. 6.2. Hence the minimization implied in Eq. 6.2 chooses one out of these four CPC points. Moreover, the case the numerical value of the cross section for a non-trivial choice of the phase coincides with the value of a

[3] Within this section the significances $\mathcal{S}$ and $\overline{\mathcal{S}}$ are treated equally, i.e. I do not distinguish between the two different treatments of the physical masses. Therefore the phase-dependence of the cross sections discussed here may originate from any of the three sources mentioned in Sec. 4.4, which generalization does not affect this section's results adversely.

[4] In general, a cross section could depend on more than just two phases. For example, in $\tilde{\tau}$ pair production the phase ϕ_A of the soft, trilinear coupling can not be removed from high-energy phenomena and ϕ_A enters as a third phase. However, the case of only two phases being relevant for collider physics is more than sufficient to derive and understand the basic properties of the significances. The extension to more than two phases may be somewhat tedious, but is principally self-evident.

[5] Here I assume that both phases are available over their complete range. The case of restricted phases will be discussed later. Furthermore, due to the properties of cosine-like functions $[f(\phi) = f(2\pi - \phi) = f(-\phi)]$ the discussion of the interval $[0, \pi]$ is sufficient.

CPC cross section, is referred to as "the cross section takes a CPC-like value". Hence, the properties of significances may be reduced to the phase-dependence of the cross section by the following three statements:

Statement I
If the variation of the phase ϕ between the two CPC *choices* 0 *and* π *with a fixed CPC choice for the second phase leads to a variation of the cross section* σ *between the two CPC cross sections* σ_1^{CPC} *and* σ_2^{CPC} *such that the cross section takes no CPC-like value on* $]0,\pi[$*, then the corresponding significance* $\mathcal{S}$ *has two local minima (*0*,* π*) and a global maximum in* $\phi_{12} \in]0,\pi[$*.*

Statement II
If the variation of the phase ϕ between the two CPC choices 0 *and* π *with a fixed CPC choice for the second phase leads to a variation of the cross section* σ *between the two* CPC *cross sections* σ_1^{CPC} *and* σ_2^{CPC} *such that the cross section* σ *takes a CPC-like value* σ_3^{CPC} *for some* $\phi_3 \in]0,\pi[$*, where* σ_3 *can be any cross section out of the four* CPC *cross sections, then the first statement can be applied to the subintervals* $]0,\phi_3[$ *and* $]\phi_3,\pi[$*. Therefore the significance* $\mathcal{S}$ *will take three local minima (at* 0*,* ϕ_3*, and* π*) and two local maxima.*

Statement III
If the variation of the phase between ϕ the two CPC choices 0 *and* π *with a fixed CPC choice for the second phase leads to a variation of the cross section* σ *between the two* CPC *cross sections* σ_1^{CPC} *and* σ_2^{CPC} *such that the cross section takes* n *CPC-like values* σ_n^{CPC} *for* $\phi_n \in]0,\pi[$ *then the first statement can be applied to the* $n+1$ *subintervals* $]0,\phi_1[, \ldots,]\phi_{n-1},\phi_n[$*, and* $]\phi_n,\pi[$*. In this case the significance will have* $n+2$ *local minima and* $n+1$ *local maxima.*

Since statement II and III follow directly from the stated suitable decomposition of $]0,\pi[$ into subintervals from statement I, only statement I is derived here and the second and third one are considered as justified under certain specifications to be given later.
The presence of local minima at the boundaries 0 and π of $[0,\pi]$ follows trivially from Eq.6.2.[6] The expected existence of a global maximum is most easily understood by interpreting the significance $\mathcal{S}$ as a relative norm acting on cross sections. Using this interpretation of $\mathcal{S}$ as a norm, it is of striking clarity that for a certain value ϕ_{12} of the phase ϕ, the cross section $\sigma(\phi_{12})$ has equal distance to both CPC reference points. Hence, seen from the point of view of the minimization instruction in Eq. 6.2, the two CPC reference points are equal; this equality then results in a global maximum for $\mathcal{S}(\sigma)$ at ϕ_{12}. Furthermore, in ϕ_{12} both absolute size and sign of the slope of $\mathcal{S}$ change.[7] Given the values of σ_1^{CPC} and σ_2^{CPC} the value ϕ_{12}, which maximizes the significance, is derived from

$$\frac{\left|\sigma(\phi_{12}) - \sigma_1^{\mathrm{CPC}}\right|}{\sqrt{\sigma_1^{\mathrm{CPC}}}} \stackrel{!}{=} \frac{\left|\sigma(\phi_{12}) - \sigma_2^{\mathrm{CPC}}\right|}{\sqrt{\sigma_2^{\mathrm{CPC}}}}, \tag{6.4}$$

[6] The physical interpretation of these minima is straightforward, CPC-cross sections are simply insensitive to CP-violating phases.

[7] The change of the sign of the slope is trivial, whereas the change of the slope is due to the change of the CPC reference point, i.e. ,among others, the denominator in Eq. 6.2 changes.

and ϕ_{12} is determined independently from the integrated luminosity $\mathcal{L}$ by

$$\sigma(\phi_{12}) = \sqrt{\sigma_1^{\mathrm{CPC}}\sigma_2^{\mathrm{CPC}}}. \tag{6.5}$$

Statement I is valid for every cross section if the following two conditions are fulfilled:

a.) σ is strictly monotone on $]0,\pi[$,

b.) none of the remaining two CPC points lays between σ_1^{CPC} and $\sigma_2^{\mathrm{CPC}}]$, i.e. $\sigma_l \notin [\sigma_1^{\mathrm{CPC}}, \sigma_2^{\mathrm{CPC}}]$ for $l = 3, 4$.

If the second condition is not satisfied, statement II or the generalized formulation in statement III may be applied. Moreover, statement II (or statement III) also apply if the first condition is violated such that σ possesses a local extremum $\sigma_{ext.}$ with either $\min(\sigma_1, \sigma_2) > \sigma_{ex}$ or $\max\left(\sigma_1^{\mathrm{CPC}}, \sigma_2^{\mathrm{CPC}}\right) < \sigma_{ex}$.
When generalizing statement I to statements II and III, some attention has to be focused on Eq. 6.5; in the general case it reads

$$\sigma\left(\phi_{i,i+1}\right) = \sqrt{\sigma_i^{\mathrm{CPC}}\sigma_{i+1}^{\mathrm{CPC}}}, \tag{6.6}$$

when σ_i and σ_{i+1} are two *different* CPC cross sections that define $[\phi_i, \phi_{i+1}]$. If σ_i and σ_{i+1} are identical, i.e. σ takes an extremum in $\phi_{ext} \in\ ]\phi_i, \phi_{i+1}[$ with $\sigma(\phi_{ext}) \notin [\sigma_i, \sigma_{i+1}]$, then Eq. 6.6 must replaced by

$$\phi_{i,i+1} = \phi_{ext}. \tag{6.7}$$

The three statements given above, together with the added specifications, are sufficient to understand the behavior of significances. The transfer of the general conditions and their implications to practical cross sections will be studied for three examples in the next section.

6.2.2 Examples

As examples the three toy-model cross sections σ_i and the associated significances $\mathcal{S}(\sigma_i)$ are now briefly investigated. The first two cross sections are chosen such that they depend solely on the phase ϕ, while the third one depends on two phases ϕ and ω

$$\sigma_1(\phi) = 3 + 2\cos\phi, \tag{6.8a}$$

$$\sigma_2(\phi) = 4 + \cos\phi - \cos^2\phi, \tag{6.8b}$$

$$\sigma_3(\phi, \omega) = 4 + 2\cos\phi + \cos\omega. \tag{6.8c}$$

Here the interest is in the shape of $\mathcal{S}(\sigma_i)$ when ϕ is varied between 0 and π.
First of all, σ_1 is a monotone cross section on $]0,\pi[$ (see Fig. 6.1.a) and hence statement I from Sec. 6.2.1 is sufficient to derive the properties of $\mathcal{S}(\sigma_1)$. As predicted $\mathcal{S}(\sigma_1)$ has two minima (at 0 and π) and a maximum at ϕ_{12}^1, see Fig. 6.1.d.
The phase-dependence of σ_2 is shown in Fig. 6.1.b; due to the negative $\cos^2$-term, σ_2 is not monotone on $]0,\pi[$, i.e. $\sigma_2(0) = \sigma_2(\pi/2)$, and σ_2 takes a global maximum on $]0,\pi/2[$. Such a case is covered by statement II together with Eq. 6.7, and indeed the significance $\mathcal{S}(\sigma_2)$ possesses three minima and two maxima (ϕ_{ext}, ϕ_{12}^2) as illustrated in Fig. 6.1.e.

Finally, we observe that the four CPC reference cross sections for σ_3 fulfill $\sigma_3(0,0) > \sigma_3(0,\pi) > \sigma_3(\pi,0) > \sigma_3(\pi,\pi)$. Now, if ϕ is varied from $(0,0)$ to $(\pi,0)$ then σ_3 coincidents with $\sigma_3(0,\pi)$ for some value ϕ_3^3 of the phase ϕ, see Fig. 6.1.c. Again such a case is covered by statement II and we expect $S(\sigma_3)$ to have three minima and two maxima (ϕ_{13}^3, ϕ_{32}^3); this is observed in Fig. 6.1.f.

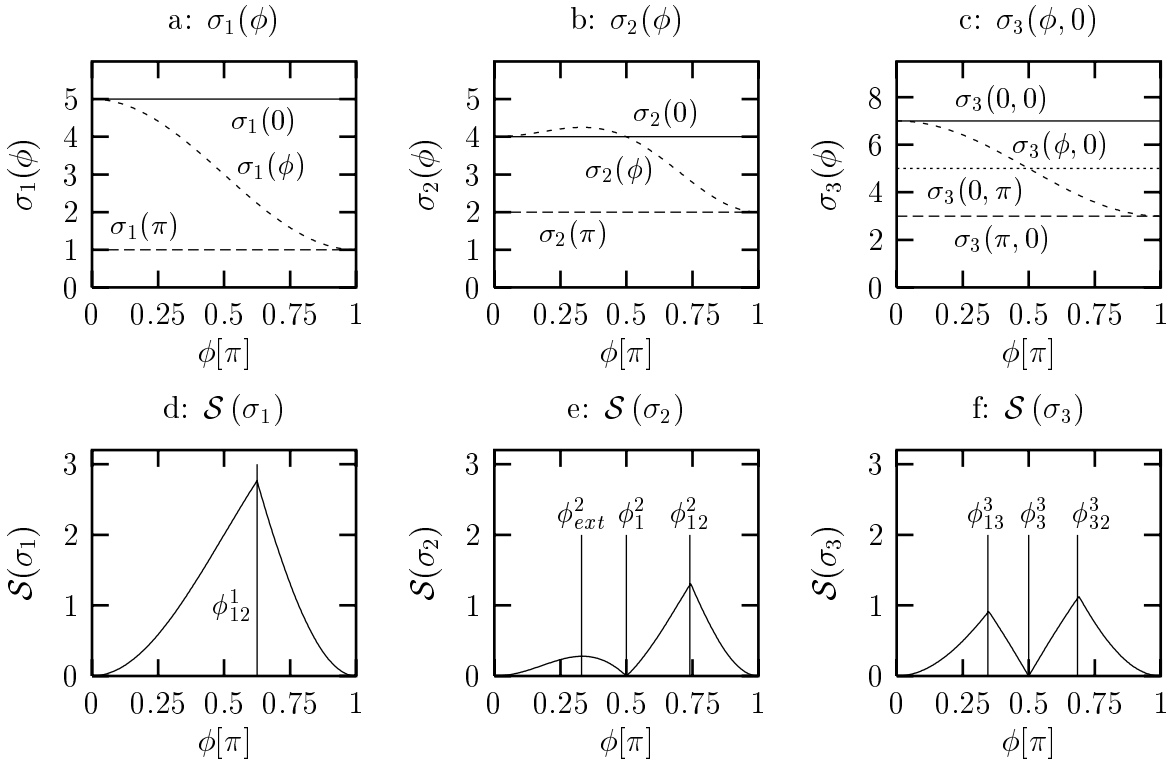

Figure 6.1: The significances $\mathcal{S}(\sigma_i)$ (lower panels) of the three toy-model cross section σ_i (upper panels) as examples of the determination of significances by their associated cross sections. The cross sections are given in arbitrary units of squared length $[\mathrm{LE}]^2$, for the integrated luminosity $\mathcal{L}$ I took $5 \times [\mathrm{LE}]^{-2}$.

Together with the discussion of constraint ranges for phases in Sec. 6.2.4 the examples basically cover all patterns for significances that are discussed within the numerical analysis. Of course, in this analysis the situation concerning the variation of phases is not as simple as assumed here. More precisely, in most cases the phase ϕ_1 is varying within the range $[\phi_1, \phi_{max}] \cup [\phi'_{max}, \pi]$ whereas the phase ϕ_μ shows some finite scatter around 0 (or/and π depending on the scenario). However, the elementary outcome of the discussion in Sec. 6.2.1 and the examples given here can be transferred to the numerical analysis.

6.2.3 Correlations

In the numerical analysis of Chapter 7 the correlations between significances of different modes will be studied. To provide a better understanding of the upcoming figures, the correlation between $\mathcal{S}(\sigma_1)$ and $\mathcal{S}(\sigma_3)$ is shown and briefly discussed here. The correlation between $\mathcal{S}(\sigma_1)$ and $\mathcal{S}(\sigma_3)$ is illustrated in Fig. 6.2.c, whereas Fig. 6.2.b just repeats $\mathcal{S}(\sigma_3)$ and Fig. 6.2.a shows the phase ϕ plotted against $\mathcal{S}(\sigma_1)$. The observed correlation pattern

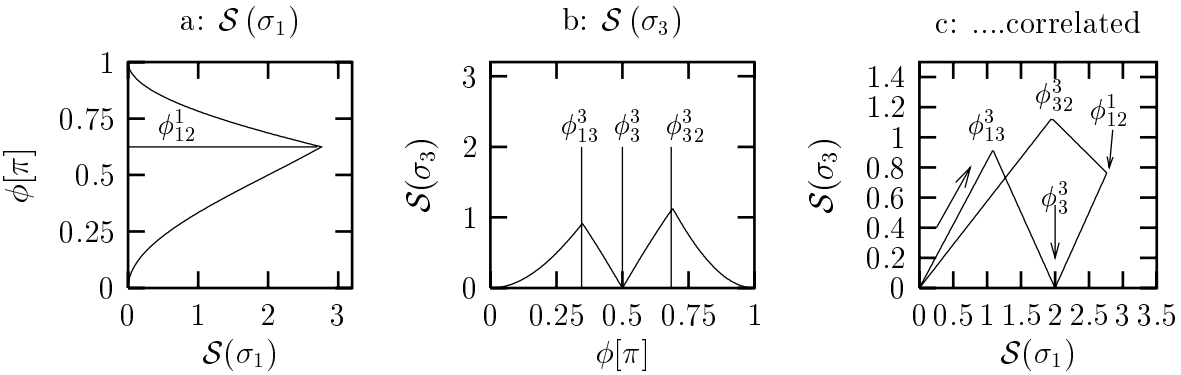

Figure 6.2: The correlation of the significances $\mathcal{S}(\sigma_1)$ (left panel) and $\mathcal{S}(\sigma_3)$ (middle panel) as an example. The correlation pattern of $\mathcal{S}(\sigma_3)$ against $\mathcal{S}(\sigma_1)$ (right panel) can be understood directly from the two left panels. The arrow in the right panel indicates the direction of increasing ϕ. All conventions as in Fig. 6.1.

can now be explained as follows:

1.) From the starting point $\phi = 0$ both significances increase with ϕ until $\phi = \phi^3_{13}$. Here $\mathcal{S}(\sigma_3)$ is maximal at the first kink.

2.) For $\phi^3_3 > \phi > \phi^3_{13}$ the significance $\mathcal{S}(\sigma_1)$ continues to increase whereas $\mathcal{S}(\sigma_3)$ decreases to reach the second minimum at ϕ^3_3. This corresponds to the second kink.

3.) For $\phi > \phi^3_3$ both significances increase again, until $\phi = \phi^1_{12}$ is reached at the third kink, where $\mathcal{S}(\sigma_1)$ is maximal.

4.) From this kink onwards $\mathcal{S}(\sigma_1)$ decreases continously towards its minimum for $\phi = \pi$.

5.) The fourth and last kink is generated when ϕ passes ϕ^3_{32} and $\mathcal{S}(\sigma_3)$ begins to decrease in order to reach the minimal value for $\phi = \pi$.

Despite its simplicity this example of a correlation pattern covers and explains almost all correlation patterns that are found in the numerical analysis. Of course, correlations of "simpler" significances are trivially covered by this example.

6.2.4 Constrained ranges for phases

Assuming more physical ranges for the phases naturally affects the behavior of the significances chosen as examples in Sec. 6.2.2. First of all, if a physical bound excludes CPC-points that correspond to intermediate CPC-values when the cross section is scanned between two allowed CPC choices the number of extrema is reduced correspondingly. If, for example, the CPC-point $(0, \pi)$ was excluded during scanning ϕ for σ_3, then the significance $\mathcal{S}(\sigma_3)$ would reveal the same properties as $\mathcal{S}(\sigma_1)$ in Fig. 6.1.d.
Secondly, if the physical bounds forbid a subinterval around one of the two CPC points that were initially used as boundaries of the scan, then the significance receives a local extremum at the physically allowed boundary $\phi_{\max}$ for ϕ. The magnitude of this "new" minimum depends on whether the former maximizing value ϕ_{12} is included in the physically allowed range or not. In case of inclusion one obtains $S(\phi_{12}) \leq S(\phi_{max})$ while $S(\phi_{12}) > S(\phi_{max})$

holds for the contrary case. Examples for such a behavior are given for $\mathcal{S}(\sigma_1)$ in Figs. 6.3.a and 6.3.b.
Finally, if the effect of the physical bound only consists of cutting out a range $[\phi_{min}, \phi_{max}]$ from a subinterval $[\phi_i, \phi_{i+1}]$ without reducing the number of available CPC reference points, then the behavior of the studied significance is essentially unchanged; only the corresponding subinterval is missing. An example of such a case is illustrated in Fig. 6.3.c.

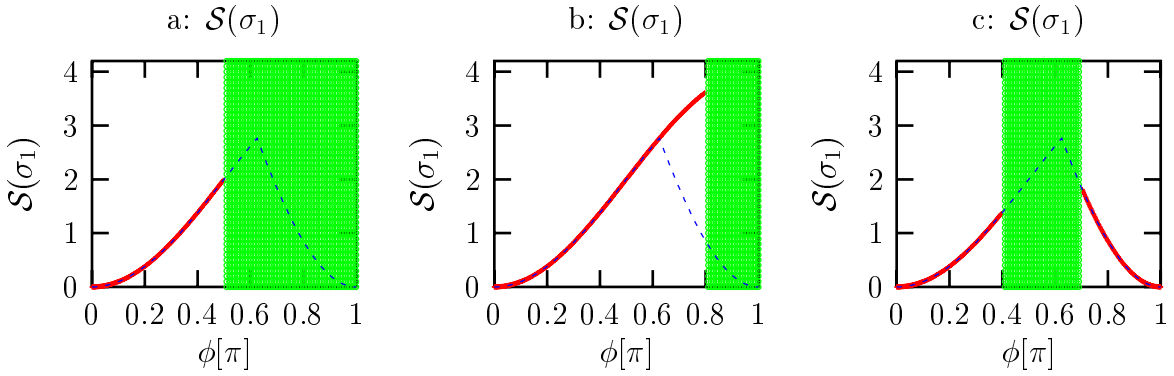

Figure 6.3: The examples for the possible impact of physical bounds on the phase ϕ in the case of $\mathcal{S}(\sigma_1)$. The shaded region indicates the subinterval for ϕ excluded by a physical bound. The solid (red) line shows $\mathcal{S}(\sigma_1)$ with the bound imposed, the dashed (blue) one recalls $\mathcal{S}(\sigma_1)$ without the bound on ϕ. All conventions as in Fig. 6.1.

Chapter 7

Numerical analysis

The thesis has now reached the stage where numerical results for our high-energy observables can be presented. First the available observables are briefly recalled and the enormous number of possible correlations between these observables is estimated. Sec. 7.2.1 collects the numerical results for the cross sections; the impact of CP-odd phases on these (CP-even) observables is discussed in Sec. 7.2.2. Afterwards the results of the (T-odd) normal components of polarization vectors are given in Sec. 7.2.3. Finally, in Sec. 7.3 a few of the possible correlations between phase-sensitive quantities are studied. More details on the code used to obtain these results appear in App. E.

7.1 Overview and organizing principle

The number of observables provided by the numerical calculation is quite large; regardless of $\sqrt{s}$, i.e. the kinematical accessibility of production channels, two low-energy and 64 high-energy observables are available. The 64 high-energy observables consist of 19 total, unpolarized cross sections, each with two significances $\mathcal{S}$ and $\overline{\mathcal{S}}$, as well as the seven independent normal components of the polarization vectors in the off-diagonal production of $\tilde{\chi}$ final states. This already amounts to 128 different correlations among low- and high-energy observables. The number of possible correlations between the high-energy observables is still larger by far. First, for each of the 19 production channels there are 3 correlations between CPC high-energy observables. Secondly, each of the 7 off-diagonal $\tilde{\chi}$ production modes allows three additional correlations between CPC and CPV high-energy observables within a production channel. Moreover, there are 171 possibilities to choose a pair of two distinguished production modes, each pair offering 3×3 different correlations of CPC high-energy observables; in total this amounts to 1539 correlations of CPC high-energy observables of different modes. In contrast, there are only 21 correlations of CPV high-energy observables from two different production modes. Finally, CPV and CPC high-energy observables of different production modes can be correlated. This corresponds to $7 \times 18 \times 3$ additional correlations. Adding up, the overall number of possible correlations a priori is of order 2,000, and a clear organizing principle to obtain a compact and meaningful presentation of the numerical results is necessary.
Of course, the information provided by the total cross sections and the corresponding sig-

nificances $\mathcal{S}$, respectively $\overline{\mathcal{S}}$, can be considered redundant.[1] Hence σ can be eliminated as a quantity other observables may correlate with.[2] Unfortunately, this restriction merely roughly halves the number of possible correlations.
As a next restriction, $\overline{\mathcal{S}}$ can be removed from the discussion in the sense that it is sufficient to study the correlation between $\mathcal{S}$ and $\overline{\mathcal{S}}$ for each mode. The reason for this is that the correlation between any other observable, say $\mathcal{X}$ and $\overline{\mathcal{S}}$, can be derived from the correlation between $\mathcal{X}$ and $\mathcal{S}$ and the correlation between $\mathcal{S}$ and $\overline{\mathcal{S}}$, i.e. the information contained in $\mathcal{C}(\mathcal{X},\overline{\mathcal{S}})$ is redundant to the information contained in $\mathcal{C}(\mathcal{X},\mathcal{S})$ if $\mathcal{C}(\mathcal{S},\overline{\mathcal{S}})$ is known.[3] For similar reasons it is not necessary to investigate the correlations between CPC and CPV high-energy observables originating from two different production channels. Applying these three considerations one is left with 270 possible correlations, if no production mode is distinguished from the others.
A criterion to distinguish production channels from each other is obviously given by the significances and, if available, by the normal components of polarization vectors. In order to find such accented production channels, the numerical results for the total cross sections, the significances $\mathcal{S}$ and $\overline{\mathcal{S}}$, and the normal component of polarization vectors $P_N^{i(j),ij}$ are presented in a tabular form and discussed briefly in Secs. 7.2.1–7.2.3. These tables are used to select a few production channels with high sensitivity to phases as well as a few promising production channels with sizeable $P_N^{i(j),ij}$. Once this reduced set of high-energy observables is selected, some correlations among these observables and with the low-energy observables are studied in Secs. 7.3.1–7.3.3. The limited set of correlations obtained by this "selective" procedure is sufficient to reveal the basic patterns that may appear when observables are correlated and to discuss the underlying physics of such correlations.

7.2 Discussion of the results

7.2.1 Cross sections

As discussed in Sec. 3.3.1, the SUSY parameters are chosen such that selectron pair production as well as production of the two lighter neutralinos or charginos is already possible at the the first stage of a FLC operating at $\sqrt{s} = 500\text{GeV}$. However, in scenario B2 the Higgsino-like states are not accessible at this energy. I take therefore in this scenario $\sqrt{s} = 800\text{GeV}$ when discussing reactions where at least one $\tilde{\chi}_3^0$, $\tilde{\chi}_4^0$, or $\chi_2^\pm$ state is produced. Note that all current FLC designs foresee an upgrade to at least that energy. A similar treatment is used in scenario B3, except for the $\tilde{\chi}_1^0\tilde{\chi}_{3,4}^0$ final state, which in this case is already accessible at $\sqrt{s} = 500\text{GeV}$.
Table 7.1 shows the maximal allowed cross sections for the 19 different production channels discussed in Secs. 4.3 and 4.4, for the three scenarios B1, B2, and B3, and the same choices for $\tan\beta$ employed in Sec. 3.3. Only combinations of phases that are allowed by the low-energy constraints on d_e and a_μ have been included in the maximization. These cross sections have been calculated at tree-level, as described in Secs. 4.3.1–4.3.4. Correc-

[1] Recall that $\mathcal{S}$ and $\overline{\mathcal{S}}$ summarize the phase-sensitivity of the total cross section using two different treatments of the physical masses.

[2] Nevertheless, the numerical results for σ are still relevant as they directly show the accessibility and serve to estimate the event rates for a given production channel.

[3] Here the notation $\mathcal{C}(\mathcal{X},\mathcal{Y})$ for the correlation between the observables $\mathcal{X}$ and $\mathcal{Y}$ was introduced.

tions due to initial-state radiation and beamstrahlung have been ignored. These effects are often larger than the dependence on CP-violating phases; they should therefore certainly be included in any future experimental analysis (along with radiative corrections, which will likely be known before the first FLC commences operations). However, they are largely independent of CP-phases, and should therefore not affect the upcoming conclusions. In Secs. 2.3.3, 4.4.3, and 5.5 it was noted that the two heaviest, Higgsino-like neutralinos are close in mass if $|\mu| > M_2, |M_1|$ and $|\mu|^2 \gg M_Z^2$; the degeneracy is only lifted at $\mathcal{O}(M_Z^2/(|\mu|^2 - M_2^2)$ and $\mathcal{O}(M_Z^2/(|\mu|^2 - |M_1|^2)$ (as well as by radiative corrections, which however are sizeable only in the presence of large A-terms in the stop sector [114, 115]). Numerically, it can be observed that the relative difference between $m_{\tilde{\chi}_3^0}$ and $m_{\tilde{\chi}_4^0}$ ranges from 24% to 35% in scenario B1, but only from 0.2% to 3.5% (0.1% to 7.5%) in scenario B2 (B3). Since the production of nearly degenerate particles is difficult to distinguish experimentally, one simply sums over the production of $\tilde{\chi}_3^0$ and $\tilde{\chi}_4^0$ in scenarios B2 and B3. In particular, only results for a single process of heavy Higgsino-like neutralino pair production are shown in these cases. Recall that the same treatment was used in Secs. 4.4.3 and 5.5, see Eq. 4.28 and Tab. 4.3, respectively Eqs. 5.24, 5.25 and Tab. 5.1. As is well known [66, 97, 103], many of the discussed cross sections can be enhanced by a factor of a few if both beams are polarized. Moreover, the discussions of Secs. 4.4.1 and 4.4.3 indicate that the greatest sensitivity to phases comes (through ϕ_1) from the interference of $SU(2)$ and $U(1)_Y$ interactions; these contributions will be suppressed if one chooses e_R^- beams, since e_R^- is a singlet under $SU(2)$. However, the sensitivity to other combinations of phases is enhanced for different choices of beam polarizations. Therefore only results for unpolarized beams are shown, with the understanding that in many cases the cross section (phase sensitivity) could be enhanced by a factor of 4(2) if fully polarized beams were available.
Table 7.1 shows that the cross sections for selectron pair production are generically bigger at e^-e^- colliders than at e^+e^- colliders [94, 95]. This difference is only partially compensated by the higher e^+e^- luminosity, if one assumes $\int \mathcal{L}dt = 500(100)\text{fb}^{-1}$ for e^+e^- (e^-e^-) collisions. These relatively conservative values are used since efficiency factors are not included. These are expected to reduce the event samples that are actually available by a factors of few, the precise value depending on both the process under consideration and the sparticle spectrum. Moreover, at e^-e^- colliders the diagonal chirality-conserving modes have higher cross sections than the off-diagonal chirality-violating mode; recall that the latter is P-wave suppressed near threshold, see Eqs. 4.13 and 4.14. At e^+e^- colliders the diagonal selectron production modes are P-wave suppressed, see Eqs. 4.8 and 4.9; this explains the rather small cross sections for $\tilde{e}_L^-\tilde{e}_L^+$ production. Finally, the selectron production cross sections are highest in scenario B3, since selectron masses are somewhat smaller than in the other two scenarios; this effect is particularly significant for $\tilde{e}_L^-\tilde{e}_L^+$ production, which is a P-wave process comparatively close to threshold. The strong dependence of the maximal $\tilde{e}_L^-\tilde{e}_L^-$ production cross section in this scenario follows from the fact that the region near $\phi_1 = \phi_\mu = 0$ is excluded by the constraint from a_μ for $\tan\beta = 20$, see Fig. 3.2.f. The biggest cross sections at e^-e^+ collisions are those for $\tilde{e}_R^-\tilde{e}_R^+$, $\tilde{\chi}_1^+\tilde{\chi}_1^-$, and $\tilde{\chi}_1^0\tilde{\chi}_1^0$ production. However, the latter leads to an invisible, and hence undetectable, final state if $\tilde{\chi}_1^0$ is a stable LSP; I will therefore not analyze it further. These large cross sections can be explained by noting that all three modes are above to a fair degree threshold and hence, compared with other modes, not phase space suppressed. Secondly, $\tilde{e}_R^-\tilde{e}_R^+$ and $\tilde{\chi}_1^-\tilde{\chi}_1^+$ receive large s-channel contributions, whereas for $\tilde{\chi}_1^0\tilde{\chi}_1^0$ the coupling of left- and right-handed selectrons to the Bino-component results in sizeable t-channel contributions. This implies

	B1		B2		B3	
$\tan\beta$	3	12	3	12	10	20
$\tilde{e}^-_R\tilde{e}^-_R$	378	371	398	390	513	512
$\tilde{e}^-_L\tilde{e}^-_R$	79.8	79.0	80.3	75.1	181	182
$\tilde{e}^-_L\tilde{e}^-_L$	272	261	281	270	523	378
$\tilde{e}^-_R\tilde{e}^+_R$	180	172	182	176	296	293
$\tilde{e}^-_L\tilde{e}^+_R$	106	104	96.5	94.5	168	160
$\tilde{e}^-_L\tilde{e}^+_L$	8.3	7.2	8.0	6.9	60.9	60.3
$\tilde{\chi}^-_1\tilde{\chi}^+_1$	250	212	144	126	175	170
$\tilde{\chi}^-_1\tilde{\chi}^+_2$	179	173	16.0*	7.5*	43.6*	38.7*
$\tilde{\chi}^-_2\tilde{\chi}^+_2$	–	–	–	–	85.9*	89.4*
$\tilde{\chi}^0_1\tilde{\chi}^0_1$	201	197	236	231	271	271
$\tilde{\chi}^0_1\tilde{\chi}^0_2$	130	120	140	132	159	161
$\tilde{\chi}^0_1\tilde{\chi}^0_3$	46.8	41.2	6.4*	5.7*	20.1	19.7
$\tilde{\chi}^0_1\tilde{\chi}^0_4$	52.8	53.7				
$\tilde{\chi}^0_2\tilde{\chi}^0_2$	74.6	49.6	58.5	49	76.2	68.9
$\tilde{\chi}^0_2\tilde{\chi}^0_3$	73.6	77.7	5.1*	5.2*	22.3*	21.4*
$\tilde{\chi}^0_2\tilde{\chi}^0_4$	27.1	22.8				
$\tilde{\chi}^0_3\tilde{\chi}^0_3$	0.26	0.43	–	–	38.3*	38.6*
$\tilde{\chi}^0_3\tilde{\chi}^0_4$	36.6	36.0				
$\tilde{\chi}^0_4\tilde{\chi}^0_4$	–	–				

Table 7.1: Maximal values of the total cross sections [in fb] for unpolarized $e^\pm$ beams, for the scenarios defined in Table 3.2 . "–" means that the corresponding mode is not accessible. In scenarios B2 and B3 I have summed over the production of the heavy Higgsino–like neutralinos, as described in the text. The beam energy is 500 GeV in most cases, but has been raised to 800 GeV for the production of $\tilde{\chi}^\pm_2$ and $\tilde{\chi}^0_{3,4}$ states in scenarios B2 and B3 as indicated by the asterisk. Note that the charge–conjugate mode is included if it is distinct from the listed one.

that for the two lightest $\tilde{\chi}$ final states the gaugino-like nature (or sizeable gaugino components) are crucial. A similar argument also holds for the modes $\tilde{\chi}^0_1\tilde{\chi}^0_2$ and $\tilde{\chi}^0_2\tilde{\chi}^0_2$. Again a (still) sizeable phase space goes hand in hand with the gaugino-like nature of the final states, and one finds acceptably large cross sections. Contrariwise, the cross sections for producing two heavy charginos or neutralinos are suppressed both by phase space and their Higgsino-like nature. Finally, the production of one light and one heavy $\tilde{\chi}$ state is possible in all three scenarios. Since, as discussed in Secs. 4.4.2 and 4.4.3, these cross sections are non-vanishing only in the presence of Higgsino-gaugino mixing, they fall with increasing $|\mu|$ (B1 $\rightarrow$ B3 $\rightarrow$ B2). Nevertheless, even in scenario B2 one will have several thousand events containing these Higgsino-like states. For the other channels, typically several tens

of thousands of events will be available, meaning that the cross section could be measured with a statistical uncertainty of 1% or less.

7.2.2 Significances

The maximal possible values for the significances $\mathcal{S}$ and $\overline{\mathcal{S}}$ of Eqs. 6.2 and 6.3 that can be found in the three scenarios are summarized in Tab. 7.2. The $\tilde{e}_L^-\tilde{e}_L^-$ mode shows the strongest phase-dependence of all selectron production channels, i.e. the highest significance, largely independent of $|\mu|$ and $\tan\beta$. The $\tan\beta$-dependence of $\mathcal{S}$ in scenario B3 is due to the fact that the point $\phi_1 = \phi_\mu = 0$ is excluded by the a_μ constraint at $\tan\beta = 20$, but still allowed at $\tan\beta = 10$, as shown in Fig. 3.2.c, and $S(\tilde{e}_L^-\tilde{e}_L^-)$ behaves similar to the example illustrated in Fig. 6.3.b. As expected from Tab. 4.1 the mixed $\tilde{e}_L^-\tilde{e}_R^+$ mode is the most promising selectron production mode for our purposes at e^+e^- colliders. It would allow to unambiguously detect (at more than five statistical standard deviations) the presence of CP-violating phases over much of the allowed parameter space, although the effect diminishes with increasing $|\mu|$ and increasing $\tan\beta$ (except in scenario B3, for the reason given above). For both these modes $\mathcal{S}$ and $\overline{\mathcal{S}}$ give very similar results. With the exception of scenario B1 with strong Higgsino-gaugino mixing, $\tilde{e}_R$ pair production at both e^-e^- and e^+e^- colliders is much less promising, especially if the physical masses of $\tilde{\chi}_1^0$, $\tilde{\chi}_3^0$, and $\tilde{\chi}_1^\pm$ are held fixed, i.e. for $\overline{\mathcal{S}}$. Similarly, $\tilde{e}_L^-\tilde{e}_R^-$ is also relatively insensitive to phases, but here the sensitivity to phases decreases if the physical masses are allowed to vary with phases, i.e. $\mathcal{S} < \overline{\mathcal{S}}$. Most of these features can be understood from the discussion of Tab. 4.1 in Sec .4.4.1.

The poor phase sensitivity of the $\tilde{e}_L^-\tilde{e}_L^+$ mode relative to the $\tilde{e}_L^-\tilde{e}_R^+$ mode can partly be explained by the smaller cross section of the former mode; recall that the significances scale with the square root of the number of events. In addition, closer inspection of the matrix elements shows that in the case of $\tilde{e}_L^-\tilde{e}_L^+$ production, the terms proportional to $\cos\phi_1$ and $\cos(\phi_1+\phi_\mu)$ are suppressed by extra factors[4] of $\sin^2\theta_W$ and $\sin^4\theta_W$ relative to the leading phase-independent terms; for the $\tilde{e}_L^-\tilde{e}_R^+$ mode the corresponding factors are 1 and $\sin^2\theta_W$, respectively.

Concerning the $\tilde{e}_L^-\tilde{e}_L^-$ and $\tilde{e}_R^-\tilde{e}_R^+$ mode, the similar, yet respectively quite different results for $\mathcal{S}$ and $\overline{\mathcal{S}}$ have already been explained in Sec. 4.4.1. Here it was noted that the dominant phase-dependence of the former mode is of order M_Z^0. Hence both treatments of the physical neutralino masses only lead to subleading phase-dependences and very similar results for $\mathcal{S}$ and $\overline{\mathcal{S}}$ must be expected. Furthermore, in the same section it was pointed out that the phase-dependence of the latter mode is dominated by phase-dependent corrections to the neutralino masses. Therefore, if these masses are kept fixed the dominant phase-dependences are eliminated and $\overline{\mathcal{S}} < \mathcal{S}$ is observed. Concerning the remaining four selectron production modes, it has already been emphasized in Sec. 4.4.1 that the revelation of the dominant phase-dependence (either from coupling or from kinematical effects) strongly depends on the given choices for SUSY and collider parameters. Hence the results of such an analysis can not be generalized, and I do not attempt to explain the different relative sizes of $\mathcal{S}$ and $\overline{\mathcal{S}}$ in the $\tilde{e}_R^-\tilde{e}_R^-$, $\tilde{e}_L^\pm\tilde{e}_R$, and $\tilde{e}_L^+\tilde{e}_L^-$ modes. However, the presence of three different hierarchies ($\mathcal{S} < \overline{\mathcal{S}}$, $\mathcal{S} \simeq \overline{\mathcal{S}}$, $\mathcal{S} > \overline{\mathcal{S}}$) in general can be explained by con-

[4] These terms also come with relative factors $|M_1|/M_2$ and $|M_1|^2/M_2^2$, respectively. These factors lead to some additional suppression of the phase-dependence in $\tilde{e}_L^-\tilde{e}_L^+$.

	B1				B2				B3			
$\tan\beta$	3		12		3		12		10		20	
	$\mathcal{S}$	$\bar{\mathcal{S}}$	$\mathcal{S}$	$\bar{\mathcal{S}}$	$\mathcal{S}$	$\bar{\mathcal{S}}$	$\mathcal{S}$	$\bar{\mathcal{S}}$	$\mathcal{S}$	$\bar{\mathcal{S}}$	$\mathcal{S}$	$\bar{\mathcal{S}}$
$\tilde{e}_R^-\tilde{e}_R^-$	3.7	17.0	0.8	5.0	2.9	1.0	0.8	0.4	0.5	1.1	0.3	0.8
$\tilde{e}_L^-\tilde{e}_R^-$	3.0	10	2.8	4.7	0.9	2.5	0.8	1.3	2.7	4.2	2.9	4.1
$\tilde{e}_L^-\tilde{e}_L^-$	61	60	61	60	59	57	59	59	90	90	136	136
$\tilde{e}_R^-\tilde{e}_R^+$	10	27	2.2	7.8	6.7	1.1	1.8	0.5	4.3	2.6	3.0	2.1
$\tilde{e}_L^-\tilde{e}_R^+$	43	68	32	39	16	16	11	12	20	23	22	24
$\tilde{e}_L^-\tilde{e}_L^+$	1.9	3.3	1.5	0.9	1.2	1.3	0.5	0.7	3.3	4.0	3.5	3.8
$\tilde{\chi}_1^-\tilde{\chi}_1^+$	0.4	0.9	< 0.1	2.5	25	1.6	2.8	0.2	1.3	0.3	0.6	0.6
$\tilde{\chi}_1^-\tilde{\chi}_2^+$	< 0.1	1.8	< 0.1	6.4	$70^\star$	$70^\star$	$3.5^\star$	$3.5^\star$	$2.4^\star$	$1.7^\star$	$1.4^\star$	$2.9^\star$
$\tilde{\chi}_2^-\tilde{\chi}_2^+$	–	–	–	–	–	–	–	–	$1.4^\star$	$1.6^\star$	$0.7^\star$	$1.5^\star$
$\tilde{\chi}_1^0\tilde{\chi}_2^0$	41	46	34	32	81	81	92	92	100	100	94	94
$\tilde{\chi}_1^0\tilde{\chi}_3^0$	56	73	30	29	$9.9^\star$	$10.5^\star$	$6.2^\star$	$6.2^\star$	21.5	23.8	21.1	23.2
$\tilde{\chi}_1^0\tilde{\chi}_4^0$	92	104	82	89								
$\tilde{\chi}_2^0\tilde{\chi}_2^0$	74	90	56	66	11	8.2	5.2	5.2	17	18	18	19
$\tilde{\chi}_2^0\tilde{\chi}_3^0$	16	37	7.0	2.9	$6.0^\star$	$6.2^\star$	$2.9^\star$	$2.8^\star$	$1.9^\star$	$1.1^\star$	$3.1^\star$	$2.0^\star$
$\tilde{\chi}_2^0\tilde{\chi}_4^0$	20	14	5.5	5.6								
$\tilde{\chi}_3^0\tilde{\chi}_3^0$	6.3	5.4	8.4	9.3	–	–	–	–	$2.4^\star$	$3.1^\star$	$2.6^\star$	$3.4^\star$
$\tilde{\chi}_3^0\tilde{\chi}_4^0$	9.3	11	9.3	10								
$\tilde{\chi}_4^0\tilde{\chi}_4^0$	–	–	–	–								

Table 7.2: The maximal significances $\mathcal{S}$ of Eq. 6.2 and $\bar{\mathcal{S}}$ of Eq. 6.3 that can be found for choices of phases which are compatible with all low–energy constraints. The scenarios B1, B2 and B3 have been defined in Table 3.2. Notation and calculational procedures are as in Table 7.1.

sidering that coupling and kinematical effects can have a relative sign, i.e. can contribute constructively or destructively to the total phase-dependence. The former case always leads to $\mathcal{S} > \overline{\mathcal{S}}$, whereas in the latter case the hierarchy is controlled by the relative size of both contributions to the total phase-dependence. This consideration holds for any mode where coupling and kinematical effects contribute at the same order in M_Z and where these contributions are of the same size. For example, from $\mathcal{S} \simeq \overline{\mathcal{S}}$, as observed for the $\tilde{e}_L^-\tilde{e}_R^+$ mode, it can be concluded that the coupling effects dominate heavily the kinematical or that both contributions have a relative sign and the ratio of the kinematical contribution to the coupling contribution is roughly two.

Turning to chargino modes, it is observed that they are sensitive to phases only in scenario B2, with large $|\mu|$, and for small $\tan\beta$. The only relevant phase here is ϕ_μ. Recall from the discussion of Sec. 3.3 that the maximal allowed value of this phase scales like $|\mu|^2$. This means that the maximal deviation of $|\cos\phi_\mu|$ from unity scales like $|\mu|^4$. In case of

$\tilde{\chi}_1^-\tilde{\chi}_1^+$ production, the main phase sensitivity[5] derives from the phase-dependence of $m_{\tilde{\chi}_1^\pm}$, which gives an extra factor of $\sin 2\beta/|\mu|$. Altogether the maximal $\mathcal{S}\left(\tilde{\chi}_1^-\tilde{\chi}_1^+\right)$ therefore scales like $|\mu|^3 \sin 2\beta$; this reproduces the numerical behavior in scenarios B2 and B3, with little Higgsino-gaugino mixing. A similar scaling also holds for the mixed $\tilde{\chi}_1^-\tilde{\chi}_2^+$ mode. However, in this case the cross section itself vanishes in the absence of Higgsino-gaugino mixing, implying that now the phase-dependent terms are of same order in M_W as the phase-independent ones; see the discussion of Sec. 4.4.2. Moreover, the significant phase-dependence proportional to $\sin 2\beta/|\mu|$ now derives from the $Z\tilde{\chi}_1^-\tilde{\chi}_2^+$ coupling instead of from the phase-dependence of the chargino masses. The latter phase-dependence is of relative order M_W^2, and could only contribute if this suppressing factor was compensated by a kinematical enhancement near threshold as suggested by Eq. 4.27. As both definitions of the significance give very similar results, this is not the case. Finally, the very strong $\tan\beta$ dependence of these significances, as observed in scenario B2, is due to the fact that values of ϕ_μ near π are only allowed for small $\tan\beta$ in this case; see Fig. 3.2.b.

In contrast to the chargino modes, some neutralino modes are promising for all considered scenarios, the noticeable exception being the production of two heavier neutralinos.[6] This is true in particular for the $\tilde{\chi}_1^0\tilde{\chi}_2^0$ mode. It was found in Sec. 4.4.3 that in this case both the total cross section and the phase-dependence (on ϕ_1) already start at $\mathcal{O}(M_Z^0)$, i.e. they are *not* suppressed for large $|\mu|$ or large $\tan\beta$. Indeed, one finds that this mode often allows a somewhat better sensitivity than the celebrated $\tilde{e}_L^-\tilde{e}_L^-$ mode. The mixed Higgsino-gaugino modes also do well, especially for not too large values of $|\mu|$. As expected from the discussion of Tab. 4.3, the $\tilde{\chi}_1^0\tilde{H}$ is somewhat more promising than the $\tilde{\chi}_2^0\tilde{H}$ mode. The rather good phase sensitivity of the $\tilde{\chi}_2^0\tilde{\chi}_2^0$ mode at first seems surprising, given that the phase-dependence only enters at $\mathcal{O}(M_Z^2)$, whereas the cross section is $\mathcal{O}(M_Z^0)$. However, closer inspection of the sensitivities for the $\tilde{\chi}_2^0\tilde{\chi}_2^0$ and $\tilde{\chi}_1^0\tilde{H}$ modes shows that the relative factor between them is in fact $\mathcal{O}(|M_1|/M_Z)$, which is close to unity in the studied case. Note that the relatively large size of the $\tilde{\chi}_2^0\tilde{\chi}_2^0$ cross sections facilitates its precise measurements and therefore increases the significances. However, as remarked at the end of Sec. 6.1 the mixed $\tilde{\chi}_1^0\tilde{H}$ final state is still considered to be more promising, since it will be less sensitive to systematic uncertainties.

Concerning the quite similar results for $\mathcal{S}$ and $\overline{\mathcal{S}}$ in $\tilde{\chi}_1^0\tilde{\chi}_2^0$, $\tilde{\chi}_1^0\tilde{H}$, and $\tilde{\chi}_2^0\tilde{H}$ production, this observation once again points to the fact that for these three production cross sections, phase-dependent and phase-independent terms are of same order in M_Z and hence kinematical effects only lead to subleading phase-dependences; i.e. the different treatments of the kinematical masses do not result in different values for $\mathcal{S}$ and $\overline{\mathcal{S}}$. Contrariwise, for $\tilde{\chi}_2^0\tilde{\chi}_2^0$ production, phase-dependences from coupling and kinematical effects contribute at the same order of M_Z, hence $\mathcal{S} \neq \overline{\mathcal{S}}$ should be expected. In this case the unexpectedly similar values of $\mathcal{S}$ and $\overline{\mathcal{S}}$ (for some scenarios) are due to "accidental" kinematical fine-tuning.

[5] The dominance of the "kinematical effect" in $\tilde{\chi}_1^-\tilde{\chi}_1^+$ production for scenario B2 is obvious when $\mathcal{S}$ and $\overline{\mathcal{S}}$ are compared.

[6] Since these modes were already disfavored in Sec. 4.4.3, they are not commented on any further here.

7.2.3 Polarizations

It has been emphasized earlier that, strictly speaking, the significances $\mathcal{S}$ and $\overline{\mathcal{S}}$ only measure deviations from the CP-conserving MSSM, regardless of the origin of these deviations; i.e. they do not directly measure CP-violation. Direct evidence for CP-violation might be found in the measurement of the T-odd normal component of $\tilde{\chi}$ polarization vectors introduced and discussed in Chapter 5. The maximal possible absolute values for these "polarization asymmetries" for scattering angle $\theta = \pi/2$ are collected in Tab. 7.3. Recall that a nonzero asymmetry can emerge only from the production of two *different* $\tilde{\chi}$ states, and that the asymmetry will be larger for the *lighter* of the two final states. However, the polarization can only be measured through $\tilde{\chi}$ decay products; therefore the polarization of the $\tilde{\chi}_1^0$, which is probably the LSP, is not considered.
As expected from Sec. 5.4, chargino polarization is indeed too small to be useful, except in scenario B2 with large $|\mu|$ and small $\tan\beta$. Recall from the discussion in Sec. 5.4 that this asymmetry (for the lighter chargino) scales like $|\mu| \sin 2\beta \sin\phi_\mu$; it was found in Sec. 3.3 that the upper bound on $|\sin\phi_\mu|$ scales like $|\mu|^2$. Altogether, the maximal value of P_N of the lighter chargino therefore scales like $|\mu|^3$. The very rapid decrease of this polarization with increasing $\tan\beta$ is partly due to the explicit $\sin 2\beta$ dependence, and partly due to the disappearance of the band around $\phi_\mu \simeq \pi$, see Fig. 3.2.b.
In scenarios with large $|\mu|$ (B2, B3) the $\tilde{\chi}_1^0\tilde{\chi}_2^0$ mode again proves the most sensitive to CP-violating phases. Eq. 5.23 shows that in this case a nonzero P_N already emerges at $\mathcal{O}(M_Z^0)$ and remains finite both for large $|\mu|$ and large $\tan\beta$. This well describes the behavior seen in cases where the perturbative diagonalization of the neutralino mass matrix is reliable. Moreover, recall from Tab. 7.1 that this mode has a fairly high cross section. This is important, since even with perfect (100%) analyzing power one needs nearly 1,000 events to detect a 10% asymmetry at the 3σ level.

	i	B1		B2		B3	
$\tan\beta$		3	12	3	12	10	20
$\tilde{\chi}_1^-\tilde{\chi}_2^+$	$\tilde{\chi}_1^-$	1.4	0.2	57*	5.2*	1.6*	0.9*
$\tilde{\chi}_1^0\tilde{\chi}_2^0$	$\tilde{\chi}_2^0$	6.4	7.8	34	33	31	31
$\tilde{\chi}_1^0\tilde{\chi}_3^0$	$\tilde{\chi}_3^0$ $(\tilde{H})$	22	27	7.2*	2.4*	6.3	6.8
$\tilde{\chi}_1^0\tilde{\chi}_4^0$	$\tilde{\chi}_4^0$ $(\tilde{H})$	5.5	6.6				
$\tilde{\chi}_2^0\tilde{\chi}_3^0$	$\tilde{\chi}_2^0$	5.5	6.4	23*	7.8*	9.7*	9.9*
$\tilde{\chi}_2^0\tilde{\chi}_4^0$	$\tilde{\chi}_2^0$	45	30				
$\tilde{\chi}_3^0\tilde{\chi}_4^0$	$\tilde{\chi}_3^0$ $(\tilde{H})$	4.9	6.8	–	–	1.9*	1.8*

Table 7.3: Maximal absolute values of $P_N^{i,ij}$ in percent. The scattering angle θ is set to $\frac{\pi}{2}$. Notations and conventions are as in Table 7.1.

As expected from the earlier discussion of Tab. 5.1, the mixed Higgsino-gaugino modes also have sizeable asymmetries even for large $|\mu|$, the heavier $\tilde{\chi}_2^0\tilde{H}$ mode being more promising. However, the relatively small cross sections of these modes imply that one would need a very large luminosity for a meaningful measurement of polarization asymmetries in these modes, except in scenario B1 with strong Higgsino-gaugino mixing. Indeed, in this last

case the $\tilde{\chi}_1^0\tilde{\chi}_3^0$ and $\tilde{\chi}_2^0\tilde{\chi}_4^0$ modes are far more promising than the $\tilde{\chi}_1^0\tilde{\chi}_2^0$ mode.
As noted earlier in this thesis the spin of the produced $\tilde{\chi}$ particles can only be determined on a statistical basis by (partly) reconstructing their decays. Therefore it is encouraging that recent dedicated studies demonstrated sensitivity to phases in the neutralino mass matrix using T-odd variables constructed in $e^+e^- \to \tilde{\chi}_1^0\tilde{\chi}_i^0$ with $\tilde{\chi}_i^0 \to \tilde{\chi}_1^0 l^+l^-$ [58], $\tilde{\chi}_i^0 \to \tilde{\chi}_1^0 Z$ [60], and $\tilde{\chi}_i^0 \to \tilde{\tau}_1^\pm\tau^\mp \to \tau^+\tau^-$ [59, 116]. The latter decay chain will be discussed intensively in Part III.

7.3 Correlations between observables

In addition to their absolute sizes, the correlations between various phase-dependent quantities are also of interest. Such correlations can provide stringent tests of the MSSM, since they are a consequence of the limited number of parameters affecting these leptonic observables in the MSSM. Recall that all the given high-energy observables (cross sections and polarizations) depend on the phase ϕ_μ; most of them also depend on the phase ϕ_1, the exception being observables related to chargino pair production. In Sec. 3.3 it was observed that ϕ_μ is tightly constrained by the low-energy observables $(a_\mu)_{\rm SUSY}$ and (especially) $(d_e)_{\rm SUSY}$, while ϕ_1 in most cases can take any value (for some combination of the other phases). Moreover, the d_e constraint enforces a tight correlation between ϕ_1 and ϕ_μ, see Fig. 3.2.
Therefore this section is devoted to the presentation of a few of the large number of possible correlations. Motivated by the findings of Secs. 7.2.1 to 7.2.3 the focus is strictly on high-energy observables associated with $\tilde{e}_L^-\tilde{e}_L^-$, $\tilde{e}_L^-\tilde{e}_R^+$, $\tilde{\chi}_1^-\tilde{\chi}_2^+$, $\tilde{\chi}_1^0\tilde{\chi}_2^0$, and $\tilde{\chi}_1^0\tilde{\chi}_3^0$ production modes. For all remaining production channels the high-energy observables were found to be less promising. However, the various correlations discussed here cover the "range" of correlation patterns and therefore are representative. Correlations between $\mathcal{S}$ and $\overline{\mathcal{S}}$ are not presented here; they are either trivial (if the leading phase-dependence of a cross section is of same order in $M_{Z(W)}$ as the leading phase-independent contributions) or depend strongly on the choices for SUSY parameters and $\sqrt{s}$. The latter point was already emphasized during the discussions in Sec. 4.4, and the numerical results for $\mathcal{S}$ and $\overline{\mathcal{S}}$ were commented on in Sec. 7.2.2.

7.3.1 Low- and high-energy quantities

The presentation of selected numerical results starts with comparing high- and low-energy quantities in Fig. 7.1. Obviously the phase-sensitive high-energy observables are *not* correlated at all with $(d_e)_{\rm SUSY}$. This is true both for T-even observables (Fig. 7.1.a) and T-odd ones (Fig. 7.1.b); in scenarios with strong Higgsino-gaugino mixing (Fig. 7.1.a) and in scenarios where this mixing is suppressed (Fig. 7.1.b); and for quantities that depend on ϕ_1 and ϕ_μ (Fig. 7.1.a) as well as those that depend only on ϕ_μ (Fig. 7.1.b). This can be explained by the observation made at the end of Sec. 3.3.3, namely that $(d_e)_{\rm SUSY}$ itself is not correlated with any of the phases after scanning over the other two phases; recall that the low-energy observables also depend on ϕ_A. For example, except at the very edges of the allowed range of ϕ_μ, $(d_e)_{\rm SUSY}$ can still take on any value within its experimentally allowed range even after ϕ_μ is fixed. This is due to the variation of ϕ_1 and ϕ_A.
On the other hand, in some cases significant correlations between high-energy observables

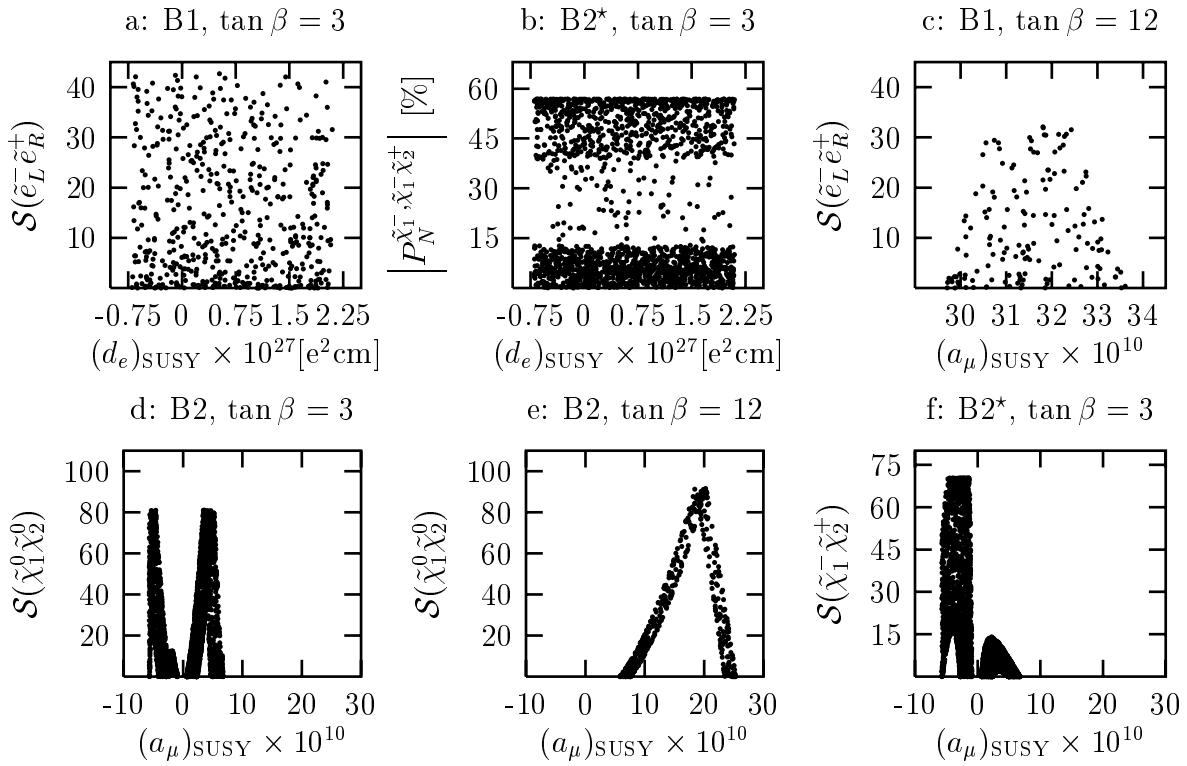

Figure 7.1: Correlations between low– and high–energy quantities. Most high–energy observables have been computed at $\sqrt{s} = 500$ GeV, except for panels b) and f), which are for $\sqrt{s} = 800$ GeV. The parameter sets B1 and B2 have been defined in Table 1, and the significance $\mathcal{S}$ is defined via Eq. 6.2.

and $(a_\mu)_{\rm SUSY}$ are observed. A cosine-like dependence of $(a_\mu)_{\rm SUSY}$ on ϕ_1 was observed in Fig. 3.6 for scenarios B2 and B3; in some cases (e.g. B2 at small $\tan\beta$), two separate bands of $(a_\mu)_{\rm SUSY}$ values exist, corresponding to $\cos\phi_\mu \simeq \pm 1$. However, in scenario B1 $(a_\mu)_{\rm SUSY}$ shows very little correlation with ϕ_1, see Figs. 3.6.a,d. Correspondingly, Fig. 7.1.c shows no correlation for scenario B1, while Figs. 7.1.d–f reveal significant correlations between $(a_\mu)_{\rm SUSY}$ and T-even high-energy observables for scenario B2. Comparison of panels d and e shows that this correlation becomes stronger at larger $\tan\beta$. This is due to the diminished role of ϕ_A and the reduced width of the allowed band in the (ϕ_μ, ϕ_1) plane; the overall size of $|(a_\mu)_{\rm SUSY}|$ also increases with increasing $\tan\beta$, see Eq. 3.17b. Finally, Fig. 7.1.f illustrates that high-energy observables whose only phase sensitivity is through ϕ_μ also correlate with ϕ_μ. Note in particular that $\mathcal{S}(\tilde{\chi}_1^+\tilde{\chi}_2^-)$ is much bigger for $(a_\mu)_{\rm SUSY} < 0$ (which corresponds to $\phi_\mu \simeq \pi$) than for $(a_\mu)_{\rm SUSY} > 0$ (which corresponds to $|\phi_\mu| \ll 1$). This confirms the explanation that was given in the discussion of Tab. 7.2 for the very strong $\tan\beta$ dependence of this quantity. For this class of observables, the correlation with $(a_\mu)_{\rm SUSY}$ also becomes stronger with increasing $\tan\beta$; however, as remarked in Secs. 4.4.2 and 5.4, the sensitivity to ϕ_μ at least disappears proportional to $\sin 2\beta$.

7.3.2 Significances of different modes

In most cases, different phase sensitive high-energy observables are strongly correlated with each other. This is illustrated by Fig. 7.2, where the two significances that are usually most

promising, i.e. for the $\tilde{e}_L^-\tilde{e}_L^-$ and $\tilde{\chi}_1^0\tilde{\chi}_2^0$ final states, are plotted against each other. The simplest correlation obtains for scenarios B3 for $\tan\beta = 20$, shown in panel f. In this case the constraint on $(a_\mu)_{\rm SUSY}$ excludes values of ϕ_1 near 0 as well as ϕ_μ near π, see Fig. 3.2.f. Hence the minimization in the definition of $\mathcal{S}$ in Eq. 6.2 only goes over the single CPC point $\phi_\mu = 0$, $\phi_1 = \pi$. The strong correlation observed in Fig. 7.2.f then follows from the fact that both significances shown here are in leading order of M_Z essentially proportional to $\cos\phi_1$ as explained in Secs. 4.4.1 and 4.4.3. The next simplest situation obtains if both

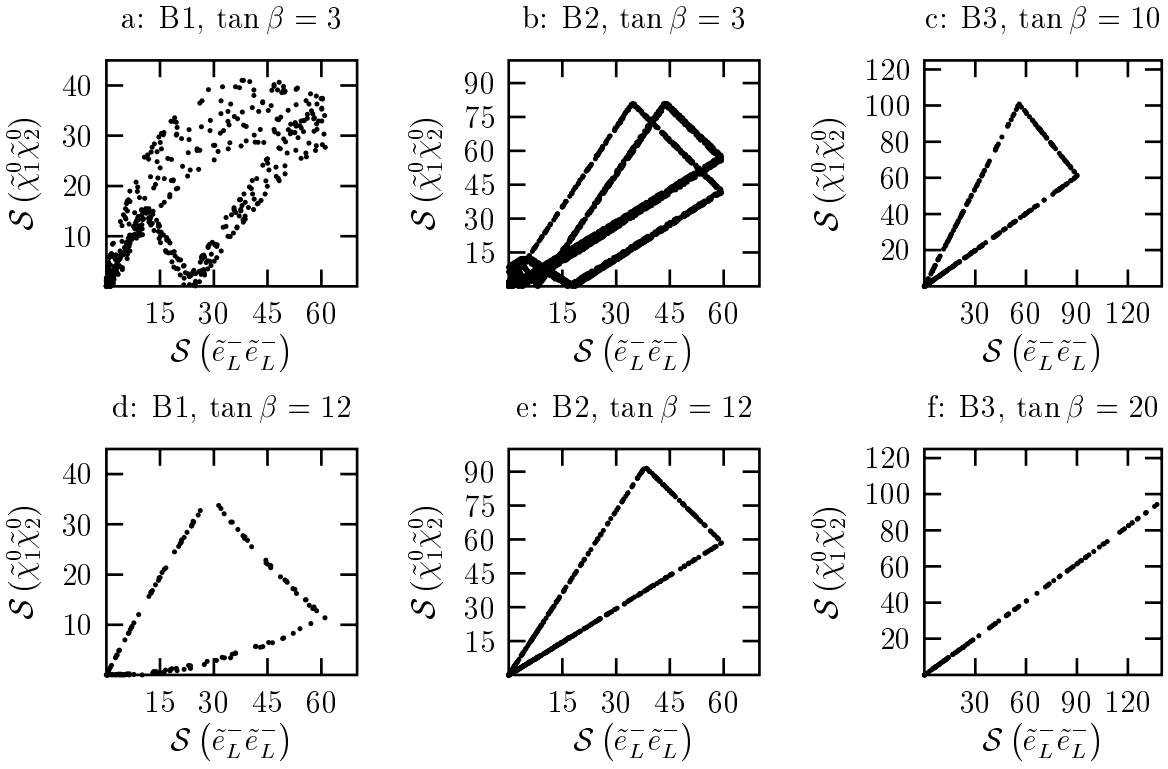

Figure 7.2: Correlations between the significances, defined as in Eq. 6.2, for the processes $e^-e^- \to \tilde{e}_L^-\tilde{e}_L^-$ and $e^+e^- \to \tilde{\chi}_1^0\tilde{\chi}_2^0$, both taken at $\sqrt{s} = 500$ GeV.

$\phi_1 = 0$ and $\phi_1 = \pi$ are allowed, but $\phi_\mu = \pi$ is still forbidden, and $\tan\beta$ is not too small [panels c, d, and e]. Now the minimization in Eq. 6.2 runs through two CPC points. Recall that this minimization is performed independently for the two significances shown in Fig. 7.2. The upper (lower) branch connected to the origin is populated by combinations of phases where both significances are minimized by $\phi_1 = 0$ ($\phi_1 = \pi$). These two bands are connected by sets of points where our algorithm picks the CPC point $\phi_1 = 0$ for $\mathcal{S}(\tilde{e}_L^-\tilde{e}_L^-)$, but chooses the point $\phi_1 = \pi$ for $\mathcal{S}(\tilde{\chi}_1^0\tilde{\chi}_2^0)$.

Fig. 7.2.a shows that in scenario B1 the correlations get weaker at smaller $\tan\beta$. To understand this, recall that B1 has strong Higgsino-wino mixing, and hence a relatively strong dependence on ϕ_μ through the combination $\cos(\phi_1 + \phi_\mu)$, which linearly depends on ϕ_μ when $|\phi_1|$ and $|\phi_1 - \phi_\mu|$ are sizeable. In contrast, $\cos\phi_\mu$ only depends quadratically on ϕ_μ for small $|\phi_\mu|$, and can therefore, as a good approximation, be set to 1 in scenario B1, see Figs. 3.2.a,d. This dependence on ϕ_μ will be numerically different for the two modes present, loosening the correlation. This effect is important only at small $\tan\beta$ for two reasons. First, all contributions to our cross sections that are sensitive to ϕ_μ are suppressed by a factor $\sin 2\beta$ at large $\tan\beta$. Secondly, the upper bound on $|\phi_\mu|$ was

observed to decrease with increasing $\tan\beta$ for scenario B1.
Fig. 7.2.a shows another new effect on the lower branch, where both significances are evaluated with the CPC point $\phi_\mu = \phi_1 = 0$. The cross section for $\tilde{\chi}_1^0\tilde{\chi}_2^0$ production in this case reveals a non-monotonous dependence on ϕ_1. As expected from the expansion of the result in Eq. 4.26 in powers of M_Z using Eqs. 2.39–2.44, this cross section reaches its absolute minimum at $\cos\phi_1 = +1$, where the S-wave contribution vanishes. However, $\cos\phi_1 = -1$ is also a (local) minimum, the maximum being reached at $\cos\phi_1 \simeq -0.8$; recall that the expansion in powers of M_Z is not reliable for scenario B1, since $M_2 = |\mu|$. As a result of this non-monotonous behavior, the cross section at $\cos\phi_1 \simeq -0.6$ becomes identical to that at $\cos\phi_1 = -1$. Since $\sigma(\tilde{e}_L^-\tilde{e}_L^-)$ does decrease monotonically with $\cos\phi_1$, values of $\cos\phi_1 \simeq -0.6$ give rise to scenarios with very small $\mathcal{S}(\tilde{\chi}_1^0\tilde{\chi}_2^0)$ but sizeable $\mathcal{S}(\tilde{e}_L^-\tilde{e}_L^-)$. The comparison of Figs. 7.2.b and 7.2.e shows that the correlation becomes weaker also for smaller $\tan\beta$ in scenario B2. This is partly due to the width of the allowed band in the (ϕ_μ, ϕ_1) plane decreasing with increasing $\tan\beta$, see Fig. 3.2. In addition, in scenario B2 with $\tan\beta = 3$, the low-energy constraints also allow values of ϕ_μ near π. One can then find values of ϕ_1 not far from π where $\sigma(\tilde{\chi}_1^0\tilde{\chi}_2^0)$ for CPV points with $|\phi_\mu| \ll 1$ is very close to this cross section at the point $\phi_\mu = \phi_1 = \pi$. This again leads to scenarios where $\mathcal{S}(\tilde{\chi}_1^0\tilde{\chi}_2^0)$ is very small but $\mathcal{S}(\tilde{e}_L^-\tilde{e}_L^-)$ is sizeable. The existence of different allowed CPC points also explains the occurrence of additional bands in Fig. 7.2.b. In some cases the correlations

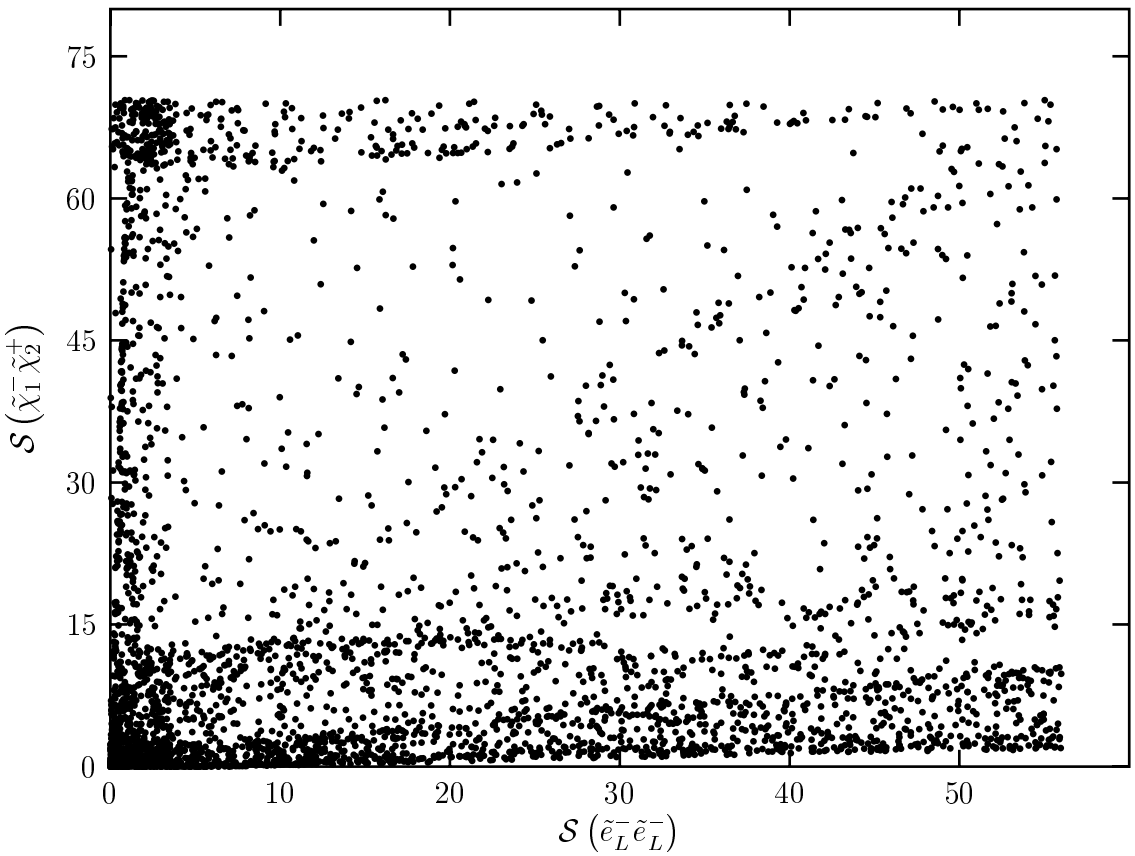

Figure 7.3: Correlation between the significances for the processes $e^-e^- \to \tilde{e}_L^-\tilde{e}_L^-$ and $e^+e^- \to \tilde{\chi}_1^-\tilde{\chi}_2^+$, both taken at $\sqrt{s} = 800$ GeV, for scenario B2 with $\tan\beta = 3$.

between the significances of different production modes are quite weak. The most extreme

case that can be found in the complete set of correlations is shown in Fig. 7.3 and occurs for B2 at $\tan\beta = 3$, in the case of the significances $\mathcal{S}(\tilde{e}_L^-\tilde{e}_L^-)$ and $\mathcal{S}(\tilde{\chi}_1^-\tilde{\chi}_2^+)$. Tab. 7.2 shows that here (and only here) $\sigma(\tilde{\chi}_1^-\tilde{\chi}_2^+)$ allows a significant probe of the phase ϕ_μ, whereas $\mathcal{S}(\tilde{e}_L^-\tilde{e}_L^-)$ is always almost determined by ϕ_1. Moreover, Fig. 3.2.b shows that in the allowed band with $\phi_\mu \simeq \pi$, the deviation $|\phi_\mu - \phi_1|$ becomes maximal for ϕ_1 quite close to $\pm\pi$. This leads to scenarios with large $\mathcal{S}(\tilde{\chi}_1^-\tilde{\chi}_2^+)$, but very small $\mathcal{S}(\tilde{e}_L^-\tilde{e}_L^-)$. Conversely, $||\cos\phi_1| - 1|$ can be quite large for small $|\phi_\mu|$, leading to scenarios with $\mathcal{S}(\tilde{e}_L^-\tilde{e}_L^-) \gg \mathcal{S}(\tilde{\chi}_1^-\tilde{\chi}_2^+)$, although the latter cannot be strictly zero if the former is bigger than 10. However, it was noticed earlier that other combinations of parameters do not allow meaningful probes of ϕ_μ using high-energy quantities. Therefore it can be concluded that in most cases, significances that can be large are also fairly strongly correlated. Furthermore most of these correlations can be understood by arguments similar to those given in the discussion of Fig. 7.2 and with help of the examples given in Secs. 6.2.2–6.2.4.

7.3.3 Significances and polarizations

Finally, in Fig. 7.4 the correlations between the normal component of the polarization vector of the heavier neutralino in mixed neutralino pair production and the significance of the same mode are shown. For scenarios B2 and B3 $\tilde{\chi}_1^0\tilde{\chi}_2^0$ production is used, whereas in scenario B1 $\tilde{\chi}_1^0\tilde{\chi}_3^0$ production is used; recall that this final state was found to be more promising in Tabs. 7.2 and 7.3. These figures appear somewhat simpler than those in

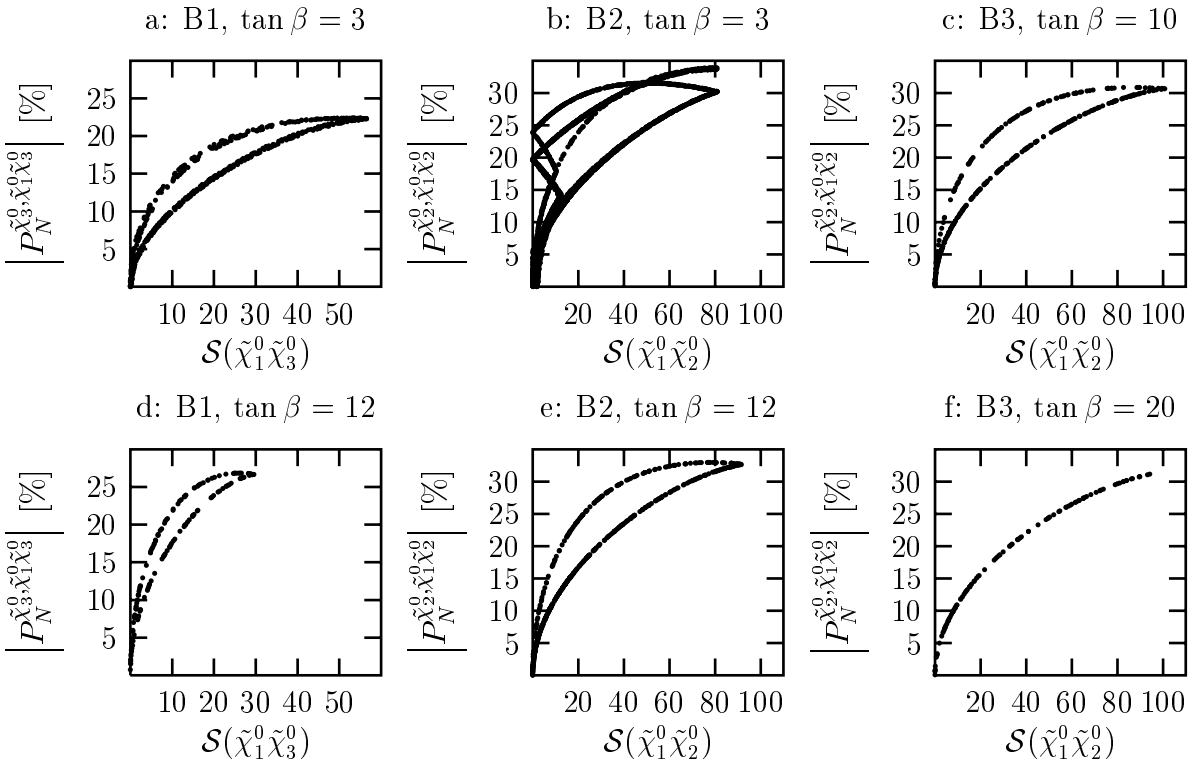

Figure 7.4: Correlation between the significance $\mathcal{S}$ and the absolute value of normal polarization P_N, measured at scattering angle $\theta = \pi/2$, for mixed neutralino pair production at $\sqrt{s} = 500$ GeV. For scenarios B2 and B3 $\tilde{\chi}_1^0\tilde{\chi}_2^0$ production is considered, but replaced by the $\tilde{\chi}_1^0\tilde{\chi}_3^0$ final state for scenario B1.

Fig. 7.2, since now the existence of two allowed CPC points only results in two bands, as compared to three in Fig. 7.2. Of course, scenarios with a single allowed CPC point (Fig. 7.2.f) once more only yield a single band. In panel b, again scenarios with sizeable phases, hence sizeable $|P_N^{\tilde{\chi}_2^0,\tilde{\chi}_1^0\tilde{\chi}_2^0}|$, and yet vanishing $\mathcal{S}(\tilde{\chi}_1^0\tilde{\chi}_2^0)$ are found; an analogous behavior was observed in Fig. 7.2.b.
More importantly, Fig. 7.4 shows that the polarization $|P_N|$ increases much more quickly as the (relevant) phase ϕ_1 is moved from 0 to π than the significance $\mathcal{S}$ does. The reason for this is that $|P_N|$, being T-odd, has a sine-like dependence on ϕ_1, i.e. grows linearly with $|\phi_1|$ or $|\phi_1 - \pi|$. In contrast, the T- and CP-even quantity $\mathcal{S}$ has a cosine-like dependence on all phases, and thus only grows proportional to $|\phi_1|^2$ or $|\phi_1 - \pi|^2$. T-odd observables like P_N are therefore in principle better suited to probe small phases.

Part III

Analysis of a decay chain

Chapter 8

Introduction and a SUSY scenario

8.1 Introduction

Contrarily to the rather general scenarios used in Part II this part of the thesis uses rather large masses for first and second generation sfermions well above 1TeV to satisfy the severe bounds from leptonic dipole moments. As discussed in Chapter 3 such a choice of mass parameters allows a "trivial" suppression of SUSY contributions to leptonic dipole moments[1] and hence phases of $\mathcal{O}(1)$. In addition, other difficulties associated with potentially large flavour changing neutral currents, see [117] for example, and rapid proton decay in SUSY GUTs [118] prefer very heavy first two generations sfermions [61–63]. Contrarily, in such models third generation sfermions are expected to be rather light ("inverted hierarchy"); this expectation is motivated by the central role of third generation sfermions in the naturalness problem and by their large Yukawa couplings which substantially reduce their masses at the weak scale. Therefore SUSY scenarios with $\mathcal{O}(1)$ CP-violating phases and relatively small masses for third generation sfermions can be considered as well motivated and phenomenological viable.

If such SUSY scenarios with an inverted hierarchy were realized by nature an FLC operating with a CMS energy of $\sqrt{s} = 500\text{GeV}$ is expected to produce some light neutralinos, charginos and third generation sfermions, whereas the remaining parts of the SUSY particle spectrum are not accessible [88]. Hence the stau sector should allow the first measurements of CP-violating phases within such models. The main focus of Part III is on the CP-violating phase $\phi_{\tilde{\tau}}$ associated with left-right mixing in the stau sector (see Sec. 2.2.1). As discussed within this section left-right mixing in the slepton sector is enhanced for large values of $\tan\beta$. This is fortunate, since such large values for $\tan\beta$ of up to 50 are preferred by some $SO(10)$ GUT models with Yukawa unification [119,120], while values of $\tan\beta$ near unity are severely constrained by Higgs searches at LEP [121]. Later in Chapter 9 it will be observed that already a rather moderate value of $\tan\beta = 10$ is sufficient to generate sizeable CP-violating effects.

From the phenomenological point of view the crucial question concerning the measurement of the CP-violating phase $\phi_{\tilde{\tau}}$ is which observable is sensitive to this phase and in addition offers a comfortable experimental environment. A priori the stau sector is expected to be advantageous for constructing CP-violating observables since the τ lepton as a decay

[1] Chapter 3 only discussed the electric dipole moment of the electron d_e, however statements similar to those in Sec. 3.2.3 also hold for d_n and d_{Hg}.

product of the stau also decays. The decays of the τ lepton allow a reconstruction of the τ lepton polarization using the energy distribution of the τ lepton decay products. Unfortunately, in the simplest decay channel $\tilde{\tau}_a^\pm \to \tau^\pm \tilde{\chi}_1^0$ the invisibility of the neutralino $\tilde{\chi}_1^0$, which is still assumed to be the LSP, allows only two measurable vectors, the three momentum and the polarization of the τ lepton. With only these two three-vectors available no CP-violating observable can be constructed, hence two step decay cascades offering more three-vectors have to be employed. Among these two step decay cascades, the decay of the second lightest neutralino $\tilde{\chi}_2^0$ into a stau and τ lepton, followed by the stau decay, is one of the most promising candidates especially if $\tan\beta$ is not too small. First of all, $\tilde{\chi}_1^0\tilde{\chi}_2^0$ production has one of the lowest thresholds of all SUSY processes with visible final states. Secondly, for the mass order $m_{\tilde{\chi}_1^0} < m_{\tilde{\tau}_1} < m_{\tilde{\chi}_2^0}$, the decay $\tilde{\chi}_2^0 \to \tilde{\tau}_1^\pm \tau^\mp$ has a large branching ratio, often near 100%. Finally, the final state offers twice the number of three-momenta (compared to $\tilde{\tau}_a^\pm \to \tau^\pm \tilde{\chi}_1^0$) and the intermediate $\tilde{\chi}_2^0$ is polarized, hence CP-odd observables can be constructed.[2] Several previous studies [57, 58, 84, 122–124] have focused on $\tilde{\chi}_2^0 \to l^+ l^- \tilde{\chi}_1^0$ decays with $l = (e, \mu, \tau)$ and used the triple product of the $l^\pm$ momenta with the incident e^- beam momentum as CP-odd observable. A common finding of these studies is that with this triple product CP-violation in the neutralino sector can be probed, but *no* sensitivity to $\phi_{\tilde{\tau}}$ can be achieved. Here the focus is on the case $l = \tau$ and CP-odd observables involving the spin of the τ lepton produced in the first step of $\tilde{\chi}_2^0$ decay. The same process, $e^+e^- \to \tilde{\chi}_1^0\tilde{\chi}_2^0 \to \tilde{\chi}_1^0\tilde{\chi}_1^0\tau^+\tau^-$, has recently also been studied in [59]. However, this study assumes universal soft breaking masses for e and τ. As it will be clarified in Sec. 9.1.2 this leads a priori to a much larger cross section for $\tilde{\chi}_1^0\tilde{\chi}_2^0$ production. On the other hand the experimental bound on d_e as discussed in Chapter 3 will severely constrain the size of CP-phases and in turn also the size of CP-odd observables. This point was not included in [59].

In order to obtain a detailed study of CP-odd observables first restrictions on SUSY parameter space are derived in Sec. 8.2. Results for the production cross sections for $e^+e^- \to \tilde{\chi}_1^0\tilde{\chi}_2^0$ as signal process and $e^+e^- \to \tilde{\tau}_i^\pm \tilde{\tau}_j^\mp$ as possible background process are given in Sec. 9.1 using polarized incident beams. The decay of $\tilde{\tau}_i$ and $\tilde{\chi}_2^0$ are treated in Sec. 9.2 with a special emphasis on the τ lepton polarization. In Secs. 9.1 and 9.2 the mixing patterns and interaction Lagrangian discussed in Chapter 2 are applied. The discussion of further experimental issues in Sec. 9.2.3 finally allows the characterization of "optimized" parameter sets. Using such a parameter set a Monte Carlo study is performed, its results are finally presented as completion of Chapter 9.

8.2 A SUSY scenario

The CP-noninvariant MSSM with sizeable values for $\tan\beta$ is in continuation of Part II still used as general framework. Contrarily to Part II first and second generation sfermions are assumed to be heavy enough to decouple from the theory for a 500 GeV FLC. As already stated and in Chapter 3 and Sec. 8.1 a large CP violating phase in the stau sector is then consistent with the current experimental bounds on d_e, d_n and d_{Hg}. The CMS energy $\sqrt{s}$ is chosen such that $\tilde{\chi}_1^0\tilde{\chi}_2^0$ production is possible and $\tilde{\chi}_1^0\tilde{\chi}_3^0$ production is beyond kinematical accessibility. Furthermore, it is also assumed that the stau sector can be studied in $\tilde{\tau}_1^\pm \tilde{\tau}_{1,2}^\mp$

[2] As stated in Chapter 5 the CPT theorem is assumed to hold, hence CP and T-violation are not distinguished.

production, by a possible adjustment of $\sqrt{s}$ to higher values if necessary. Furthermore, the assumption of R-parity conservation and that hence the lightest neutralino $\tilde{\chi}_1^0$ is the LSP is kept. This is important since then the decay products of any SUSY particle contain at least one LSP which escapes from detection.
The fundamental SUSY parameters of the chargino, neutralino and slepton sector were given within Sec. 2.2 and summarized in Sec. 2.4. Specifying $\tilde{l} = \tilde{\tau}$ and using the convention $\phi_2 = 0$, the seven real parameters and the three phases involved are

$$\{|M_1|,\ M_2,\ |\mu|,\ \tan\beta,\ m_{\tilde{\tau}_L},\ m_{\tilde{\tau}_R},\ |A_{\tilde{\tau}}|\} \quad \text{and} \quad \{\phi_\mu,\ \phi_1,\ \phi_{A_\tau}\}\,. \tag{8.1}$$

Concerning the chargino and neutralino sector strategies for the determination of $|M_1|$, M_2, and $|\mu|$ have been worked out in great detail [50, 66–68]. Since the mixing patterns in the chargino and neutralino sector are rather insensitive to $\tan\beta$ for large values of this parameter, a determination of $\tan\beta$ for values larger than ≈ 10 is rather difficult within the chargino and neutralino sector. In such a situation the decay $\tilde{\tau}_1^\pm \to \tilde{\chi}_1^0 \tau^\pm$, in particular the longitudinal polarization of the τ lepton, which could be measured with an accuracy of 5%, proves as useful [125, 126]. The measurement of the longitudinal τ polarization with the error margins given above, can be used to determine high values of $\tan\beta$ with an accuracy of 5% [127]. In addition, Ref. [127] also showed that the measurement of both $\tilde{\tau}_i$ masses in combination with the $\tilde{\tau}_1^\pm \tilde{\tau}_1^\mp$ production cross section in the CP-conserving case allows a determination of $|A_\tau|$ if $|\mu|$ is known from other measurements: under favorable circumstances an error of about 5% in $\tan\beta$ and of about 5% in $m_{\tilde{\tau}_2}$ would result in the measurement of $|A_\tau|$ with an accuracy of about 8%. However, none of these observables is sensitive to the CP-violating phase $\phi_{\tilde{\tau}}$ in the stau sector.[3] On the other hand, this phase cannot be determined independently of the other parameters in the stau sector.
Therefore the following observables in the neutralino and stau sector are relevant for a detailed study of CP-odd observables in $e^+e^- \to \tilde{\chi}_1^0 \tilde{\chi}_2^0 \to \tilde{\chi}_1^0 \tilde{\chi}_1^0 \tau^\pm \tau^\mp$:

1. The masses $m_{\tilde{\tau}_{1,2}}$ of the staus and the masses $m_{\tilde{\chi}_{1,2}^0}$ of the two lighter neutralinos.

2. The cross sections for neutralino pair production, $\sigma(\tilde{\chi}_1^0 \tilde{\chi}_2^0)$, as signal process and for stau pair production, $\sigma\left(\tilde{\tau}_1^\pm \tilde{\tau}_{1,2}^\mp\right)$, as SUSY background process; in both cases longitudinal polarization of the incident beams is included.

3. The average polarizations of the intermediate, neutralino $\tilde{\chi}_2^0$ and of the τ leptons produced in the decay cascade.

4. The spin/momentum correlations between the intermediate, neutralino $\tilde{\chi}_2^0$ and the τ lepton from the decay $\tilde{\chi}_2^0 \to \tilde{\tau}_1^\pm \tau^\mp$ and the spin/angular/momentum correlations of the two final τ leptons.

The masses were essentially covered in Secs. 2.2.1 and 2.2.3 and are of interest here since these parts of the mass spectrum control the decay patterns and have influence on the experimental accessibility of CP-odd observables discussed in the latter sections. The cross sections are important since they indicate the order of magnitude of signal and background events and hence point to possibilities to suppress the SUSY background processes.

[3] More precisely, all these observables contain a cosine-like dependence on some rephasing invariant combinations of the phases ϕ_μ, ϕ_1, and ϕ_{A_τ}, but none of these observables is sufficient to distinguish between CP-violating and CP-conserving models.

The quantities summarized in the third item estimate the sensitivity of observables to the CP-violating phase $\phi_{\tilde{\tau}}$ and contain first informations on the parameter dependence of the observables themselves. Note that all physical quantities summarized above have some dependence on the CP-violating phases in the neutralino sector, in the stau sector or in both sectors. However, in Secs. 9.2.2, 9.2.3, and 9.3 it will be shown that only observables involving components of the τ spin orthogonal to the τ momentum have a potential to probe $\phi_{\tilde{\tau}}$.
Obviously, the details of the decay pattern depend on the neutralino and stau mass spectra. Restricted to the case where the decay of $\tilde{\chi}_2^0$ into a stau is allowed, i.e. $m_{\tilde{\chi}_2^0} > m_{\tilde{\tau}_1}$, the following two mass spectra have to be considered:

SPECTRUM I SPECTRUM II

These spectra result in different decay patterns:

$$\text{SPECTRUM I:} \quad \tilde{\tau}_2^{\pm} \to \tau^{\pm}\tilde{\chi}_{1,2}^0, \quad \tilde{\chi}_2^0 \to \tau^{\pm}\tilde{\tau}_1^{\mp}, \quad \tilde{\tau}_1^{\pm} \to \tau^{\pm}\tilde{\chi}_1^0; \tag{8.2a}$$

$$\text{SPECTRUM II:} \quad \tilde{\chi}_2^0 \to \tau^{\pm}\tilde{\tau}_{1,2}^{\mp}, \quad \tilde{\tau}_2^{\pm} \to \tau^{\pm}\tilde{\chi}_1^0, \quad \tilde{\tau}_1^{\pm} \to \tau^{\pm}\tilde{\chi}_1^0. \tag{8.2b}$$

In the case of SPECTRUM I, the production process $e^+e^- \to \tilde{\chi}_2^0\tilde{\chi}_2^0$ may also be possible if $\tilde{\tau}_1^{\pm}\tilde{\tau}_2^{\mp}$ is accessible. The former production modes leads to events with four τ leptons and two LSP's in the final state through the sequential decay $\tilde{\chi}_2^0 \to \tau^-\tau^+\tilde{\chi}_1^0$. Since the decay patterns of SPECTRUM II in Eq. 8.2b will lead to additional event topologies from $\tilde{\chi}_1^0\tilde{\chi}_2^0$ production, which require an independent analysis, SPECTRUM I is in the focus for the remainder.
Considering the decay patterns in Eq. 8.2a the production cross sections for $e^+e^- \to \tilde{\chi}_1^0\tilde{\chi}_2^0$ and $e^+e^- \to \tilde{\tau}_1^{\pm}\tilde{\tau}_1^{\mp}$ can give rise to the same final state with two τ leptons and two LSP's, while the process $e^+e^- \to \tilde{\tau}_1^{\pm}\tilde{\tau}_2^{\mp}$ could eventually lead to 2 (or 4) τ leptons and 2 LSP's, or 2τ's+$2\nu_\tau$'s+2 LSP's if the decays $\tilde{\tau}_2^{\pm} \to \tilde{\chi}_1^{\pm}\nu_\tau$ and $\tilde{\chi}_1^{\pm} \to \tilde{\tau}_1^{\pm}\nu_\tau$ are kinematically allowed.
Since it is already known that the τ lepton polarization from $\tilde{\tau}_1$ decays is rather insensitive to the CP-violating phase $\phi_{\tilde{\tau}}$ (see Sec. 8.1), it is crucial to find some distinct features to disentangle these production channels leading to the same final state 2τ + 2LSP. First of all, a simple assumption is that $\tilde{\chi}_1^0\tilde{\chi}_2^0$ production is studied at a beam energy where $\tilde{\tau}_1^{\pm}\tilde{\tau}_2^{\mp}$ production is not accessible. This eliminates one "background process" and leaves us with at most two competing processes; note that $\tilde{\chi}_1^0\tilde{\chi}_2^0$ production becomes possible at lower energy than $\tilde{\tau}_1$ pair production if $m_{\tilde{\tau}_1} > (m_{\tilde{\chi}_1^0} + m_{\tilde{\chi}_2^0})/2$. If kinematical accessible, $\tilde{\tau}_1^{\pm}\tilde{\tau}_1^{\mp}$ production tends to yield the two τ leptons back to back, whereas $\tilde{\chi}_1^0\tilde{\chi}_2^0$ would have them more collinear, since they originate from the same parent $\tilde{\chi}_2^0$. However, since above threshold $\sigma\left(\tilde{\tau}_1^{\pm}\tilde{\tau}_1^{\mp}\right) \gg \sigma\left(\tilde{\chi}_1^0\tilde{\chi}_2^0\right)$, angular distributions will not be sufficient to suppress the background from $\tilde{\tau}_1$ pair production. Therefore later onwards in Secs. 9.2.3 and 9.3 SUSY parameters will be chosen such that the τ energy distributions from the competing processes do not overlap and hence can be used to distinguish between the final states from signal and background processes.

Chapter 9

Production cross sections and decays

9.1 Production cross sections

Concerning the production cross sections for $e^+e^- \to \tilde{\tau}_i^\pm \tilde{\tau}_j^\mp$ and $e^+e^- \to \tilde{\chi}_1^0 \tilde{\chi}_2^0$ as well as the polarization vectors of the produced neutralinos one is in the fortunate situation that most work was already completed in Secs. 4.3.1, 4.3.4, and 5.3.2. Hence the results from these sections can be transferred with minor modifications.

9.1.1 Stau pair production

In principle the calculation of the total and differential cross section for $e^+e^- \to \tilde{\tau}_i^\pm \tilde{\tau}_j^\mp$ is identical to the calculation of the corresponding quantities for $e^+e^- \to \tilde{e}_i^\pm \tilde{e}_j^\mp$ presented in Sec. 4.3.1. The only differences are the absence of the t-channel contribution[1] and the presence of left-right mixing in the stau sector.[2] Incorporating these two differences the general helicity amplitudes for $e^+e^- \to \tilde{\tau}_i^\pm \tilde{\tau}_j^\mp$ are

$$\langle \sigma, -\sigma \rangle_{ij} = -e^2 \sin\theta \lambda_{ij}^{\frac{1}{2}} Z_{ij}^\sigma, \tag{9.1}$$

where the kinematics are chosen as in Sec. 4.2 and the kinematical function λ_{ij} is defined in Eq. C.3. The vector chiral couplings are

$$Z_{ij}^\sigma = \delta_{ij} + D_Z \frac{\sin^2\theta_W - \frac{1-\sigma}{4}}{\cos^2\theta_W \sin^2\theta_W} \left[\sin^2\theta_W \delta_{ij} - \frac{1}{2} \left(U_{\tilde{\tau}}\right)_{1i}^\star \left(U_{\tilde{\tau}}\right)_{1j} \right]. \tag{9.2}$$

The dimensionless Z boson propagator D_Z was introduced in Eq. 4.1 and $\sigma = \{+,-\} \equiv \{R,L\}$ denotes the helicity of the two incident electrons. The calculation of the total, unpolarized cross section is straightforward, one finds

$$\sigma_{ij} = \frac{\pi\alpha^2}{6s} \lambda_{ij}^{\frac{3}{2}} \left[|Z_{ij}^-|^2 + |Z_{ij}^+|^2 \right]. \tag{9.3}$$

With the parametrization introduced in Eq. 2.7 the total and differential, polarized and unpolarized cross sections for diagonal production modes $\tilde{\tau}_i^\pm \tilde{\tau}_i^\mp$ depend on $\cos 2\theta_{\tilde{\tau}}$, i.e. are parabolic functions in $\cos 2\theta_{\tilde{\tau}}$. As suggested by [127], measuring unpolarized and polarized cross sections fixes $\cos 2\theta_{\tilde{\tau}}$ uniquely, in the parametrization of Eq. 2.7 this is consequently

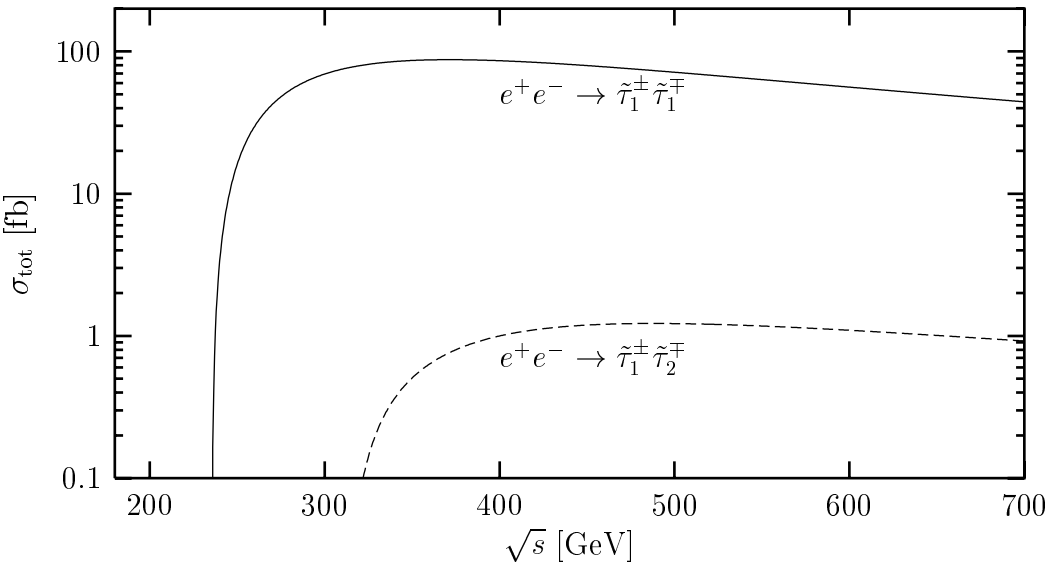

Figure 9.1: The total cross sections for $e^+e^- \to \tilde{\tau}_1^\pm \tilde{\tau}_1^\mp$ and $e^+e^- \to \tilde{\tau}_1^\pm \tilde{\tau}_2^\mp$ as a function of $\sqrt{s}$. Parameters are set as explained in the text.

sufficient to fix $\theta_{\tilde{\tau}}$ up to a sign ambiguity. The total, unpolarized cross sections for $e^+e^- \to \tilde{\tau}_1^\pm \tilde{\tau}_1^\mp$ and $e^+e^- \to \tilde{\tau}_1^\pm \tilde{\tau}_2^\mp$ are presented in Fig. 9.1 as functions of the CMS energy $\sqrt{s}$ for the following choice of SUSY parameters

$$\begin{aligned} m_{\tilde{\tau}_L} = 185\text{GeV}, \quad m_{\tilde{\tau}_R} = 115\text{GeV}, \quad |\mu| = 200\text{GeV}, \quad |A_\tau| = 1\text{TeV}, \\ \phi_\mu = 0, \qquad \phi_{A_\tau} = 0, \qquad \tan\beta = 10. \end{aligned} \tag{9.4}$$

First of all, the total cross section for $\tilde{\tau}_1^\pm \tilde{\tau}_1^\mp$ production amounts to about 100 fb, offering large enough statistics for a detailed probe of the $\tilde{\tau}_1$ sector. Secondly, the cross sections are P-wave suppressed near threshold, $\sigma_{\rm tot} \propto \lambda_{ij}^{\frac{3}{2}}$ as in Eq. 9.3, and rise slowly near threshold. This behavior makes a determination of $\tilde{\tau}$ masses through threshold scans rather difficult. Finally, the suppression of $\tilde{\tau}_1^\pm \tilde{\tau}_2^\mp$ production compared to $\tilde{\tau}_1^\pm \tilde{\tau}_1^\mp$ production results from the smallness of the off-diagonal coupling in Eq. 9.2.

9.1.2 Neutralino pair production

As discussed in Chapter 8 first generation sfermions are assumed to decouple from the theory for a 500 GeV FLC. This implies that the selectron exchange contributions included to $\tilde{\chi}_i^0 \tilde{\chi}_j^0$ production in Sec. 4.3.4 are absent here, therefore the bilinear charges in Eqs. 4.23 reduce to

$$Q_{LL}^{ij} = -\left(Q_{LR}^{ij}\right)^\star = \alpha_L D_Z Z_{ij}^\star, \tag{9.5a}$$

$$Q_{RR}^{ij} = -\left(Q_{RL}^{ij}\right)^\star = -\alpha_R D_Z Z_{ij}, \tag{9.5b}$$

where $\alpha_L = (\sin^2\theta_W - \frac{1}{2})/(\sin^2\theta_W \cos^2\theta_W)$ and $\alpha_R = 1/\cos^2\theta_W$. The matrix Z_{ij} was defined in Eq. 2.51. Note that the definition of $Z_{ij} \propto (N_{3i}N_{3j}^\star - N_{4i}N_{4j}^\star)$ implies the CP-relation $Z_{ij} = (Z_{ji})^\star$, and hence $Q_{\alpha\beta}^{ij} = (Q_{\alpha\beta}^{ji})^\star$ if the Z-boson width is neglected.

[1] There is no coupling $e\tilde{\tau}_j\tilde{\chi}_i^0$ if R-parity is conserved.

[2] Due to the large tau mass left-right mixing in the stau sector is not negligible as discussed in Sec. 2.2.1.

It is known that polarized electron and positron beams are useful to determine the wave-functions of the neutralinos [67,128] and may enhance the production cross sections. Using the helicity amplitudes in Eqs. 4.19 together with the bilinear charges from Eqs. 9.5 and polarisation density matrices[3] as in Eqs. C.20 and C.21 the polarized, differential cross section reads

$$\frac{d\sigma_{ij}}{d\Omega} = 2^{-\delta_{ij}} \frac{\alpha^2}{16s} \lambda_{ij}^{\frac{1}{2}} \left\{ \left[(1 - P_L \overline{P}_L) + \xi (P_L - \overline{P}_L) \right] \Sigma_U + P_T \overline{P}_T \cos\eta \Sigma_T \right\}, \tag{9.6}$$

where $\xi = (\alpha_R^2 - \alpha_L^2)/(\alpha_R^2 + \alpha_L^2) = -0.147$ and η is introduced in Eq. C.22. If the Z-width is neglected the Z-propagator is real and the coefficients $\Sigma_{U,T}$ are

$$\Sigma_U = 2D_Z^2(\alpha_R^2 + \alpha_L^2) \left\{ \left[1 - \Delta_{ij}^2 + \lambda_{ij} \cos^2\theta_i \right] |Z_{ij}|^2 - 4\mu_i\mu_j \mathcal{R}\mathrm{e}\left[Z_{ij}^2 \right] \right\}, \tag{9.7a}$$

$$\Sigma_T = 4\lambda_{ij} D_Z^2 \alpha_R \alpha_L |Z_{ij}|^2 \sin^2\theta_i, \tag{9.7b}$$

with λ_{ij} and Δ_{ij} as given in Eqs. C.3 and C.16, respectively. The coefficients $\Sigma_{U,T}$ reveal two remarkable points about the cross sections for neutralino pair production: First, the only angular dependence is through the polar angle θ_i of the produced $\tilde{\chi}_i^0$ exclusively. Second, the dependence of the cross section on neutralino mixing is completely described by the two quantities $|Z_{ij}|^2$ and $\mathcal{R}\mathrm{e}\left[Z_{ij}^2\right]$ for each production mode $\tilde{\chi}_i^0\tilde{\chi}_j^0$. This implies that transversely polarized beams do not offer any independent information on neutralino mixing. Therefore the opportunity of transversely polarized beams is not further investigated in the remainder, i.e. $P_T = \overline{P}_T = 0$ is used from now onwards.
In order to probe the stau sector through the subsequent decay $\tilde{\chi}_2^0 \to \tilde{\tau}_1^\pm \tau^\mp$ following $e^+e^- \to \tilde{\chi}_1^0\tilde{\chi}_2^0$, the first question is whether the $\tilde{\chi}_1^0\tilde{\chi}_2^0$ production cross section is sufficiently large. The cross section $\sigma_{\mathrm{tot}}\,(e^+e^- \to \tilde{\chi}_1^0\tilde{\chi}_2^0)$ as a function of $\sqrt{s}$ with $\tan\beta = 10$ and $\phi_1 = 0$ is shown in Fig. 9.2 for three different choices of ϕ_μ. The beam polarizations are set as $P_L = -0.8$ and $\overline{P}_L = 0.6$, which maximizes the cross section if $|P_L| \leq 0.8$ and $|\overline{P}_L| \leq 0.6$. The same choice of beam polarization minimizes the $\tilde{\tau}_1$ pair background if $m_{\tilde{\tau}_R} < m_{\tilde{\tau}_L}$ as expected in most SUSY scenarios. Moreover, the gaugino mass unification relation $M_2 = 3/5 \cot^2\theta_W |M_1|$ with $\phi_1 = 0$ is employed. For $\phi_\mu = 0$, the parameters are set as

$$|M_1| = 85\mathrm{GeV}, \quad |\mu| = 200\mathrm{GeV}, \quad \tan\beta = 10. \tag{9.8}$$

For $\phi_\mu = \pi/3$ and $\phi_\mu = \pi/2$, parameters are chosen to yield (partly) the same neutralino mass spectrum as the parameters set in Eq. 9.8, i.e.

$$m_{\tilde{\chi}_1^0} = 76.5 \pm 0.1\mathrm{GeV}, \quad m_{\tilde{\chi}_2^0} = 132.2 \pm 0.1\mathrm{GeV}, \quad m_{\tilde{\chi}_3^0} > 200\mathrm{GeV}. \tag{9.9}$$

First of all, it may be observed that large values of ϕ_μ increase the cross section slightly. Secondly, the smallness of the cross section compared with the results in Tab. 7.1 is due to the absence of the selectron exchange diagrams. Dropping these diagrams eliminates the leading contribution of $\mathcal{O}(M_Z^0)$ and reduces the cross section for $\tilde{\chi}_1^0\tilde{\chi}_2^0$ production to a $\mathcal{O}(M_Z^4)$ effect within the reliability of the perturbative treatment of neutralino mixing presented in Sec. 2.3.3. Nevertheless, using the quite conservative estimate of $500\mathrm{fb}^{-1}$ for the luminosity of an FLC (see Sec. 7.2.1) a few thousand events are available for further analysis.

[3] Put $P_L^1 = P_L$, $P_T^1 = P_T$, $P_L^2 = \overline{P}_L$, and $P_T^2 = \overline{P}_T$.

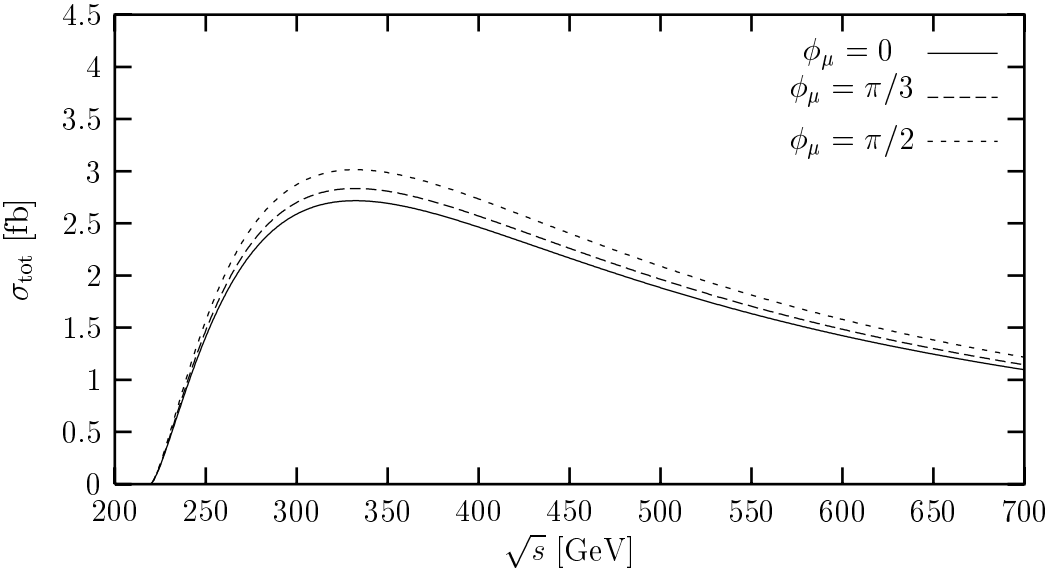

Figure 9.2: The total, polarized cross section for $\tilde{\chi}_1^0\tilde{\chi}_2^0$. Parameters are set as explained in the text.

9.1.3 Neutralino polarization vectors

Further information on neutralino mixing in general and especially on the chiral structure of the neutralinos is contained in the neutralino polarization vectors. Following the definitions of Sec. 5.3.1 and using the general results for fermion polarization vector components in $e^+e^- \to 2f$ with polarized beams from Sec. 5.3.2 together with the modified bilinear charges from Eq. 9.5, one finds the following, compact results for the polarization vector component of $\tilde{\chi}_i^0$ in $\tilde{\chi}_i^0\tilde{\chi}_j^0$ production[4]

$$P^i_{L,T,N} = P^{i,ij}_{L,T,N} = \frac{\xi(1 - P_L\overline{P}_L) + (P_L - \overline{P}_L)}{(1 - P_L\overline{P}_L) + \xi(P_L - \overline{P}_L)} \cdot \frac{\Delta^{i,ij}_{L,T,N}}{\Delta^{ij}_U}. \tag{9.10}$$

The coefficients $\Delta^{i,ij}_{L,T,N}$ and Δ^{ij}_U are

$$\Delta^{i,ij}_L = 2\cos\theta_i \left\{(1 - \bar{\Delta}_{ij})|Z_{ij}|^2 - 2\mu_i\mu_j \mathcal{R}\mathrm{e}\left[(Z_{ij})^2\right]\right\}, \tag{9.11a}$$

$$\Delta^{i,ij}_T = -2\sin\theta_i \left\{\mu_i(1 - \Delta_{ij})|Z^2_{ij}| - \mu_j(1 + \Delta_{ij})\mathcal{R}\mathrm{e}\left[\left(Z^2_{ij}\right)\right]\right\}, \tag{9.11b}$$

$$\Delta^{i,ij}_N = 2\mu_j\lambda_{ij}^{\frac{1}{2}}\sin\theta_i \mathcal{I}\mathrm{m}\left[(Z_{ij})^2\right], \tag{9.11c}$$

$$\Delta^{ij}_U = \left[1 - \Delta^2_{ij} + \lambda_{ij}\cos\theta_i\right]|Z_{ij}|^2 - 4\mu_i\mu_j\mathcal{R}\mathrm{e}\left[(Z_{ij})^2\right], \tag{9.11d}$$

where the quantity $\bar{\Delta}_{ij}$ was defined in Eq. 5.17. Since the parameter ξ is small, sizeable polarization vector components of the produced neutralinos require the presence of large beam polarizations P_L and $\overline{P}_L$.
In Fig. 9.3 the components of the polarization of $\tilde{\chi}_2^0$ are presented as a function of $\cos\theta_{\tilde{\chi}_2^0}$ with a CP-violating choice for the phases ϕ_1 and ϕ_μ. Note that the sizeable beam polarizations $P_L = -0.8$ and $\overline{P}_L = 0.6$ indeed do generate a substantial polarization of the

[4] Compared with Chapter 5 the short-handed notation $P^i_{L,T,N}$ is used for $P^{i,ij}_{L,T,N}$.

neutralino. In Sec. 9.2.2 it will be illustrated that a non-vanishing polarization of the neutralino $\tilde{\chi}_2^0$ is essential for probing CP-violation through the CP-violating phase $\phi_{\tilde{\tau}}$ in the stau sector.

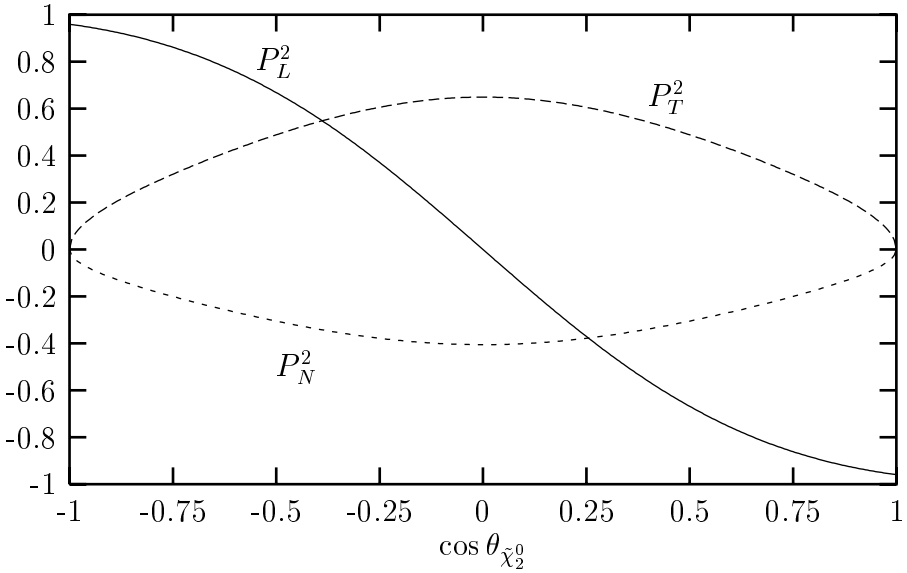

Figure 9.3: Polarization vector components $P_{L,T,N}^2$ of $\tilde{\chi}_2^0$ in $\tilde{\chi}_2^0\tilde{\chi}_1^0$ production as a function of $\cos\theta_{\chi_2^0}$. The collider parameters are $\sqrt{s} = 300\text{GeV}$, $P_L = -0.8$, and $\overline{P}_L = 0.6$. The real SUSY parameters are set as in Eq. 9.4, but the phases are changed to $\phi_1 = \phi_\mu = \pi/4$.

9.2 Decays of sparticles

The next step in modeling the discussed decay chain consists in calculating the decay distributions and polarization vector components of τ leptons for the decays $\tilde{\tau}_a^\mp \to \tau^\mp \tilde{\chi}_i^0$ and $\tilde{\chi}_i^0 \to \tilde{\tau}_a^\mp \tau^\pm$.

9.2.1 Stau decays

The decay distribution of the stau decay $\tilde{\tau}_a^\mp \to \tau^\mp \tilde{\chi}_i^0$ and the polarization 4-vector of the final τ lepton in the rest frame of the tau slepton are given by

$$\frac{d\Gamma_\mp}{d\Omega_1^\star} = \frac{\lambda^{\frac{1}{2}}}{64\pi^2 m_{\tilde{\tau}_a}} \left(\left|Q_{ia}^R\right|^2 + \left|Q_{ia}^L\right|^2 \right) \left\{ 1 - \frac{m_\tau^2}{m_{\tilde{\tau}_a}^2} - \frac{m_{\tilde{\chi}_i^0}^2}{m_{\tilde{\tau}_a}^2} - 2\frac{m_\tau m_{\tilde{\chi}_i^0}}{m_{\tilde{\tau}_a}^2} \mathcal{A}_T^{ia} \right\}, \tag{9.12}$$

$$\mathcal{P}_\mu^{\tau^\mp} = \mp \frac{\mathcal{A}_L^{ia}}{1 - 2\frac{m_\tau m_{\tilde{\chi}_i^0}}{m_{\tilde{\tau}_a}^2 - m_\tau^2 - m_{\tilde{\chi}_i^0}^2} \mathcal{A}_T^{ia}} \left(\frac{m_\tau q_{i\mu}}{k_1 \cdot q_i} - \frac{k_{1\mu}}{m_\tau} \right), \tag{9.13}$$

where $d\Omega_1^\star = d\cos\theta_1^\star d\phi_1^\star$ is the solid angle of the τ lepton in the $\tilde{\tau}_a^\mp$ rest frame, k_1 and q_i are the 4-momenta of the the τ lepton $\tau^\mp$ and the neutralino $\tilde{\chi}_i^0$, and the phase space factor λ is to be evaluated as $\lambda\left(m_{\tilde{\tau}_a}^2, m_\tau^2, m_{\tilde{\chi}_i^0}^2\right)$. The couplings $Q_{ia}^{L,R}$ are related to the

neutralino-fermion-sfermion couplings $n_{L,i\alpha}$ and $n_{R,i\alpha}$ in Eqs. 3.16c and 3.16d via ($\alpha = a$)

$$Q^L_{ia} = -n^\star_{Li\alpha} = \frac{-e}{\sqrt{2}\sin\theta_W}\left[\left(N^\star_{2i} + \tan\theta_W N^\star_{1i}\right)\left(U_{\tilde\tau}\right)_{La} - \sqrt{2}Y_\tau N^\star_{3i}\left(U_{\tilde\tau}\right)_{Ra}\right], \quad (9.14a)$$

$$Q^R_{ia} = -n^\star_{Ri\alpha} = \frac{e}{\sqrt{2}\sin\theta_W}\left[2\tan\theta_W N_{1i}\left(U_{\tilde\tau}\right)_{Ra} + \sqrt{2}Y_\tau N_{3i}\left(U_{\tilde\tau}\right)_{La}\right]. \quad (9.14b)$$

where the reduced Yukawa coupling Y_τ is defined by Eq. 2.58 as $Y_\tau = m_\tau/(\sqrt{2}M_W\cos\beta)$. For the sake of a compact notation three τ polarization asymmetries are introduced as

$$\mathcal{A}^{ia}_L = \frac{\left|Q^R_{ia}\right|^2 - \left|Q^L_{ia}\right|^2}{\left|Q^R_{ia}\right|^2 + \left|Q^L_{ia}\right|^2}, \qquad \mathcal{A}^{ia}_T = \frac{2\mathcal{R}\mathrm{e}\left[Q^R_{ia}Q^{L\star}_{ia}\right]}{\left|Q^R_{ia}\right|^2 + \left|Q^L_{ia}\right|^2}, \qquad \mathcal{A}^{ia}_N = \frac{2\mathcal{I}\mathrm{m}\left[Q^R_{ia}Q^{L\star}_{ia}\right]}{\left|Q^R_{ia}\right|^2 + \left|Q^L_{ia}\right|^2}. \quad (9.15)$$

The average polarization of the τ lepton can be measured through τ lepton decays within the detector [129–131]. Eq. 9.13 indicates that it is purely longitudinally polarized;[5] its degree of polarization is given by

$$P^{\tau^\mp}_L = \pm\frac{\lambda^{\frac{1}{2}}\left(m^2_{\tilde\tau_a}, m^2_\tau, m^2_{\tilde\chi^0_i}\right)\mathcal{A}^{ia}_L}{m^2_{\tilde\tau_a} - m^2_\tau - m^2_{\tilde\chi^0_i} - 2m_\tau m_{\tilde\chi^0_i}\mathcal{A}^{ia}_T} \to \pm\mathcal{A}^{ia}_L \quad \text{for} \quad m_{\tilde\tau_a} \gg m_\tau. \quad (9.16)$$

In the rest frame of the stau slepton the decay distribution given by Eq. 9.12 is isotropic, as in all two body decays of scalar particles. The degree of longitudinal polarization in Eq. 9.16 is constant over phase space, depending on the couplings $Q^{R,L}_{ia}$. The magnitude of $P^{\tau^\mp}_L$ depends not only on the left-right mixing in the stau sector but also on the neutralino mixing as shown in Eq. 9.14. Since the gaugino interaction with (s)fermions preserves chirality while the Higgsino interaction action flips chirality, $P^{\tau^\mp}_L$ is sensitive to the τ Yukawa coupling [125, 126]. Note that τ mass effects, which have been neglected in [59, 125–127, 132], introduce some dependence of $P^{\tau^\mp}_L$ on the phase $\phi_{\tilde\tau}$, via A^{ia}_T. However, this dependence is almost always too weak to allow a measurement of this phase through $\tilde\tau_1 \to \tau\chi^0_1$ decays. Not only is $m_\tau m_{\tilde\chi^0_1} \ll m^2_{\tilde\tau_1} - m^2_\tau - m^2_{\tilde\chi^0_1}$ unless $m_{\tilde\chi^0_1}$ is very close to $m_{\tilde\tau_1}$, the coefficient $\mathcal{A}^{11}_T$ is usually also significantly smaller in magnitude than 1.
At this stage it is instructive to consider some limiting cases of the decay $\tilde\tau_1 \to \tau\tilde\chi^0_1$ in the limit $m_{\tilde\tau_1} \gg m_\tau$, involving the couplings $Q^{R,L}_{11}$. If the lightest neutralino is a pure Bino, the degree of longitudinal polarization of the τ lepton becomes

$$P^{\tau^\mp}_L\left(\tilde\tau^\mp_1 \to \tau^\mp\tilde B\right) = \pm\frac{4\sin^2\theta_{\tilde\tau} - \cos^2\theta_{\tilde\tau}}{4\sin^2\theta_{\tilde\tau} + \cos^2\theta_{\tilde\tau}}, \quad (9.17)$$

which has some dependence on the stau mixing angle, which is most probably already known from $\tilde\tau^\mp_i\tilde\tau^\pm_j$ production cross sections once $P^{\tau^\mp}_L$ is measured. If the lighter stau is right-handed, one has

$$P^{\tau^\mp}_L\left(\tilde\tau^\mp_R \to \tau^\mp\tilde\chi^0_1\right) = \pm\frac{2\tan^2\theta_W|N_{11}|^2 - Y^2_\tau|N_{31}|^2}{2\tan^2\theta_W|N_{11}|^2 + Y^2_\tau|N_{31}|^2}. \quad (9.18)$$

This ratio will deviate significantly from unity only if $\tan\beta$ is large, so that Y_τ becomes comparable to the $U(1)_Y$ gauge coupling, *and* the LSP has a significant Higgsino component. Since in most models, including the numerical examples to be presented below, the

[5] The boost in the lab frame will in general produce a small transverse polarization; however, it is suppressed by a factor m_τ/E_τ.

LSP is indeed Bino-like and $\tilde{\tau}_1$ is dominantly $\tilde{\tau}_R$, i.e. $\theta_{\tilde{\tau}}$ is near $\pi/2$, the polarization of $\tau^{\mp}$ from $\tilde{\tau}_1^{\mp}$ decays is usually quite close to ± 1, with little dependence on SUSY parameters (within the ranges allowed by the model) [133]. Measuring this polarization can thus test this (large) class of models, but is often not very useful for determining parameters.

9.2.2 Neutralino decays

As already discussed in Sec. 8.1 the following neutralino production process with the succeeding decay chain attracts the main interest of the thesis within Part III:

$$e^+ + e^- \to \tilde{\chi}_j^0 + \tilde{\chi}_i^0$$
$$\tilde{\chi}_i^0 \to \tau^{\mp} + \tilde{\tau}_a^{\pm}$$
$$\tilde{\tau}_a^{\pm} \to \tau^{\pm} + \tilde{\chi}_1^0$$

As described in Secs. 5.3.1 and 5.3 the produced spin-one-half neutralino is polarized through its production. Therefore non-trivial spin correlations between the decaying neutralino and the tau lepton produced in the first step of the $\tilde{\chi}_i^0$ decay are generated. In order to describe the decay distribution and the tau polarization, a "starred" coordinate system is defined, where the $(x^\star, z^\star)$ plane is still the production plane of the neutralino pair, but the neutralino $\tilde{\chi}_i^0$ momentum points along the $z^\star$ axis. The "starred" set of axes is thus related to the coordinate system used in Sec. 9.1.2 through a rotation around the $y = y^\star$ axis by the production angle $\theta_{\tilde{\chi}_i^0}$. In this coordinate system the polarization vector of the neutralino $\tilde{\chi}_i^0$ is $\vec{P}^i = (P_T^i, P_N^i, P_L^i)$ in the rest frame of the neutralino. The expressions for the polarization vector components were given in Eqs. 9.10 and 9.11.
Using the polar and azimuthal angle $\theta_2^\star$ and $\phi_2^\star$ of the τ momentum direction with respect to the neutralino momentum direction in the rest frame of the neutralino, the angular distribution and polarization vector of the τ lepton are given by

$$\frac{d\Gamma_{\mp}}{d\Omega_2^\star} = \frac{\lambda^{\frac{1}{2}}}{64\pi^2} E_\tau \left(\left| Q_{ia}^R \right|^2 + \left| Q_{ia}^L \right|^2 \right) \left[1 + \mu_\tau \mathcal{A}_T^{ia} \pm \beta_\tau \mathcal{A}_L^{ia} \left(\vec{P}^i \cdot \hat{s}_3^\star \right) \right], \tag{9.19}$$

$$P_L^{\tau^{\mp}} = \frac{\pm\beta_\tau \mathcal{A}_L^{ia} + (1 + \mu_\tau \mathcal{A}_T^{ia}) \left(\vec{P}^i \cdot \hat{s}_3^\star \right)}{1 + \mu_\tau \mathcal{A}_T^{ia} \pm \beta_\tau \mathcal{A}_L^{ia} \left(\vec{P}^i \cdot \hat{s}_3^\star \right)}, \tag{9.20a}$$

$$P_T^{\tau^{\mp}} = \frac{(\mu_\tau + \mathcal{A}_T^{ia}) \left(\vec{P}^i \cdot \hat{s}_1^\star \right) - \beta_\tau \mathcal{A}_N^{ia} \left(\vec{P}^i \cdot \hat{s}_2^\star \right)}{1 + \mu_\tau \mathcal{A}_T^{ia} \pm \beta_\tau \mathcal{A}_L^{ia} \left(\vec{P}^i \cdot \hat{s}_3^\star \right)}, \tag{9.20b}$$

$$P_N^{\tau^{\mp}} = \frac{(\mu_\tau + \mathcal{A}_T^{ia}) \left(\vec{P}^i \cdot \hat{s}_2^\star \right) + \beta_\tau \mathcal{A}_N^{ia} \left(\vec{P}^i \cdot \hat{s}_1^\star \right)}{1 + \mu_\tau \mathcal{A}_T^{ia} \pm \beta_\tau \mathcal{A}_L^{ia} \left(\vec{P}^i \cdot \hat{s}_3^\star \right)}. \tag{9.20c}$$

The energy of the τ lepton in the $\tilde{\chi}_i^0$ rest frame is

$$E_\tau = \frac{m_{\tilde{\chi}_i^0}}{2} \left(1 + \frac{m_\tau^2}{m_{\tilde{\chi}_i^0}^2} - \frac{m_{\tilde{\tau}_a}^2}{m_{\tilde{\chi}_i^0}^2} \right). \tag{9.21}$$

The kinematical function λ has to be evaluated using the argument $\left(1, m^2_{\tilde{\tau}_a}/m^2_{\tilde{\chi}^0_i}, m^2_\tau/m^2_{\tilde{\chi}^0_i}\right)$. The reduced mass μ_τ of the τ lepton is m_τ/E_τ and the τ lepton's speed β_τ is given by $\beta_\tau = \lambda^{\frac{1}{2}}/\left[1 - \left(m^2_{\tilde{\tau}_a} - m^2_\tau\right)/m^2_{\tilde{\chi}^0_i}\right]$. Finally, the three unit vectors $\hat{s}^\star_{1,2,3}$ are defined by

$$\hat{s}^\star_1 = (\cos\theta^\star_2 \cos\phi^\star_2, \cos\theta^\star_2 \sin\phi^\star_2, -\sin\theta^\star_2)\,, \tag{9.22a}$$

$$\hat{s}^\star_2 = (-\sin\phi^\star_2, \cos\phi^\star_2, 0)\,, \tag{9.22b}$$

$$\hat{s}^\star_3 = (\sin\theta^\star_2 \cos\phi^\star_2, \sin\theta^\star_2 \sin\phi^\star_2, \cos\theta^\star_2)\,. \tag{9.22c}$$

Note that $P^{\tau^\mp}_T$, $P^{\tau^\mp}_N$, $P^{\tau^\mp}_L$ are the polarization components of the τ polarization vector in the τ rest frame along the $\hat{s}^\star_1$, $\hat{s}^\star_2$, $\hat{s}^\star_3$ directions, respectively. Combining the three polarization components leads to the τ polarization 3-vector

$$\vec{P}^{\tau^\mp} = \frac{(\mu_\tau + \mathcal{A}^{ia}_T)\,\vec{P}^i + \left[(1-\mu_\tau)\,(1-\mathcal{A}^{ia}_T)\left(\vec{P}^i \cdot \hat{s}^\star_3\right) \pm \beta_\tau \mathcal{A}^{ia}_L\right]\hat{s}^\star_3 - \beta_\tau \mathcal{A}^{ia}_N \left(\vec{P}^i \times \hat{s}^\star_3\right)}{1 + \mu_\tau \mathcal{A}^{ia}_T \pm \beta_\tau \mathcal{A}^{ia}_L \left(\vec{P}^i \cdot \hat{s}^\star_3\right)}. \tag{9.23}$$

The polarization 4-vector of the τ lepton in the neutralino rest frame can be obtained by applying a Lorentz boost along the $\hat{s}^\star_3$ direction with the τ lepton speed β_τ to the 4-vector $(0, \vec{P}^{\tau^\mp})$.

In Part III the main focus is the decay $\tilde{\chi}^0_2 \to \tau^\mp \tilde{\tau}^\pm_1$. If the decaying neutralino $\tilde{\chi}^0_2$ is unpolarized ($\vec{P}^i = 0$), only the polarization asymmetry $\mathcal{A}^{21}_L$ as defined in Eq. 9.15 can be determined by measuring the longitudinal polarization of the τ lepton.[6] Some limiting cases of this asymmetry are

$$\mathcal{A}^{21}_L\left(\tilde{\chi}^0_2 = \tilde{W}_3\right) = -1, \tag{9.24a}$$

$$\mathcal{A}^{21}_L\left(\tilde{\chi}^0_2 = \tilde{H}^0_1\right) = \cos 2\theta_{\tilde{\tau}}, \tag{9.24b}$$

$$\mathcal{A}^{21}_L\left(\tilde{\tau}_1 = \tilde{\tau}_R\right) = \frac{2|N_{12}|^2 \tan^2\theta_W - Y^2_\tau |N_{32}|^2}{2|N_{12}|^2 \tan^2\theta_W + Y^2_\tau |N_{32}|^2}. \tag{9.24c}$$

The GUT relation $|M_1| \simeq 0.5 M_2$ suppresses the value of $|N_{12}|$ in most of the parameter space, but for $|\mu| > M_2$, $|N_{32}|$ is also suppressed. Even a small $\tilde{\tau}_L$ component in $\tilde{\tau}_1$ can therefore change $\mathcal{A}^{21}_L$ significantly, making it a far more sensitive probe of SUSY parameters than $\mathcal{A}^{11}_L$.

If the polarization of the decaying neutralino $\tilde{\chi}^0_2$ is sizeable, which is possible only with the longitudinal polarization of the $e^\pm$ beams, $\mathcal{A}^{21}_T$ and $\mathcal{A}^{21}_N$ become measurable. The explicit expression of the numerator of $\mathcal{A}^{32}_N$ is (besides $e^2/\sin^2\theta_W$)

$$\begin{aligned}
\mathcal{I}\mathrm{m}\left[Q^R_{21} Q^{L\star}_{21}\right] \propto\ & \sqrt{2}\tan\theta_W Y_\tau \sin^2\theta_{\tilde{\tau}} \mathcal{I}\mathrm{m}\left[N_{12} N_{32}\right] \\
& -\frac{Y_\tau}{\sqrt{2}} \cos^2\theta_{\tilde{\tau}} \mathcal{I}\mathrm{m}\left[N_{32}\left(N_{22} + \tan\theta_W N_{12}\right)\right] \\
& -\tan\theta_W \sin\theta_{\tilde{\tau}} \cos\theta_{\tilde{\tau}} \mathcal{I}\mathrm{m}\left[N_{12}\left(N_{22} + \tan\theta_W N_{12}\right) e^{i\phi_{\tilde{\tau}}}\right] \\
& +Y^2_\tau \sin\theta_{\tilde{\tau}} \cos\theta_{\tilde{\tau}} \mathcal{I}\mathrm{m}\left[N_{32} N_{32} e^{-i\phi_{\tilde{\tau}}}\right].
\end{aligned} \tag{9.25}$$

[6] Note that $\mu_\tau \ll 1$ and hence $P^{\tau^\mp}_L \simeq \pm\beta_\tau \mathcal{A}^{21}_L$.

The numerator of $\mathcal{A}_T^{21}$ is obtained by replacing $\mathcal{I}\mathrm{m}$ by $\mathcal{R}\mathrm{e}$ in the equation above. The CP-violating phase $\phi_{\tilde{\tau}}$ from stau left-right mixing is present in the two last terms of Eq. 9.25. Note that these contributions to $\mathcal{A}_N^{ia}$ (and $\mathcal{A}_T^{ia}$) are only non-zero in the presence of nontrivial left-right mixing in the stau sector. This point is rather expectable since the phase $\phi_{\tilde{\tau}}$ is associated with the off-diagonal entries of the stau mixing matrix $U_{\tilde{\tau}}$ from Eq. 2.7. These two contributions thus increase with increasing $\tan\beta$; in particular this increase is rapid for the last contribution, due the factor Y_τ^2, but this term is only important for $\tan\beta > 20$. On the other hand, if the $U(1)_Y$ gaugino mass is real, which is true in our convention if gaugino mass unification also holds for their phases, the first two terms in Eq. 9.25 are proportional to $\sin 2\beta$, i.e. they become small as $\tan\beta$ becomes large. Finally, recall that $\tilde{\chi}_1^0$ and $\tilde{\chi}_2^0$ have to have significant Higgsino components in order to obtain a sizeable $\tilde{\chi}_1^0\tilde{\chi}_2^0$ production cross section, see Eq. 2.51.[7] Therefore the necessary conditions for the studied process to be sensitive to the phase $\phi_{\tilde{\tau}}$ are:

- sizeable left-right mixing in the stau sector, this prefers large values of $\tan\beta$;
- sizeable gaugino–Higgsino mixing, which requires $|\mu|$ not to be too large.

9.2.3 Numerical results for tau polarization asymmetries

Before numerical results of the τ polarization asymmetries for a sample parameter set can be presented, some discussions of experimental issues are in order here. Since the final state consists of two τ leptons with two LSP's, the first question is whether and how the two τ leptons originating from the primary and secondary decay can be distinguished. For example, the negatively charged τ lepton can be produced through the following decay channels:

$$\text{DECAY I}: \quad \tilde{\chi}_2^0 \to \tilde{\tau}_1^+\tau^- \quad \text{followed by} \quad \tilde{\tau}_1^+ \to \tilde{\chi}_1^0\tau^+, \tag{9.26a}$$

$$\text{DECAY II}: \quad \tilde{\chi}_2^0 \to \tilde{\tau}_1^-\tau^+ \quad \text{followed by} \quad \tilde{\tau}_1^- \to \tilde{\chi}_1^0\tau^-. \tag{9.26b}$$

If these two processes are indistinguishable, a substantial reduction of the efficiency is inevitable; recall from the discussion in Sec. 9.2.1 that the (almost purely longitudinal) polarization of the τ lepton produced in $\tilde{\tau}$ decay depends only very weakly on $\phi_{\tilde{\tau}}$.
In the rest frame of $\tilde{\chi}_2^0$, the τ^- energy from DECAY I is given by Eq. 9.21 with $i = 2$ and $a = 1$, whereas for DECAY II the τ lepton energy in the same reference frame is distributed over

$$E_{\tau^-} \in \left[\gamma_{\tilde{\tau}_1}E_\tau^\star - \gamma_{\tilde{\tau}_1}\beta_{\tilde{\tau}_1}\left|\vec{p}_\tau^{\,\star}\right|, \gamma_{\tilde{\tau}_1}E_\tau^\star + \gamma_{\tilde{\tau}_1}\beta_{\tilde{\tau}_1}\left|\vec{p}_\tau^{\,\star}\right|\right]. \tag{9.27}$$

Here, $E_\tau^\star$ is the energy of the τ lepton from $\tilde{\tau}_1$ decay in the $\tilde{\tau}_1$ rest frame, given as

$$E_\tau^\star = \frac{m_{\tilde{\tau}_1}}{2}\left(1 + \frac{m_\tau^2}{m_{\tilde{\tau}_1}^2} - \frac{m_{\tilde{\chi}_1^0}^2}{m_{\tilde{\tau}_1}^2}\right), \tag{9.28}$$

and $|\vec{p}_\tau^{\,\star}| = \sqrt{E_\tau^2 - m_\tau^2}$. The boost factors $\gamma_{\tilde{\tau}_1} = E_{\tilde{\tau}_1}/m_{\tilde{\tau}_1}$ and $\gamma_{\tilde{\tau}_1}\beta_{\tilde{\tau}_1} = \sqrt{E_{\tilde{\tau}_1}^2/m_{\tilde{\tau}_1}^2 - 1}$ describe the boost from the rest frame of $\tilde{\tau}_1$ to the rest frame of $\tilde{\chi}_2^0$, with the energy of $\tilde{\tau}_1$

[7] However, if $\tilde{\chi}_1^0$ was Higgsino-like, the $\tilde{\chi}_2^0 - \tilde{\chi}_1^0$ mass splitting would be small, making the ordering $m_{\tilde{\chi}_1^0} < m_{\tilde{\tau}_1} < m_{\tilde{\chi}_2^0}$ assumed in this analysis implausible.

in the second frame given as

$$E_{\tilde{\tau}_1} = \frac{m_{\tilde{\chi}_2^0}}{2}\left(1 - \frac{m_\tau^2}{m_{\tilde{\chi}_2^0}^2} + \frac{m_{\tilde{\tau}_1}^2}{m_{\tilde{\chi}_2^0}^2}\right). \tag{9.29}$$

The final boost into the lab frame will again broaden the energy distribution of the τ lepton from the $\tilde{\tau}_1$ decay and will in addition lead to a broad energy distribution for the τ lepton from the $\tilde{\chi}_2^0$ decay. Nevertheless, for some choices of the parameters the ranges of these energy distributions do not overlap. In such a fortunate situation the question which τ lepton originates from the $\tilde{\chi}_2^0$ decay can be answered using the energies of the two τ leptons. However, the neutrino(s) produced in the succeeding decay of the τ limit(s) the measurement of the τ energy. Especially in the decay modes $\tau \to \pi\nu$ and $\tau \to e\nu\nu$, $\mu\nu\nu$, usually less than half of the τ energy is visible. On the other hand, in the decays $\tau \to \rho\nu$ or $\tau \to a_1\nu$ the substantial mass of the ρ or a_1 meson enhances the visible energies of the τ lepton.

As remarked earlier, the situation is cleanest if the two τ energy distributions show little or no overlap even after the boost to the lab frame. One rather safe case is when $m_{\tilde{\tau}_1}$ is close to either $m_{\tilde{\chi}_1^0}$ or $m_{\tilde{\chi}_2^0}$. In this case the signal usually has one rather hard and one rather soft τ so that the overlap of the two τ energy distributions is not serious. Moreover this signal is easy to distinguish from the possible background process $e^+e^- \to \tilde{\tau}_1^\pm\tilde{\tau}_1^\mp$ followed by $\tilde{\tau}_1^\pm \to \tau^\pm\tilde{\chi}_1^0$ which tends to have either two soft tau leptons (if $m_{\tilde{\tau}_1}$ is close to $m_{\tilde{\chi}_1^0}$) or two hard ones (if $m_{\tilde{\tau}_1}$ is close to $m_{\tilde{\chi}_2^0}$).

The second issue is the measurement of the τ polarization, which is analyzed through its decay distributions with the decay modes $\tau \to \pi\nu$, $\rho\nu$, $a_1\nu$, $e\nu\nu$, $\mu\nu\nu$. The $\tau \to \pi\nu$ decay mode is useful for determing the τ polarization only if the τ energy is known, which is the case in $e^+e^- \to \tau^+\tau^-$ production studied at LEP, but not in the case studied here. Therefore only the final states $\rho\nu$ and $a_1\nu$ with the combined branching ratio of about 34% are considered here: The energy distribution of ρ or a_1 decay products can determine the ρ or a_1 polarization which can specify, in turn, the τ polarization [129–131]. Unfortunately, the efficiency of the τ transverse polarization measurement is usually smaller than that of the τ longitudinal polarization [134], and is further reduced as the τ energy increases. Since the τ^- energy is approximately proportional to the mass difference between $\tilde{\chi}_2^0$ and $\tilde{\tau}_1$, the following mass spectrum is best suited to clearly probe $\mathcal{A}_{T,N}^{21}$:

After this discussion of experimental issues concerning a clear probe of $\mathcal{A}_{T,N}^{21}$ which led to mass spectrum for which this probe would be easiest, the final issue is how to fix the SUSY parameters without a single signal of supersymmetric particles. Within this part of the thesis the major goal is to study the dependence of $\mathcal{A}_{L,T,N}^{21}$ on the phase $\phi_{\tilde{\tau}}$. However, a variation of this phase through a variation of the phases ϕ_μ and/or ϕ_A while keeping all the other SUSY parameters fixed results in differing mass spectra for the neutralino and stau sectors. As these masses most likely will be measured much earlier than the polarizations observables investigated here, such a treatment of SUSY parameters is rather unreasonable. The neutralino and stau sector is determined by the real parameters $|\mu|$, $|M_1|$, M_2, $\tan\beta$, $m_{\tilde{\tau}_L}$, $m_{\tilde{\tau}_R}$, and the three phases ϕ_μ, ϕ_1, and ϕ_A if the GUT relation $M_2 = 3/5\cot^2\theta_W|M_1|$ and the convention $\phi_2 = 0$ are used. As noted earlier, $m_{\tilde{\tau}_R}$ is expected to be smaller than

$m_{\tilde{\tau}_L}$ since $\tilde{\tau}_R$ has no $SU(2)$ interactions. For definiteness, the following SUSY parameters are fixed

$$\tan\beta = 10, \quad \phi_1 = 0, \quad |A_\tau| = 1\text{TeV}, \tag{9.30}$$

while all other, remaining SUSY parameters are a priori varied. Considering the optimal scenario for probing $\phi_{\tilde{\tau}}$ derived above, the neutralino and stau mass spectrum and the stau mixing angle are fixed as

$$\begin{array}{lll} m_{\tilde{\chi}_1^0} = 80 \pm 0.5\text{GeV}, & m_{\tilde{\chi}_2^0} = 140 \pm 0.5\text{GeV}, & m_{\tilde{\chi}_3^0} = 225 \pm 5\text{GeV}, \\ m_{\tilde{\tau}_1} = 130 \pm 0.1\text{GeV}, & m_{\tilde{\tau}_2} = 210 \pm 1\text{GeV}, & \theta_{\tilde{\tau}}[\pi] = -0.477 \pm 0.006. \end{array} \tag{9.31}$$

Using these bounds, the mass parameters (in GeV) are constrained as

$$M_1 \in [81.8, 88.3], \quad |\mu| \in [206, 220], \quad m_{\tilde{\tau}_R} \in [122.5, 128.5], \quad m_{\tilde{\tau}_L} - m_{\tilde{\tau}_R} \in [72, 82.5], \tag{9.32}$$

while the CP-violating phase $\phi_{\tilde{\tau}}$ is completely unconstrained.

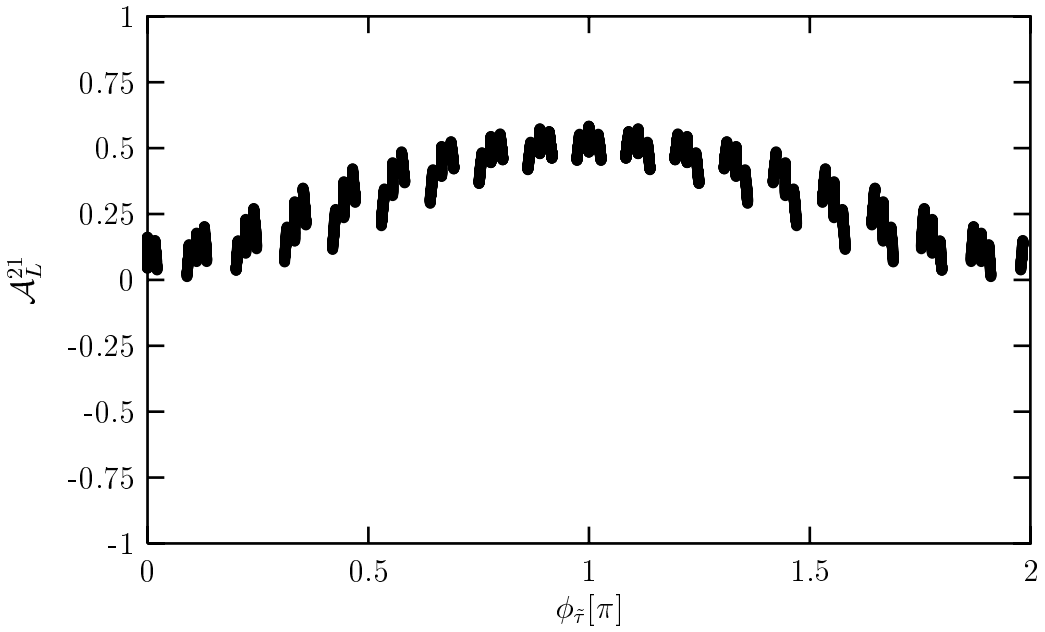

Figure 9.4: The longitudinal polarization asymmetry $\mathcal{A}_L$ of τ^- from DECAY I. Parameters are as discussed in the text.

Figure 9.4 presents the longitudinal polarization asymmetry of the τ^- lepton produced in DECAY I, while Fig. 9.5 shows its transversal and normal polarization asymmetries. The finite spread of points for a fixed value of $\phi_{\tilde{\tau}}$ is attributed to the choice of the SUSY scenario by fixing the neutralino and stau mass spectra within finite error margins, rather than fixing the fundamental SUSY parameters. The dominant dependence of $\mathcal{A}_L^{21}$ on $\phi_{\tilde{\tau}}$ is introduced through this procedure (see Fig. 9.4), mostly through the change of the decomposition of $\tilde{\chi}_2^0$. Earlier it has been shown that this quantity is very sensitive to various SUSY parameters. However, the spread of the points is too large to allow a good measurement of $\phi_{\tilde{\tau}}$. In contrast, Fig. 9.5 clearly illustrates that $\mathcal{A}_T^{21}$ and $\mathcal{A}_N^{21}$ are quite sensitive to this phase. As expected from Eq. 9.15, which reveals $(\mathcal{A}_L^{ia})^2 + (\mathcal{A}_T^{ia})^2 + (\mathcal{A}_N^{ia})^2 = 1$ after a short calculation, these two polarization asymmetries show complementary behavior: When $|\mathcal{A}_N^{21}| \approx 1$ (particularly when Q_{21}^R is almost real and Q_{21}^L is almost imaginary or vice versa), $\mathcal{A}_T^{21}$ becomes minimized; when $|\mathcal{A}_T^{21}| \approx 1$ (particularly when both Q_{21}^R and Q_{21}^L are almost either real or imaginary) $\mathcal{A}_N^{21}$ becomes minimized.

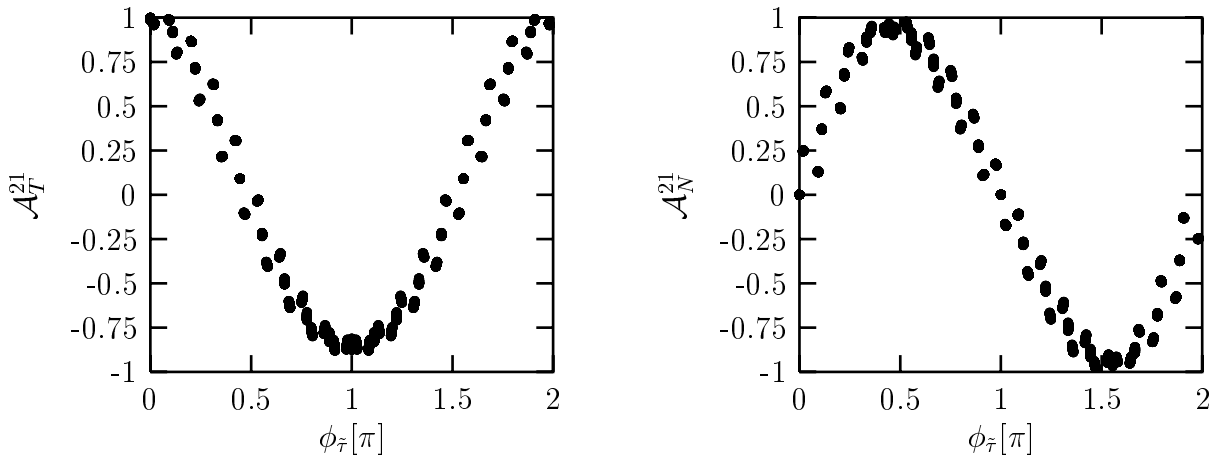

Figure 9.5: The transverse and normal polarization asymmetries $\mathcal{A}_T$ and $\mathcal{A}_N$ of τ^- from DECAY I. Parameters are as discussed in the text.

9.3 Case studies

In the previous sections it has been illustrated that the τ polarization asymmetries $\mathcal{A}_{T,N}^{21}$ lead to a sensitive dependence of the polarization of the τ lepton from the decay $\tilde{\chi}_2^0 \to \tau^{\pm}\tilde{\tau}_1^{\mp}$ on the phase $\phi_{\tilde{\tau}}$. Unfortunately the polarization asymmetries $\mathcal{A}_{T,N}^{21}$ cannot be extracted directly from the measurable τ polarization unless the event can be reconstructed completely. In the case at hand a complete event construction would be possible (up to possible discrete symmetries) if the masses of all participating SUSY particles were known, *and* if the τ energies could be measured. Since even in the $\tau \to \rho\nu$, $a_1\nu$ decays a significant fraction of the τ energy will usually be carried away by the neutrinos such an approach is impractical. Since obviously the direct reconstruction of τ lepton polarization asymmetries is practically impossible this section is devoted to a discussion of the τ polarization in the lab frame, as a function of kinematical variables that are also defined in the lab frame. To this end the τ four-momentum, whose spatial component in the "starred" coordinate system, i.e. in the neutralino rest frame, points in the direction of the unit vector $\hat{s}_3^\star$ defined in Eq. 9.22c, is boosted into the lab frame. In order to describe the behavior of the τ lepton produced in the second step of the $\tilde{\chi}_2^0$ decay, $\tilde{\tau}_1$ decays have to be modeled in the $\tilde{\tau}_1$ rest frame as described in Sec. 9.2.1, afterwards this decay has to be boosted into the lab frame. Altogether five angular variables have to be integrated: the production angle θ_2 used in Sec. 9.1.2, and the angles $\theta_1^\star$, $\phi_1^\star$, and $\theta_2^\star$, $\phi_2^\star$ describing $\tilde{\tau}_1^{\pm} \to \tau^{\pm}\tilde{\chi}_1^0$ and $\tilde{\chi}_2^0 \to \tilde{\tau}_1^{\pm}\tau^{\mp}$ decays, respectively. This is done using Monte Carlo methods.
Using the achievements of the previous chapter two points in the parameter space defined by Eqs. 9.30 and 9.31 are chosen. Both have

$$m_{\tilde{\tau}_L} = 205\text{GeV}, \quad m_{\tilde{\tau}_R} = 124\text{GeV}, \quad |\mu| = 215\text{GeV}, \tag{9.33}$$

Set I is chosen to conserve CP, whereas CP is violated for Set II:

$$\text{Set I}: \quad |M_1| = 87.5\text{GeV}, \quad \phi_\mu = 0, \quad \phi_{A_\tau} = \pi \quad \Rightarrow \phi_{\tilde{\tau}} = \pi; \tag{9.34a}$$

$$\text{Set II}: \quad |M_1| = 84.3\text{GeV}, \quad \phi_\mu = \frac{\pi}{2}, \quad \phi_{A_\tau} = \frac{\pi}{2} \quad \Rightarrow \phi_{\tilde{\tau}} = \frac{\pi}{2}. \tag{9.34b}$$

Note that the phase of μA_τ is the same for both sets, hence $|Z_{\tilde{\tau}}|$ and in consequence of this the mixing angle $\theta_{\tilde{\tau}}$ is identical in both cases, see Eqs. 2.4 and 2.9. Contrariwise, the

phase $\phi_{\tilde{\tau}}$ differs between SET I ($\phi_{\tilde{\tau}} = \pi$) and SET II ($\phi_{\tilde{\tau}} = \pi/2$).
The CMS energy is chosen as $\sqrt{s} = 300$GeV, comparison with Fig. 9.2 indicates that the signal cross section $e^-e^+ \to \tilde{\chi}_1^0\tilde{\chi}_2^0$ is near its maximum values for this choice. Unfortunately, for this choice of the CMS energy the background process $e^+e^- \to \tilde{\tau}_1^\pm\tilde{\tau}_1^\mp$ is also significantly above threshold, see Fig. 9.1 where the cross sections has a slightly lower threshold. The incident beam polarizations are set to $P_L = -0.8$ and $\overline{P}_L = 0.6$, as discussed earlier such a choice suppresses the cross section for $\tilde{\tau}_1^\pm\tilde{\tau}_1^\mp$ production significantly, see Sec. 9.1.1, and is on the other hand sufficient to obtain a sizeable polarization for the intermediate $\tilde{\chi}_2^0$, see Sec. 9.1.3.

As advertised earlier signal and background process can be separated by the energy

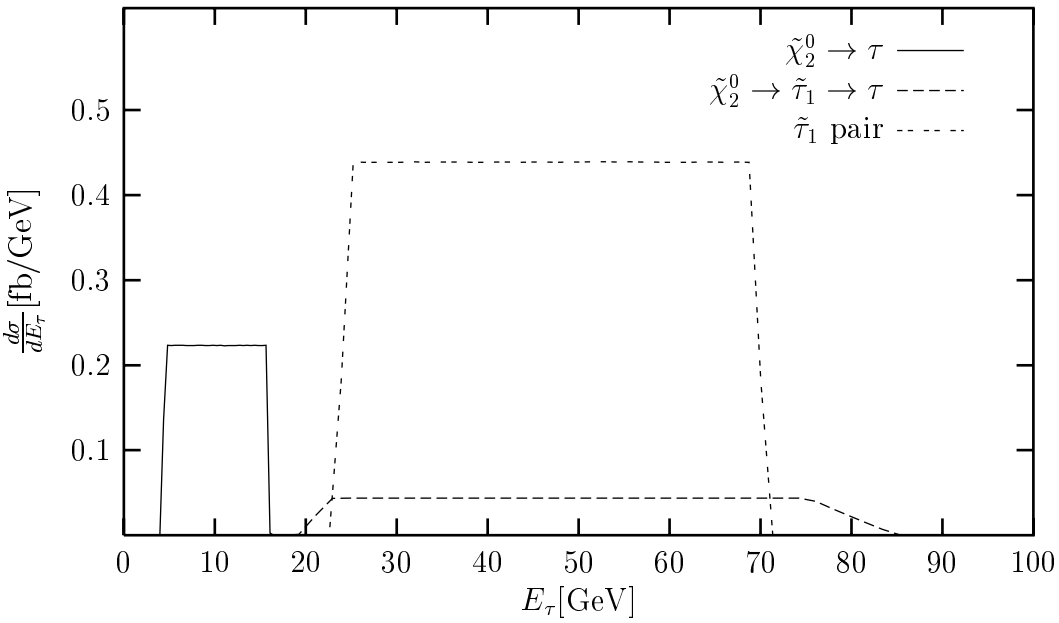

Figure 9.6: Energy distribution of the "soft" (solid) and "hard" (dashed) τ lepton from $\tilde{\chi}_2^0$ decay, as well as for the τ lepton from $\tilde{\tau}_1$ pair production and decay (double-dashed). Parameters are as in Eqs. 9.30, 9.33, and 9.34a.

distributions of the τ leptons, the same distributions are also sufficient to distinguish between the τ lepton from the primary decay of $\tilde{\chi}_2^0$ and the one from the secondary decay $\tilde{\tau}_1^\pm \to \tau^\pm\tilde{\chi}_1^0$. To this end the three resulting τ energy distributions in the lab frame are displayed in Fig. 9.6. Since both parameter sets lead to (essentially) the same mass spectrum, this figure is valid for SET I and SET II. The solid curve gives the energy distribution for the "soft" τ lepton from the primary $\tilde{\chi}_2^0$ decay, whereas the dashed curve is for the "hard" τ lepton produced in the second $\tilde{\chi}_2^0$ decay step. As advertised earlier these two distributions do not overlap[8] and are hence well suited to distinguish between the τ leptons from primary and secondary decay step of $\tilde{\chi}_2^0$. Moreover, the energy distribution from $e^+e^- \to \tilde{\tau}_1^\pm\tilde{\tau}_1^\mp \to \tau^\pm\tau^\mp\tilde{\chi}_1^0\tilde{\chi}_1^0$ (double-dashed curve) is also well separated from that of the "soft" τ lepton from $\tilde{\chi}_2^0$. Note that the energy distribution for the "soft" τ lepton is completely flat. Comparing with Fig. 9.3, which uses very similar parameters and shows that the intermediate $\tilde{\chi}_2^0$ can be strongly polarized this behavior appears as a surprise. The energy of the "soft" τ lepton in the rest frame depends only on the angle $\theta_2^\star$, the

[8] At higher $\sqrt{s}$ some overlap between these distributions does occur.

minimal (maximal) values given by $\cos\theta_2^\star = -1(1)$. Furthermore, Eq. 9.19 shows that the angular dependence of the angular decay distribution for $\tilde{\chi}_2^0$ is given by $\vec{P}^2 \cdot \hat{s}_3^\star$, integrating over the azimuthal angle $\phi_2^\star$ reduces the angular dependence to $P_L^2 \cos\theta_2^\star$. In turn the longitudinal polarization of $\tilde{\chi}_2^0$ is, according to Eqs. 9.10 and 9.11, proportional[9] to $\cos\theta_2$. Integrating over $\cos\theta_2$ will therefore lead to a vanishing *average* longitudinal polarization P_L^2, and finally to flat energy distributions of the primary $\tilde{\chi}_2^0$ decay products. The angular

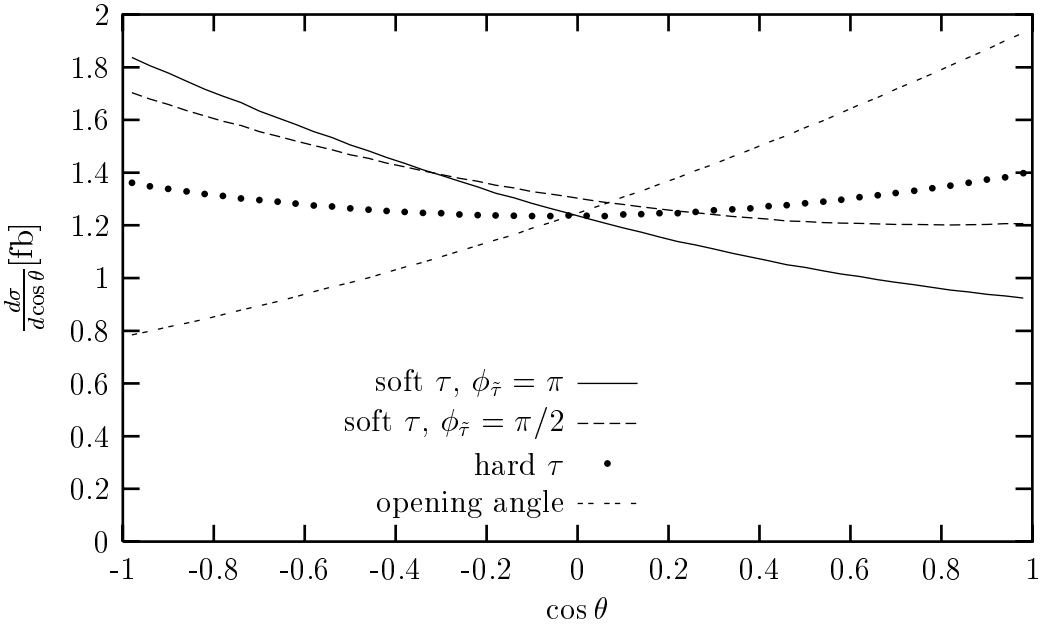

Figure 9.7: Angular distributions of the τ leptons from $\tilde{\chi}_2^0\tilde{\chi}_1^0$ production and decay. Parameters are as described in the text.

distributions of the τ leptons from DECAY I of Eq. 9.26a are shown in Fig. 9.7. The solid and dotted curves show the differential cross section as function of the cosine of the angle between the incident e^- beam and the direction of the "soft" and the "hard" τ lepton, respectively; the corresponding distributions for DECAY II can be obtained by sending $\cos\theta \to -\cos\theta$. The "soft" τ lepton shows quite a pronounced forward-backward asymmetry. This can again be explained from Eqs. 9.19, 9.10, and 9.11. In the case that the intermediate $\tilde{\chi}_2^0$ goes in forward direction, $\cos\theta_2 > 0$, its longitudinal polarization P_L^2 is negative according to Fig. 9.3. Since $\mathcal{A}_L^{21} > 0$, see Fig. 9.4, this means that the "soft" τ lepton will be emitted preferentially in the direction opposite to that of $\tilde{\chi}_2^0$, i.e. in backward direction. On the other hand, if $\cos\theta_2 < 0$ the longitudinal polarization P_L^2 is positive and the "soft" τ lepton will be emitted preferentially collinear with $\tilde{\chi}_2^0$, i.e. again in backward direction. The size of this effect depends on the longitudinal polarization asymmetry $\mathcal{A}_L^{21}$: Fig. 9.4 reveals a smaller value for $\mathcal{A}_L^{21}$ for SET II with $\phi_{\tilde{\tau}} = \pi/2$ compared to SET I with $\phi_{\tilde{\tau}} = \pi$. The dashed curve in Fig. 9.7 indeed shows a less pronounced forward-backward asymmetry for SET II. Finally, the double-dashed curve shows the differential cross section as a function of the opening angle between the "soft" and the "hard" τ lepton, $\theta_{\tau\tau}$. As expected from the discussion at the end of Sec. 8.2 this distribution peaks at small angles, i.e. $\cos\theta_{\tau\tau}$ near 1. However, this peak is not very pronounced, since the boost from the $\tilde{\chi}_2^0$ rest frame to the lab frame is not very large. This distribution is the same for DECAY I

[9] More precisely, $P_L^2 \propto \cos\theta_2/(1 + b\cos^2\theta_2)$. This does not spoil the argumentation above.

and DECAY II.

In the discussion of Sec. 9.2.3 it was observed that the main sensitivity to the phase

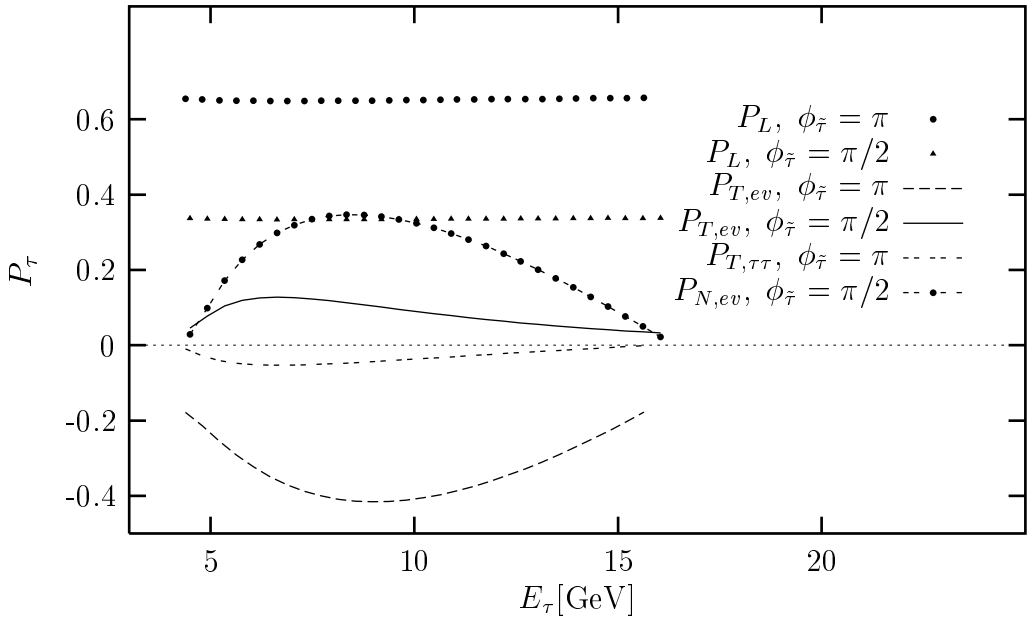

Figure 9.8: Energy dependence of the components of the polarization vector of the τ^- produced in Decay I. The transverse T and normal N components are defined either with respect to the plane spanned by the e^- and τ 3–momenta (subscript "ev"), or with respect to the plane spanned by the 3–momenta of the two τ leptons in the final state (subscript "$\tau\tau$"). Phase $\phi_{\tilde\tau} = \pi(\pi/2)$ refers to parameter SET I (SET II).

$\phi_{\tilde\tau}$ comes from the components of the τ lepton polarization that are orthogonal to the τ lepton three momentum. In principle, both polarization asymmetries $\mathcal{A}_T^{21}$ and $\mathcal{A}_N^{21}$ are equally well suited to determine this phase. However, the observation of a CP- or T-odd quantity would clearly be a more convincing proof of CP-violation in the stau and/or neutralino sector. The choice of beam polarization implies that the initial state is not CP self-conjugate. On the other hand, since the Born approximation is used and finite width effects are neglected here, the T transformation can be replaced by the naive $\tilde{T}$ transformation, which was briefly discussed in Sec. 5.1. Remember that the positive z- and x-directions of our coordinate system were defined by the three-momentum of the incident e^- beam and the transverse component of the three-momentum of the produced $\tilde\chi_2^0$. In this coordinate system a $\tilde{T}$-transformation, which reverses the directions of all three-momenta and spins, amounts to changing the y-components of all three momenta and spins; recall that the y axis is the same in the original coordinate system and the "starred" one introduced in Sec. 9.2.2. Practically speaking the $\tilde{T}$ conjugate of some kinematic configuration can therefore be obtained by simply sending $\phi_1^\star \to -\phi_1^\star$ and $\phi_2^\star \to -\phi_2^\star$. The existence of $\tilde{T}$-violation, and hence of CP-violation, is established if some observable takes *different* values for some configuration and the $\tilde{T}$ conjugate one. Note that these two configurations result in the same τ energies; the angular variables whose distributions are shown in Fig. 9.7 also remain unchanged.

The simplest such observables involve the triple product of three momentum or spin vectors. The triple product of the momenta of the final-state leptons with the incoming e^-

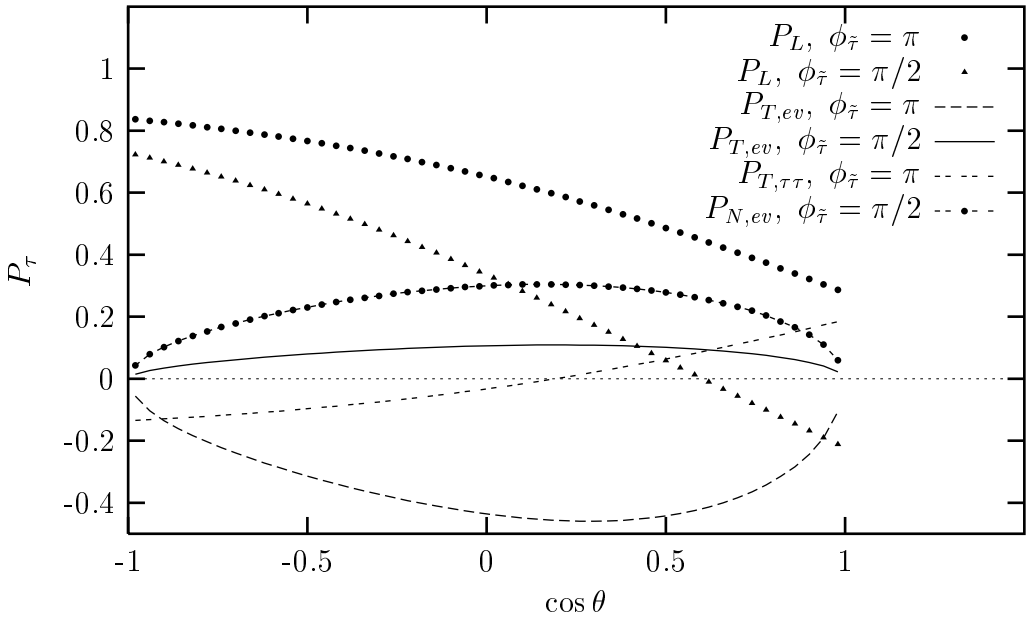

Figure 9.9: Dependence of the components of the polarization vector of the τ^- produced in Decay I on the cosine of the angle between this τ^- and the e^- beam. Parameters and notation are as in Fig. 9.8.

momentum has been studied in refs. [57, 58, 84, 122–124]. As mentioned in Sec. 8.1 this observable shows sensitivity to the CP-violating phases in the neutralino sector, but is not sensitive to $\phi_{\tilde\tau}$. This observation can be traced back to the fact that the τ lepton energy distribution only depends on $\mathcal{A}_L^{21}$, not on $\mathcal{A}_{T,N}^{21}$. Therefore the component of the "soft" τ polarization that is normal either to the "event" plane defined by the e^- beam and the three-momentum of this τ, or normal to the "$\tau\tau$" plane spanned by the three momenta of the two τ's in the final state is studied here. In both cases the "transverse" component of the τ polarization that lies in this plane is also analyzed.

The dependence of the τ polarization of the "soft" τ lepton on its energy is shown in Fig. 9.8 for DECAY I. The dotted and triangled curves show the longitudinal polarizations for SET I and SET II, respectively. It may be observed that this component is essentially independent of E_τ after integrating over the production angle θ_2. Up to terms of order m_τ^2 the longitudinal polarization component is boost-invariant. Its average value can thus be calculated from Eqs. 9.19 and 9.20a to

$$\langle P_L^{\tau^\mp}\rangle \simeq \mp\frac{\beta_\tau \mathcal{A}_L^{21}}{1+\mu_\tau \mathcal{A}_T^{21}}, \tag{9.35}$$

which well describes the numerical results presented in Fig. 9.8. Note in particular that this component of the polarization has opposite sign for DECAY II, where the "soft" τ lepton is positively charged.

The dashed and solid curves show the transverse polarization in the "event" plane for SET I and SET II, respectively. This polarization component clearly reflects the behavior of $\mathcal{A}_T^{21}$ as shown in Fig. 9.5, being sizeable and negative for $\phi_{\tilde\tau}=\pi$, but small for $\phi_{\tilde\tau}=\pi/2$. It has some dependence on the τ energy, reaching its maximal absolute value for some intermediate E_τ. Such values for E_τ correspond to small values of $\cos\theta_2^\star$, i.e. $|\sin\theta_2^\star|\simeq 1$,

which in turn maximizes the product $\vec{P}^2 \cdot \hat{s}_1^\star$ that multiplies $\mathcal{A}_T^{21}$ in Eq. 9.20b; recall from Fig. 9.3 that P_L^2 is the potentially biggest component of $\vec{P}^2$. In contrast, the double-dashed curve shows that the transverse polarization in the "$\tau\tau$" plane is small even for $\phi_{\tilde{\tau}} = \pi/2$. It should be suspected that such a small polarization, of less than 5%, will be very difficult to measure.

The dashed curve with dots in Fig. 9.8 shows the τ polarization normal to the "event" plane for SET II; since this polarization component is a $\tilde{T}$-odd quantity, it vanishes for SET I. It again tracks the behavior shown in Fig. 9.5, being large and positive for $\phi_{\tilde{\tau}} = \pi/2$. Also like $P_{T,ev}^\tau$, it shows a pronounced maximum at intermediate values of E_τ. Note that the product $\vec{P}^2 \cdot \hat{s}_1^\star$, which is maximized in this region of phase space, now multiplies the CP-odd quantity $\mathcal{A}_N^{21}$ in Eq. 9.20c. The τ polarization normal to the "$\tau\tau$" plane (not shown) is always much smaller than the one normal to the "event" plane.

Fig. 9.9 shows the same τ polarization components as in Fig. 9.8 as functions of the cosine of the angle θ_τ between the incoming e^- and the outgoing τ three momenta. It may be observed that the longitudinal τ polarization depends quite strongly on this angle. A value of $\cos\theta_\tau$ near -1 is easiest to achieve if $\cos\theta_2 \simeq -1$ and $\cos\theta_2^\star \simeq +1$, which results in $\vec{P}^2 \cdot \hat{s}_3^\star > 0$ after integrating over $\phi_2^\star$, so that both terms in the numerator of Eq. 9.20a are positive. In contrast, $\cos\theta_\tau \simeq 1$ is most easily achievable if $\cos\theta_2 \simeq \cos\theta_2^\star \simeq +1$, which gives a negative product $\vec{P} \cdot \hat{s}_3^\star$. For the parameters in SET II, where $\mathcal{A}_L^{21}$ is smaller, this even leads to negative P_L^τ in the forward direction. As before, P_L^τ has to be reversed for DECAY II.

The overall behavior of the transverse and normal components defined with respect to the "event" plane again follows the behavior of $\mathcal{A}_T^{21}$ and $\mathcal{A}_N^{21}$, respectively, as displayed in Fig. 9.5. Above it has been observed that these components reach their maximal values if $|\sin\theta_2^\star| \simeq 1$, which implies small $\cos\theta_2^\star$ and also the lab system variable $|\cos\theta_\tau|$ well away from unity. On the other hand, the transverse τ polarization defined with respect to the "$\tau\tau$" plane can now reach up to 20% for the parameters in SET I, which however is still well below the maximal value of $|P_{T,ev}^\tau|$.

Finally, the components of $\vec{P}^\tau$ were also investigated as functions of the opening angle between the τ leptons in the final state. However, the numerical results revealed only a very weak dependence on this angle in all cases; hence these results are not shown here. Note that the opening angle between the two τ leptons is independent of the production angle θ_2, and only weakly dependent on the $\tilde{\chi}_2^0$ decay angle $\theta_2^\star$. It has been seen above that these two variables largely determine the τ polarization. Integrating over them thus essentially reduces these polarizations to their average values.

Part IV

Summary

Chapter 10

Summary

This final chapter summarizes the most important findings of my thesis. First, Parts II and III are treated on separate footing in Secs. 10.1 and 10.2. In each of these sections the underlying assumptions are recalled and the most interesting results are resumed. Afterwards both sections are compared and combined to obtain more generalized conclusions in Sec. 10.3. Finally, a short outlook on possible developments in the discussed field is given.

10.1 Summary of Part II

In part II of this thesis the question to what extent the phases of dimensionful parameters in the MSSM Lagrangian can be determined from leptonic observables was discussed in great detail. All relevant results for low- and high-energy observables were presented and discussed using semi-analytical approximations obtained from a perturbative diagonalization of sparticle mass matrices. A detailed numerical analysis was performed for three sets of points in parameter space. The results of this numerical analysis and the conclusions following from them were broadly discussed. During this discussion the "initial" questions as summarized in Sec. 1.3 were clearly answered.
The main assumption within Part II was the universality of soft breaking parameters for first and second generation sleptons. Since no observables involving third generation (s)particles were investigated through Part II the only dimensionful, complex parameters are the Higgsino mass parameter μ, the $U(1)_Y$ gaugino mass M_1, and the leptonic trilinear soft breaking parameter A_l. The phases of these parameters are measured relative to the $SU(2)$ gaugino mass M_2, which is taken to be real and positive by convention for most of the analytical results and in the numerical analysis. The additional assumptions made on the relation of $|M_1|$ to M_2 and the relation of $m^2_{\tilde{l}_L}$ to $m^2_{\tilde{l}_R}$ serve no special purpose, both refer to models with universal gaugino and scalar masses at the GUT scale. In contrast to the first assumption which has quite important consequences and implications for the analysis in Part II, these two assumptions can be considered as arbitrary and can be dropped in any further applications of the developed code.
The main focus of Part II is clearly on quantities that can be measured at an FLC using the e^+e^- and e^-e^- option, nevertheless the low-energy constraints from d_e and a_μ were first analyzed in great detail. Given the numerically studied scenarios with moderate slepton masses it is well known that sizeable phases of dimensionful parameters are only allowed if the chargino and neutralino contributions to d_e cancel each other to a precision given by

the current experimental measurement of d_e. In agreement with earlier work [22, 23] it was found that—unless $|\mu| \gg M_2, m_{\tilde{l}}$—the phases of M_1 and A_l may take any value for some combination of the other phases. Contrarily, the phase of μ is tightly constrained with the maximal deviation from 0 or π scaling like $|\mu|^2$. The perhaps unexpected result during the analysis of low-energy constraints was the fact that further improved measurements of d_e will not significantly reduce the allowed ranges for any of these three phases after scanning over the other two phases in this case. This statement holds independently of whether the improved measurements lead to an improved, upper bound on $|d_e|$ or establish a non-vanishing value above the SM-prediction. In contrast, improved measurements of a_μ, if combined with improved SM predictions for the hadronic contributions, have the power to further restrict the allowed ranges of these phases.
After the discussion of low-energy constraints from leptonic dipole moments the course of my thesis turned to high-energy observables and I broadly studied the phase-dependences of a rather large set of total, unpolarized cross sections and their sensitivity to phases. After the semi-analytical discussion of cross sections with the goal to isolate the dominant sources of phase-dependences in a given production mode I introduced a measure to quantify the impact of non-trivial CP-odd phases on CP-even cross sections. This measure was referred to as significance. These significances determine the statistical significance with which the presence of non-trivial phases can be determined in a given production channel. For the $\tilde{e}_L^- \tilde{e}_L^-$ mode, which was already known [96] to depend strongly on the relative phase between M_1 and M_2, a significance of 60–90 standard deviations was found. However, since several neutralino production channels have comparable or even better sensitivity to the same phase this result does necessarily argue in favor of an e^-e^- collider. In particular, for $|\mu| > M_2$ the $\tilde{\chi}_1^0 \tilde{\chi}_2^0$ production mode reveals significances of 80 or more standard deviations from the CP-conserving MSSM and is still doing quite well (~ 30 standard deviations) for $|\mu| \approx M_2$. Moreover, the $\tilde{e}_L^- \tilde{e}_R^+$ production mode is still rather promising, showing somehow smaller significances between 10 and 70 standard deviations depending on the scenario. Note that the term of the cross section dependent on the relative phase between M_1 and M_2 is for the former two modes (within the reliability of the semi-analytical treatment of cross sections) independent of $\sin 2\beta$ and allows a determination of this phase even for quite small values of $\tan\beta$. Concerning the chargino production modes the numerically found significances are in general discouragingly small and indicate that these production channels most probably are not useful for the determination of phases. For the given choice of slepton masses $m_{\tilde{l}} \approx 200\text{GeV}$ the only significant dependence in chargino production on phases over the complete experimentally allowed parameter space occurs for $|\mu| > 2M_2$. The d_e constraint on the phase of μ, which is the only phase entering chargino production modes, becomes weaker for larger slepton masses. Hence the minimal ratio $|\mu|/M_2$ where chargino production can become useful for probing CP violating phases should decrease for larger $m_{\tilde{l}}$. However, since the relevant significances of all chargino production modes scale like $\sin 2\beta$, these production modes will be useful only for quite small values of $\tan\beta$. However, since the introduced significances only measure the deviation of cross sections from the predictions of the CP-conserving MSSM, all measurements of cross sections—regardless of their significances—are not sufficient to distinguish between the CP-violating MSSM and other, possible extensions of the MSSM without new CP-phases. This is the reason for studying the component of the polarization vector of produced charginos and neutralinos normal to the production plane. This polarization vector component is a CP-odd quantity and hence could in principle be used to establish CP-violation in the MSSM.

I found that these components can reach values exceeding 30% in the production of two different neutralinos. In particular the normal component of the polarization vector of the heavier neutralino in $\tilde{\chi}_1^0\tilde{\chi}_2^0$ production shows quite promising values. Again, chargino modes are apparently rather useless, in general they offer quite small normal components. Only for $|\mu| > M_2$ and small $\tan\beta$ the lighter chargino in $\tilde{\chi}_1^-\tilde{\chi}_2^+$ production offers values larger than in the neutralino modes. Note that recent studies [58–60] as well as the findings of Part III indicate that such large CP-odd polarizations might indeed lead to measurable CP-asymmetries in the phase space distributions of $\tilde{\chi}$ decay products.
Finally, the various correlations between phase-dependent observables were studied. Here no correlation was found between d_e and any phase-sensitive high-energy observable. This is due to the rather precise cancellation required between the different contributions to d_e and implies that further improved measurements of d_e will not further restrict the ranges for phase-sensitive high-energy observables. In contrast correlations were observed between a_μ and phase-sensitive high-energy observables. These correlations allow the conclusion that improved measurements and better predictions for the hadronic contribution to a_μ have the power to restrict the possible ranges of high-energy observables. Finally, most pairs of high-energy observables are strongly correlated. This reflects that most of them probe, given the strongly constrained phase of μ in our scenarios, the phase of M_1. This set of correlations is rather fortunate and should be important, since the measurement of one phase-sensitive high-energy observable in turn constrains the allowed ranges for most of the remaining phase-sensitive high-energy observables and hence allows stringent tests of the model itself. However, in scenarios with large $|\mu|$ and small $\tan\beta$ the phase of μ can still play an important role, in particular in chargino production modes. In that case phase-sensitive high-energy observables correlate poorly with those in the neutralino or slepton sector. This lack of correlations underscores the importance of measuring as many phase-sensitive observables as possible.
Altogether it may be concluded that even after including the current low-energy constraints most of the considered high-energy observables still show a significant dependence on the constrained phases. Unfortunately, the measurement of cross sections is not sufficient to establish CP-violation in the MSSM, for this purpose a non-vanishing value of some CP-odd observable has to be measured.

10.2 Summary of Part III

Motivated by the promising numerical results for the normal component of the polarization vector of the heavier neutralino in $\tilde{\chi}_1^0\tilde{\chi}_2^0$ production the course of my thesis swayed to the investigation of possible CP-asymmetries in neutralino pair production followed by decays of sparticles. In particular the $\tilde{\chi}_1^0\tilde{\chi}_2^0$ production followed by the two step decay $\tilde{\chi}_2^0 \to \tilde{\tau}_1^\pm\tau^\mp \to \tilde{\chi}_1^0\tau^\pm\tau^\mp$ was studied in great detail. During a study of the production cross sections for $\tilde{\chi}_1^0\tilde{\chi}_2^0$ as signal and for $\tilde{\tau}_1^\pm\tilde{\tau}_{1(2)}^\mp$ as possible SUSY background as well as of the primary $\tilde{\chi}_2^0 \to \tilde{\tau}^\pm\tau^\mp$ decay and the secondary/background decays $\tilde{\tau}_1^\mp \to \tau_1^\pm\tilde{\chi}_1^0$ it was observed that the polarization vector components of the τ lepton from the primary decay that are orthogonal to the τ momentum are very sensitive to the CP-odd phase $\phi_{\tilde{\tau}}$ from stau left-right mixing. In contrast, the polarization vector of the τ lepton from the secondary/background decay is mainly longitudinal to the τ momentum and rather insensitive to $\phi_{\tilde{\tau}}$. This observation directly implied that mass spectra which experimentally

allow a reconstruction of the origins of the two τ leptons in the final state and a distinction between signal and background final states are strongly preferred. A case study using Monte Carlo techniques performed for such optimized mass spectra revealed that much of the orthogonal polarization vector components of the τ lepton from the primary $\tilde{\chi}_2^0$ decay survives after boosting into the laboratory frame. The most sensitive regions in phase space involve both intermediate values of the energy of the τ lepton and of its angle with respect to the beam direction. In particular, for a CP-phase $\phi_{\tilde{\tau}} = \pi/2$, a CP-violating normal component was found in excess of up to 30% in certain regions of phase space. During this analysis the absolute necessity of strong (longitudinal) beam polarization was clearly underscored.

Of course, this quite promising result depends strongly on the assumptions that were made during the analysis.

To begin with, an inverted hierarchy with very heavy first and second generation sleptons was assumed. On the one hand this is a rather conservative assumption since it reduces the signal cross section by two orders of magnitude. On the other hand it is a quite optimistic assumption as it removes the stringent constraints on CP-violating phases from the measurements of leptonic dipole moments, in particular those from d_e. Note that this assumption would practically be excluded once an excess in a_μ has to be accounted into the MSSM. In the case that $\tilde{\tau}_1$ lies in mass between the two lighter neutralinos this assumption also implies that the investigated decay mode has a branching ratio near to 100%. Note that the mass parameters in the gaugino sector were chosen such that relatively small neutralino masses are obtained and the competing two body decays $\tilde{\chi}_2^0 \to \tilde{\chi}_1 Z$ and $\tilde{\chi}_2^0 \to \tilde{\chi}_1^0 h$ are closed. However, for gaugino-like neutralinos (which in general have a sizeable mass splitting) these two competing decays have rather small branching ratios, even if they were allowed.

A second important assumption is that left-right mixing in the stau sector should be sizeable. This assumption is motivated by the point that the phase $\phi_{\tilde{\tau}}$ looses its physical meaning in the absence of left-right mixing. In the numerical studies of $\tilde{\chi}_2^0$ decay in its rest frame it was observed that a quite moderate value of $\tan\beta = 10$ is already sufficient for the pursued purpose and generates sizeable effects. Note that for this choice of $\tan\beta$ neutralino masses and couplings begin to decouple from the phase of μ, i.e. show little sensitivity to ϕ_μ. Together with the universality assumption on gaugino masses at the GUT scale extended to their phases, i.e. $\phi_1 = \phi_2 = 0$, the CP-observables are indeed mostly attributed to the CP-violating phases in the stau sector.

Finally, the third assumption was that $\tilde{\tau}_1$ is quite close in mass to $\tilde{\chi}_2^0$. In this case the origin of the two τ leptons in the final state can be reconstructed experimentally in an event-by-event analysis; more precisely the energy of a τ lepton indicates whether it originates from the primary decay of $\tilde{\chi}_2^0$ or from the secondary decay of $\tilde{\tau}_1$. This is an important point since only the τ leptons from the $\tilde{\chi}_2^0$ decay have sizeable polarization components orthogonal to their momentum and since the efficiency of the reconstruction of the τ polarization is known to decrease with increasing τ energy. This implies that in contrary case—$\tilde{\tau}_1$ being close in mass to $\tilde{\chi}_1^0$—a reduction of the efficiency of the reconstruction of the τ polarization has to be accepted. In the worst case, i.e. if no distinction between τ leptons from the primary decay and from the secondary decay would be possible, averaging of the τ polarizations would be necessary and hence the asymmetries would be reduced by a factor two.

To summarize, within the inverted hierarchy models, the main assumption is thus that $\tilde{\chi}_2^0 \to \tilde{\tau}_1 \tau$ two body-decays are open, but $\tilde{\chi}_2^0 \to \tilde{\tau}_2 \tau$ two body decays are closed. In

the case that the second decay mode also is open several more decay chains need to be investigated. In the case they cannot be distinguished in the experiment the necessary averaging over them could lead to a further reduction of the τ polarization. However, in most SUSY models the region in parameter space with $m_{\tilde{\tau}_2} < m_{\tilde{\chi}^0_2}$ is quite small, whereas $m_{\tilde{\tau}_1} > m_{\tilde{\chi}^0_2}$ seems quite feasible. Obviously, in such regions of parameter space the two body decay $\tilde{\chi}^0_2 \to \tilde{\tau}_1 \tau$ is closed. If the competing two body decays were also closed, the decay $\tilde{\chi}^0_2 \to \tilde{\chi}^0_1 \tau^\pm \tau^\mp$ would still have a large, often dominant branching ratio, in many cases the dominant contributions would arise from virtual $\tilde{\tau}$ exchange [135–137]. Hence it may be assumed that in this case again sizeable polarizations with sensitivity to $\phi_{\tilde{\tau}}$ can be found. In the case that the competing two body decays were open the final state of interest would receive only very small contributions from virtual $\tilde{\tau}$ exchange and $\tilde{\chi}^0_2$ decays would not be a good probe of $\phi_{\tilde{\tau}}$. However, assuming that a sizeable beam energy will be available, the decays of heavier neutralinos may then be useful to extract information on the phase $\phi_{\tilde{\tau}}$ in such a case.
Altogether, it has to be concluded that neutralino decays into τ pairs offer a good, indeed probably the best possibility to probe CP violation in the stau sector at an FLC.

10.3 Synthesis and Outlook

In general the approaches to address possibly non-vanishing CP-phases of dimensionful parameters in the MSSM Lagrangian pursued in Parts II and III are quite different. This difference is not only reflected by the different assumptions made for the soft breaking parameters of the slepton sector but also—and actually much stronger—by the presented methods for studying the impact of non-vanishing phases.
In principle, the complete analysis presented in Part II can be understood as a "blind box" analysis. Given any parameter set satisfying universality for the first and second generation sleptons' soft breaking parameters the analysis calculates the low-energy allowed ranges for the phases of the dimensionful parameters as well as the significances of the various cross sections and the size of the normal components of polarization vectors in chargino and neutralino production.
In contrast, the analysis of CP-asymmetries in $e^- e^+ \to \tilde{\chi}^0_1 \tilde{\chi}^0_1 \tau^\pm \tau^\mp$ with sensitivity to the the CP-phase $\phi_{\tilde{\tau}}$ in the stau sector already starts with rather comfortable assumptions and modifies them during the analysis in order to obtain sizeable and experimentally well accessible CP-asymmetries. The transfer of the obtained numerical results from the studied parameter point to larger regions in parameter space hence depends strongly on the assumptions made and leads, roughly speaking, more to expectations than to general predictions. Unfortunately, due to the requirement of partly reconstructed kinematics for each event the involved experimental issues are much more difficult than those for measuring total cross sections and hence such restrictive assumptions can not be avoided. This implies that it is rather preferable to know as much details of the mass spectra before efforts are made to measure CP-asymmetries.
Altogether it can be concluded that total cross sections and CP-asymmetries offer a complementary access to CP-violating in the MSSM. This complementarity is essentially attributed to the fact that former show a cosine-like dependence on phases, whereas the latter ones have a sine-like dependence. This implies that the former ones are rather insensitive to small phases (perhaps the most likely scenario) and the measurement of (or

bounds on) CP-violating asymmetries will have to be used in this case. Contrariwise, if some CP-phase is near $\pi/2$, where the CP-odd asymmetries are close to maximal, these are not well suited to determine the value of this phase. Hence in such a case some cross sections will have the edge in the determination of this phase.
Also, there is some complementarity between high-energy observables involving selectrons on the one side and the low-energy observables d_e and a_μ and the CP-asymmetries involving the stau sector on the other side. Only the latter two depend on the phase of the corresponding trilinear soft breaking terms, whereas the former ones have only to probe the phases of M_1 and μ. This implies that in order to extract information on the phase of the soft trilinear coupling, given universality of these terms for all three generations, both low-energy observables and high-energy observables involving the stau sector have to be measured.
Finally, it may be concluded that measurements at high-energy colliders will be necessary to pin down the phases of dimensionful parameters. Both precision measurements of CP-even quantities like total cross sections and masses as well as searches for CP-asymmetries are promising in certain regions of parameter space. For both purposes an FLC seems to be ideally suited.

Part V

Appendices

Appendix A

More details about the perturbative treatment of particle mixing

A.1 Generalities

The basic idea for a perturbative treatment of a problem like

$$UM = \mathrm{diag}(\lambda_i)U, \tag{A.1}$$

is to expand the mass eigenvalues α_i, the mass matrix M, and either the mixing matrices U or the eigenstates v_i into a power series in some suitable perturbative parameter λ, $\lambda \ll 1$:

$$\alpha_i \simeq \alpha^{(0)} + \lambda^1\delta\alpha^{(1)} + \lambda^2\delta\alpha^{(2)} + \lambda^3\delta\alpha^{(3)} + \cdots, \tag{A.2a}$$

$$U \simeq U^{(0)} + \lambda^1\delta U^{(1)} + \lambda^2\delta U^{(2)} + \lambda^3\delta U^{(3)} + \cdots, \tag{A.2b}$$

$$v_i \simeq v_i^{(0)} + \lambda^1\delta v_i^{(1)} + \lambda^2\delta v_i^{(2)} + \lambda^3\delta v_i^{(3)} + \cdots, \tag{A.2c}$$

$$M \simeq M^{(0)} + \lambda^1\delta M^{(1)} + \lambda^2\delta M^{(2)} + \lambda^3\delta M^{(3)} + \cdots. \tag{A.2d}$$

As the mass matrix is a dimensionful quantity, its dimension fixes the maximum power of λ in its expansion.[1] The corrections to the mass eigenvalues and the mixing matrices (eigenvectors) in order λ^n are then obtained by inserting the decompositions in Eq. A.2 into Eq. A.1, then expanding and dropping all terms with λ^m, $m > n$. Imposing the unitarity of the mixing matrix U or ortho-normality of the eigenvectors v_i up to $\mathcal{O}(\lambda^n)$

$$(v_i^{(0)} + \lambda^1\delta v_i^{(1)} + \cdots)(v_j^{(0)} + \lambda^1\delta v_j^{(1)} + \cdots) \stackrel{!}{=} \delta_{ij} + \mathcal{O}(\lambda^{n+1}), \tag{A.3a}$$

$$(U^{(0)} + \lambda^1\delta U^{(1)} + \cdots)(U^{(0)} + \lambda^1\delta U^{(1)} + \cdots)^\dagger \stackrel{!}{=} \delta_{ij} + \mathcal{O}(\lambda^{n+1}), \tag{A.3b}$$

completes the set of equations for the determination of the $\mathcal{O}(\lambda^n)$ corrections.

[1] The expansion parameter λ is associated with a ratio of mass scales within the mass matrix M. Hence, concerning the mass matrix the use of "decomposition" instead of "expansion" would actually be more appropriate.

A.2 Perturbative chargino mixing

After separating the Dirac phases, which will be treated at the end of this section, from U_R the series for the mixing matrices U_L and V_R, the squared mass eigenvalues Λ_i, and the matrices $M_L = M_C M_C^\dagger$ and $M_R = M_C^\dagger M_C$ are introduced as

$$M_R = M_R^{(0)} + \lambda \delta M_R^{(1)} + \lambda^2 \delta M_R^{(2)} \ldots, \tag{A.4a}$$

$$M_R = M_L^{(0)} + \lambda \delta M_L^{(1)} + \lambda^2 \delta M_L^{(2)} \ldots, \tag{A.4b}$$

$$\Lambda_i \simeq \Lambda_i^{(0)} + \lambda \delta \Lambda_i^{(1)} + \lambda^2 \delta \Lambda_i^{(2)} + \cdots, \tag{A.4c}$$

$$(V_R)_{ij} \simeq \left(V_R^{(0)}\right)_{ij} + \lambda \left(\delta V_R^{(1)}\right)_{ij} + \lambda^2 \left(\delta V_R^{(2)}\right)_{ij} + \cdots = \delta_{ij} + \lambda \beta_{ij} + \lambda^2 \beta'_{ij} \ldots, \tag{A.4d}$$

$$(U_L)_{ij} \simeq \left(U_L^{(0)}\right)_{ij} + \lambda \left(\delta U_L^{(1)}\right)_{ij} + \lambda^2 \left(\delta U_L^{(2)}\right)_{ij} + \cdots = \delta_{ij} + \lambda \epsilon_{ij} + \lambda^2 \epsilon'_{ij} \ldots. \tag{A.4e}$$

The dimensionless parameter λ corresponds M_W (divided by some SUSY mass scale in the chargino mass matrix), i.e. $\mathcal{O}(\lambda^n) = \mathcal{O}(M_W^n)$.
Putting the expansions into the equations

$$V_R M_R = \mathrm{diag}\,(\Lambda_i)\, V_R, \tag{A.5a}$$

$$U_L M_L = \mathrm{diag}\,(\Lambda_i)\, U_L, \tag{A.5b}$$

I find the following equations by sorting after powers of λ

$$\lambda^{(0)}: \quad \left(M_R^{(0)}\right)_{ik} = \Lambda^{(0)} \delta_{ik}, \tag{A.6a}$$

$$\lambda^{(1)}: \quad \epsilon_{ij} \left(M_R^{(0)}\right)_{jk} + \left(\delta M_R^{(1)}\right)_{ik} = \delta \Lambda_i^{(1)} \delta_{ik} + \Lambda_i^{(0)} \epsilon_{ik}, \tag{A.6b}$$

$$\begin{aligned} \lambda^{(2)}: \quad & \left(\delta M_R^{(2)}\right)_{ik} + \epsilon_{ij} \left(\delta M_R^{(1)}\right)_{jk} + \epsilon'_{ij} \left(M_R^{(0)}\right)_{jk} \\ & = \delta \Lambda_i^{(2)} \delta_{ik} + \delta \Lambda_i^{(1)} \epsilon_{ik} + \Lambda_i^{(0)} \epsilon'_{ik}, \end{aligned} \tag{A.6c}$$

and similar relations for M_L, β_{ij} and β'_{ij}. From these equations it is straightforward to find the zeroth order squared masses[2]

$$\Lambda_1^{(0)} = |M_2|^2, \quad \Lambda_2^{(0)} = |\mu|^2, \tag{A.7}$$

and the higher corrections to the squared masses and the mixing matrices

$$\delta \Lambda_i^{(1)} = 0, \tag{A.8a}$$

$$\delta \Lambda_i^{(2)} = \frac{(\Lambda_i^{(0)} - \Lambda_j^{(0)}) \left(M_R^{(2)}\right)_{ii} + \left|\left(M_R^{(1)}\right)_{ji}\right|^2}{\Lambda_i^{(0)} - \Lambda_j^{(0)}}, \quad \text{with } i \neq j, \tag{A.8b}$$

$$\epsilon_{ij} = \frac{\left(\delta M_R^{(1)}\right)_{ij}}{\Lambda_i^{(0)} - \Lambda_j^{(0)}}, \quad \text{for } i \neq j, \tag{A.8c}$$

[2] The ordering $|M_2| < |\mu|$ is assumed.

$$\epsilon'_{ij} = 0, \quad \text{for} \quad i \neq j. \tag{A.8d}$$

During this calculation it is important to notice that the 2×2 matrices $M^{(0)}_{L(R)}$ and $\delta M^{(2)}_{L(R)}$ are diagonal while $\delta M^{(1)}_{L(R)}$ is off-diagonal and that most sums collapse due to this fact. From unitarity we find

$$\epsilon_{ij} = -\epsilon^{\star}_{ji}, \tag{A.9a}$$

$$\mathcal{R}\mathrm{e}\left[\epsilon_{ii}\right] = 0, \tag{A.9b}$$

$$2\mathcal{R}\mathrm{e}\left[\epsilon'_{ii}\right] = -|\epsilon_{ij}|^2. \tag{A.9c}$$

After a few manipulations of the original equations using the obtained results, one can furthermore show

$$\mathcal{I}\mathrm{m}\left[\epsilon_{ii}\right] = 0. \tag{A.10}$$

Since the perturbative results must respect the properties of the analytic parameterization to any order in perturbation theory, we can directly conclude that

$$\mathcal{I}\mathrm{m}\left[\epsilon'_{ii}\right] = 0. \tag{A.11}$$

All corresponding results for β_{ij} and β'_{ij} are obtained with the identical procedure manner and are given by Eq. A.8 after the replacements $M_L \to M_R$ and $\epsilon_{ij} \to \beta_{ij}$, with this replacement Eqs. A.9 to A.11 read analogously.
The Dirac phases γ_1 and γ_2 can be extracted from

$$P^{\dagger} = V_R M_C U_L^{\dagger} \left[\mathrm{diag}\left([\Lambda_1^{(0)} + \lambda^2\delta\Lambda_1^{(2)}]^{1/2}, [\Lambda_2^{(0)} + \lambda^2\delta\Lambda_2^{(2)}]^{1/2}\right)\right]^{-1}. \tag{A.12}$$

Inserting $M_C = M_C^{(0)} + \lambda\delta M_C^{(1)}$ and the expansion for U_L and V_R given in Eq. A.4, perturbative results for $\sin\gamma_i$ and $\cos\gamma_2$ and hence for $\tan\gamma_i$ can be derived. The derivation of these results is not as simple as the calculation of the corrections to the mixing matrix, so I do not give the results explicitly here and refer to the ones given in Sec. 2.3.2.
The formalism for a perturbative diagonalization of the chargino mass matrix can easily be extended to higher orders of perturbation theory, but for Part II of my thesis the knowledge of the leading corrections is sufficient.

A.3 Perturbative neutralino mixing

The starting point for a perturbative diagonalization of the neutralino mass matrix is

$$M_N N = N^{\star}\mathrm{diag}\left(m_{\tilde{\chi}^0_1}, m_{\tilde{\chi}^0_2}, m_{\tilde{\chi}^0_3}, m_{\tilde{\chi}^0_4}\right) = N^{\star} M_N^d, \tag{A.13}$$

or in terms of eigenstates

$$M_N \tilde{\chi}_i^{0\star} = \tilde{\chi}_i^0 M_N^d = m_i \tilde{\chi}_i^0. \tag{A.14}$$

Then the perturbative series for the mass matrix M_N, the eigenstates $\tilde{\chi}^0_i$, and the masses m_i are introduced as

$$M_N = M_N^{(0)} + \lambda\delta M_N^{(1)}, \tag{A.15a}$$

$$\tilde{\chi}_i^0 \simeq \tilde{\chi}_i^{0,(0)} + \lambda\tilde{\chi}_i^{0,(1)} + \lambda^2\tilde{\chi}_i^{0,(2)} + \cdots, \tag{A.15b}$$

$$m_i \simeq m_i^{(0)} + \lambda\delta m_i^{(1)} + \lambda^2\delta m_i^{(2)} + \cdots, \tag{A.15c}$$

with the eigenstates $\tilde{\chi}_i^0$ expanded and decomposed as

$$\tilde{\chi}_i^{0,(0)} = e^{i\Psi_i}\tilde{\chi'}_i^{0,(0)}, \tag{A.16a}$$

$$\tilde{\chi}_i^{0,(1)} = e^{i\Psi_i}\sum c_{ij}\tilde{\chi'}_j^{0,(0)}, \tag{A.16b}$$

$$\tilde{\chi}_i^{0,(2)} = e^{i\Psi_i}\sum d_{ij}\tilde{\chi'}_j^{0,(0)}. \tag{A.16c}$$

Here λ is a dimensionless parameter which only serves for counting the orders of the perturbation theory.[3] Plugging these decompositions into Eq. A.14 and sorting by powers of λ, one finds

$$\lambda^0\ (\simeq M_Z^0): \quad M_N^{(0)}\tilde{\chi}_i^{0,(0)\star} = \tilde{\chi}_i^{0,(0)}, \tag{A.17a}$$

$$\lambda^1\ (\simeq M_Z^1): \quad M_N^{(0)}\tilde{\chi}_i^{0,(1)\star} + \delta M_N^{(1)}\tilde{\chi}_i^{0,(0)\star} = m_i^{(0)}\tilde{\chi}_i^{0,(1)} + \delta m_i^{(1)}\tilde{\chi}_i^{0,(0)}, \tag{A.17b}$$

$$\lambda^2\ (\simeq M_Z^2): \quad M_N^{(0)}\tilde{\chi}_i^{0,(2)\star} + \delta M_N^{0,(1)\star} = m_i^{(0)}\tilde{\chi}_i^{0,(2)} + \delta m_i^{(1)}\tilde{\chi}_i^{0,(1)} + \delta m_i^{(2)}\tilde{\chi}_i^{0,(0)}. \tag{A.17c}$$

After defining

$$\tilde{\chi'}_j^{0,(0)T} M_N^{(0)}\tilde{\chi}_i^{0,(0)} = \left(M_N^{(0)}\right)_{ji}, \tag{A.18a}$$

$$\tilde{\chi'}_j^{0,(0)T}\delta M_N^{(1)}\tilde{\chi}_i^{0,(0)} = \left(\delta M_N^{(1)}\right)_{ji}, \tag{A.18b}$$

one finds by multiplying Eqs. A.17 with $\tilde{\chi'}_j^{0,(0)T}$ and by inserting the expansion of the eigenstates as in Eq. A.16 the following relations

$$\left(M_N^{(0)}\right)_{ji} = m_i^{(0)}e^{i2\Psi_i}\delta_{ij}, \tag{A.19a}$$

$$\left(\delta M_N^{(1)}\right)_{ji} = \delta m_i^{(1)}\delta_{ij}e^{i2\Psi_i} + c_{ij}m_i^{(0)}e^{i2\Psi_i} - c_{ij}^\star m_j^{(0)}e^{i2\Psi_j}, \tag{A.19b}$$

$$\sum c_{ik}^\star\left(\delta M_N^{(1)}\right)_{jk}e^{-i2\Psi_i} = m_i^{(0)}d_{ij} - m_j^{(0)}e^{i2(\Psi_j-\Psi_i)}d_{ij}^\star + \delta m_i^{(2)}\delta_{ij}. \tag{A.19c}$$

The zeroth order phases and masses are then given by Eq. A.19a as

$$m_1^{(0)} = |M_1|, \quad m_2^{(0)} = |M_2|, \quad m_3^{(0)} = m_4^{(0)} = |\mu|, \tag{A.20a}$$

$$\Psi_1 = -\phi_1/2, \quad \Psi_2 = -\phi_2/2, \quad \Psi_3 = -(\phi_\mu+\pi)/2, \quad \Psi_4 = -\phi_\mu/2, \tag{A.20b}$$

while Eq. A.19b determines the first order corrections, for which we find

$$\delta m_i^{(1)} = 0, \tag{A.21a}$$

$$\mathcal{I}\mathrm{m}\left[c_{ii}\right] = 0, \tag{A.21b}$$

[3] $\mathcal{O}(\lambda^n)$ corresponds to $\mathcal{O}(M_Z^n)$.

$$c_{ij} = \left(\delta M_N^{(1)}\right)_{ji} \frac{m_i^{(0)} e^{-i2\Psi_i} + m_j^{(0)} e^{2i\Psi_j}}{m_i^{(0)2} - m_j^{(0)2}}, \quad i \neq j. \tag{A.21c}$$

Imposing the ortho-normality of the $\tilde{\chi'}_i^0$ up $\mathcal{O}(\lambda)$ we obtain two additional relations for the $\mathcal{O}(\lambda)$ corrections

$$c_{ij} = -c_{ji}^\star, \tag{A.22a}$$

$$\mathcal{R}\mathrm{e}\left[c_{ii}\right] = 0. \tag{A.22b}$$

Note that the $\mathcal{O}(\lambda)$ corrections to gaugino-gaugino mixing are either excluded by

$$\left(M_N^{(0)}\right)_{12} = \left(M_N^{(0)}\right)_{21} = 0,$$

or by the ortho-normality conditions. The second point is still true for the diagonal corrections to Higgsino-Higgsino mixing, whereas the off-diagonal corrections c_{34} and c_{43} remain correlated to each other but undetermined. This behavior results from the un-lifted degeneracy of the Higgsino mass eigenstates. As one can show these two entries do not affect our observables in a perturbative analysis, and hence can be set to zero by hand. The $\mathcal{O}(\lambda^2)$ corrections are obtained from Eq. A.19c, after some manipulations the results read

$$\delta m_i^{(2)} = \sum_{k,k\neq i} \frac{\left(\delta M_N^{(1)}\right)_{ki} \left(\delta M_N^{(1)}\right)_{ik}}{m_i^{(0)2} - m_k^{(0)2}} \left\{ m_i^{(0)} + m_k^{(0)} \cos\left[2(\Psi_i + \Psi_k)\right] \right\}, \tag{A.23a}$$

$$\mathcal{I}\mathrm{m}\left[d_{ii}\right] = -\sum_{k,k\neq i} \frac{\left(\delta M_N^{(1)}\right)_{ki} \left(\delta M_N^{(1)}\right)_{ik}}{2\left(m_i^{(0)2} - m_k^{(0)2}\right)} \frac{m_k^{(0)}}{m_i^{(0)}} \sin\left[2(\Psi_i + \Psi_k)\right], \tag{A.23b}$$

$$\begin{aligned} d_{ij} = \frac{1}{m_i^{(0)2} - m_j^{(0)2}} \sum_{k,k\neq i} \frac{\left(\delta M_N^{(1)}\right)_{ki} \left(\delta M_N^{(1)}\right)_{kj}}{m_i^{(0)2} - m_k^{(0)2}} \Big[& m_i^{(0)2} + m_i^{(0)} m_k^{(0)} e^{-i2(\psi_i + \Psi_k)} \\ & + m_i^{(0)} m_j^{(0)} e^{i2(\Psi_j - \Psi_i)} + m_k^{(0)} m_i^{(0)} e^{i2(\Psi_k + \Psi_j)} \Big], \quad i \neq j. \end{aligned} \tag{A.23c}$$

The additional relations from ortho-normality up to $\mathcal{O}(\lambda^2)$ are

$$2\mathcal{R}\mathrm{e}\left[d_{ii}\right] = -\sum_k |c_{ik}|^2, \tag{A.24a}$$

$$d_{ji}^\star = -d_{ij} - \sum_k c_{ik} c_{jk}^\star. \tag{A.24b}$$

Again the off-diagonal corrections to Higgsino-Higgsino mixing are correlated to each other, but remain undetermined due to the un-lifted degeneracy between the Higgsino mass eigenstates. Since they do not, like c_{34} and c_{43}, affect the observables, they are set to zero by hand. Using all these results the neutralino mixing matrix in the perturbative treatment reads

$$N = (\tilde{\chi}_1, \tilde{\chi}_2, \tilde{\chi}_3, \tilde{\chi}_4)^\star \tag{A.25}$$

$$= \begin{pmatrix} e^{-i\phi_1/2}(1+d^\star_{11}) & e^{-i\phi_2/2}d^\star_{21} & e^{-i(\phi_\mu+\pi)/2}c^\star_{31} & e^{-i\phi_\mu/2}c^\star_{41} \\ e^{-i\phi_1/2}d^\star_{12} & e^{-i\phi_2/2}(1+d^\star_{22}) & e^{-i(\phi_\mu+\pi)/2}c^\star_{32} & e^{-i\phi_\mu/2}c^\star_{42} \\ \frac{e^{-i\phi_1/2}}{\sqrt{2}}(c^\star_{13}+c^\star_{14}) & \frac{e^{-i\phi_2/2}}{\sqrt{2}}(c^\star_{23}+c^\star_{24}) & \frac{e^{-i(\phi_\mu+\pi)/2}}{\sqrt{2}}(1+d^\star_{33}) & \frac{e^{-i\phi_\mu/2}}{\sqrt{2}}(1+d^\star_{44}) \\ \frac{e^{-i\phi_1/2}}{\sqrt{2}}(c^\star_{13}-c^\star_{14}) & \frac{e^{-i\phi_2/2}}{\sqrt{2}}(c^\star_{23}-c^\star_{24}) & \frac{e^{-i(\phi_\mu+\pi)/2}}{\sqrt{2}}(1+d^\star_{33}) & -\frac{e^{-i\phi_\mu/2}}{\sqrt{2}}(1+d^\star_{44}) \end{pmatrix} \quad \text{(A.26)}$$

As already mentioned, corrections to gaugino-gaugino and Higgsino-Higgsino mixing occur in $\mathcal{O}(M_Z^2)$ while corrections to gaugino-Higgsino mixing are already an $\mathcal{O}(M_Z)$-effect. Corrections to the physical masses are also an $\mathcal{O}(M_Z^2)$-effect. The formalism presented here can easily be extended to higher orders in λ ($\equiv M_Z$) by adding the required terms in the series given by Eq. A.17 and keeping the corresponding terms in Eq. A.16. The calculation will merely get more tedious and the results more lengthier. However, for the purposes of Part II a calculation up to second order in M_Z is sufficient.

A.4 Perturbative parameter adjustment

In Part II the thesis discusses the possibility to keep phase-dependent kinematical masses fixed by an adjustment of the absolute values of input parameters. That is to say, the variation of the kinematical masses along with the variation of the phases is absorbed into a change of the absolute values of parameters. This procedure can be written as

$$m_i^{CPC}(\alpha_i) \stackrel{!}{=} m_i(\phi_i, \alpha_i + \delta\alpha_i), \quad \text{(A.27)}$$

where m_i^{CPC} is the kinematical mass of particle i and is fixed with respect to any CP-conserving reference point (CPC) depending on a set of parameters α_i. The adjustment of these parameters in presence of non-vanishing phases ϕ_i is denoted by $\delta\alpha_i$. In general, Eq. A.27 corresponds to a set of non-linear equations and has to be treated numerically.
If only the dimensionful parameters in the chargino and neutralino mass matrix, i.e. $|M_1|$, $|M_2|$, and $|\mu|$, are varied, correspondingly at most three masses can be kept at CPC-values. In the numerical analysis we choose the masses of $\tilde{\chi}_1^0$, $\tilde{\chi}_3^0$, and $\tilde{\chi}_1^\pm$. For these particle masses fixed the parameter adjustment can be discussed perturbatively, i.e. the three equations from Eq. A.27 can be solved to give perturbative expressions for $\delta|M_1|$, $\delta|M_2$, and $\delta|\mu|$. Using the results for the $\mathcal{O}(M_Z^2)$ shifts of the mass eigenvalues as given in Eqs. 2.40 and 2.35, the corresponding shifts in the parameters read

$$\delta|M_1| = \frac{|\mu| M_Z^2 \sin^2\theta_W}{|\mu|^2 - |M_1|^2} \sin 2\beta \left[\cos(\phi_\mu + \phi_1) - \cos(\phi_\mu + \phi_1)|_{CPC}\right], \quad \text{(A.28a)}$$

$$\delta|M_2| = \frac{|\mu| M_Z^2 \cos^2\theta_W}{|\mu|^2 - |M_2|^2} \left[\cos(\phi_\mu + \phi_2) - \cos(\phi_\mu + \phi_2)|_{CPC}\right], \quad \text{(A.28b)}$$

$$\delta|\mu| = -\frac{1-\sin 2\beta}{2} M_Z^2 \left\{ \frac{|M_1| \sin^2\theta_W}{|\mu|^2 - |M_1|^2} \left[\cos(\phi_\mu + \phi_1) - \cos(\phi_\mu + \phi_1)|_{CPC}\right] + \frac{|\mu| \cos^2\theta_W}{|\mu|^2 - |M_2|^2} \left[\cos(\phi_\mu + \phi_2) - \cos(\phi_\mu + \phi_2)|_{CPC}\right] \right\}, \quad \text{(A.28c)}$$

where $|_{CPC}$ indicates that the corresponding cosine-terms have to be evaluated with the given combination of the "trivial" phases, i.e. these terms are either 1 or -1 corresponding to $\phi_\mu + \phi_{1(2)} = 0, 2\pi$ or $\phi_\mu + \phi_{1(2)} = \pi$. The results in Eq. A.28 show clearly that the shifts in the absolute values of the varied parameters are indeed of $\mathcal{O}(M_Z^2)$.

Appendix B

More details on the calculation of the SUSY contributions to d_e and a_μ

B.1 Calculation of leptonic dipole moments

B.1.1 Generalities

The calculation of the SUSY contributions to a_μ and d_e mediated by chargino and neutralino exchange follows [54] closely. Guided by this work one starts with a generalized interaction Lagrangian as given by [54]

$$\mathcal{L} = eV_\mu^{(k)}\overline{\Psi}_j\gamma_\mu(V_{jl} - A_{jl}\gamma_5)\Psi_l + e\left\{\overline{\Psi}_f(S_{jk} - P_{jk}\gamma_5)\Psi_k\Phi_j + h.c.\right\} + ieG_{jk}V^\mu\Phi_j^\dagger \overleftrightarrow{\partial}_\mu \Phi_k\,, \tag{B.1}$$

where several terms contained in [54] have been dropped already since they are irrelevant for the SUSY one loop contributions to be calculated later onwards. Vector bosons are denoted by $V_\mu^{(k)} = A_\mu, Z_\mu$; fermions and scalar bosons by Ψ_k and Φ_k, respectively. Following [54] the relevant generic vertices are:

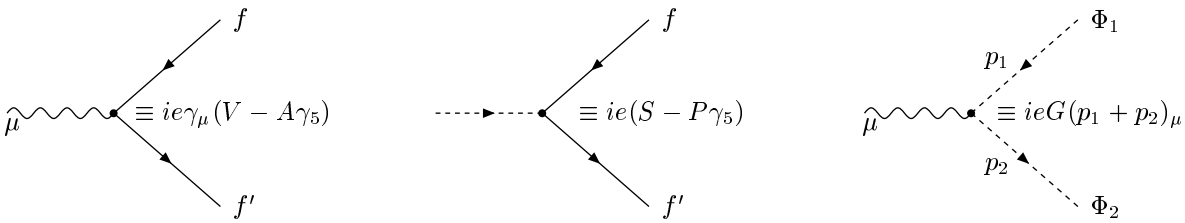

Figure B.1: Generic vertices determined by Eq. B.1.

Given these vertices the generic contributions to lepton form factors in the effective Vff-vertex from fermion exchange with two scalars (type A) and from scalar exchange with two fermions (type B) may be calculated. The corresponding diagrams are depicted in Fig B.2, the left one resulting later in the neutralino contribution and the right one into the chargino contribution, when the generic interaction Lagrangian in Eq. B.1 is identified with the SUSY interaction Lagrangian from Sec. 2.5 and the generic boson V is specified as photon. In Apps. B.1.2 and B.1.3 the most important steps during the calculation of these two generic diagrams are summarized and performed up to a stage where the results can

Figure B.2: Generic diagrams for the fermion exchange with two scalars (left) and for the scalar exchange with two fermions (right).

be compared with [54]. Note that this reference neither presents any intermediate steps nor executes the limit $s \to 0$ of vanishing vector boson momentum. Furthermore, it only gives the explicit results for the generic one loop contributions and specifies the generic vertices for the MSSM, but does not explicitly show the result for the lepton form factors from neutralino and chargino exchange, i.e. explicit results for $(d_f)_{\text{SUSY}}$ and $(a_f)_{\text{SUSY}}$ are missing. Contrarily, in App. B.1.4 these results, being of central importance for this thesis, are derived from the results of Apps. B.1.2 and B.1.3. Several properties of and manipulations on the loop functions appearing throughout the calculation of the lepton form factors are collected in App. B.2, whereas the Gordon identities used in the calculation are summarized in App. B.3. The basic reason for using [54] as guideline is that this work reveals somewhat more technical details on the calculation of the lepton form factors than most other references [22, 24, 55] do.

B.1.2 Calculation of diagram type A (neutralino)

The complete diagram of type A contributions is shown in Fig. B.3, including the precise vertices and the complete momentum configuration. Using standard propagators for the exchanged scalars j, k and the exchanged fermion l together with a careful treatment of the internal Majorana fermion line the one-loop contribution $(F_A)_{jlk}$ from diagrams of type A to the invariant Feynman amplitude reads as

$$(F_A)_{jlk} = \overline{u}_{p_2} \mu^{4-D} \int \frac{d^D q}{(2\pi)^D} \frac{e^3 (S^\star_{kl} + \gamma_5 P^\star_{kl})(\not{q} + M_l)(S_{jl} - \gamma_5 P_{jl})(2q - p_1 - p_2)_\mu G_{jk}}{\left[q^2 - M_l^2 + i\epsilon\right]\left[(q-p_1)^2 - M_j^2 + i\epsilon\right]\left[(q-p_2)^2 - M_k^2 + i\epsilon\right]} u_{p_1}. \tag{B.2}$$

Some attention has to be focused on the Majorana nature of the exchanged fermion, regarding the correct treatment of vertices with Majorana fermions as well as propagators of Majorana fermions [138] is of great benefit. The chiral structure of $(F_A)_{jlk}$ can be simplified. After introducing four effective vertex factors A^i_{jlk} as

$$A^1_{jlk} = G_{jk}\left(S_{jl} S^\star_{kl} + P_{jl} P^\star_{kl}\right) = (A^1_{klj})^\star, \tag{B.3a}$$

$$A^2_{jlk} = G_{jk}\left(S_{jl} P^\star_{kl} + P_{jl} S^\star_{kl}\right) = (A^2_{klj})^\star, \tag{B.3b}$$

$$A^3_{jlk} = G_{jk}\left(S_{jl} S^\star_{kl} - P_{jl} P^\star_{kl}\right) = (A^3_{klj})^\star, \tag{B.3c}$$

$$A^4_{jlk} = G_{jk}\left(S_{jl} P^\star_{kl} - P_{jl} S^\star_{kl}\right) = -(A^4_{klj})^\star, \tag{B.3d}$$

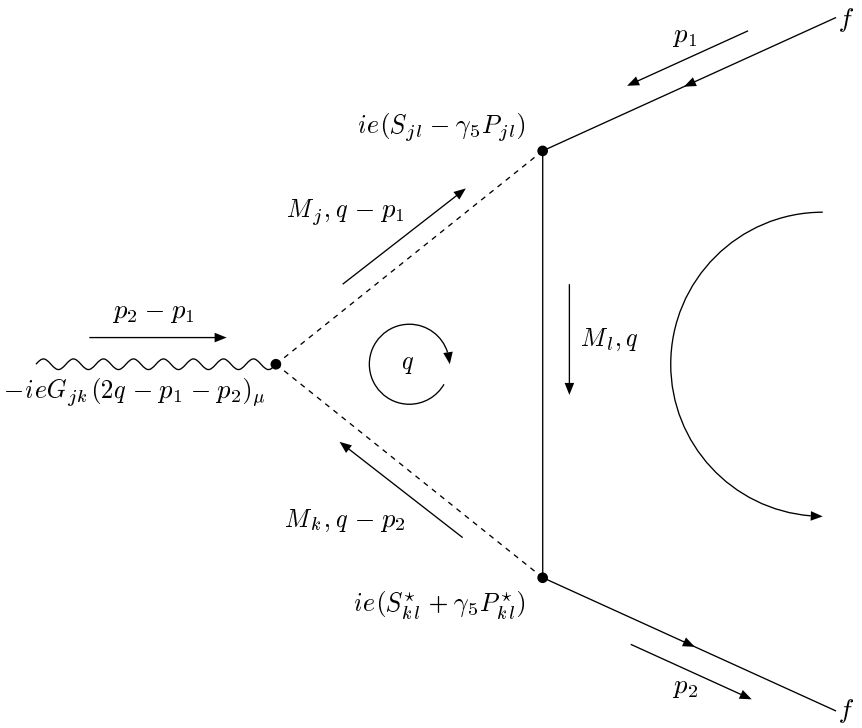

Figure B.3: Diagram for type A contributions with specified vertices and complete momentum configuration. The clockwise running loop momentum is labeled by q. Arrows on solid lines indicate the fermion flow, the circled arrow on the right refers to the flow of fermion number. The momentum flow is indicated by the smaller, solid arrows close to the particle lines.

the nominator of the integrand in $(F_A)_{jlk}$ reduces to

$$\left[\not{q}\left(A^1_{jlk} - \gamma_5 A^2_{jlk}\right)(2q - p_1 - p_2)_\mu + M_l\left(A^3_{jlk} + \gamma_5 A^4_{jlk}\right)(2q - p_1 - p_2)_\mu\right]. \tag{B.4}$$

The next step is to eliminate the q-integration formally by rewriting the Feynman amplitude $(F_A)_{jlk}$ in terms of tensor integrals. Using the conventions for the three-point functions in the orthogonal decomposition as specified in App. B.2.3, $(F_A)_{jlk}$ may be rewritten as

$$\begin{aligned}(F_A)_{jlk} = \frac{ie^3}{16\pi^2}\overline{u}_{p_2}\Big\{&\gamma^\alpha\left[2C_{\alpha\mu} - (p_1+p_2)_\mu C_\alpha\right]_{ljk}\left(A^1_{jlk} - \gamma_5 A^2_{jlk}\right)\\ &+ M_l\left[2C_\mu - (p_1+p_2)_\mu C_0\right]_{ljk}\left(A^3_{jlk} + \gamma_5 A^4_{jlk}\right)\Big\}u_{p_1}.\end{aligned} \tag{B.5}$$

The notation $\left[C_{\{0,\mu,\mu\nu\}}\right]_{ljk}$ denotes the argument of the tensor integrals $\left[C_{\{0,\mu,\mu\nu\}}\right]_{ljk} = C_{\{0,\mu,\mu\nu\}}(p_1, p_2, M_l, M_j, M_k)$. At this stage of the calculation the explicit use of the orthogonal decomposition for the tensor integrals $C_{\alpha\mu}$ and C_μ as given in Eqs. B.36 of App. B.2.3 is convenient. The advantage of this decomposition consists in the appearance of $p_{-\mu} \equiv (p_2 - p_1)_\mu$ corresponding to the vector boson momentum. Anticipating the vector boson on-shell condition $p_{-\mu}\epsilon^\mu = 0$ all terms proportional to $p_{-\mu}$ can be dropped

immediately. Furthermore terms proportional to $g_{\alpha\mu}$ only lead to corrections of V_f^V and A_f^V. Hence the relevant parts of the tensor integrals are

$$\gamma^\alpha C_{\alpha\mu}|_{\text{rel.}} = \not{p}_+ p_{+\mu} C_2^{++} - \not{p}_- p_{+\mu} C_2^{+-}, \tag{B.6a}$$

$$\gamma^\alpha C_\alpha|_{\text{rel.}} = \not{p}_+ C_1^+ - \not{p}_- C_1^-, \tag{B.6b}$$

$$C_\mu|_{\text{rel.}} = p_{+\mu} C_1^+. \tag{B.6c}$$

The contracted combinations $\not{p}_\pm$ of external fermion momenta are eliminated with use of the fermion on-shell conditions as given in Eq. B.58

$$\overline{u}_{p_2} \not{p}_+ (A + B\gamma_5) u_{p_1} = \overline{u}_{p_2} 2mA u_{p_1}, \tag{B.7a}$$

$$\overline{u}_{p_2} \not{p}_- (A + B\gamma_5) u_{p_1} = \overline{u}_{p_2} 2m\gamma_5 B u_{p_1}. \tag{B.7b}$$

Employing all these simplifications and manipulations the relevant part of the Feynman amplitude $(F_A)_{jlk}$ reads as

$$\begin{aligned}(F_A)_{jlk}\Big|_{\text{rel.}} = ie\frac{\alpha}{4\pi}\overline{u}_{p_2} p_{+\mu} \Big\{ &\left[2m_f (2C_2^{++} - C_1^+)_{ljk} A^1_{jlk} + M_l (2C_1^+ - C_0)_{ljk} A^3_{jlk}\right] \\ &+ \left[2m_f (2C_2^{+-} - C_1^-)_{ljk} A^2_{jlk} + M_l (2C_1^+ - C_0)_{ljk} A^4_{jlk}\right] \gamma_5 \Big\} u_{p_1}.\end{aligned} \tag{B.8}$$

Finally the momentum $p_{+\mu} = (p_1 + p_2)_\mu$ is eliminated via the Gordon identities in App. B.3. By comparing $(F_A)_{jlk}$ with the effective Vff vertex in Eq. 3.3 the contributions arising from type A diagrams to the form factors $a_f^V(s)$ and $d_f^V(s)$ are given by

$$\left(\frac{a_f^V}{2m_f}\right)_{A,jlk} = \frac{-\alpha}{4\pi}\left[2m_f \left(2C_2^{++} - C_1^+\right)_{ljk} A^1_{jlk} + M_l \left(2C_1^+ - C_0\right)_{ljk} A^3_{jlk}\right] \tag{B.9a}$$

$$\left(\frac{d_f^V}{e}\right)_{A,jlk} = \frac{i\alpha}{4\pi}\left[2m_f \left(2C_2^{+-} - C_1^-\right)_{ljk} A^2_{jlk} + M_l \left(2C_1^+ - C_0\right)_{ljk} A^4_{jlk}\right] \tag{B.9b}$$

To obtain the final result one has to sum over all particles that can be present in the loop diagram of type A

$$\left(\frac{a_f^V}{2m_f}\right)_A = \sum_{j,k,l}\left(\frac{a_f^V}{2m_f}\right)_{A,jlk}, \qquad \left(\frac{d_f^V}{e}\right)_A = \sum_{j,k,l}\left(\frac{d_f^V}{e}\right)_{A,jlk}. \tag{B.10}$$

Employing the symmetry properties of A^i_{jlk} (see Eq. B.3) and of the loop functions (see App. B.2.3) under the exchange $j \leftrightarrow k$ simplifies the summation; in terms of initial couplings S, P, and G the two form factors read

$$\begin{aligned}\left(\frac{a_f^V}{2m_f}\right)_A = \frac{-\alpha}{4\pi}\Bigg\{ &2m_f \sum_{j,k,l} (2C_2^{++} - C_1^+)_{ljk} \mathcal{R}\text{e}\left[G_{jk}\left(S_{jl}S^\star_{kl} + P_{jl}P^\star_{kl}\right)\right] \\ &+ \sum_{j,k,l} M_l (2C_1^+ - C_0)_{ljk} \mathcal{R}\text{e}\left[G_{jk}\left(S_{jl}S^\star_{kl} - P_{jl}P^\star_{kl}\right)\right]\Bigg\},\end{aligned} \tag{B.11a}$$

$$\left(\frac{d_f^V}{e}\right)_A = \frac{-\alpha}{4\pi}\Bigg\{2m_f \sum_{j,k,l} (2C_2^{+-} - C_1^-)_{ljk} \mathcal{I}\text{m}\left[G_{jk}\left(S_{jl}P^\star_{kl} + P_{jl}S^\star_{kl}\right)\right]$$

$$+ \sum_{j,k,l} M_l (2C_1^+ - C_0)_{ljk} \mathcal{I}\mathrm{m}\left[G_{jk}\left(S_{jl} P_{kl}^\star - P_{jl} S_{kl}^\star\right)\right] \Bigg\} . \qquad \text{(B.11b)}$$

After including an additional minus sign[1] for C_1^- and C_2^{+-} these results agree with [54].

B.1.3 Calculation of diagram type B (chargino)

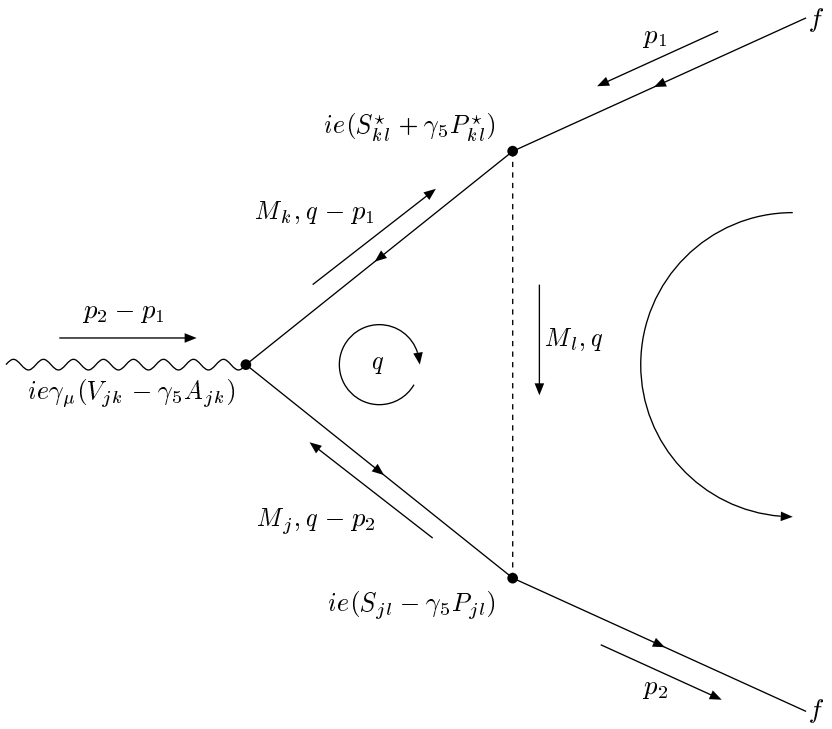

Figure B.4: Diagram for type B contributions with specified vertices and complete momentum configuration. The clockwise running loop momentum is labeled by q. Arrows on solid lines indicate the fermion flow, the circled arrow on the right refers to the flow of fermion number. The momentum flow is indicated by the smaller, solid arrows close to the particle lines.

The complete diagram of type B contributions is shown in Fig. B.4, including the precise vertices and the complete momentum configuration. Using standard propagators for the exchanged fermions j, k and the exchanged scalar l the one-loop contribution $(F_B)_{jlk}$ from diagrams of type B to the invariant Feynman amplitude reads as

$$(F_B)_{jlk} = -e^3 \overline{u}_{p_2} \mu^{4-D} \int \frac{d^D q}{(2\pi)^D} \qquad \text{(B.12)}$$
$$\times \left\{ \frac{\left(S_{jl} - \gamma_5 P_{jl}\right)\left(\not{q} - \not{p}_2 - M_j\right)\gamma_\mu \left(V_{jk} - \gamma_5 A_{jk}\right)\left(\not{q} - \not{p}_1 - M_k\right)\left(S_{kl}^\star + \gamma_5 P_{kl}^\star\right)}{\left[q^2 - M_l^2 + i\epsilon\right]\left[(q-p_1)^2 - M_j^2 + i\epsilon\right]\left[(q-p_2)^2 - M_k^2 + i\epsilon\right]} \right\} u_{p_1}.$$

[1] This is due to the slightly differing ordering of arguments in $[C_{0,\mu,\mu\nu}]_{ljk} = C_{0,\mu,\mu\nu}\,(p_1, p_2, M_l, M_j, M_k)$ compared with $[C_{0,\mu,\mu\nu}]_{kjl} = C_{0,\mu,\mu\nu}\,(p_1, p_2, M_l, M_k, M_j)$ in [54].

First of all, for the further calculation it is worth to notice that the term proportional to the product of the fermion masses $M_k M_l$ has the Lorentz structure $\gamma_\mu(A + B\gamma_5)$, and hence only contributes to the form factors A_f^V and V_f^V. Thus this term can be dropped immediately as we are only interested in the form factors a_f^V and d_f^V. The chiral structure of $(F_B)_{jkl}$ can be simplified, by introducing six effective vertex factors B^i_{jlk} as

$$B^1_{jlk} = V_{jk}\left(S_{jl}S^\star_{kl} + P_{jl}P^\star_{kl}\right) + A_{jk}\left(S_{jl}P^\star_{kl} + P_{jl}S^\star_{kl}\right) = \left(B^1_{klj}\right)^\star, \tag{B.13a}$$

$$B^2_{jlk} = V_{jk}\left(S_{jl}P^\star_{kl} + P_{jl}S^\star_{kl}\right) + A_{jk}\left(S_{jl}S^\star_{kl} + P_{jl}P^\star_{kl}\right) = \left(B^2_{klj}\right)^\star, \tag{B.13b}$$

$$B^3_{jlk} = V_{jk}\left(S_{jl}S^\star_{kl} - P_{jl}P^\star_{kl}\right) + A_{jk}\left(S_{jl}P^\star_{kl} - P_{jl}S^\star_{kl}\right) = \left(B^5_{klj}\right)^\star, \tag{B.13c}$$

$$B^4_{jlk} = V_{jk}\left(S_{jl}P^\star_{kl} - P_{jl}S^\star_{kl}\right) + A_{jk}\left(S_{jl}S^\star_{kl} + P_{jl}P^\star_{kl}\right) = -\left(B^6_{klj}\right)^\star, \tag{B.13d}$$

$$B^5_{jlk} = V_{jk}\left(S_{jl}S^\star_{kl} - P_{jl}P^\star_{kl}\right) - A_{jk}\left(S_{jl}P^\star_{kl} - P_{jl}S^\star_{kl}\right) = \left(B^3_{klj}\right)^\star, \tag{B.13e}$$

$$B^6_{jlk} = V_{jk}\left(S_{jl}P^\star_{kl} + P_{jl}S^\star_{kl}\right) - A_{jk}\left(S_{jl}S^\star_{kl} - P_{jl}P^\star_{kl}\right) = -\left(B^4_{klj}\right)^\star, \tag{B.13f}$$

the nominator of the integrand in $(F_B)_{jkl}$ reduces to

$$(\not{q}\gamma_\mu\not{q} - \not{p}_2\gamma_\mu\not{q} - \not{q}\gamma_\mu\not{p}_1)\left(B^1_{jlk} + \gamma_5 B^2_{jlk}\right) - M_j\gamma_\mu\not{q}\left(B^3_{jlk} + \gamma_5 B^4_{jlk}\right) - M_k\not{q}\gamma_\mu\left(B^5_{jlk} + \gamma_5 B^6_{jlk}\right), \tag{B.14}$$

where all terms that are proportional either to $\not{p}_{1(2)}$ or to bilinears of these momenta have been dropped. The reason for this is that such terms further reduce to the Lorentz structure $\gamma_\mu(A + B\gamma_5)$ by the fermion on-shell conditions and hence only contribute to the form factors A_f^V and V_f^V. By formally performing the loop momentum integration one obtains[2]

$$\begin{aligned}(F_B)_{jlk} = \frac{-ie^3}{16\pi^2}\overline{u}_{p_2}\Big\{&\left[\gamma^\alpha\gamma_\mu\gamma^\beta C_{\alpha\beta} - \not{p}_2\gamma_\mu\gamma^\alpha C_\alpha - \gamma^\alpha\gamma_\mu\not{p}_1 C_\alpha\right]_{lkj}\left(B^1_{jlk} + \gamma_5 B^2_{jlk}\right) \\ &- M_j\gamma_\mu\gamma^\alpha\left[C_\alpha\right]_{lkj}\left(B^3_{jlk} + \gamma_5 B^4_{jlk}\right) - M_k\gamma^\alpha\gamma_\mu\left[C_\alpha\right]_{lkj}\left(B^5_{jlk} + \gamma_5 B^6_{jlk}\right)\Big\}u_{p_1}.\end{aligned} \tag{B.15}$$

Again the orthogonal decomposition of the tensor integrals is convenient. Employing this decomposition and standard manipulations of products of γ-matrices the relevant parts of the tensor integrals read as

$$\gamma^\alpha\gamma_\mu\gamma^\beta C_{\alpha\beta}\big|_{\text{rel.}} = 2\left[\not{p}_+ p_{+\mu} C_2^{++} + 2\left(p_{1\mu}\not{p}_1 - \not{p}_2 p_{2\mu}\right)C_2^{+-}\right], \tag{B.16a}$$

$$\gamma_\mu\gamma^\alpha C_\alpha\big|_{\text{rel.}} = 2p_{2\mu}\left(C_1^+ - C_1^-\right), \tag{B.16b}$$

$$\gamma^\alpha\gamma_\mu C_\alpha\big|_{\text{rel.}} = 2p_{1\mu}\left(C_1^+ + C_1^-\right). \tag{B.16c}$$

All terms that either contribute only to A_f^V and V_f^V, i.e. terms proportional to $\gamma_\mu\not{p}_i$ and $\gamma_\mu\not{p}_i\not{p}_j$, or vanish by imposing the vector boson on-shell condition, i.e. terms proportional to $p_{-\mu}$, have been dropped immediately. The relevant part of the contribution $(F_B)_{jlk}$ is then given as

$$(F_B)_{jlk}\Big|_{\text{rel.}} = -2\frac{ie\alpha}{4\pi}\overline{u}_{p_2}\left\{\left[\not{p}_+ p_{+\mu} C_2^{++} + 2\left(p_{1\mu}\not{p}_1 - \not{p}_2 p_{2\mu}\right)C_2^{+-}\right.\right.$$

[2]Note that compared to the calculation of diagram type A the masses have been arranged differently. Therefore the loop functions $\left[C_{\{0,\mu,\mu\nu\}}\right]_{lkj}$ are identical to $\left[C_{\{0,\mu,\mu\nu\}}\right]_{kjl}$ in [54].

$$
\begin{aligned}
&- p_{2\mu}\not{p}_2 \left(C_1^+ - C_1^-\right) - p_{1\mu}\not{p}_1 \left(C_1^+ + C_1^-\right)\big]_{lkj} \left[B^1_{jlk} + \gamma_5 B^2_{jlk}\right] \\
&- M_j p_{2\mu} \left(C_1^+ - C_1^-\right)_{lkj} \left[B^3_{jlk} + \gamma_5 B^4_{jlk}\right] \\
&- M_k p_{1\mu} \left(C_1^+ + C_1^-\right)_{lkj} \left[B^5_{jlk} + \gamma_5 B^6_{jlk}\right] \Big\} u_{p_1}. \qquad \text{(B.17)}
\end{aligned}
$$

Using the fermion on-shell condition and $2p^\mu_{1,2} = p^\mu_+ \mp p^\mu_-$ together with the vector boson on shell-condition further simplifies the relevant part of the amplitude $(F_B)_{jlk}$

$$
\begin{aligned}
(F_B)_{jlk}\Big|_{\text{rel}} = -\frac{ie\alpha}{4\pi}\overline{u}_{p_2} p\!\!\!/_{+\mu} \Big\{ & 2m_f \left[2C_2^{++} - C_1^+\right]_{lkj} B^1_{jlk} - 2m_f\gamma_5 \left[2C_2^{+-} - C_1^-\right] B^2_{jlk} \\
& - M_j \left[C_1^+ - C_1^-\right]_{lkj} \left[B^3_{jlk} + \gamma_5 B^4_{jlk}\right] \\
& - M_k \left[C_1^+ + C_1^-\right]_{lkj} \left[B^5_{jlk} + \gamma_5 B^6_{jlk}\right] \Big\} u_{p_1}. \qquad \text{(B.18)}
\end{aligned}
$$

Using the Gordon identities from App. B.3 to eliminate $p_{+\mu}$ and comparing with Eq. 3.3 reveals the contributions from type B diagrams to the form factors $a_f^V(s)$ and $d_f^V(s)$ as

$$
\begin{aligned}
\left(\frac{a_f^V}{2m_f}\right)_{B,jlk} = \frac{\alpha}{4\pi} \Big\{ & 2m_f \left[2C_2^{++} - C_1^+\right]_{lkj} B^1_{jlk} \\
& - M_j \left[C_1^+ - C_1^-\right]_{lkj} B^3_{jlk} - M_k \left[C_1^+ + C_1^-\right]_{lkj} B^5_{jlk} \Big\} \qquad \text{(B.19a)} \\
\left(\frac{d_f}{e}\right)_{B,jlk} = i\frac{\alpha}{4\pi} \Big\{ & 2m_f \left[2C_2^{+-} - C_1^-\right]_{lkj} B^2_{jlk} \\
& + M_j \left[C_1^+ - C_1^-\right]_{lkj} B^4_{jlk} + M_k \left[C_1^+ + C_1^-\right]_{lkj} B^6_{jlk} \Big\}. \qquad \text{(B.19b)}
\end{aligned}
$$

As illustrated in Eq. B.10 one finally has to sum over all particles that can be present in the loop diagram of type B. Employing the symmetry properties of B^i_{jlk} (see Eq. B.13) and of the loop functions (see App. B.2.3) under the exchange $j \leftrightarrow k$ simplifies the summation, in terms of initial couplings S, P, V, and A the two form factors read

$$
\begin{aligned}
\left(\frac{a_f^V}{2m_f}\right)_B = \frac{\alpha}{4\pi} \sum_{j,k,l} \Big\{ & 2m_f \left[C_2^{++} - C_1^+\right]_{lkj} \mathcal{R}\mathrm{e}\left[V_{jk}\left(S_{jl}S^\star_{kl} + P_{jl}P^\star_{kl}\right) + A_{jk}\left(S_{jl}P^\star_{kl} + P_{jl}S^\star_{kl}\right)\right] \\
& - 2M_k \left[C_1^+ + C_1^-\right]_{lkj} \mathcal{R}\mathrm{e}\left[V_{jk}\left(S_{jl}S^\star_{kl} - P_{jl}P^\star_{kl}\right) - A_{jk}\left(S_{jl}P^\star_{kl} - P_{jl}S^\star_{kl}\right)\right] \Big\} \qquad \text{(B.20a)} \\
\left(\frac{d_e}{e}\right)_B = -\frac{\alpha}{4\pi} \sum_{j,k,l} \Big\{ & 2m_f \left[C_2^{+-} - C_1^-\right]_{lkj} \mathcal{I}\mathrm{m}\left[V_{jk}\left(S_{jl}P^\star_{kl} + P_{jl}s^\star_{kl}\right) + A_{jk}\left(S_{jl}S^\star_{kl} + P_{jl}P^\star_{kl}\right)\right] \\
& - 2M_k \left[C_1^+ + C_1^-\right]_{lkj} \mathcal{I}\mathrm{m}\left[V_{jk}\left(P_{jl}S^\star_{kl} - S_{jl}P^\star_{kl}\right) + A_{jk}\left(S_{jl}S^\star_{kl} - P_{jl}P^\star_{kl}\right)\right] \Big\} \qquad \text{(B.20b)}
\end{aligned}
$$

Again these results agree with [54].

B.1.4 Final results

The first step to obtain the final results for $d_e^\gamma(0)$ and $a_\mu^\gamma(0)$ is to specify the vector boson as photon, in which case the couplings between the vector boson and the two scalars, respectively two fermions simplify to

$$G_{jk} = \delta_{jk}, \quad V_{jk} = \delta_{jk}, \quad A_{jk} = 0. \tag{B.21}$$

Secondly, the generic scalar and pseudoscalar coupling S and P may be expressed in terms of chiral couplings L and R,

$$S_{ij} = \frac{L_{ij} + R_{ij}}{2}, \quad P_{ij} = \frac{L_{ij} - R_{ij}}{2}, \tag{B.22}$$

which implies for bilinears of S and P

$$|S_{ij}|^2 + |P_{ij}|^2 = \frac{1}{2}\left(|L_{ij}|^2 + |R_{ij}|^2\right), \tag{B.23a}$$

$$|S_{ij}|^2 - |P_{ij}|^2 = \mathcal{R}\mathrm{e}\left[L_{ij}R_{ij}^\star\right], \tag{B.23b}$$

$$S_{ij}P_{ij}^\star - P_{ij}S_{ij}^\star = i\mathcal{I}\mathrm{m}\left[L_{ij}^\star R_{ij}\right]. \tag{B.23c}$$

Hence the contributions to $a_f^\gamma(s)$ and $d_f^\gamma(s)$ from type A and type B diagrams in terms of chiral couplings ($L(R)_{ij,A} \neq L(R)_{ij,B}$) read

$$\left(\frac{a_f^\gamma}{2m_f}\right)_A = -\frac{\alpha}{4\pi}\sum_{jl}\Big\{m_f\left[|L_{jl,A}|^2 + |R_{jl,A}|^2\right]\left[2C_2^{++} - C_1^+\right]_{ljj} + M_l\mathcal{R}\mathrm{e}\left[L_{jl,A}R_{jl,A}^\star\right]\left[2C_1^+ - C_0\right]_{ljj}\Big\}, \tag{B.24a}$$

$$\left(\frac{a_f^\gamma}{2m_f}\right)_B = \frac{\alpha}{4\pi}\sum_{jl}\Big\{m_f\left[|L_{jl,B}|^2 + |R_{jl,B}|^2\right]\left[2C_2^{++} - C_1^+\right]_{ljj} - 2M_j\mathcal{R}\mathrm{e}\left[L_{jl,B}R_{jl,B}^\star\right]\left[2C_1^+\right]_{ljj}\Big\}, \tag{B.24b}$$

$$\left(\frac{d_e^\gamma}{e}\right)_A = -\frac{\alpha}{4\pi}\sum_{jl}M_l\mathcal{I}\mathrm{m}\left[L_{jl,A}^\star R_{jl,A}\right]\left[2C_1^+ - C_0\right]_{ljj}, \tag{B.24c}$$

$$\left(\frac{d_e^\gamma}{e}\right)_B = -\frac{\alpha}{4\pi}\sum_{jl}M_l\mathcal{I}\mathrm{m}\left[L_{jl,B}^\star R_{jl,B}\right]\left[2C_1^+\right]_{ljj}. \tag{B.24d}$$

Note that $k = j$ as enforced by the photon vertices is used here, this eliminates contributions proportional to C_1^- and C_2^{+-}. By identifying the couplings $L_{ij,A}$ and $R_{ij,A}$ with those in Eqs. 3.16c and 3.16d, respectively $L_{ij,B}$ and $R_{ij,B}$ with those in Eqs. 3.16a and 3.16b via

$$L_{ij,A} = \frac{n_{Lj\alpha}}{e}, \quad R_{ij,A} = \frac{n_{Rj\alpha}}{e}, \tag{B.25a}$$

$$L_{ij,B} = \frac{c_{Lj}\delta_{l\tilde{\nu}}}{e}, \quad R_{ij,B} = \frac{c_{Rj}\delta_{l\tilde{\nu}}}{e}, \tag{B.25b}$$

and using the expansions of the appearing combinations for loop functions in external momenta from App. B.2.6 the final result for the neutralino and chargino loop contributions to $a_f \equiv a_f^\gamma(0)$ and $d_f \equiv d_f^\gamma(0)$ are found to be

$$a_f^{\tilde{\chi}^0} = \frac{-1}{192\pi^2} \sum_{i,\alpha} \left\{ \frac{m_f^2}{M_\alpha^2} f_3\left(z_{\alpha i}\right) \left[|n_{L,i\alpha}|^2 + |n_{R,i\alpha}|^2 \right] + \frac{4m_f}{M_i} f_2\left(z_{\alpha i}\right) \mathcal{R}\mathrm{e}\left[n_{L,i\alpha}^\star n_{R,i\alpha} \right] \right\}, \tag{B.26a}$$

$$d_f^{\tilde{\chi}^0} = \frac{-e}{96\pi^2} \sum_{i,\alpha} \left\{ \frac{1}{M_i} f_2\left(z_{\alpha i}\right) \mathcal{I}\mathrm{m}\left[n_{L,i\alpha}^\star n_{R,i\alpha} \right] \right\}, \tag{B.26b}$$

$$a_f^{\tilde{\chi}^\pm} = \frac{1}{192\pi^2} \sum_{i} \left\{ \frac{m_f^2}{M_i^2} f_3\left(z_i\right) \left[|c_{Li}|^2 + |c_{Ri}|^2 \right] + 8 \frac{m_f}{M_i} f_1\left(z_i\right) \mathcal{R}\mathrm{e}\left[c_{Li}^\star c_{Ri} \right] \right\}, \tag{B.26c}$$

$$d_f^{\tilde{\chi}^\pm} = \frac{e}{96\pi^2} \sum_{i} \left\{ \frac{2}{M_i} f_1\left(z_i\right) \mathcal{I}\mathrm{m}\left[c_{Li}^\star c_{Ri} \right] \right\}. \tag{B.26d}$$

Setting $i = 1, \ldots 4$; $\alpha = L, R$; and $z_{\alpha i} = M_\alpha^2 / M_i^2$ for the neutralino contribution and $i = 1, 2$ with $z_i = M_i^2 / M_{\tilde{\nu}}^2$ for the chargino contribution as well as $f \equiv e$ or $f \equiv \mu$ the results in Eqs. B.26 reproduce the results for both SUSY contributions to d_e and a_μ as given in Sec. 3.2.1.

B.2 Relevant loop functions

To make this thesis self-contained the relevant loop functions and their most important features are briefly presented here. N-point functions which are not appearing during the calculation of the form factors a_f^V and d_f^V are not discussed here.

B.2.1 Introducing scalar and tensor integrals

For the calculation of the leptonic dipole moments it is necessary to calculate scalar and tensor three-point functions $C_{\{0,\mu,\mu\nu\}}$. In general these three-point functions are associated with the diagrammatical structure and configuration of momenta as shown in Fig. B.5.
In the covariant, standard decomposition the three-point functions are usually defined as [139]

$$C_{\{0,\mu,\mu\nu\}} = \frac{16\pi^2}{i} \mu^{4-D} \int \frac{d^D l}{(2\pi)^D} \frac{\{1, l_\mu, l_\mu l_\nu\}}{\left[(l+p_1)^2 - M_1^2 + i\epsilon\right] \left[(l+p_2)^2 - M_2^2 + i\epsilon\right] \left[l^2 - M_0^2 + i\epsilon\right]}, \tag{B.27}$$

where μ is a parameter of mass dimension and serves to keep the dimension of the integrals fixed for varying dimension D [139]. The reason for calculating these integrals in D dimensions is the fact that integrals that are divergent in four dimensions converge for $D \neq 4$ dimensions. By going to D dimensions these UV divergencies are regularized and correspond to singularities in $(D-4)$. More details on this dimensional regularization may be found in [70, 71, 139]. The infinitesimal imaginary parts $i\epsilon$ are needed to regulate singularities of the integrand in Eq. B.27 [139]. After integration they determine the correct imaginary parts of logarithms and dilogarithms, furthermore the correct choices ensure

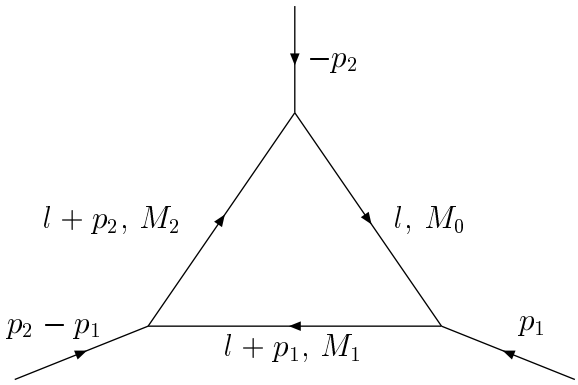

Figure B.5: General configuration for momenta and masses as used for the standard definition of three-point functions. The flow of momentum is indicated by arrows.

causality [139].
Later onwards the tensor three-point functions $C_{\mu,\mu\nu}$ are reduced to one- and two-point functions, these are introduced as

$$A_0 = \frac{16\pi^2}{i}\mu^{4-D}\int \frac{d^D l}{(2\pi)^D}\frac{1}{[l^2 - M_0^2 + i\epsilon]}, \tag{B.28a}$$

$$B_{\{0,\mu\}} = \frac{16\pi^2}{i}\mu^{4-D}\int \frac{d^D l}{(2\pi)^D}\frac{\{1, l_\mu\}}{[(l+p_1)^2 - M_1^2 + i\epsilon]\,[l^2 - M_0^2 + i\epsilon]}. \tag{B.28b}$$

The arguments of the tensor integrals A_0, $B_{\{0,\mu\}}$, and $C_{\{0,\mu,\mu\nu\}}$ consist of independent external momenta and the internal masses, i.e.

$$A_0 = A_0\left(M_0\right), \tag{B.29a}$$

$$B_{\{0,\mu\}} = B_{\{0,\mu\}}\left(p_1, M_0, M_1\right), \tag{B.29b}$$

$$C_{\{0,\mu,\mu\nu\}} = C_{\{0,\mu,\mu\nu\}}\left(p_1, p_2, M_0, M_1, M_2\right). \tag{B.29c}$$

The N-point functions A_0, $B_{\{0,\mu\}}$, and $C_{\{0,\mu,\mu\nu\}}$ are the only ones that appear during the calculation of the form factors a_f^V and d_f^V.

B.2.2 Reduction of tensor integrals

In the "standard" decomposition the tensor integrals are expanded into symmetric Lorentz-structures constructed from the available, external momenta $p_{i\mu}$ and the metric tensor $g_{\mu\nu}$, i.e. [139]

$$B_\mu = p_{1\mu} B_1, \tag{B.30a}$$

$$C_\mu = p_{1\mu} C_1 + p_{2\mu} C_2, \tag{B.30b}$$

$$C_{\mu\nu} = p_{1\mu}p_{1\nu}C_{11} + p_{2\mu}p_{2\nu}C_{22} + p_{2\mu}p_{1\nu}C_{21} + p_{1\mu}p_{2\nu}C_{12} + g_{\mu\nu}C_{00}. \tag{B.30c}$$

By contracting with external momenta p_i^μ and/or the metric tensor $g^{\mu\nu}$ the tensor integrals decomposed in Eq. B.30 are reduced to tensor integrals with less powers of the internal momentum l_μ in the nominator and/or less propagator factors in the nominator. Following

the general method described by [139] one finds for the two-point function B_μ and the three-point functions $C_{\{\mu,\mu\nu\}}$ after some tedious calculations

$$B_1 = \frac{1}{2p_1^2}\left[A_0(M_0) - A_0(M_1) - f_1 B_0(p_1, M_0, M_1)\right], \tag{B.31a}$$

$$\begin{pmatrix} C_1 \\ C_2 \end{pmatrix} = \frac{1}{2\left[p_1^2 p_2^2 - (p_1 p_2)^2\right]} \begin{pmatrix} p_2^2 & -p_1 p_2 \\ -p_1 p_2 & p_1^2 \end{pmatrix} \begin{pmatrix} R^1 \\ R^2 \end{pmatrix} \tag{B.31b}$$

$$\begin{pmatrix} C_{11} & C_{21} \\ C_{12} & C_{22} \end{pmatrix} = \frac{1}{2\left[p_1^2 p_2^2 - (p_1 p_2)^2\right]} \begin{pmatrix} p_2^2 & -p_1 p_2 \\ -p_1 p_2 & p_1^2 \end{pmatrix} \begin{pmatrix} R_1^1 - 2C_{00} & R_2^1 \\ R_1^2 & R_2^2 - 2C_{00} \end{pmatrix}. \tag{B.31c}$$

The coefficients R_i and R_i^j are given as

$$R^1 = B_0(p_2, M_0, M_2) - B_0(p_{21}, M_1, M_2) - f_1 C_0, \tag{B.32a}$$

$$R^2 = B_0(p_1, M_0, M_1) - B_0(p_{21}, M_1, M_2) - f_2 C_0, \tag{B.32b}$$

$$R_1^1 = -f_1 C_1 - B_1(p_{12}, M_2, M_1), \tag{B.32c}$$

$$R_2^1 = -f_1 C_2 + B_1(p_{12}, M_2, M_1) + B_0(p_{12}, M_2, M_1) - B_1(p_2, M_0, M_2), \tag{B.32d}$$

$$R_1^2 = B_1(p_1, M_0, M_1) - B_1(p_{12}, M_2, M_1) - f_2 C_1, \tag{B.32e}$$

$$R_2^2 = -f_2 C_2 + B_0(p_{12}, M_2, M_1) + B_1(p_{12}, M_2, M_1), \tag{B.32f}$$

where $f_i = p_i^2 - M_i^2 + M_0^2$ and $p_{12} = -p_{21} = p_1 - p_2$ were introduced. Moreover, the argument $(p_1, p_2, M_0, M_1, M_2)$ of $C_{\{0,1,2\}}$ has been dropped. The coefficient C_{00} has to be calculated separately, one finds

$$C_{00} = \frac{1}{2}\frac{1}{D-2}\left[2M_0^2 C_0 + f_1 C_1 + f_2 C_2 + B_0(p_{12}, M_2, M_1)\right].$$

By restricting to singularities in $(D-4)$ and non-vanishing parts for $D \to 4$, this simplifies to

$$C_{00} = \frac{1}{4}\left[B_0(p_{12}, M_2, M_1) + f_1 C_1 + f_2 C_2 + 2M_0^2 C_0 + 1\right] + \mathcal{O}(D-4). \tag{B.33}$$

The determinant present in Eqs. B.31b and B.31c

$$p_1^2 p_2^2 - (p_1 p_2)^2 = \frac{1}{2}\left[(p_1^2 - p_1 p_2)(p_2^2 + p_1 p_2) + (p_1^2 + p_1 p_2)(p_2^2 - p_1 p_2)\right], \tag{B.34}$$

indicates that the reduction formula for C_μ and $C_{\mu\nu}$ become singular if the moment are collinear, i.e. $p_1 = \pm p_2$. As this collinearity is implied by the limit $s \to 0$ of vanishing vector boson momentum, this limit causes a priori some worries. However, closer inspection of the combinations of the relevant loop functions during the calculations of App. B.2.5 reveals that in the case of d_f^γ and a_f^γ additional factors $p_1^2 - p_1 p_2$ and $p_2^2 - p_1 p_2$ arise in these relevant combinations of loop functions. These factors cancel with the collinear singularities from Eq. B.34.

B.2.3 Orthogonal decomposition and symmetries

An alternative way to describe the Lorentz structure of tensor integrals is used by [54], here the general three-point functions are given as

$$C_{\{0,\mu,\mu\nu\}} = \frac{16\pi^2}{i}\mu^{4-D}\int \frac{d^D l}{(2\pi)^D}\frac{\{1, l_\mu, l_\mu l_\nu\}}{[(l-p_1)^2 - M_1 + i\epsilon]\,[(l-p_2)^2 - M_2^2 + i\epsilon]\,[l^2 - M_0^2 + i\epsilon]}, \tag{B.35}$$

i.e. the loop momentum l_μ is assigned opposite[3] to Eq. B.27. Instead of the covariant decomposition in Eq. B.30 the three-point functions are decomposed using the combinations $p_{\pm\mu} = (p_1 \pm p_2)_\mu$ as follows

$$C_\mu = p_{+\mu} C_1^+ + p_{-\mu} C_1^-, \tag{B.36a}$$

$$C_{\mu\nu} = p_{+\mu}p_{+\nu} C_2^{++} + p_{-\mu}p_{-\nu} C_2^{--} + (p_{+\mu}p_{-\nu} + p_{-\mu}p_{+\nu})\, C_2^{+-} + g_{\mu\nu} C_2^{00}. \tag{B.36b}$$

Using the basic relation between orthogonally decomposed and covariantly decomposed three-point functions

$$C^{\text{ortho.}}_{\{0,\mu,\mu\nu\}}\big|_{l_\mu \to -l_\mu} = C^{\text{cova.}}_{\{0,\mu,\mu\nu\}}, \tag{B.37}$$

one finds by expanding the linears and bilinears of $p_{\pm\mu}$ the following relations between the coefficients $C_{i(j)}$ of the covariant decomposition and the coefficients $C_i^{\alpha(\beta)}$ of the orthogonal decomposition

$$C_1^+ = -\frac{1}{2}(C_1 + C_2), \tag{B.38a}$$

$$C_1^- = -\frac{1}{2}(C_1 - C_2), \tag{B.38b}$$

$$C_2^{++} = \frac{1}{4}(C_{11} + C_{22} + C_{12} + C_{21}), \tag{B.38c}$$

$$C_2^{--} = \frac{1}{4}(C_{11} + C_{22} - C_{12} - C_{21}), \tag{B.38d}$$

$$C_2^{+-} = \frac{1}{4}(C_{11} - C_{22}), \tag{B.38e}$$

$$C_2^{00} = C_{00}. \tag{B.38f}$$

Noticing the invariance of the three-point functions under the simultaneous exchange $p_1 \leftrightarrow p_2$ and $M_1 \leftrightarrow M_2$, the following properties of the coefficients $C_i^{\alpha(\beta)}$ under this exchange are evident

$$C_0(p_1, p_2, M_0, M_1, M_2) = C_0(p_2, p_1, M_0, M_2, M_1), \tag{B.39a}$$

$$C_1^\alpha(p_1, p_2, M_0, M_1, M_2) = \alpha C_1^\alpha(p_2, p_1, M_0, M_2, M_1), \tag{B.39b}$$

$$C_2^{\alpha\beta}(p_1, p_2, M_0, M_1, M_2) = \alpha\beta C_2^{\alpha\beta}(p_2, p_1, M_0, M_2, M_1), \tag{B.39c}$$

$$C_2^{00}(p_1, p_2, M_0, M_1, M_2) = C_2^{00}(p_2, p_1, M_0, M_2, M_1). \tag{B.39d}$$

The dependence of the loop functions on the external momenta is exclusively given by the three Lorentz scalars p_1^2, p_2^2, and $p_1 p_2$. Moreover, considering two equal mass on-shell

[3] This assignment is in particular relevant for C_μ.

fermions, the Lorentz scalars $p_1^2 \equiv p_2^2 \equiv m_f^2$ and $p_1 p_2$ are invariant under the exchange of the external momenta. Hence the simultaneous exchange $p_1 \leftrightarrow p_2$ and $M_1 \leftrightarrow M_2$ is equivalent to the single exchange $M_1 \leftrightarrow M_2$ in this case. Using the short-handed notation $C_{\{0,\mu,\mu\nu\}}(p_1, p_2, M_l, M_j, M_k) = \left[C_{\{0,\mu,\mu\nu\}}\right]_{ljk}$ Eqs. B.39 reduce to

$$\left[C_0\right]_{ljk} = \left[C_0\right]_{lkj}, \tag{B.40a}$$

$$\left[C_1^\alpha\right]_{ljk} = \alpha \left[C_1^\alpha\right]_{lkj}, \tag{B.40b}$$

$$\left[C_2^{\alpha\beta}\right]_{ljk} = \alpha\beta \left[C_2^{\alpha\beta}\right]_{lkj}, \tag{B.40c}$$

$$\left[C_2^{00}\right]_{ljk} = \left[C_2^{00}\right]_{lkj}. \tag{B.40d}$$

Trivially, this implies

$$\left[C_1^-\right]_{ljj} = \left[C_2^{+-}\right]_{ljj} = 0, \tag{B.41}$$

if $p_1^2 = p_2^2 = m_f^2$.

B.2.4 Scalar integrals

Only the scalar integrals $A_0(M_0)$, $B_0(p_1, M_0, M_1)$, and $C_0(p_1, p_2, M_0, M_1, M_2)$ have to be calculated explicitly, all other tensor integrals can be reduced to those three scalar integrals. Following standard text books [70, 71, 140] one finds

$$A_0(M_0) = M_0^2 \left[\Delta - \log\left(\frac{M_0^2}{\mu^2}\right) + 1\right] + \mathcal{O}(D-4), \tag{B.42a}$$

$$B_0(p_1, M_0, M_1) = \Delta - \int_0^1 dx \log\left[\frac{x p_1^2 - x(p_1^2 - M_1^2 + M_0^2) + M_0^2 - i\epsilon}{\mu^2}\right] + \mathcal{O}(D-4), \tag{B.42b}$$

$$C_0(p_1, p_2, M_0, M_1, M_2) = -\int_0^1 dx \int_0^{1-x} dy \left\{\left[x^2 p_1^2 + y^2 p_2^2 + 2xy p_1 p_2 - x(p_1^2 - M_1^2 + M_0^2) - y(p_2^2 - M_2^2 + M_0^2) - M_0^2 + i\epsilon\right]^{-1}\right\}, \tag{B.42c}$$

where $\Delta = 1/(4-D) + \log 4\pi - \gamma_E$ and γ_E is the Euler constant. The variables x and y denote two Feynman parameters which were used to linearize the denominators of the integrands.[4] As the numerical factor $\log 4\pi - \gamma_E$ is absorbed in Δ these numerical factors cancel in a given combination of loop functions only if the singularities in $D-4$ cancel, i.e. when the considered combination is UV-finite. Moreover, note that C_0 is already UV-finite. For the purposes pursued here it is slightly more convenient to keep the Feynman parameters at this stage and to integrate them out after the appearing loop functions have been expanded in the external momenta.

B.2.5 Divergent parts of loop integrals and effective loop functions

As stated in Sec. 3.1 it is not possible within renormalizable theories to write down contributions to the form factors d_f^V and a_f^V at tree level, hence counterterms for d_f^V and a_f^V

[4] Using $\frac{1}{ab} = \int_0^1 dx \left[a(1-x) + bx\right]^{-2}$ and $\frac{1}{abc} = 2\int_0^1 dx \int_0^{1-x} dy \left[(c-a)y + (b-a)x + a\right]^{-3}$.

are forbidden. This implies that the singularities appearing in the combinations of loop functions contributing to d_f^V and A_f^V have to cancel among each other, i.e. these contributions have to be UV-finite. This postulate provides a stringent test for the consistency of the calculation performed within Apps. B.1.2 and B.1.3. The divergent parts of all loop functions discussed so far are

$$(D-4)A_0(M_0) = -2M_0^2 + \mathcal{O}(D-4), \tag{B.43a}$$

$$(D-4)B_0(p_1, M_0, M_1) = -2 + \mathcal{O}(D-4), \tag{B.43b}$$

$$(D-4)C_0(p_1, p_2, M_0, M_1, M_2) = \mathcal{O}(D-4), \tag{B.43c}$$

$$(D-4)B_1(p_1, M_0, M_1) = 1 + \mathcal{O}(D-4), \tag{B.43d}$$

$$(D-4)C_i(p_1, p_2, M_0, M_1, M_2) = \mathcal{O}(D-4) \quad \{i\} = \{1,2\}, \tag{B.43e}$$

$$(D-4)C_{ij}(p_1, p_2, M_0, M_1, M_2) = \mathcal{O}(D-4) \quad \{i,j\} = \{1,2\}, \tag{B.43f}$$

$$(D-4)C_{00}(p_1, p_2, M_0, M_1, M_2) = -\frac{1}{2} + \mathcal{O}(D-4). \tag{B.43g}$$

These divergent parts as far as shown here agree with [139].
Now the combinations of the orthogonal decomposition coefficients $C_i^{\alpha(\beta)}$ appearing in d_f^γ and a_f^γ (see Eqs. B.11b and B.20) are defined as "effective loop functions" $F_i(m_f, M_l, M_j)$ via

$$\begin{aligned} F_1(m_f, M_l, M_j) &= \lim_{s\to 0} \left\{ C_1^+ \left(m_f, m_f, M_l, M_j, M_j\right) \right\} \\ &= -\frac{1}{2} \lim_{s\to 0} \left\{ \left[C_1 + C_2\right] \left(m_f, m_f, M_l, M_j, M_j\right) \right\}, \end{aligned} \tag{B.44a}$$

$$\begin{aligned} F_2(m_f, M_l, M_j) &= \lim_{s\to 0} \left\{ \left[2C_1^+ - C_0\right] \left(m_f, m_f, M_l, M_j, M_j\right) \right\} \\ &= -\lim_{s\to 0} \left\{ \left[C_1 + C_2 + C_0\right] \left(m_f, m_f, M_l, M_j, M_j\right) \right\}, \end{aligned} \tag{B.44b}$$

$$\begin{aligned} F_3(m_f, M_l, M_j) &= \lim_{s\to 0} \left\{ \left[2C_2^{++} - C_1^+\right] \left(m_f, m_f, M_l, M_j, M_j\right) \right\} \\ &= -\frac{1}{2} \lim_{s\to 0} \left\{ \left[C_{11} + C_{12} + C_{21} + C_{22} + C_1 + C_2\right] \left(m_f, m_f, M_l, M_j, M_j\right) \right\}, \end{aligned} \tag{B.44c}$$

where the limit $s \to 0$ of vanishing momentum for vector boson V is already performed and $M_k \equiv M_j$ as enforced by the photon vertices is used. Taking this limit is straightforward, the collinear singularities discussed at the end of App. B.2.2 cancel with suitable factors from the nominators of the effective loop functions. Using the reduction formula from Eqs. B.31 for covariant decomposed tensor integrals one finds for the effective loop functions $F_i(m_f, M_l, M_j)$

$$\begin{aligned} F_1(m_f, M_l, M_j) = \frac{1}{4m_f^2} \big[& B_0(m_f, M_l, M_j) - B_0(0, M_j, M_j) \\ & -(m_f^2 - M_j^2 + M_l^2) C_0(m_f, m_f, M_l, M_j, M_j) \big], \end{aligned} \tag{B.45a}$$

$$\begin{aligned} F_2(m_f, M_l, M_j) = \frac{-1}{2m_f^2} \big[& B_0(m_f, M_l, M_j) - B_0(0, M_j, M_j) \\ & +(m_f^2 + M_j^2 - M_l^2) C_0(m_f, m_f, M_l, M_j, M_j) \big], \end{aligned} \tag{B.45b}$$

$$F_3(m_f,M_l,M_j)=\frac{1}{8m_f^2}\Big\{\,[2B_0(m_f,M_l,M_j)-1-B_0(0,M_j,M_j)$$
$$-2(m_f^2-M_j^2+2M_l^2)C_0(m_f,m_f,M_l,M_j,M_j)\big]$$
$$+\frac{1}{m_f^2}\left[A_0(M_l)-A_0(M_j)-(m_f^2-M_j^2+M_l^2)B_0(m_f,M_l,M_j)\right]$$
$$-\frac{6(m_f^2-M_j^2+M_l^2)}{4m_f^2}\left[B_0(m_f,M_l,M_j)-B_0(0,M_j,M_j)\right.$$
$$\left.-\;(m_f^2-M_j^2+M_l^2)C_0(m_f,s,M_l,M_j,M_j)\right]\Big\}. \tag{B.45c}$$

Using the results in Eq. B.43 the singularities of the functions $F_i(m_f,M_l,M_j)$ are extracted, one finds

$$(D-4)F_i(m_f,M_l,M_j)=\mathcal{O}(D-4),\quad \text{for}\;\; i=1,2,3; \tag{B.46}$$

as expected. The structure of the functions $F_i(m_f,M_l,M_j)$ is generalized as

$$F_i(m_f,M_l,M_j)=\frac{1}{m_f^2}\sum_m c_m^i(m_f,M_l,M_j)G_m(m_f,M_l,M_j),\quad i=1,2; \tag{B.47a}$$

$$F_3(m_f,M_l,M_j)=\frac{1}{m_f^4}\sum_m c_m^3(m_f,M_l,M_j)G_m(m_f,M_l,M_j), \tag{B.47b}$$

where the five scalar integrals $A_0(M_l)$, $A_0(M_j)$, $B_0(m_f,M_l,M_j)$, $B_0(0,M_j,M_j)$, and $C_0(m_f,m_f,M_l,M_j,M_j)$ are referred to by G_m.

B.2.6 Expansion in external momenta

A suitable parameter for the expansion of loop functions in external momenta is given by the ratio $\beta=m_f^2/M_l^2$. In our case the lepton is specified either as electron or as muon, whereas the loop mass M_l is either a neutralino mass or the sneutrino mass; in all cases $\beta\ll 1$ holds. The generalized, effective loop functions $F_i(m_f,M_l,M_j)$ from Eq. B.47 are first rewritten as

$$\overline{F}_i(\beta,M_j/M_l)=\frac{1}{m_f^2}\sum_m \overline{c}_m^i(\beta,M_j/M_l)\overline{G}_m(\beta,M_j/M_l),\quad i=1,2; \tag{B.48a}$$

$$\overline{F}_3(\beta,M_j/M_l)=\frac{1}{m_f^4}\sum_m \overline{c}_m^3(\beta,M_j/M_l)\overline{G}_m(\beta,M_j/M_l), \tag{B.48b}$$

and then formally expanded as

$$\overline{F}_i(\beta,M_j/M_l)=\frac{1}{m_f^2}\left(\overline{F}_i^{(0)}+\beta\overline{F}_i^{(1)}+\beta^2\overline{F}_i^{(2)}+\ldots\right),\quad i=1,2; \tag{B.49a}$$

$$\overline{F}_3(\beta,M_j/M_l)=\frac{1}{m_f^4}\left(\overline{F}_3^{(0)}+\beta\overline{F}_i^{(1)}+\beta^2\overline{F}_i^{(2)}+\ldots\right), \tag{B.49b}$$

where the Taylor coefficients $\overline{F}_i^{(n)}$ are

$$\overline{F}_i^{(0)}=\overline{F}_i\big|_{\beta=0}=\sum_m \overline{c}_m^i\overline{G}_m\big|_{\beta=0}, \tag{B.50a}$$

$$\overline{F}_i^{(1)} = \sum_m \left(\frac{\partial \overline{c}_m^i}{\partial \beta} \overline{G}_m + \overline{c}_m^i \frac{\partial \overline{G}_m}{\partial \beta} \right) \Bigg|_{\beta=0}, \tag{B.50b}$$

$$\overline{F}_i^{(2)} = \frac{1}{2} \sum_m \left(\frac{\partial^2 \overline{c}_m^i}{\partial \beta^2} \overline{G}_m + \overline{c}_m^i \frac{\partial^2 \overline{G}_m}{\partial \beta^2} + \frac{\partial \overline{c}_m^i}{\partial \beta} \frac{\partial \overline{G}_m}{\partial \beta} \right) \Bigg|_{\beta=0}. \tag{B.50c}$$

Since the form factors d_f^γ and a_f^γ are at least finite[5] for vanishing fermion mass m_f, the Taylor coefficients $\overline{F}_i^{(n)}$ have to satisfy

$$\overline{F}_i^{(0)} = 0, \tag{B.51a}$$

$$\overline{F}_3^{(1)} = 0. \tag{B.51b}$$

These conditions imply that the scalar integrals B_0 and C_0 have to be expanded up to $\mathcal{O}(\beta^2)$ in order to obtain the correct results for the form factors a_f^γ and d_f^γ.
The next step consists in rewriting and expanding the scalar loop functions A_0, B_0, and C_0. For this intention in addition to β a second, dimensionless quantity $A = (M_j^2 - M_l^2)/M_l^2$ is introduced and the finite parts of the loop functions are rewritten as

$$A_0(M_l)|_{\text{fin.}} = M_l^2 \left(1 - \log \left[\frac{M_l^2}{\mu^2} \right] \right), \tag{B.52a}$$

$$A_0(M_j)|_{\text{fin.}} = (1+A) \left[A_0(M_l)|_{\text{fin.}} - M_l^2 \log[1+A] \right], \tag{B.52b}$$

$$B_0(0, M_l, M_j)|_{\text{fin.}} = -\log \left[\frac{M_l^2}{\mu^2} \right] - \log[1+A], \tag{B.52c}$$

$$B_0(\beta, A, M_l)|_{\text{fin.}} = -\log \left[\frac{M_l^2}{\mu^2} \right] - \int_0^1 dx \log \left[(x^2 - x)\beta + Ax + 1 \right], \tag{B.52d}$$

$$C_0(\beta, A, M_l)|_{\text{fin.}} = \frac{-1}{M_l^2} \int_0^1 dx \int_0^{1-x} dy \left[(x^2 + xy - y^2 - x - y)\beta + (x+y)A + 1 \right]^{-1}, \tag{B.52e}$$

where some of the Feynman integrations have already been performed. The infinitesimal, imaginary parts $i\epsilon$ have been dropped, because they are formally relevant only for the zeroth order Taylor coefficients $B_0^{(0)}$ and $C_0^{(0)}$; a closer inspection of the relevant integrals for these coefficients shows that neither the argument of the logarithm in $B_0^{(0)}$ nor the denominator in $C_0^{(0)}$ contains a zero within the integration area. Moreover, the integrands for the remaining Taylor coefficients are formally independent of ϵ and furthermore do not contain singularities or zeros in the integration area.
The Taylor coefficients $B_0^{(n)}$ and $C_0^{(n)}$ are defined by the expansions of the scalar integrals $B_0(\beta, A, M_l)$ and $C_0(\beta, A, M_l)$ as

$$\begin{aligned} B_0(\beta, A, M_l) &= B_0^{(0)} + B_0^{(1)}\beta + B_0^{(2)}\beta^2 + \dots \\ &= B_0|_{\beta=0} + \frac{\partial B_0}{\partial \beta}\bigg|_{\beta=0} \beta + \frac{1}{2} \frac{\partial^2 B_0}{\partial \beta^2}\bigg|_{\beta=0} \beta^2 + \dots, \end{aligned} \tag{B.53a}$$

[5] In Sec. 3.1 these form factors were associated with chirality flipping operators, this implies $\lim_{m_f \to 0}(d_f^\gamma) = \lim_{m_f \to 0}(a_f^\gamma) = 0$.

$$C_0(\beta, A, M_l) = C_0^{(0)} + C_0^{(1)}\beta + C_0^{(2)}\beta^2 + \dots$$
$$= C_0|_{\beta=0} + \left.\frac{\partial C_0}{\partial \beta}\right|_{\beta=0} \beta + \frac{1}{2}\left.\frac{\partial^2 C_0}{\partial \beta^2}\right|_{\beta=0} \beta^2 + \dots . \tag{B.53b}$$

By calculating these derivatives and performing the Feynman integration over x (and y) one finds after some tedious calculations

$$B_0^{(0)} = -\log\left[\frac{M_l^2}{\mu^2}\right] + \frac{1}{A}\left[A - (1+A)\log[1+A]\right], \tag{B.54a}$$

$$B_0^{(1)} = \frac{1}{2A^3}\left[A^2 + 2A - 2(1+A)\log[1+A]\right], \tag{B.54b}$$

$$B_0^{(2)} = \frac{1}{3A^5}\left[A^3 + 12A^2 + 12A - 6(A^2+3A+2)\log[1+A]\right], \tag{B.54c}$$

$$C_0^{(0)} = \frac{-1}{A^2 M_l^2}, \left[A - \log[1+A]\right], \tag{B.54d}$$

$$C_0^{(1)} = \frac{-1}{2A^4 M_l^2}, \left[A^2 - 6A - (4A+6)\log[1+A]\right], \tag{B.54e}$$

$$C_0^{(2)} = \frac{-2}{3A^6 M_l^2}, \left[A^3 + 21A^2 + 30A - (9A^2 + 36A + 30)\log[1+A]\right]. \tag{B.54f}$$

Contrariwise, the expansion of the coefficients $\overline{c}_j^i$ is almost trivial. After some further, tedious calculations one finds for the effective loop functions

$$\overline{F}_1(\beta, A, M_l) = \frac{1}{4M_l^2}\frac{1}{A^3}\left[A^2 - 2A + 2\log[1+A]\right] + \mathcal{O}(\beta), \tag{B.55a}$$

$$\overline{F}_2(\beta, A, M_l) = \frac{1}{2M_l^2}\frac{1}{A^3}\left[A^2 + 2A + 2(1+A)\log[1+A]\right] + \mathcal{O}(\beta), \tag{B.55b}$$

$$\overline{F}_3(\beta, A, M_l) = \frac{1}{12M_l^2}\frac{1}{A^4}\left[A^3 - 3A^2 - 6A + 6(1+A)\log[1+A]\right] + \mathcal{O}(\beta). \tag{B.55c}$$

Introducing $z_{jl} = 1 + A = M_j^2/M_l^2$ the effective loop functions are finally given as

$$\overline{F}_1 = \frac{-1}{6}\frac{1}{M_j^2} f_1(z_{jl}) + \mathcal{O}(m_f^2/M_l^2), \tag{B.56a}$$

$$\overline{F}_2 = \frac{1}{6}\frac{1}{M_l^2} f_2(z_{jl}) + \mathcal{O}(m_f^2/M_l^2), \tag{B.56b}$$

$$\overline{F}_3 = \frac{1}{24}\frac{1}{M_j^2} f_3(z_{jl}) + \mathcal{O}(m_f^2/M_l^2), \tag{B.56c}$$

where the functions $f_i(z)$ were defined in Eq. 3.15 and are normalized as $f_i(1) = 1$.

B.3 Gordon identities

The Gordon identities relevant for the calculation of the dipole moments are [54]

$$2m_f \bar{u}_q \gamma^\mu v_{\bar{q}} = \left\{\bar{u}_q (q-\bar{q})^\mu v_{\bar{q}} + i\bar{u}_q (q+\bar{q})_\nu \sigma^{\mu\nu} v_{\bar{q}}\right\}, \tag{B.57a}$$

$$2m_f \bar{u}_q \gamma^\mu \gamma_5 v_{\bar{q}} = \{\bar{u}_q (q+\bar{q})^\mu \gamma_5 v_{\bar{q}} + i\bar{u}_q (q-\bar{q})_\nu \sigma^{\mu\nu} \gamma_5 v_{\bar{q}}\}\,, \tag{B.57b}$$

$$0 = \{\bar{u}_q (q+\bar{q})^\mu v_{\bar{q}} + i\bar{u}_q (q-\bar{q})_\nu \sigma^{\mu\nu} v_{\bar{q}}\}\,, \tag{B.57c}$$

$$0 = \{\bar{u}_q (q-\bar{q})^\mu \gamma_5 v_{\bar{q}} + i\bar{u}_q (q+\bar{q})_\nu \sigma^{\mu\nu} \gamma_5 v_{\bar{q}}\}\,. \tag{B.57d}$$

Using the Dirac equation

$$\not{p}\, u = m\, u, \tag{B.58a}$$

$$\overline{u}\, \not{p} = m\, \overline{u}, \tag{B.58b}$$

the Gordon identities can be checked directly.

Appendix C

Formula for the calculation of cross sections

C.1 Details of the road map

C.1.1 Kinematics

Working in the CMS frame with total energy $\sqrt{s}$ and neglecting the electron mass, the (first) electron and positron (second electron) momenta can be written as

$$p_1^\mu = \frac{\sqrt{s}}{2}(1,0,0,1)\,, \tag{C.1a}$$

$$p_2^\mu = \frac{\sqrt{s}}{2}(1,0,0,-1)\,. \tag{C.1b}$$

The outgoing momenta of the produced superparticles b and c are

$$k_1^\mu = \frac{\sqrt{s}}{2}\left(1+\frac{m_b^2-m_c^2}{s}, \lambda_{bc}^{\frac{1}{2}}\sin\theta, 0, \lambda_{bc}^{\frac{1}{2}}\cos\theta\right), \tag{C.2a}$$

$$k_2^\mu = \frac{\sqrt{s}}{2}\left(1-\frac{m_b^2-m_c^2}{s}, -\lambda_{bc}^{\frac{1}{2}}\sin\theta, 0, -\lambda_{bc}^{\frac{1}{2}}\cos\theta\right), \tag{C.2b}$$

here λ_{bc} denotes the usual two body final state kinematical function

$$\lambda_{bc} = \lambda\left(1, \frac{m_b^2}{s}, \frac{m_c^2}{s}\right), \tag{C.3a}$$

$$\lambda(1,x,y) = 1+x^2+y^2-2(x+y+xy). \tag{C.3b}$$

Furthermore the kinematical invariants (Mandelstam variables) are

$$s = (p_1+k_1)^2, \tag{C.4a}$$

$$t = (p_1-k_1)^2, \tag{C.4b}$$

$$u = (p_1-k_2)^2. \tag{C.4c}$$

C.1.2 Two body phase space

According to [141] the two body phase space is given as

$$d\Phi_2 = \frac{1}{16\pi^2}\frac{d^3k_1}{E_1}\frac{d^3k_2}{E_2}\delta\left(E_1+E_2-2E\right)\delta^3\left(k_1+k_2\right). \tag{C.5}$$

Performing the implied integrations one finds

$$\frac{d\Phi_2}{d\Omega} = \frac{1}{32\pi^2}\lambda\left(1,\mu_1^2,\mu_2^2\right)^{\frac{1}{2}}. \tag{C.6}$$

Following [142] the flux factor reads

$$F = 2s\lambda\left(1,\mu_e^2,\mu_e^2\right)^{\frac{1}{2}}, \tag{C.7}$$

where μ_e, μ_1, and μ_2 are the reduced masses $(m/\sqrt{s})$ of the incident electrons and the produced particles, respectively. Taking the limit of (kinematical) massless electrons, $\mu_e \to 0$, the complete phase space factor is finally found to be

$$\frac{1}{F}\frac{d\Phi_2}{d\Omega} = \frac{1}{64\pi^2}\frac{1}{s}\lambda\left(1,\mu_1^2,\mu_2^2\right)^{\frac{1}{2}}. \tag{C.8}$$

C.1.3 Helicity amplitudes

The basic idea for helicity amplitudes techniques as introduced in [143] is a change from the generic four spinors to two component Weyl-spinors as helicity eigenstates

$$\frac{\vec{p}\vec{\sigma}}{|\vec{p}|}\chi_\lambda(p) = \lambda\chi_\lambda(p), \tag{C.9}$$

where $\vec{\sigma} = (\sigma_1,\sigma_2,\sigma_3)$ are the standard Pauli matrices. The two component Weyl spinors are related to four component spinors by

$$P_\alpha u(p,\lambda) \equiv u_\alpha(p,\lambda) = \omega_{\alpha\lambda}(p)\chi_\lambda(p), \tag{C.10a}$$

$$P_\alpha v(p,\lambda) \equiv v_\alpha(p,\lambda) = \alpha\lambda\omega_{-\alpha\lambda}(p)\chi_{-\lambda}(p), \tag{C.10b}$$

where $\omega_{\alpha\lambda}(p) = (E+\alpha\lambda|\vec{p}|)^{\frac{1}{2}}$. The helicity eigenstates for the ingoing particles are chosen as

$$\chi_+(p_1) = \begin{pmatrix}1\\0\end{pmatrix}, \qquad \chi_-(p_1) = \begin{pmatrix}0\\1\end{pmatrix}, \tag{C.11a}$$

$$\chi_+(p_2) = \begin{pmatrix}0\\-1\end{pmatrix}, \quad \chi_-(p_2) = \begin{pmatrix}1\\0\end{pmatrix}, \tag{C.11b}$$

and

$$\chi_+(k_1) = \begin{pmatrix}\cos\frac{\theta}{2}\\ \sin\frac{\theta}{2}\end{pmatrix}, \qquad \chi_-(k_1) = \begin{pmatrix}-\sin\frac{\theta}{2}\\ \cos\frac{\theta}{2}\end{pmatrix}, \tag{C.12a}$$

$$\chi_+(k_2) = \begin{pmatrix}-\sin\frac{\theta}{2}\\ \cos\frac{\theta}{2}\end{pmatrix}, \quad \chi_-(k_2) = \begin{pmatrix}\cos\frac{\theta}{2}\\ \sin\frac{\theta}{2}\end{pmatrix}, \tag{C.12b}$$

for the outgoing particles.[1] With these conventions it is straightforward to obtain the following results for the scalar and vectorial fermionic string associated with massless fermions

$$\overline{v}\left(p_2,\sigma_2\right)P_\alpha u\left(p_1,\sigma_1\right)=-\alpha\sqrt{s}\delta_{\alpha\sigma_1}\delta_{\sigma_1\sigma_2}, \tag{C.13a}$$

$$\overline{v}\left(p_2,\sigma_2\right)\gamma^\mu P_\alpha u\left(p_1,\sigma_1\right)=\sqrt{s}\delta_{\alpha\sigma_1}\delta_{\sigma_2,-\sigma_1}\left(0,1,i\sigma_1,0\right), \tag{C.13b}$$

where the four choices in Eq. C.13b correspond to $\mu=0,1,2,3$. In the case of neutralinos or charginos with non-negligible mass only the vectorial string is required. It can be written as

$$\begin{aligned}\overline{u}_i\left(k_1,\lambda_1\right)\gamma^\mu P_\beta\, v_j\left(k_2,\lambda_2\right)=\frac{\sqrt{s}}{2}\Big[&\sqrt{1-\eta^2_{\beta\lambda_1}}\delta_{\lambda_1\lambda_2}\left(\beta,\lambda_1\sin\theta,0,\lambda_1\cos\theta\right)\\&+\sqrt{\left(1+\beta\lambda_1\eta_{\beta\lambda_1}\right)\left(1+\beta\lambda_1\eta_{-\beta\lambda_1}\right)}\delta_{\lambda_1,-\lambda_2}\left(0,\cos\theta,-i\lambda_1,-\sin\theta\right)\Big],\end{aligned} \tag{C.14}$$

where

$$\eta_{\beta\lambda_1}=\lambda_{ij}^{\frac{1}{2}}+\beta\lambda_1\Delta_{ij}, \tag{C.15}$$

and

$$\Delta_{ij}=\frac{m_i^2-m_j^2}{s}. \tag{C.16}$$

C.1.4 Polarisation density matrices

After the calculation of helicity amplitudes the polarization of the incoming electron and positron (second electron) is incorporated by polarization density matrices ρ^1 and ρ^2. The initial state polarization averaged, squared (helicity) matrix element is then given as [143]

$$\overline{|\mathcal{M}_{ij}|^2}=\mathcal{T}\nabla\left[\mathcal{M}_{ij}\rho^2\mathcal{M}_{ij}^\dagger\left(\rho^1\right)^T\right]=\sum_{\sigma_1,\sigma_1',\sigma_2,\sigma_2'}\langle\sigma_1\sigma_2\rangle\langle\sigma_1'\sigma_2'\rangle^\star\rho^1_{\sigma_1\sigma_1'}\rho^2_{\sigma_2\sigma_2'}, \tag{C.17}$$

when two scalar particles produced. In case two fermions are produced, their helicity has to be included and the formula for the *initial* state polarization averaged, squared matrix element reads

$$\overline{|\mathcal{M}_{ij}^{\lambda_1\lambda_2,\lambda_1'\lambda_2'}|^2}=\sum_{\sigma_1,\sigma_1',\sigma_2,\sigma_2'}\langle\sigma_1\sigma_2,\lambda_1\lambda_2\rangle\langle\sigma_1'\sigma_2',\lambda_1'\lambda_2'\rangle^\star\rho^1_{\sigma_1\sigma_1'}\rho^2_{\sigma_2\sigma_2'}. \tag{C.18}$$

As long as the final state polarizations are of no interest, the initial state polarization averaged and final state helicity summed, squared matrix element is obtained as

$$\overline{|\mathcal{M}_{ij}|^2}=\sum_{\lambda_1\lambda_2}\overline{|\mathcal{M}_{ij}^{\lambda_1\lambda_2}|^2}=\sum_{\sigma_1,\sigma_1',\sigma_2,\sigma_2'}\delta^{\lambda_1\lambda_2,\lambda_1'\lambda_2'}_{\lambda_1\lambda_1'}\delta_{\lambda_2\lambda_2'}\langle\sigma_1\sigma_2,\lambda_1\lambda_2\rangle\langle\sigma_1'\sigma_2',\lambda_1'\lambda_2'\rangle^\star\rho^1_{\sigma_1\sigma_1'}\rho^2_{\sigma_2\sigma_2'}, \tag{C.19}$$

Finally, the polarization density matrices read

$$\rho^-_{\sigma_1\sigma_1'}=\frac{1}{2}\begin{pmatrix}1+P_L^1 & P_T^1e^{-i\alpha_1}\\ P_T^1e^{i\alpha_1} & 1-P_L^1\end{pmatrix}, \tag{C.20}$$

[1] The convention for a momentum-dependent Weyl spinor for fermions going in the $-z$ direction used here differs by an overall sign from that of [143].

and

$$\rho^{-}_{\sigma_1\sigma_1'} = \frac{1}{2}\begin{pmatrix} 1+P_L^2 & -P_T^2 e^{i\alpha_2} \\ -P_T^2 e^{-i\alpha_2} & 1-P_L^2 \end{pmatrix}. \tag{C.21}$$

Here P_L and P_T denote the longitudinal and transversal polarization, respectively, α is the angle between each transversal polarization and the normal direction of the event plane. If these angles are replaced by the azimuthal angle ϕ and their rotation invariant difference η via

$$\alpha_1 = \phi, \tag{C.22a}$$

$$\alpha_2 = \eta - \phi, \tag{C.22b}$$

they lead to a non-trivial dependence of polarized cross sections for non-vanishing transversal polarizations.

C.1.5 Fierz rearrangement

During the calculation of the 2 fermion $\rightarrow$ 2 fermion cross sections a Fierz-rearrangement has to be applied to get identical current structures for the s-channel and the t-/u-channel contributions. The generic s-channel amplitude has already the structure of e^--current$\otimes$ neutralino(chargino)-current

$$\mathcal{M}^s = \overline{v}(e^+)\gamma_\mu P_\alpha Q_s^\alpha u(e^-) \otimes \overline{u}_i \gamma^\mu P_\beta Q_s^\beta v_j, \tag{C.23}$$

whereas the t-channel amplitude consists of two "mixed" currents

$$\mathcal{M}^t = \overline{u}_i P_\alpha Q_t^\alpha u(e^-) \otimes \overline{v}(e^+) P_\beta Q_t^\beta v_j. \tag{C.24}$$

By a Fierz re-arrangement given as

$$\overline{u}_i P_\alpha u(e^-) \otimes \overline{v}(e^+) P_\beta v_j = \frac{1}{2}\overline{v}(e^+)\gamma_\mu P_\alpha u(e^-) \otimes \overline{u}_i \gamma^\mu P_\beta v_j, \tag{C.25}$$

the t-(u-)channels can be transformed into the desired current structure and finally the complete amplitude may be written as

$$\mathcal{M} = Q^{\alpha\beta}\overline{v}(e^+)\gamma_\mu P_\alpha u(e^-) \otimes \overline{u}_i \gamma^\mu P_\beta v_j, \tag{C.26}$$

where

$$Q^{\alpha\beta} = Q_s^\alpha Q_s^\beta + \frac{1}{2} Q_t^\alpha Q_t^\beta. \tag{C.27}$$

More details on Fierz-transformations may be found in standard text books such as [70] or in [143].

C.2 Neutralino functions

After introducing two effective neutralino mixing coefficients

$$V_L^j = \frac{N_{1j}}{2\cos\theta_W} + \frac{N_{2j}}{2\sin\theta_W}, \tag{C.28a}$$

$$V_R^j = \frac{N_{1j}}{\cos\theta_W}, \tag{C.28b}$$

two dimensionless neutralino functions for the t- and u-exchanges are defined as

$$M_{\alpha\beta}\,(s,t/u) = \sum_{k=1}^{4} m_{\tilde{\chi}_k^0}\sqrt{s} V_\alpha^k V_\beta^k D_{t,u}^k, \tag{C.29a}$$

$$N_{\alpha\beta}\,(s,t/u) = \sum_{k=1}^{4} s V_\alpha^k V_\beta^{k,\star} D_{t,u}^k, \tag{C.29b}$$

where the propagators D_t^k and D_u^k have been defined in Eq. 4.6. Very similar neutralino functions were introduced in [94,95]; it was seen in Sec. 4.3.1 and 4.3.2 that they allow to give compact expressions for the slepton production amplitudes.

C.3 Analytical phase space integration

Without specifying the nature of the exchanged and produced particles the most general differential cross section for the studied processes may symbolically be written as

$$\frac{d\sigma_{ij}}{d\cos\theta} \propto \left| \sum_l \right.$$ 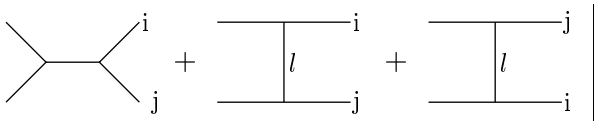 $$\left. \right|^2 \otimes \left(1, \cos\theta, \cos^2\theta\right), \tag{C.30}$$

where the diagrams from left to right symbolize the s-, t-, and u-channel contribution; the factors 1, $\cos\theta$, and $\cos^2\theta$ summarize all possible terms in the scattering angle. In the case that several particles can be exchanged in the t- and u-channel these are denoted by l. The problem of the analytical phase space integration of such a differential cross section is then addressed as follows:
First the appearing t- and u-channel propagators $D_t(s)$ and $D_u(s)$ are generalized to

$$D_{\gamma,l}^{ij} = \frac{1}{A_{ij,l} + \gamma\cos\theta B_{ij}} = \begin{cases} \frac{s}{2} D_t(s) & \text{if} \quad \gamma = 1 \\ \frac{s}{2} D_u(s) & \text{if} \quad \gamma = -1 \end{cases}, \tag{C.31}$$

where

$$A_{ij,l} = \mu_i^2 + \mu_j^2 - 1 - 2\mu_l^2, \quad B_{ij} \equiv \lambda_{ij}^{\frac{1}{2}}. \tag{C.32}$$

Treating the implicit double summation in Eq. C.30 correctly only six combinations of propagators are possible, these are summarized in Tab. C.1. The equalities

$$D_{\gamma,l}^{ij} D_{-\gamma,l}^{ij} = \frac{1}{2A_{ij,l}} \left(D_{\gamma,l}^{ij} + D_{-\gamma,l}^{ij}\right), \tag{C.33a}$$

$$D_{\gamma,l}^{ij} D_{\delta,m}^{ij} = \frac{1}{A_{ij,l} - \delta\gamma A_{ij,m}} \left(D_{\gamma,l}^{ij} - \gamma\delta D_{\delta,m}^{ij}\right) \quad \text{for} \quad l \neq m, \tag{C.33b}$$

allow a decomposition of the differential cross section into sums of products between coupling factors and kinematical factors (with $z \equiv \cos\theta$) as

$$\frac{d\sigma_{ij}}{dz} = \sum_l \sum_{\substack{n,k=0,2 \\ \gamma=\pm}} C_{ij,l}^{nk,\gamma} F_{ij,l}^{nk,\gamma}(z) + \sum_{\substack{l,m \\ m\neq l}} \sum_{\substack{n=0,2 \\ \gamma,\delta=\pm}} C_{ij,lm}^{n1,\gamma\delta} \left[F_{ij,l}^{n1,\gamma}(z) - \delta\gamma F_{ij,m}^{n1,\delta}(z)\right], \tag{C.34}$$

where the indices i, j denote the produced particles and the subscripts l and m refer to the particles exchanged in the t- and u-channel diagrams. The superscripts γ and/or δ indicate whether t- and/or u-channel contribute. Finally, the indices n and k count the powers of $z = \cos\theta$ in the numerator and the power of involved t-/u-channel propagators, respectively, i.e.

$$F_{ij,l}^{12,-1}(z) = \frac{z}{\left(A_{ij,l} - zB_{ij}\right)^2}. \tag{C.35}$$

The coefficients $C_{ij,l}^{nk,\gamma}$ and $C_{ij,l}^{n1,\gamma\delta}$ serve to absorb all coupling coefficients as well as all θ-independent terms so that the nine "master-functions" $F_{ij,l}^{nk,\gamma}$ are functions of $A_{ij,l}$, B_{ij} and $\cos\theta$ only. For the first addend in Eq. C.34 I have used Eq. C.33a to linearize terms with $D_{\gamma,l}^{ij} D_{-\gamma,l}^{ij}$. In the second addend terms containing $D_{\gamma,l}^{ij} D_{\delta,m}^{ij}$ have been linearized with the help of Eq. C.33b. As all interferences with the s-channel diagram are included in the first addend, only one power of $D_{\gamma,l}^{ij}$ ($D_{\delta,m}^{ij}$) is contained in the second addend and the initial sum, ranging over $k = 0, 2$, collapses to $k = 1$ after the mentioned linearization.

combination	source
1	s^2
$D_{\gamma,l}^{ij}$	interferences between s- and $t(u)$-channel
$(D_{\gamma,l}^{ij})^2$	$t^2(u^2)$ for same exchanged particles
$D_{\gamma,l}^{ij} D_{-\gamma,l}^{ij}$	interferences between t- and u-channel for same exchanged particles
$D_{\gamma,l}^{ij} D_{\gamma,m}^{ij}$	$t^2(u^2)$ for different exchanged particles
$D_{\gamma,l}^{ij} D_{-\gamma,m}^{ij}$	interferences between t- and u-channel for different exchanged particles

Table C.1: All possible combinations of propagators that can arise from expanding the products in Eq. C.30.

Using the general decomposition in Eq. C.34 the analytic phase space integration

$$\sigma_{ij} = \int_{-1}^{1} dz \left(\frac{d\sigma_{ij}}{dz}\right), \tag{C.36}$$

reduces to the calculation of nine "master-integrals"

$$I_{ij,l}^{nk,\gamma}(z) = \int_{-1}^{1} dz F_{ij,l}^{nk,\gamma}(z), \tag{C.37}$$

and a "book-keeping" problem given by the correct determination of the coefficients $C_{ij,l}^{nk,\gamma}$ and $C_{ij,lm}^{k1,\gamma\delta}$ from a given differential cross section. Finally, the total cross section reads

$$\sigma_{ij} = \sum_{l} \sum_{\substack{n,k=0,2 \\ \gamma=\pm}} C_{ij,l}^{nk,\gamma} I_{ij,l}^{nk,\gamma} + \sum_{\substack{k,l \\ k\neq l}} \sum_{\substack{n=0,2 \\ \gamma,\delta=\pm}} C_{ij,lm}^{n1,\gamma\delta} \left(I_{ij,l}^{n1,\gamma} - \delta\gamma I_{ij,m}^{n1,\delta}\right). \tag{C.38}$$

The "master integrals" can be calculated easily, one finds

$$I_{ij,l}^{00,\gamma} = 2, \tag{C.39a}$$

$$I_{ij,l}^{01,\gamma} = \frac{L\left[A_{ij}, B_{ij}\right]}{B_{ij}}, \tag{C.39b}$$

$$I_{ij,l}^{02,\gamma} = 2F\left[A_{ij}, B_{ij}\right], \tag{C.39c}$$

$$I_{ij,l}^{10,\gamma} = 0, \tag{C.39d}$$

$$I_{ij,l}^{11,\gamma} = \frac{1}{\gamma B_{ij}^2}\left\{2B_{ij} - A_{ij}L\left[A_{ij}, B_{ij}\right]\right\}, \tag{C.39e}$$

$$I_{ij,l}^{12,\gamma} = \frac{-1}{\gamma B_{ij}^2}\left\{2A_{ij}B_{ij}F\left[A_{ij}, B_{ij}\right] - L\left[A_{ij}, B_{ij}\right]\right\}, \tag{C.39f}$$

$$I_{ij,l}^{20,\gamma} = \frac{2}{3}, \tag{C.39g}$$

$$I_{ij,l}^{21,\gamma} = \frac{1}{B_{ij}^3}\left\{A_{ij}^2 L\left[A_{ij}, B_{ij}\right] - 2A_{ij}B_{ij}\right\}, \tag{C.39h}$$

$$I_{ij,l}^{22,\gamma} = \frac{2}{B_{ij}^3}\left\{A_{ij}^2 B_{ij}F\left[A_{ij}, B_{ij}\right] + B_{ij} - A_{ij}L\left[A_{ij}, B_{ij}\right]\right\}. \tag{C.39i}$$

where

$$L\left[A_{ij}, B_{ij}\right] = \log\left[\frac{A_{ij} + B_{ij}}{A_{ij} - B_{ij}}\right], \tag{C.40a}$$

$$F\left[A_{ij}, B_{ij}\right] = \frac{1}{A_{ij}^2 - B_{ij}^2}. \tag{C.40b}$$

Of course, the coefficients $C_{ij,l}^{nk,\gamma}$ and $C_{ij,lm}^{n1,\gamma\delta}$ still have to be determined for each process. However, after this "book keeping" task is performed the general expression for σ_{ij} in terms of "master integrals" and coupling coefficients indeed provides a complete, analytical result for the phase space integration of the investigated cross sections. This analytical result can easily be implemented in the code and allows a much faster numerical evaluation of cross sections than any numerical subroutine for the phase space integration could provide.

C.4 Perturbative treatment of cross sections

This part of the appendices briefly introduces two concepts that were used for the derivation of perturbative expressions for the phase-dependences of cross sections: a general decomposition of the (differential) cross section by sources and by powers of the perturbative parameter and an approach for the diagrammatical expansion of cross sections.

C.4.1 Decomposition of cross sections

The class of cross sections that is considered within this work depends on absolute values of SUSY parameters α_i and SUSY phases ϕ_j and may be generically written as

$$\sigma \equiv (\alpha_i, \phi_j) = c_0\overline{K}\left(\alpha_i, \phi_j\right) + c\left(\alpha_i, \phi_j\right)K\left(\alpha_i, \phi_j\right) \equiv c_0\overline{K} + cK, \tag{C.41}$$

where c_0 collects all SUSY independent couplings factor and $c\left(\alpha_i, \phi_j\right)$ all SUSY dependent. $\overline{K}$ and K summarize all kinematical factors, both depend on (α_i, ϕ_j). The contribution to

σ in n.th order of the generic expansion parameter λ reads

$$\sigma^{(n)} = \lambda^n c_0 \overline{K}^{(n)} + \lambda^n \sum_{k=0}^{n} c^{(k)} K^{(n-k)}, \tag{C.42}$$

where $\overline{K}^{(l)}$, $K^{(l)}$, and $c^{(l)}$ denote the coefficients of the l.th order of λ in the expansions of $\overline{K}$, K and c. The coupling coefficients $c(\alpha_i, \phi_j)$ always contain at least two mixing matrix elements.[2] Hence the expansion of $c(\alpha_i, \phi_j)$ can only be calculated exactly up to the same order of λ as the expansions of the mixing matrices have been performed. As mixing matrices have only been calculated up to second order, (the reliable part of) the expansion of σ reads

$$\begin{aligned}\sigma = {} & c_0 \overline{K}^{(0)} + c^{(0)} K^{(0)} + \lambda \left[c_0 \overline{K}^{(1)} + c^{(1)} K^{(0)} + c^{(0)} K^{(1)} \right] \\ & + \lambda^2 \left[c_0 \overline{K}^{(2)} + c^{(2)} K^{(0)} + c^{(1)} K^{(1)} + c^{(0)} K^{(2)} \right] + \underbrace{\sum_{n>2} \sigma^{(n)}}_{\text{undetermined}} .\end{aligned} \tag{C.43}$$

The next observation is that the coefficient $c^{(1)}$ vanishes for all considered cross sections. In the case of $\tilde{\chi}\tilde{\chi}$ pair production one power of λ corresponds to a $\mathcal{O}(\lambda)$ bilinear (in mixing matrix elements) of type "gaugino-Higgsino" multiplied with a $\mathcal{O}(\lambda^0)$ bilinear either of the type "gaugino-gaugino" or of the type "Higgsino-Higgsino". Such a product of bilinears is forbidden as a contribution to a cross section with definite final states since each of these bilinear refers to a final state. For selectron modes the two relevant vertices contain only gauge-interactions. Hence gaugino-Higgsino mixing, being the only mixing at $\mathcal{O}(\lambda)$, cannot contribute to cross sections at $\mathcal{O}(\lambda)$. Finally, as no physical mass is shifted at $\mathcal{O}(\lambda)$ the coefficients $\overline{K}^{(1)}$ and $K^{(1)}$ are identical to zero. Therefore the expansion of the cross section up to second order perturbation theory finally is

$$\sigma = c_0 \overline{K}^{(0)} + c^{(0)} K^{(0)} + \lambda^2 \left[c_0 \overline{K}^{(2)} + c^{(2)} K^{(0)} + c^{(0)} K^{(2)} \right], \tag{C.44}$$

where the coefficients $\overline{K}^{(2)}$ and $K^{(2)}$ are explicitly given as

$$\overline{K}^{(2)} = \sum_k \left. \frac{\partial \overline{K}}{\partial m_k^2} \right|_{\lambda=0} \cdot \delta m_k^{2(2)}, \tag{C.45a}$$

$$K^{(2)} = \sum_k \left. \frac{\partial K}{\partial m_k^2} \right|_{\lambda=0} \cdot \delta m_k^{2(2)}. \tag{C.45b}$$

The expression in Eq. C.44 can be used to extract the sources of possible phase-dependences either for fixed SUSY parameters or for fixed physical masses. In the first case the phase-dependent part of the expanded cross section σ_{ϕ_j} is given as

$$\sigma_{\phi_j} = c_{\phi_j}^{(0)} K^{(0)} + \lambda^2 \left[c_0 \overline{K}_{\phi_j}^{(2)} + c_{\phi_j}^{(2)} K^{(0)} + c^{(0)} K_{\phi_j}^{(2)} \right], \tag{C.46}$$

[2] For all s-channel diagrams the $Z\tilde{\chi}\tilde{\chi}$-vertex is proportional to a bilinear of mixing matrix elements or contains no such matrix elements, whereas the vertices $\gamma\tilde{f}\tilde{f}$, $Z\tilde{f}\tilde{f}$ and $\gamma\tilde{\chi}\tilde{\chi}$ involve none. The t- and u-channel diagrams contain two vertices either of type $f\tilde{f}\tilde{\chi}$ or $f\tilde{\nu}_f\tilde{\chi}$, each of them is linear in mixing matrix elements. Therefore, if a contribution to the cross section contains mixing matrix elements these elements are appearing at least as bilinears.

where the subscript ϕ_j implies that all phase-independent terms have been dropped. In the second case with parameter variations $\delta\alpha_l$ of second order in λ and phase-independent kinematical functions the phase-dependent part of the cross section is

$$\sigma_{\phi_j} = c^{(0)}_{\phi_j} K^{(0)} + \lambda^2 \left(\sum_l \frac{\partial c^{(0)}}{\partial \alpha_l} \cdot \delta\alpha_l \right)_{\phi_j} K^{(0)} + \lambda^2 c^{(2)}_{\phi_j} K^{(0)} + \underbrace{\lambda^4 \left(\sum_l \frac{\partial c^{(2)}}{\partial \alpha_l} \cdot \delta\alpha_l \right)_{\phi_j} K^{(0)}}_{\text{subdominant}} . \tag{C.47}$$

These decompositions nicely illustrate that with zeroth order phase-dependences present, all other sources of phase-dependences are subleading (like e.g. in the $\tilde{\chi}^0_1\tilde{\chi}^0_2$ mode). Furthermore, it can be observed that zeroth order phase-dependences exclusively originate from coupling effects. Secondly, in the case of absent zeroth order phase-dependences, i.e. $c^{(0)}_{\phi_j} = 0$, coupling effects are of same order λ as the kinematical effects (like e.g. in $\tilde{e}^-_R\tilde{e}^-_R$ mode), respectively the effects from parameter adjustment are. Moreover, if all zeroth order contributions vanish, i.e. $c_0 = c^{(0)} = 0$, phase-dependences from $\mathcal{O}(\lambda^2)$ coupling effects dominate for both treatments of the physical masses (like e.g. in the $\tilde{\chi}^0_1\tilde{\chi}^0_{\tilde{H}}$ mode).
In the case that not all physical masses are kept fixed it is obvious that coupling effects, kinematical effects and effects from parameter shifts contribute to the phase-dependence of the cross sections. For this rather complicated case the phase-dependent part σ_{ϕ_j} of the expansion of σ takes the general form

$$\begin{aligned}
\sigma_{\phi_j} = {} & c^{(0)}_{\phi_j} K^{(0)} + \lambda^2 c^{(2)}_{\phi_j} K^{(0)} + \lambda^2 \left(\sum_l \frac{\partial c^{(0)}}{\partial \alpha_l} \cdot \delta\alpha_l \right)_{\phi_j} \\
& + \lambda^2 \sum_k \left[c_0 \left. \frac{\partial \overline{K}}{\partial m_k^2} \right|_{\lambda=0} \cdot \delta m_k^{2(2)} + c^{(0)} \left. \frac{\partial K}{\partial m_k^2} \right|_{\lambda=0} \cdot \delta m_k^{2(2)} \right]_{\phi_j} \\
& + \lambda^2 \sum_{l,k} \left[c_0 \left. \frac{\partial \overline{K}}{\partial m_k^2} \cdot \frac{\partial m_k^2}{\partial \alpha_l} \right|_{\lambda=0} \cdot \delta\alpha_l + c^{(0)} \left. \frac{\partial K}{\partial m_k^2} \cdot \frac{\partial m_k^2}{\partial \alpha_l} \right|_{\lambda=0} \cdot \delta\alpha_l \right]_{\phi_j} + \mathcal{O}(\lambda^4),
\end{aligned} \tag{C.48}$$

where the index k sums over all varying masses m_k. Again, if phase-dependences of $\mathcal{O}(\lambda^0)$ are present, they dominate. Otherwise, in the case that they are absent, Eq. C.49 shows that the determination of the dominant contribution in the general case requires a precise specification of couplings, kinematics and parameters. Therefore the results of such an analysis will depend strongly on the latter ones as already pointed out before. The conclusions drawn from Eq. C.46 and C.47 have been applied in Sec. 4.4. The advantage of such decompositions clearly consists in a better overview on the bookkeeping problem and hence in a simplification of the derivation of perturbative results for cross sections.

C.4.2 Diagrammatical approach

The diagrammatical approach for deriving the leading powers in M_Z (or M_W) and sorting out the leading contributions is introduced and illustrated for the example of neutralino production. The diagrammatic approach starts with writing down the relevant tree-level diagrams and cutting the lines associated with neutralinos. Kinematical details such as distinguishing between t- and u-channel are of no importance for the ansatz. The parts of these cut lines associated with final states get labels referring to the mass eigenstates,

whereas parts of lines connected to vertices are labeled with current state indices determined uniquely by the vertices. For the case of neutralino pair production the three diagrams obtained by this description are shown in Fig. C.1. The next step is to introduce

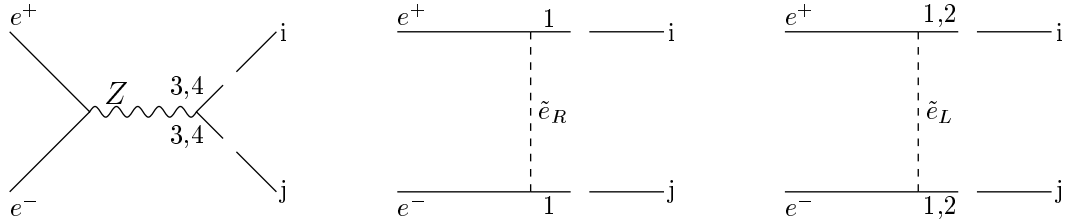

Figure C.1: Initial, "cut" diagrams for the diagrammatical approach to power-counting in neutralino production. The labels i and j denote final states. The indices at vertices indicate the current eigenstates associated with the vertex.

"links" which are used as insertions into the gaps generated by cutting neutralino lines. These links are sorted by powers of M_Z and receive labels k, l accordingly to the presence of the neutralino mixing matrix element N_{kl} in the considered order of M_Z. Consistently, if the entry N_{kl} is absent in a given order of M_Z the corresponding link between k and l does not exist. The links associated with the perturbative diagonalization of the neutralino mass matrix are shown in Fig. C.2. The perturbative expansion of the invariant amplitude

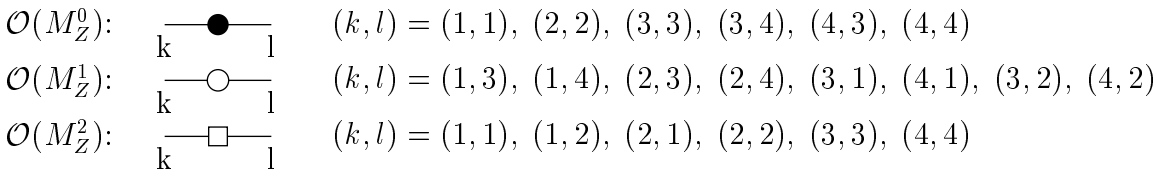

Figure C.2: "Links" for neutralino lines up to $\mathcal{O}(M_Z^2)$, the power of M_Z is indicated on the left, the links them self are displayed in the middle, and the pairs of numbers on the right summarize the possible pairs of labels for the link.

is then obtained symbolically by specifying the final state labels i and j according to the studied production mode and inserting suitable, non-vanishing links. Of course, if several links have to be inserted to close all cuts, these links can be of different order in M_Z. This procedure results in a set of diagrams with distinguished order of M_Z and one or several index pairs indicating directly what kind of mixing (gaugino-gaugino, Higgsino-Higgsino or gaugino-Higgsino) is involved. The powers of M_Z appearing in the cross section follow directly from multiplying all diagrams previously obtained among themselves.
The method is briefly illustrated for the $\tilde{\chi}_1^0\tilde{\chi}_3^0$-mode. First of all, the specified, cut diagrams are shown in Fig. C.3. . In the next step the relevant "links" have to be collected, these are summarized in Fig. C.4. By looking at the $\mathcal{O}(M_Z^0)$-links we notice immediately that all contributions to the invariant amplitude are vanishing at this order. This observation reflects the point that the $\tilde{\chi}_1^0\tilde{\chi}_3^0$ mode requires gaugino-Higgsino mixing which is an $\mathcal{O}(M_Z^1)$ effect. Similarly, there are no diagrams of $\mathcal{O}(M_Z^2)$ arising from one $\mathcal{O}(M_Z^0)$- and one $\mathcal{O}(M_z^2)$-link inserted, since the second ones are associated with gaugino-gaugino and Higgsino-Higgsino mixing. Also there are no $\mathcal{O}(M_Z^2)$ contributions to the amplitude from two $\mathcal{O}(M_Z^1)$-links inserted, the insertion of such links would be relevant for two gaugino-like or two Higgsino-like final states. Therefore the amplitude for this example contains

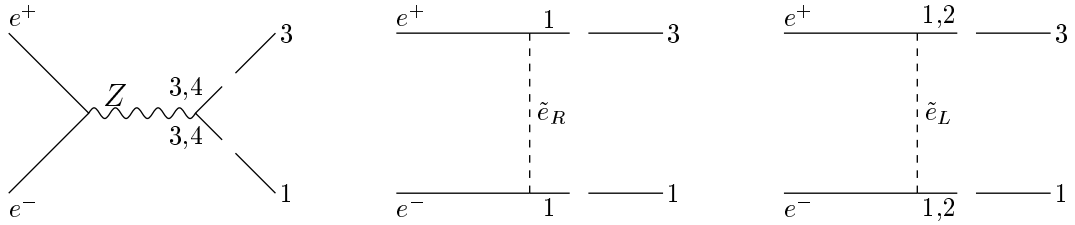

Figure C.3: "Cut" diagrams with specified final state labels for $\tilde{\chi}_1^0\tilde{\chi}_3^0$ production.

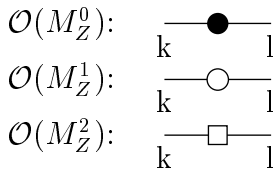

Figure C.4: Relevant "Links" for neutralino lines up to $\mathcal{O}(M_Z^2)$ for $\tilde{\chi}_1^0\tilde{\chi}_3^0$ production

only $\mathcal{O}(M_Z^1)$ terms, i.e. only insertions of one M_Z^0 link and one M_Z^1 link contribute. The corresponding diagrams with links inserted are displayed in Fig. C.5 As a matter of the fact that the leading diagrams contributing to the amplitude are $\mathcal{O}(M_Z)$, the cross section itself is in leading order[3] of $\mathcal{O}(M_Z^2)$.

The transfer of the given example to other neutralino, chargino, and selectron production modes is self-evident, only an additional description for cutting internal neutralino lines is necessary: an internal neutralino line has to be cut twice, lines connected with vertices get "current labels" as used before. The remaining internal line, i.e. the part of the neutralino line that is not connected to vertices receives a label k referring to the exchanged mass eigenstate. For $\tilde{e}_R^-\tilde{e}_R^-$ production this description leads to the cut diagram as shown in Fig. C.6.

The diagrammatical approach introduced here, while being rather intuitive, allows a systematic and straightforward determination of the relevant powers of M_Z in the perturbative expansion of the invariant amplitude and hence of the cross section itself. The advantage of this approach is that the terms which may contribute can easily be figured out and be calculated before the cross section is treated perturbatively. Compared with initially 15 diagrams for a calculation of the cross section up to $\mathcal{O}(M_Z^2)$ the simplification of the perturbative treatment is enormous. Obviously, the approach is very similar to the standard method of mass insertions in loop-calculations.

In general one might consider cutting each external (internal) neutralino line more than once (twice). However, this is *not* necessary. First, since each "link" connects current and mass eigenstates one would always have to insert an odd (even) number of cuts into external (internal) neutralino lines. If these cuts are then filled by links, the chain of links generated is equivalent to another link of higher order in M_Z. Therefore the "power-counting" described here is not affected.

[3]Unless cancellations due to the detailed structure of couplings occur. An example for such cancellations is given by the equal Higgsino modes $\tilde{\chi}_3^0\tilde{\chi}_3^0$ and $\tilde{\chi}_4^0\tilde{\chi}_4^0$: Here the diagrammatical approach predicts amplitudes of leading order $\mathcal{O}(M_Z)$, but these contributions vanish due to the structure of $Z_{33(44)}$.

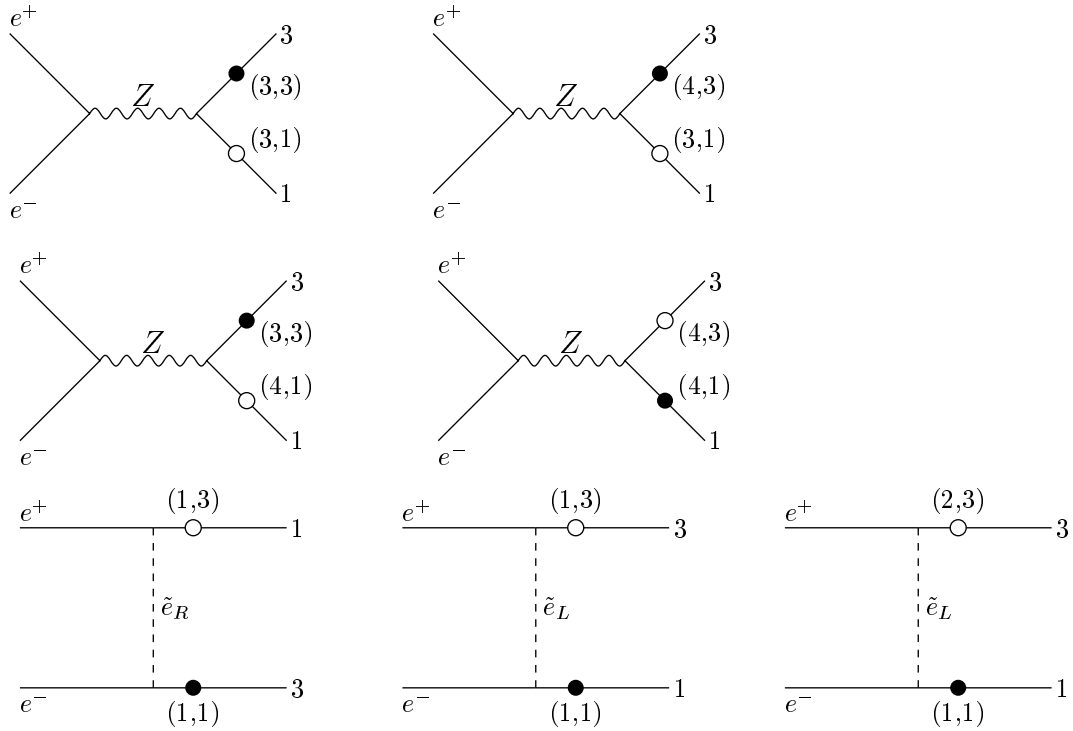

Figure C.5: The complete set of $\mathcal{O}(M_Z^1)$ diagrams contributing to the amplitude for $\tilde{\chi}_1^0\tilde{\chi}_3^0$-production. The bracketed pairs of number indicate the inserted links.

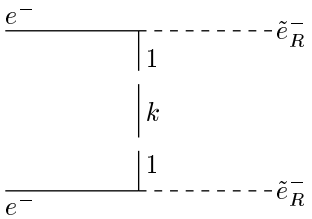

Figure C.6: Cutting of internal neutralino lines in the example of $\tilde{e}_R^-\tilde{e}_R^-$ production.

Appendix D

Polarisation vector components

D.1 The longitudinal component $P_L^{i,ij}$ as an example

In order to illustrate some details of the general calculation of polarisation vector components in the presence of initial state polarisation the basic steps in the calculation of $P_L^{i,ij} \equiv P_L^i$ are shown here as an example. The calculation starts by multiplying Eq. 5.9 with $\delta_{\bar{\lambda}\bar{\lambda}'}$ and summing over $\bar{\lambda}$ and $\bar{\lambda}'$. From this one obtains

$$\frac{1}{2N}\sum_{\sigma,\,\sigma',\,\bar{\lambda}}\langle\sigma\,{-\sigma},\lambda\bar{\lambda}\rangle\langle\sigma\,{-\sigma},\lambda'\bar{\lambda}\rangle^{\star}\rho^1_{\sigma\sigma'}\rho^2_{-\sigma-\sigma'} = \delta_{\lambda'\lambda} + (\tau_z)_{\lambda'\lambda}P_L^i + (\tau_x)_{\lambda'\lambda}P_T^i + (\tau_y)_{\lambda'\lambda}P_N^i. \quad \text{(D.1)}$$

The longitudinal component is then extracted by multiplying with $(\tau_z)_{\lambda\lambda'} \equiv \lambda\delta_{\lambda\lambda'}$ and summing over λ and λ'. This leads to

$$P_L^i = \frac{1}{4N}\sum_{\sigma,\,\sigma',\,\bar{\lambda}}\lambda\langle\sigma\,{-\sigma},\lambda\bar{\lambda}\rangle\langle\sigma\,{-\sigma},\lambda\bar{\lambda}\rangle^{\star}\rho^1_{\sigma\sigma'}\rho^2_{-\sigma-\sigma'}. \quad \text{(D.2)}$$

After inserting the polarisation density matrix elements given in Eqs. C.20 and C.21 the final result reads

$$\begin{aligned} P_L^i = \frac{1}{16N}\sum_{\lambda,\,\bar{\lambda}}\lambda\Big\{ & \left(1 - P_L^1P_L^2\right)\left(|\langle{+}{-},\lambda\bar{\lambda}\rangle|^2 + |\langle{-}{+},\lambda\bar{\lambda}\rangle|^2\right) \\ & + \left(P_L^1 - P_L^2\right)\left(|\langle{+}{-},\lambda\bar{\lambda}\rangle|^2 - |\langle{-}{+},\lambda\bar{\lambda}\rangle|^2\right) \\ & - 2P_T^1P_T^2e^{-i(\alpha_1+\alpha_2)}\langle{+}{-},\lambda\bar{\lambda}\rangle\langle{-}{+},\lambda\bar{\lambda}\rangle^{\star} \\ & - 2P_T^1P_T^2e^{i(\alpha_1+\alpha_2)}\langle{-}{+},\lambda\bar{\lambda}\rangle\langle{+}{-},\lambda\bar{\lambda}\rangle^{\star}\Big\}. \end{aligned} \quad \text{(D.3)}$$

Now the coefficients $C^k_{L,i}$ defined in Eq. 5.11b can be read off from Eq. D.3.

D.2 Polarisation vector components in terms of helicity amplitudes

During the calculation of polarisation vector components the coefficients $C^k_{\alpha,i(j)}$ of $P_\alpha^{i(j)}$ and the coefficients N_k of the normalization defined in Eqs. 5.11 have to be expressed in terms

of helicity amplitudes. For reasons of completeness these intermediate results are listed are. First of all, the coefficients N_k read

$$N_1 = \sum_{\lambda,\,\bar{\lambda},\,\sigma} |\langle \sigma\, -\sigma, \lambda\bar{\lambda}\rangle|^2, \tag{D.4a}$$

$$N_2 = \sum_{\lambda,\,\bar{\lambda},\,\sigma} \sigma |\langle \sigma\, -\sigma, \lambda\bar{\lambda}\rangle|^2, \tag{D.4b}$$

$$N_3 = -2 \sum_{\lambda,\,\bar{\lambda}} \mathcal{R}\mathrm{e}\left[\langle +-, \lambda\bar{\lambda}\rangle \langle -+, \lambda\bar{\lambda}\rangle^\star\right], \tag{D.4c}$$

$$N_4 = -2 \sum_{\lambda,\,\bar{\lambda}} \mathcal{I}\mathrm{m}\left[\langle +-, \lambda\bar{\lambda}\rangle \langle -+, \lambda\bar{\lambda}\rangle^\star\right]. \tag{D.4d}$$

The coefficients $C^k_{L,i(j)}$ in the decomposition of the longitudinal polarisation vector components are

$$C^1_{L,i} = \sum_{\lambda,\,\bar{\lambda},\,\sigma} \lambda |\langle \sigma\, -\sigma, \lambda\bar{\lambda}\rangle|^2, \tag{D.5a}$$

$$C^2_{L,i} = \sum_{\lambda,\,\bar{\lambda},\,\sigma} \lambda\sigma |\langle \sigma\, -\sigma, \lambda\bar{\lambda}\rangle|^2, \tag{D.5b}$$

$$C^3_{L,i} = -2 \sum_{\lambda,\,\bar{\lambda}} \lambda\ \mathcal{R}\mathrm{e}\left[\langle +-, \lambda\bar{\lambda}\rangle \langle -+, \lambda\bar{\lambda}\rangle^\star\right], \tag{D.5c}$$

$$C^4_{L,i} = -2 \sum_{\lambda,\,\bar{\lambda}} \lambda\ \mathcal{I}\mathrm{m}\left[\langle +-, \lambda\bar{\lambda}\rangle \langle -+, \lambda\bar{\lambda}\rangle^\star\right], \tag{D.5d}$$

$$C^1_{L,j} = \sum_{\lambda,\,\bar{\lambda},\,\sigma} \bar{\lambda} |\langle \sigma\, -\sigma, \lambda\bar{\lambda}\rangle|^2, \tag{D.5e}$$

$$C^2_{L,j} = \sum_{\lambda,\,\bar{\lambda},\,\sigma} \bar{\lambda}\sigma |\langle \sigma\, -\sigma, \lambda\bar{\lambda}\rangle|^2, \tag{D.5f}$$

$$C^3_{L,j} = -2 \sum_{\lambda,\,\bar{\lambda}} \bar{\lambda}\ \mathcal{R}\mathrm{e}\left[\langle +-, \lambda\bar{\lambda}\rangle \langle -+, \lambda\bar{\lambda}\rangle^\star\right], \tag{D.5g}$$

$$C^4_{L,j} = -2 \sum_{\lambda,\,\bar{\lambda}} \bar{\lambda}\ \mathcal{I}\mathrm{m}\left[\langle +-, \lambda\bar{\lambda}\rangle \langle -+, \lambda\bar{\lambda}\rangle^\star\right], \tag{D.5h}$$

while the coefficients $C^k_{T,i(j)}$ are given as

$$C^1_{T,i} = 2 \sum_{\sigma,\,\bar{\lambda}} \mathcal{R}\mathrm{e}\left[\langle \sigma\, -\sigma, +\bar{\lambda}\rangle \langle \sigma\, -\sigma, -\bar{\lambda}\rangle^\star\right], \tag{D.6a}$$

$$C^2_{T,i} = 2 \sum_{\sigma,\,\bar{\lambda}} \sigma\ \mathcal{R}\mathrm{e}\left[\langle \sigma\, -\sigma, +\bar{\lambda}\rangle \langle \sigma\, -\sigma, -\bar{\lambda}\rangle^\star\right], \tag{D.6b}$$

$$C^3_{T,i} = -2 \sum_{\lambda,\,\bar{\lambda}} \mathcal{R}\mathrm{e}\left[\langle +-, \lambda\bar{\lambda}\rangle \langle -+, -\lambda\bar{\lambda}\rangle^\star\right], \tag{D.6c}$$

$$C^4_{T,i} = -2\sum_{\lambda,\,\bar\lambda} \mathcal{I}\mathrm{m}\left[\langle +-,\lambda\bar\lambda\rangle\langle -+,-\lambda\bar\lambda\rangle^\star\right], \tag{D.6d}$$

$$C^1_{T,j} = 2\sum_{\sigma,\,\lambda} \mathcal{R}\mathrm{e}\left[\langle\sigma\,-\sigma,\lambda+\rangle\langle\sigma\,-\sigma,\lambda-\rangle^\star\right], \tag{D.6e}$$

$$C^2_{T,j} = 2\sum_{\sigma,\,\lambda} \sigma\mathcal{R}\mathrm{e}\left[\langle\sigma\,-\sigma,\lambda+\rangle\langle\sigma\,-\sigma,\lambda-\rangle^\star\right], \tag{D.6f}$$

$$C^3_{T,j} = -2\sum_{\lambda,\,\bar\lambda} \mathcal{R}\mathrm{e}\left[\langle +-,\lambda\bar\lambda\rangle\langle -+,\lambda-\bar\lambda\rangle^\star\right], \tag{D.6g}$$

$$C^4_{T,j} = -2\sum_{\lambda,\,\bar\lambda} \mathcal{I}\mathrm{m}\left[\langle +-,\lambda\bar\lambda\rangle\langle -+,\lambda-\bar\lambda\rangle^\star\right]. \tag{D.6h}$$

Finally I find for the coefficients of $P_N^{i(j)}$

$$C^1_{N,i} = -2\sum_{\sigma,\,\bar\lambda} \mathcal{I}\mathrm{m}\left[\langle\sigma\,-\sigma,+\bar\lambda\rangle\langle\sigma\,-\sigma,-\bar\lambda\rangle^\star\right], \tag{D.7a}$$

$$C^2_{N,i} = -2\sum_{\sigma,\,\bar\lambda} \sigma\ \mathcal{I}\mathrm{m}\left[\langle\sigma\,-\sigma,+\bar\lambda\rangle\langle\sigma\,-\sigma,-\bar\lambda\rangle^\star\right], \tag{D.7b}$$

$$C^3_{N,i} = 2\sum_{\lambda,\,\bar\lambda} \lambda\ \mathcal{I}\mathrm{m}\left[\langle +-,\lambda\bar\lambda\rangle\langle -+,-\lambda\bar\lambda\rangle^\star\right], \tag{D.7c}$$

$$C^4_{N,i} = -2\sum_{\lambda,\,\bar\lambda} \lambda\ \mathcal{R}\mathrm{e}\left[\langle +-,\lambda\bar\lambda\rangle\langle -+,-\lambda\bar\lambda\rangle^\star\right], \tag{D.7d}$$

$$C^1_{N,j} = -2\sum_{\sigma,\,\lambda} \mathcal{I}\mathrm{m}\left[\langle\sigma\,-\sigma,\lambda+\rangle\langle\sigma\,-\sigma,\lambda-\rangle^\star\right], \tag{D.7e}$$

$$C^2_{N,j} = -2\sum_{\sigma,\,\lambda} \sigma\ \mathcal{I}\mathrm{m}\left[\langle\sigma\,-\sigma,\lambda+\rangle\langle\sigma\,-\sigma,\lambda-\rangle^\star\right], \tag{D.7f}$$

$$C^3_{N,j} = 2\sum_{\lambda,\lambda} \bar\lambda\ \mathcal{I}\mathrm{m}\left[\langle +-,\lambda\bar\lambda\rangle\langle -+,\lambda-\bar\lambda\rangle^\star\right], \tag{D.7g}$$

$$C^4_{N,j} = -2\sum_{\lambda,\,\lambda} \bar\lambda\ \mathcal{R}\mathrm{e}\left[\langle +-,\lambda\bar\lambda\rangle\langle -+,\lambda-\bar\lambda\rangle^\star\right]. \tag{D.7h}$$

Again the index pair ij, referring to the final state particles, has been omitted. After replacing the generic helicity amplitudes $\langle\sigma-\sigma,\lambda\bar\lambda\rangle$ with the explicit ones from Eq. 4.19 the coefficients $C^k_{\alpha,i(j)}$ can be expressed in terms of the quartic charges given by Eq. 5.12.

Appendix E

The code

The code consists of the main program "READ.F" linked to 22 subroutines in total. This amounts to approximately 3,500 lines written in FORTRAN. Most of the code, except a few "library subroutines", were written and debugged by myself. As far as possible the produced data were compared with published numerical results. This check was fulfilled successfully. The time consumption of coding and debugging can roughly be estimated as equal to the efforts invested in Chapters 2-7. A detailed "README" is available on request. The code is introduced and summarized in Secs. E.1 and E.2, whereas Sec. E.3 points to a few (minor) shortcomings and possible improvements or extensions.

E.1 Organization and work flow

The basic operational scheme of the code as used for the numerical analysis within Part. II of this thesis is summarized in Fig. E.1. The code essentially separates into four major, logical blocks. Accordingly to their purpose these blocks are referred to as "PRESCAN", "LOW ENERGY", HIGH ENERGY", and "SIGNIFICANCE".
The code is started by RUN, the executable script-file where all the choices for SUSY parameters and the "collider parameters" $\sqrt{s}$ and θ are to be made. Furthermore the parameters to specify the scan are to be chosen here, i.e. the dimension of the scan (d=1,2,3), the number of iterations per scan loop (for d=1,2) or the number of randomly generated points for d=3. Additionally the ratio of the minimal (maximal) value of the scanned parameters to their previously fixed ("central") values may be adjusted here. In the case that phases are scanned they can be restricted either to the interval $[-\pi/2, \pi/2]$ or $[0, 2\pi]$. Moreover, for d=1 or d=2 the parameters to be scanned are to be selected, where the "collider parameters" are available opportunities. Contrarily, for d=3 the phases ϕ_μ, ϕ_1, and ϕ_A are scanned by default. Finally, for d=3 the choice between B1 and B2 or B3 has to be made explicitly. The code is "mastered" by the the main program READ.F, which serves to link the logical blocks and hence to process the scan. For any choice of the dimension of the scan the scan begins with completing the block "PRESCAN". Within this block all SM constants, SUSY and collider parameters as well as the values for the low-energy cuts are filled and the parameters to be scanned are prepared for this procedure.
Once the scan is prepared the block "LOW ENERGY" is evoked for the first time, i.e. $(d_e)_{\mathrm{SUSY}}$, $(a_\mu)_{\mathrm{SUSY}}$, the relevant part of the mass spectrum and $\sigma(\tilde{\chi}_1^\pm \tilde{\chi}_1^\mp)$ are calculated and passed to the subroutine CUTTER. Here the previously calculated low-energy observ-

ables are compared with the given bounds.

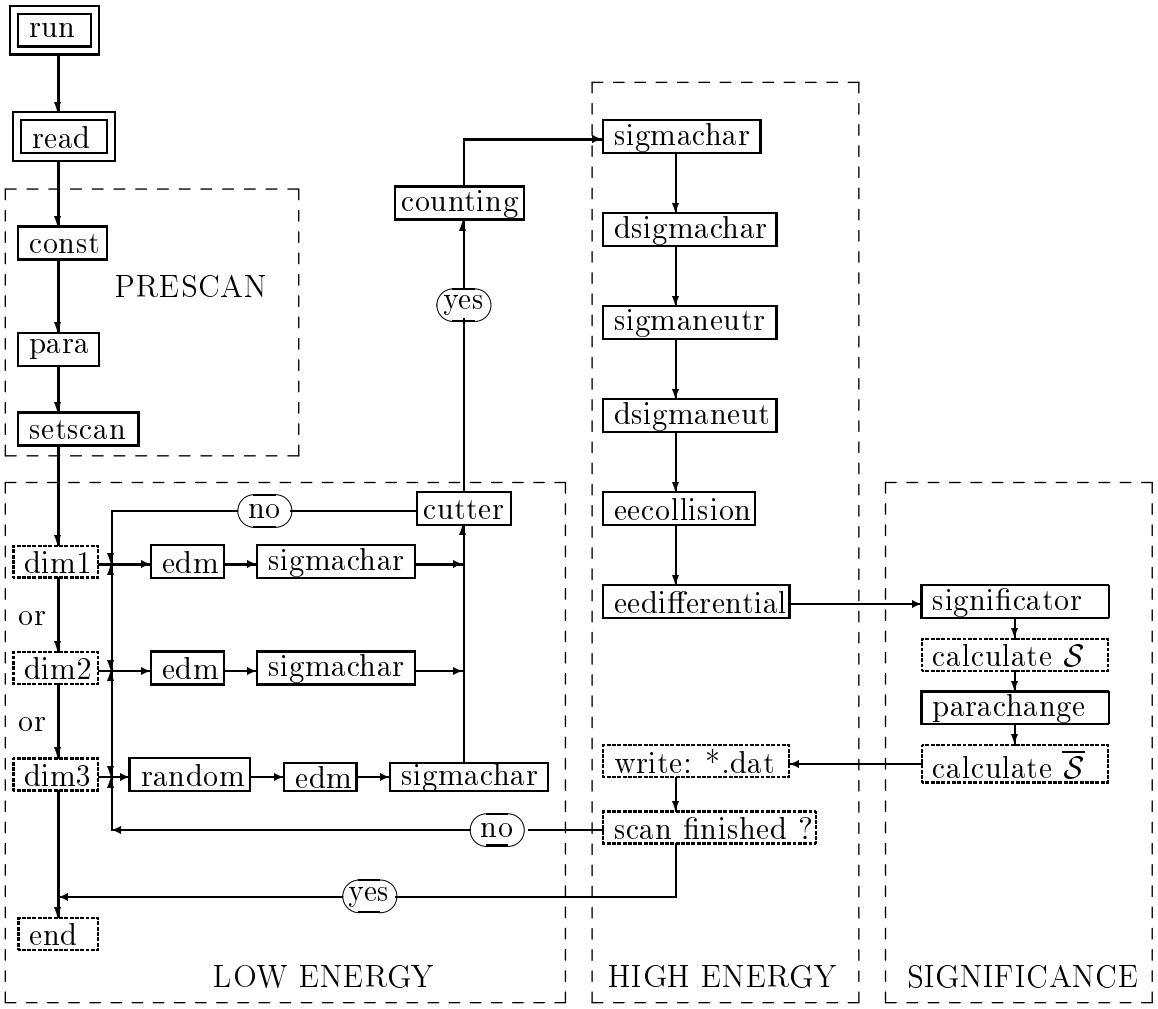

Figure E.1: Organization and work flow of the code as used for the numerical analysis. The solid boxes denote central subroutines. The minor dashed boxes indicate important steps during the processing of the scan. The major dashed boxes show the four central blocks the code is grouped in, the ellipses refer to the two most relevant if-cases during the scan. The main program "READ" and the executable file "RUN" are emphasized by doubled boxes. Several "unphysical subroutines have been omitted.

If any of these observables fails to satisfy the given experimental bound, the "LOW ENERGY" block is repeated for the next point, otherwise the "HIGH ENERGY" part is performed. Note that for d=3 a random number generator is required, whereas for d=1 or d=2 simple iterative loops are sufficient. Of course, within "LOW ENERGY" the subroutine SIGMACHAR is called using $\sqrt{s}$ as given from the last run at LEP and the running of $\alpha_{\rm QED}$ is taken into account between the "LOW ENERGY" and the "HIGH ENERGY" blocks. Intermediate between these two blocks resides the subroutine COUNTING, which serves for bookkeeping of cutting losses.

In the block "HIGH ENERGY" all differential and total cross sections as well as the polarization vector components in $\tilde{\chi}$ production are calculated for the given values of $\sqrt{s}$ and θ.
Afterwards the scan continues with the block "SIGNIFICANCE" which calculates first the significance $\mathcal{S}(f_i f_j)$ and then, after the parameters have been adjusted by PARACHANGE as described in Sec. 6.1, the significance $\overline{\mathcal{S}}(f_i f_j)$. Once the calculation of $\mathcal{S}(f_i f_j)$ and $\overline{\mathcal{S}}(f_i f_j)$ is completed all observables (of interest) are written into suitable files and the scan is either completed and ends or continues with the next iteration of the "LOW ENERGY" block.
These steps as described here and the mentioned subroutines give a basically complete overview of the code without going into too much detail. Several subroutines ("hidden" or "unphysical" ones) are not illustrative and hence not commented on here.

E.2 Physical subroutines

In this section the physical subroutines, i.e. subroutines that directly calculate observables, are summarized by their obligatory output. If present, additional outputs, benefits, and specialities are mentioned.

1. EDM

obligatory output:	$(d_e)_{\mathrm{SUSY}}$, $(a_\mu)_{\mathrm{SUSY}}$; N, $m_{\tilde{\chi}_i^0}$; U_R, U_L, $m_{\tilde{\chi}_i^\pm}$; $m_{\tilde{e}_i}$, $m_{\tilde{\mu}_i}$
additional output:	$(a_e)_{\mathrm{SUSY}}$, $(d_\mu)_{\mathrm{SUSY}}$; $U_{\tilde{e}}$, $U_{\tilde{\mu}}$
speciality:	slepton mixing
benefit:	provides mixing matrices for all other subroutines

2. SIGMACHAR

obligatory output:	$\sigma(\tilde{\chi}_i^\pm \tilde{\chi}_j^\mp)$
speciality:	no slepton mixing, analytic phase space integration

3. SIGMANEUT

obligatory output:	$\sigma(\tilde{\chi}_i^0 \tilde{\chi}_j^0)$
additional output:	polarized cross sections $\sigma^L(\tilde{\chi}_i^0 \tilde{\chi}_j^0)$, $\sigma^R(\tilde{\chi}_i^0 \tilde{\chi}_j^0)$, $\sigma^T(\tilde{\chi}_i^0 \tilde{\chi}_j^0)$
speciality:	no slepton mixing, analytic phase space integration

4. EECOLLSIONS

obligatory output:	$\sigma(\tilde{e}_\alpha^\pm \tilde{e}_\beta^-)$
speciality:	mass ordered cross sections, no slepton mixing, analytic phase space integration

5. DSIGMACHAR

obligatory output:	$\frac{d\sigma}{d\cos\theta}(\tilde{\chi}_i^\pm \tilde{\chi}_j^\mp)$, $P_N^{i(j),ij}$
additional output:	$P_{L,T}^{i(j),ij}$
speciality:	no slepton mixing

6. DSIGMANEUTR

obligatory output:	$\frac{d\sigma}{d\cos\theta}(\tilde{\chi}_i^0\tilde{\chi}_j^0)$, $P_N^{i(j),ij}$
additional output:	$P_{L,T}^{i(j),ij}$, polarized differential cross sections $\frac{d\sigma^{L,R,T}}{d\cos\theta}(\tilde{\chi}_i^0\tilde{\chi}_j^0)$
speciality:	no slepton mixing

7. EEDIFFERENTIAL

obligatory output:	$\frac{d\sigma}{d\cos\theta}(\tilde{e}_\alpha^\pm\tilde{e}_\beta^-)$
speciality:	no slepton mixing, mass ordered differential cross sections

8. SIGNIFICATOR

obligatory output:	$\mathcal{S}(f_if_j)$, $\mathcal{S}(f_if_j)$
additional output:	adjusted parameters in $\overline{\text{CPV}}_n$ that minimizes $\overline{\mathcal{S}}$ for each production mode and $\sigma\vert_{\overline{\text{CPV}}_n}$

All "obligatory"output beside the mixing matrices is directly written into files. Contrariwise the "additional" output is in most case only accessible at the level of the corresponding subroutine, i.e. can currently not be written to files.

E.3 Shortcomings and possible improvements

Most of the shortcomings that may be revealed from the code are associated with the d=3 scan. In the current version this scan is strictly limited to three, i.e. the variation of more than three parameters (SUSY and/or collider parameters) is not possible. Secondly, the 3-dimensional scan is restricted to phases only and thirdly, $\tan\beta$ has to be fixed by hand in the source files for such a scan. All these unfavorable features can easily be removed (even in the current version) by hand in the source files. But a more customer friendly version should for sure contain a solution of these problems such that *all* specifications are to be made exclusively in the executable file RUN.
A second set of deficits may be located in the treatment of initial state polarization; currently these collider parameters are only implemented for a few production channels with fixed choices of the beam polarization configuration (for example $\sigma^{L,R,T}$ in neutralino pair production). In this sense beam polarization is not included as free parameter at all. However, removing this shortcoming should be straightforward. Moreover and consequently, the results for polarization vector components in polarized two fermion production are not included, this deficit for sure has to be removed if an interface to decay chains or decay chains themselves were included. Finally, including radiative corrections both to the production cross section and to the beam performance as mentioned in Secs. 6.1 and 7.2.1, respectively, might be an issue if this code was extended.
However, still it can and has to be emphasized that this code, despite the mentioned shortcomings and possibilities for "upgrades", is indeed rather optimized for the initially given job which was defined as to check the consistency of CP-phases with low-energy bounds and, if consistent, to study the impact of these CP-phases on observables defined at the level of differential or total, unpolarized cross sections without including any decay chains.

Bibliography

[1] Hans Peter Nilles. Supersymmetry, supergravity and particle physics. *Phys. Rept.*, 110:1, 1984.

[2] Howard E. Haber and Gordon L. Kane. The search for supersymmetry: Probing physics beyond the standard model. *Phys. Rept.*, 117:75, 1985.

[3] Edward Witten. Dynamical breaking of supersymmetry. *Nucl. Phys.*, B188:513, 1981.

[4] N. Sakai. Naturalness in supersymmetric 'GUTs'. *Zeit. Phys.*, C11:153, 1981.

[5] Savas Dimopoulos and Howard Georgi. Softly broken supersymmetry and $SU(5)$. *Nucl. Phys.*, B193:150, 1981.

[6] Romesh K. Kaul and Parthasarathi Majumdar. Cancellation of quadratically divergent mass corrections in globally supersymmetric spontaneously broken gauge theories. *Nucl. Phys.*, B199:36, 1982.

[7] C. Giunti, C. W. Kim, and U. W. Lee. Running coupling constants and grand unification models. *Mod. Phys. Lett.*, A6:1745–1755, 1991.

[8] Ugo Amaldi, Wim de Boer, and Hermann Furstenau. Comparison of grand unified theories with electroweak and strong coupling constants measured at LEP. *Phys. Lett.*, B260:447–455, 1991.

[9] Paul Langacker and Ming-xing Luo. Implications of precision electroweak experiments for m_t, ρ_0, $\sin^2\theta_W$ and grand unification. *Phys. Rev.*, D44:817–822, 1991.

[10] John R. Ellis, S. Kelley, and D. V. Nanopoulos. Probing the desert using gauge coupling unification. *Phys. Lett.*, B260:131–137, 1991.

[11] Luis E. Ibanez and Graham G. Ross. $SU(2)_L \otimes U(1)$ symmetry breaking as a radiative effect of supersymmetry breaking in GUTs. *Phys. Lett.*, B110:215–220, 1982.

[12] H. Goldberg. Constraint on the photino mass from cosmology. *Phys. Rev. Lett.*, 50:1419, 1983.

[13] John R. Ellis, J. S. Hagelin, D. V. Nanopoulos, Keith A. Olive, and M. Srednicki. Supersymmetric relics from the big bang. *Nucl. Phys.*, B238:453–476, 1984.

[14] J. H. Christenson, J. W. Cronin, V. L. Fitch, and R. Turlay. Evidence for the 2π decay of the K_2^0 meson. *Phys. Rev. Lett.*, 13:138–140, 1964.

[15] A. Abashian et al. Measurement of the CP violation parameter $\sin 2\phi_1$ in B_d^0 meson decays. *Phys. Rev. Lett.*, 86:2509–2514, 2001.

[16] B. Aubert et al. Measurement of CP violating asymmetries in B_0 decays to CP eigenstates. *Phys. Rev. Lett.*, 86:2515–2522, 2001.

[17] S. Pakvasa and J. W. F. Valle. Neutrino properties before and after Kamland. *Proc. Indian Natl. Sci. Acad.*, 70A:189–222, 2004.

[18] K. Hagiwara et al. Review of particle physics. *Phys. Rev.*, D66:010001, 2002.

[19] R. J. Crewther, P. Di Vecchia, G. Veneziano, and Edward Witten. Chiral estimate of the electric dipole moment of the neutron in quantum chromodynamics. *Phys. Lett.*, B88:123, 1979.

[20] M. Kobayashi and T. Maskawa. CP violation in the renormalizable theory of weak interaction. *Prog. Theor. Phys.*, 49:652–657, 1973.

[21] A. D. Sakharov. Violation of CP invariance, C asymmetry, and baryon asymmetry of the universe. *Pisma Zh. Eksp. Teor. Fiz.*, 5:32–35, 1967.

[22] Michal Brhlik, Gerald J. Good, and Gordon L. Kane. Electric dipole moments do not require the CP-violating phases of supersymmetry to be small. *Phys. Rev.*, D59:115004, 1999.

[23] Tarek Ibrahim and Pran Nath. The neutron and the electron electric dipole moment in n = 1 supergravity unification. *Phys. Rev.*, D57:478–488, 1998. [Erratum-ibid.: D **58**: 019901 (1998), Erratum-ibid.:D **60**: 079903 (1999), Erratum-ibid.:D **60**: 119901, (1999)].

[24] A. Bartl, T. Gajdosik, W. Porod, P. Stockinger, and H. Stremnitzer. Electron and neutron electric dipole moments in the constrained MSSM. *Phys. Rev.*, D60:073003, 1999.

[25] Stefan Pokorski, Janusz Rosiek, and Carlos A. Savoy. Constraints on phases of supersymmetric flavour conserving couplings. *Nucl. Phys.*, B570:81–116, 2000.

[26] E. Accomando, R. Arnowitt, and Bhaskar Dutta. Grand unification scale CP violating phases and the electric dipole moment. *Phys. Rev.*, D61:115003, 2000.

[27] Pran Nath. CP violation via electroweak gauginos and the electric dipole moment of the electron. *Phys. Rev. Lett.*, 66:2565–2568, 1991.

[28] Yoshiki Kizukuri and Noriyuki Oshimo. The neutron and electron electric dipole moments in supersymmetric theories. *Phys. Rev.*, D46:3025–3033, 1992.

[29] P. Srivastava. *Supersymmetry, Superfields and Supergravity: An Introduction.* University of Sussex Press, (1986).

[30] J. Wess and J. Bagger. *Supersymmetry and Supergravitation.* Princeton Series in Physics. Princeton University Press, (1992).

[31] X. Tata. An introduction to supersymmetry and supersymmetry phenomenology. Lectures presented at Mt. Sorak Symp. on the Standard and Beyond, Mt. Sorak, Korea, Aug 1990.

[32] Manuel Drees. An introduction to supersymmetry. 1996. hep-ph/9611409.

[33] Stephen P. Martin. A supersymmetry primer. 1997. hep-ph/9709356.

[34] Savas Dimopoulos and David W. Sutter. The supersymmetric flavor problem. *Nucl. Phys.*, B452:496–512, 1995.

[35] David W. Sutter. The supersymmetric flavor problem and $\mu \to e\gamma$. 1995. hep-ph/9704390.

[36] Howard E. Haber. The status of the minimal supersymmetric standard model and beyond. *Nucl. Phys. Proc. Suppl.*, 62:469–484, 1998.

[37] Yosef Nir and Nathan Seiberg. Should squarks be degenerate? *Phys. Lett.*, B309:337–343, 1993.

[38] Michael Dine, Ann E. Nelson, and Yuri Shirman. Low-energy dynamical supersymmetry breaking simplified. *Phys. Rev.*, D51:1362–1370, 1995.

[39] Michael Dine, Ann E. Nelson, Yosef Nir, and Yuri Shirman. New tools for low-energy dynamical supersymmetry breaking. *Phys. Rev.*, D53:2658–2669, 1996.

[40] http://lhc-new-homepage.web.cern.ch/lhc-new-homepage/.

[41] D. P. Roy. Higgs and SUSY searches at LHC: An overview. *Acta Phys. Polon.*, B34:3417–3440, 2003.

[42] http://lcdev.kek.jp/.

[43] http://www-project.slac.stanford.edu/nlc/home.html.

[44] http://tesla-new.desy.de.

[45] http://tesla.desy.de/new_pages/TDR_CD/start.html.

[46] J. A. Aguilar-Saavedra et al. Tesla Technical Design Report Part III: Physics at an e^+e^- linear collider. 2001. hep-ph/0106315.

[47] G. A. Blair, W. Porod, and P. M. Zerwas. Reconstructing supersymmetric theories at high energy scales. *Phys. Rev.*, D63:017703, 2001.

[48] G. A. Blair, W. Porod, and P. M. Zerwas. The reconstruction of supersymmetric theories at high energy scales. *Eur. Phys. J.*, C27:263–281, 2003.

[49] J. L. Feng, M. E. Peskin, H. Murayama, and Xerxes Tata. Testing supersymmetry at the next linear collider. *Phys. Rev.*, D52:1418–1432, 1995.

[50] Toshifumi Tsukamoto, Keisuke Fujii, Hitoshi Murayama, Masahiro Yamaguchi, and Yasuhiro Okada. Precision study of supersymmetry at future linear e^+e^- colliders. *Phys. Rev.*, D51:3153–3171, 1995.

[51] T. Abe et al. Linear collider physics resource book for Snowmass 2001. 2: Higgs and supersymmetry studies. 2001. hep-ex/0106056.

[52] Koh Abe et al. Particle physics experiments at jlc. 2001. hep-ph/0109166.

[53] Jonathan L. Feng and Mihoko M. Nojiri. Supersymmetry and the linear collider. 2002. hep-ph/0210390.

[54] W. Hollik, Jose I. Illana, S. Rigolin, C. Schappacher, and D. Stockinger. Top dipole form factors and loop-induced CP violation in supersymmetry. *Nucl. Phys.*, B551:3–40, 1999.

[55] Stephen P. Martin and James D. Wells. Muon anomalous magnetic dipole moment in supersymmetric theories. *Phys. Rev.*, D64:035003, 2001.

[56] Vernon D. Barger, Tao Han, Tian-Jun Li, and Tilman Plehn. Measuring CP violating phases at a future linear collider. *Phys. Lett.*, B475:342–350, 2000.

[57] Vernon D. Barger et al. CP-violating phases in SUSY, electric dipole moments, and linear colliders. *Phys. Rev.*, D64:056007, 2001.

[58] A. Bartl, H. Fraas, O. Kittel, and W. Majerotto. CP asymmetries in neutralino production in e^+e^- collisions. *Phys. Rev.*, D69:035007, 2004.

[59] A. Bartl, T. Kernreiter, and O. Kittel. A CP asymmetry in $e^+e^- \to$ neutralino(i) neutralino(j) $\to$ neutralino(j) tau stau(k) with tau polarization. *Phys. Lett.*, B578:341–348, 2004.

[60] A. Bartl, H. Fraas, O. Kittel, and W. Majerotto. CP sensitive observables in $e^+e^- \to$ neutralino(i) neutralino(j) and neutralino decay into Z boson. 2004. hep-ph/0402016.

[61] Manuel Drees. N=1 supergravity GUTs with noncanonical kinetic energy terms. *Phys. Rev.*, D33:1468, 1986.

[62] Andrew G. Cohen, D. B. Kaplan, and A. E. Nelson. The more minimal supersymmetric standard model. *Phys. Lett.*, B388:588–598, 1996.

[63] Jonathan A. Bagger, Jonathan L. Feng, Nir Polonsky, and Ren-Jie Zhang. Superheavy supersymmetry from scalar mass A-parameter fixed points. *Phys. Lett.*, B473:264–271, 2000.

[64] Savas Dimopoulos and Scott Thomas. Dynamical relaxation of the supersymmetric CP violating phases. *Nucl. Phys.*, B465:23–33, 1996.

[65] S. Y. Choi, Manuel Drees, B. Gaissmaier, and Jae Sik Lee. CP violation in tau slepton pair production at muon colliders. *Phys. Rev.*, D64:095009, 2001.

[66] S. Y. Choi et al. Reconstructing the chargino system at e^+e^- linear colliders. *Eur. Phys. J.*, C14:535–546, 2000.

[67] S. Y. Choi, J. Kalinowski, G. Moortgat-Pick, and P. M. Zerwas. Analysis of the neutralino system in supersymmetric theories. *Eur. Phys. J.*, C22:563–579, 2001.

[68] S. Y. Choi, J. Kalinowski, G. Moortgat-Pick, and P. M. Zerwas. Analysis of the neutralino system in supersymmetric theories. (Addendum). 2002. hep-ph/0202039.

[69] Seong Youl Choi, Manuel Drees, and Benedikt Gaissmaier. Systematic study of the impact of CP-violating phases of the MSSM on leptonic high-energy observables. 2004. hep-ph/0403054.

[70] Michael Peskin and D. Schroeder. *An Introduction to Quantum Field Theory*. Perseus Books, (1995).

[71] T.Kugo. *Eichtheorie*. Springer-Verlag, (1997).

[72] S. Abel, S. Khalil, and O. Lebedev. EDM constraints in supersymmetric theories. *Nucl. Phys.*, B606:151–182, 2001.

[73] Michael Graesser and Scott Thomas. Supersymmetric relations among electromagnetic dipole operators. *Phys. Rev.*, D65:075012, 2002.

[74] G. W. Bennett et al. Measurement of the positive muon anomalous magnetic moment to 0.7-ppm. *Phys. Rev. Lett.*, 89:101804, 2002.

[75] G. W. Bennett et al. Measurement of the negative muon anomalous magnetic moment to 0.7-ppm. *Phys. Rev. Lett.*, 92:161802, 2004.

[76] Werner Bernreuther and Mahiko Suzuki. The electric dipole moment of the electron. *Rev. Mod. Phys.*, 63:313–340, 1991.

[77] M. Davier, S. Eidelman, A. Hocker, and Z. Zhang. Confronting spectral functions from e^+e^- annihilation and tau decays: Consequences for the muon magnetic moment. *Eur. Phys. J.*, C27:497–521, 2003.

[78] M. Hayakawa and T. Kinoshita. Pseudoscalar pole terms in the hadronic light-by-light scattering contribution to muon g-2. *Phys. Rev.*, D57:465–477, 1998.

[79] Masashi Hayakawa and Toichiro Kinoshita. Comment on the sign of the pseudoscalar pole contribution to the muon g-2. 2001. hep-ph/0112102.

[80] R. R. Akhmetshin et al. Reanalysis of hadronic cross section measurements at CMD-2. *Phys. Lett.*, B578:285–289, 2004.

[81] M. Davier, S. Eidelman, A. Hocker, and Z. Zhang. Updated estimate of the muon magnetic moment using revised results from e^+e^- annihilation. *Eur. Phys. J.*, C31:503–510, 2003.

[82] K. Hagiwara, A. D. Martin, Daisuke Nomura, and T. Teubner. Predictions for g-2 of the muon and $\alpha_{QED}(M_Z^2)$. 2003. hep-ph/0312250.

[83] J. F. de Troconiz and F. J. Yndurain. The hadronic contributions to the anomalous magnetic moment of the muon. 2004. hep-ph/0402285.

[84] S. T. Petcov. CP violation effect in neutralino pair production in e^+e^- annihilation and the electric dipole moment of the electron. *Phys. Lett.*, B178:57, 1986.

[85] John R. Ellis, Sergio Ferrara, and D. V. Nanopoulos. CP violation and supersymmetry. *Phys. Lett.*, B114:231, 1982.

[86] F. del Aguila, M. B. Gavela, J. A. Grifols, and A. Mendez. Specifically supersymmetric contribution to electric dipole moments. *Phys. Lett.*, B126:71, 1983. [Erratum-ibid.: Phys.Lett.B129: 77, (1983)].

[87] Manuel Drees and Stephen P. Martin. Implications of SUSY model building. 1995. hep-ph/9504324.

[88] B. C. Allanach et al. The snowmass points and slopes: Benchmarks for susy searches. *Eur. Phys. J.*, C25:113–123, 2002.

[89] Glennys R. Farrar and Pierre Fayet. Searching for the spin 0 leptons of supersymmetry. *Phys. Lett.*, B89:191, 1980.

[90] M. Gluck and E. Reya. Photino mass and selectron production in unpolarized and polarized e^+e^- annihilation. *Phys. Lett.*, B130:423, 1983.

[91] A. Bartl, H. Fraas, and W. Majerotto. Gaugino - Higgsino mixing in selectron and sneutrino pair production. *Z. Phys.*, C34:411, 1987.

[92] Xerxes Tata and Duane A. Dicus. Supersymmetric particle production at electron - positron colliders. *Phys. Rev.*, D35:2110, 1987.

[93] Howard Baer, A. Bartl, Debra Karatas, W. Majerotto, and Xerxes Tata. Searching for supersymmetry at e^+e^- supercolliders. *Int. J. Mod. Phys.*, A4:4111, 1989.

[94] Michael E. Peskin. Systematics of slepton production in e^+e^- and e^-e^- collisions. *Int. J. Mod. Phys.*, A13:2299–2306, 1998.

[95] Jonathan L. Feng and Michael E. Peskin. Selectron studies at e^-e^- and e^+e^- colliders. *Phys. Rev.*, D64:115002, 2001.

[96] Scott Thomas. CP-odd phases in slepton pair production. *Int. J. Mod. Phys.*, A13:2307–2318, 1998.

[97] C. Blochinger, H. Fraas, G. Moortgat-Pick, and W. Porod. Selectron pair production at e^-e^- and e^+e^- colliders with polarized beams. *Eur. Phys. J.*, C24:297–310, 2002.

[98] John R. Ellis, J. M. Frere, J. S. Hagelin, Gordon L. Kane, and S. T. Petcov. Search for neutral gauge fermions in e^+e^- annihilation. *Phys. Lett.*, B132:436, 1983.

[99] Vernon D. Barger, R. W. Robinett, W. Y. Keung, and R. J. N. Phillips. Production of gauge fermions at colliders. *Phys. Lett.*, B131:372, 1983.

[100] A. Bartl, H. Fraas, and W. Majerotto. Signatures of chargino production in e^+e^- collisions. *Z. Phys.*, C30:441, 1986.

[101] A. Bartl, H. Fraas, and W. Majerotto. Production and decay of neutralinos in e^+e^- annihilation. *Nucl. Phys.*, B278:1, 1986.

[102] A. Bartl, H. Fraas, W. Majerotto, and B. Mosslacher. Chargino production at LEP-200. *Z. Phys.*, C55:257–264, 1992.

[103] S. Y. Choi, M. Guchait, J. Kalinowski, and P. M. Zerwas. Chargino pair production at e^+e^- colliders with polarized beams. *Phys. Lett.*, B479:235–244, 2000.

[104] G. Valencia. Constructing CP odd observables. 1994. hep-ph/9411441.

[105] S. Y. Choi, A. Djouadi, Herbert K. Dreiner, J. Kalinowski, and P. M. Zerwas. Chargino pair production in e^+e^- collisions. *Eur. Phys. J.*, C7:123–134, 1999.

[106] J. L. Kneur and G. Moultaka. Phases in the gaugino sector: Direct reconstruction of the basic parameters and impact on the neutralino pair production. *Phys. Rev.*, D61:095003, 2000.

[107] Marco A. Diaz, Steve F. King, and Douglas A. Ross. Radiative corrections to chargino production in electron positron collisions. *Nucl. Phys.*, B529:23–61, 1998.

[108] Marco A. Diaz, Stephen F. King, and Douglas A. Ross. Radiative corrections to chargino production in electron positron collisions with polarized beams. *Phys. Rev.*, D64:017701, 2001.

[109] Piotr H. Chankowski. Radiative $SU(2) \otimes U(1)$ breaking in the supersymmetric standard model and decoupling of heavy squarks and gluino. *Phys. Rev.*, D41:2877, 1990.

[110] Hsin-Chia Cheng, Jonathan L. Feng, and Nir Polonsky. Signatures of multi-TeV scale particles in supersymmetric theories. *Phys. Rev.*, D57:152–169, 1998.

[111] Hsin-Chia Cheng, Jonathan L. Feng, and Nir Polonsky. Super-oblique corrections and non-decoupling of supersymmetry breaking. *Phys. Rev.*, D56:6875–6884, 1997.

[112] Mihoko M. Nojiri, Damien M. Pierce, and Youichi Yamada. Slepton production as a probe of the squark mass scale. *Phys. Rev.*, D57:1539–1552, 1998.

[113] Shingo Kiyoura, Mihoko M. Nojiri, Damien M. Pierce, and Youichi Yamada. Radiative corrections to a supersymmetric relation: A new approach. *Phys. Rev.*, D58:075002, 1998.

[114] Gian F. Giudice and Alex Pomarol. Mass degeneracy of the Higgsinos. *Phys. Lett.*, B372:253–258, 1996.

[115] Manuel Drees, Mihoko M. Nojiri, D. P. Roy, and Youichi Yamada. Light Higgsino dark matter. *Phys. Rev.*, D56:276–290, 1997. [Erratum-ibid.: D **64**: 039901 (2001)].

[116] S. Y. Choi, M. Drees, B. Gaissmaier, and J. Song. Analysis of CP violation in neutralino decays to tau sleptons. *Phys. Rev.*, D69:035008, 2004.

[117] F. Gabbiani, E. Gabrielli, A. Masiero, and L. Silvestrini. A complete analysis of FCNC and CP constraints in general SUSY extensions of the standard model. *Nucl. Phys.*, B477:321–352, 1996.

[118] Toru Goto and Takeshi Nihei. Effect of $RRRR$ dimension 5 operator on the proton decay in the minimal $SU(5)$ SUGRA GUT model. *Phys. Rev.*, D59:115009, 1999.

[119] B. Ananthanarayan, G. Lazarides, and Q. Shafi. Top mass prediction from supersymmetric GUTs. *Phys. Rev.*, D44:1613–1615, 1991.

[120] S. Kelley, Jorge L. Lopez, and D. V. Nanopoulos. Yukawa unification. *Phys. Lett.*, B274:387–392, 1992.

[121] Searches for the neutral higgs bosons of the MSSM: Preliminary combined results using LEP data collected at energies up to 209-GeV. 2001. hep-ex/0107030.

[122] Noriyuki Oshimo. T violation in neutralino decay. *Z. Phys.*, C41:129, 1988.

[123] Yoshiki Kizukuri and Noriyuki Oshimo. T odd asymmetry mediated by neutralino in e+ e- annihilation. *Phys. Lett.*, B249:449–454, 1990.

[124] S. Y. Choi, H. S. Song, and W. Y. Song. CP phases in correlated production and decay of neutralinos in the minimal supersymmetric standard model. *Phys. Rev.*, D61:075004, 2000.

[125] Mihoko M. Nojiri. Polarization of tau lepton from scalar tau decay as a probe of neutralino mixing. *Phys. Rev.*, D51:6281–6291, 1995.

[126] Mihoko M. Nojiri, Keisuke Fujii, and Toshifumi Tsukamoto. Confronting the minimal supersymmetric standard model with the study of scalar leptons at future linear e^+e^- colliders. *Phys. Rev.*, D54:6756–6776, 1996.

[127] E. Boos et al. Polarisation in sfermion decays: Determining $\tan\beta$ and trilinear couplings. *Eur. Phys. J.*, C30:395–407, 2003.

[128] G. Moortgat-Pick, A. Bartl, H. Fraas, and W. Majerotto. Impact of e^+ and e^- beam polarization on chargino and neutralino production at a linear collider. *Eur. Phys. J.*, C18:379–391, 2000.

[129] B. K. Bullock, K. Hagiwara, and Alan D. Martin. Tau polarization as a signal of charged higgs bosons. *Phys. Rev. Lett.*, 67:3055–3057, 1991.

[130] B. K. Bullock, K. Hagiwara, and Alan D. Martin. Tau polarization and its correlations as a probe of new physics. *Nucl. Phys.*, B395:499–533, 1993.

[131] M. Davier, L. Duflot, F. Le Diberder, and A. Rouge. The optimal method for the measurement of tau polarization. *Phys. Lett.*, B306:411–417, 1993.

[132] E. Boos, G. Moortgat-Pick, H. U. Martyn, M. Sachwitz, and A. Vologdin. Impact of tau polarization for the determination of high $\tan\beta$ and A_τ. 2002. hep-ph/0211040.

[133] Monoranjan Guchait and D. P. Roy. Using tau polarization as a distinctive SUGRA signature at LHC. *Phys. Lett.*, B541:356–361, 2002.

[134] A. Bartl, T. Kernreiter, and W. Porod. A CP sensitive asymmetry in the three-body decay $\tilde{t}_1 \to b\tilde{\nu}_\tau\tau^+$. *Phys. Lett.*, B538:59–65, 2002.

[135] Howard Baer, Chih-hao Chen, Manuel Drees, Frank Paige, and Xerxes Tata. Supersymmetry reach of Tevatron upgrades: The large tan β case. *Phys. Rev.*, D58:075008, 1998.

[136] Mihoko M. Nojiri and Youichi Yamada. Neutralino decays at the LHC. *Phys. Rev.*, D60:015006, 1999.

[137] A. Djouadi, Y. Mambrini, and M. Muhlleitner. Chargino and neutralino decays revisited. *Eur. Phys. J.*, C20:563–584, 2001.

[138] A. Denner, H. Eck, O. Hahn, and J. Kublbeck. Feynman rules for fermion number violating interactions. *Nucl. Phys.*, B387:467–484, 1992.

[139] A. Denner. Techniques for calculation of electroweak radiative corrections at the one loop level and results for W physics at LEP-200. *Fortschr. Phys.*, 41:307–420, 1993.

[140] L. H. Ryder. *Quantum Field Theory.* Cambridge University Press, (1985).

[141] M. Nikolic, editor. *Kinematics and Multiparticle Systems.* Documents on Modern Physics. Gordon and Breach, (1968).

[142] V. Barger and R. Phillips. *Collider Physics.* Addison Wesley, (1996).

[143] K. Hagiwara and D. Zeppenfeld. Helicity amplitudes for heavy lepton production in e^+e^- annihilation. *Nucl. Phys.*, B274:1, 1986.

Acknowledgments

I would like to complete my thesis with an acknowledgment to all the colleagues and friends who shared the last three years with me and accompanied me during this time.
Among all these people Professor M. Drees as my advisor takes premier place. Not only did he provide an excellent working environment as such and enabled me to attend several international workshops and conferences, but he also did guide me through the—metaphorical—mystic forest of particle physics in general and of SUSY in particular. Fortunately, I was able to profit from his vast knowledge and rich experiences within physics and beyond.
I should express my gratitude to the Deutsche Forschungsgemeinschaft, which supported most of my research under project number DR 263. Talking about funding neither Professor A. J. Buras and Professor F. von Feilitzsch nor the "Stipendienstelle des Internationalen Zentrums der Technischen Universität München" may be neglected here, the former provided helpful and welcome financial back-up in times of funding troubles, whereas the latter granted me a scholarship for finishing this thesis.
For sure, my Korean collaborators, namely Professor S .Y. Choi, J. Song, and J. S. Lee, must be acknowledged here. I shall always remember the fruitful collaboration and inspiring discussions we shared. Moreover, Professor S .Y. Choi and J. Song arranged my visit to KIAS in Seoul, whose working circumstances, friendly members and location I enjoyed very much.
Moreover, I will always keep the former and current members of the groups T31 and T30d and of the former group T30e in good memory; the great discussions on physics, life, the Universe and everything we had as well the excellent entertainment they provided can only be underestimated.
Concerning the working environment both our group secretary Karin Ramm as well as all the computing system administrators I bothered through the last years deserve my gratitude. Without such remarkable people working would have been much harder.
Finally, I would like thank to all my friends, in particular Klaus Härtl and Robert Buras, my family, in particular my parents, and—last, but definitely not least—my beloved partner Sarah. Altogether they formed an unimprovable background for doing physics and ensured that I stayed—to some extent—in touch with life and reality.

So long and thanks for the fish.

Garching, July 2004

Benedikt Gaißmaier